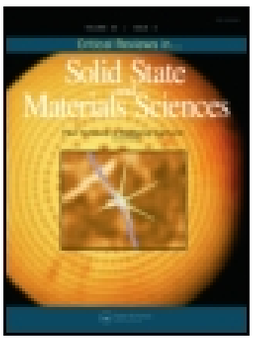

Taylor & Francis
Taylor & Francis Group

Critical Reviews in Solid State and Materials Sciences

ISSN: (Print) (Online) Journal homepage: https://www.tandfonline.com/loi/bsms20

Designing highly ductile magnesium alloys: current status and future challenges

Umer Masood Chaudry, Sravya Tekumalla, Manoj Gupta, Tea-Sung Jun & Kotiba Hamad

To cite this article: Umer Masood Chaudry, Sravya Tekumalla, Manoj Gupta, Tea-Sung Jun & Kotiba Hamad (2021): Designing highly ductile magnesium alloys: current status and future challenges, Critical Reviews in Solid State and Materials Sciences, DOI: 10.1080/10408436.2021.1947185

To link to this article: https://doi.org/10.1080/10408436.2021.1947185

Published online: 02 Aug 2021.

CRITICAL REVIEWS IN SOLID STATE AND MATERIALS SCIENCES
https://doi.org/10.1080/10408436.2021.1947185

Taylor & Francis
Taylor & Francis Group

REVIEW

Designing highly ductile magnesium alloys: current status and future challenges

Umer Masood Chaudry[a,b], Sravya Tekumalla[c], Manoj Gupta[d], Tea-Sung Jun[b], and Kotiba Hamad[a]

[a]School of Advanced Materials Science & Engineering, Sungkyunkwan University, Suwon, South Korea; [b]Department of Mechanical Engineering, Incheon National University, Incheon, South Korea; [c]School of Mechanical and Aerospace Engineering, Nanyang Technological University, Singapore; [d]Department of Mechanical Engineering, National University of Singapore, 9 Engineering Drive, Singapore

ABSTRACT

In order to reduce oil consumption and avoid fossil fuel-related environmental problems, scientists are always looking for lightweight structural materials that show high performance during both processing and application. Among various candidates, Mg seems to be the most promising. Mg is ~33, 60, and 75% lighter than Al, Ti, and steel, respectively. However, the vast applications of Mg are impeded due to its intrinsic brittleness at room temperature, which is related to the hexagonal close-packed crystal structure of Mg. In this crystal structure, the limited number of independent slip systems available at room temperature leads to brittle behavior and low fracture toughness. Thus, engineers and scientists all over the world have shown a great deal of interest in fabricating Mg-based materials with improved ductility. In this review, accordingly, the origin of low ductility in pure Mg and the fundamentals of designing highly ductile Mg alloys will be presented and critically discussed. In addition, the recent advances achieved in the field of Mg alloys with high ductility via control of structure and composition will be outlined. Finally, various properties of highly ductile Mg-based materials, including creep, fatigue, corrosion, and formability, will be discussed.

KEYWORDS

Magnesium-based materials; ductility; slip systems; atomistic mechanisms; composites; severe plastic deformation

GRAPHICAL ABSTRACT

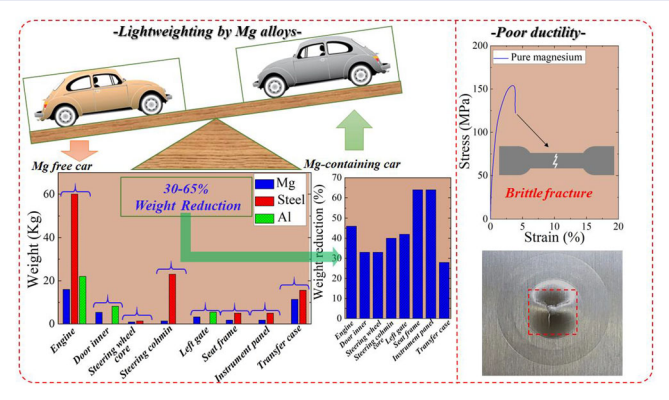

Table of contents

CONTACT Manoj Gupta mpegm@nus.edu.sg; Tea-Sung Jun t.jun@inu.ac.kr; Kotiba Hamad hamad82@skku.edu

1. Introduction

1.1. Importance of lightweight materials

Global warming is one of the most important issues that mankind is currently facing. It is a major factor in climate change, which, in addition to increasing the earth's average temperature, is also responsible for rising sea levels and frequent events of extreme weather. The intergovernmental panel on climate change (IPCC) reported that the observed high rate of global warming since the mid-20th century is dominantly caused by human activities, as illustrated by Figure 1a.[1] The major source of greenhouse gas emissions is the burning of fossil fuels, which mainly results in the emission of carbon dioxide (CO_2) gas, the largest contributor to global warming. For example, from 2007 to 2016, human activities have added 10.7×10^{12} Kg of carbon to the atmosphere each year, of which 9.4×10^{12} Kg came from the burning of fossil fuels (Figure 1b).[2] In recent years, there has been a vigorous debate over energy conservation and environmental protection. Scientists and engineers are looking for ways to mitigate the emission of CO_2 and avoid its adverse effects on the atmosphere. When looking at CO_2 emissions from the burning of oil by various sectors, it becomes evident that emissions are dominated by the transportation sector, which showed linear growth in emissions over the past five decades as presented by Figure 1c.[3] In response to tightening climate change policies and emission standards, world-leading countries have developed fuel consumption standards and regulations by implementing aggressive emission targets. For instance, the USA plans to reduce oil consumption by passenger cars from 6 L to less than 5 L per 100 km by the year 2025 (Figure 1d).[4] For this reason, developing high-performance lightweight structural materials for the automobile and aerospace industry is essential, as it would allow for simultaneous reductions in oil utilization and environmental pollution. For example, for every 100 kg weight reduction of an automobile, fuel consumption is estimated to improve by 0.9 km/L.[5] Out of various candidates, magnesium (Mg) is considered the best potential candidate to serve this purpose.

Mg is the lightest among the structural metallic materials, with a density that is 66% that of aluminum (Al), 39% that of titanium (Ti) and 23% that of steel, and is recognized as the best next-generation lightweight metallic material.[6] Mg is widely available, comprising 2.7% of the earth's crust (8th most abundant element), and can be commercially produced from ore with a purity of more than 99.8%. Hence, there are sufficient Mg resources for it to be substituted for Al and steel in diverse engineering applications. In addition to its low density and high abundance, Mg and its alloys show higher strength-to-weight ratios than other conventional materials (Figure 1e). Furthermore, because it is nontoxic to the human body and displays enhanced biodegradation and excellent biocompatibility in physiological conditions, Mg has emerged as an ideal candidate for permanent implant materials. Moreover, Mg and its alloys show superior castability, such that complex shapes can be fabricated at a high production rate. Additionally, from the viewpoint of environmental protection, Mg surpasses other materials, with a recyclability of 100%.[7] Based on the above discussed multiple advantages, Mg has been under immense investigations during last two decades as represented by Figure 1f.

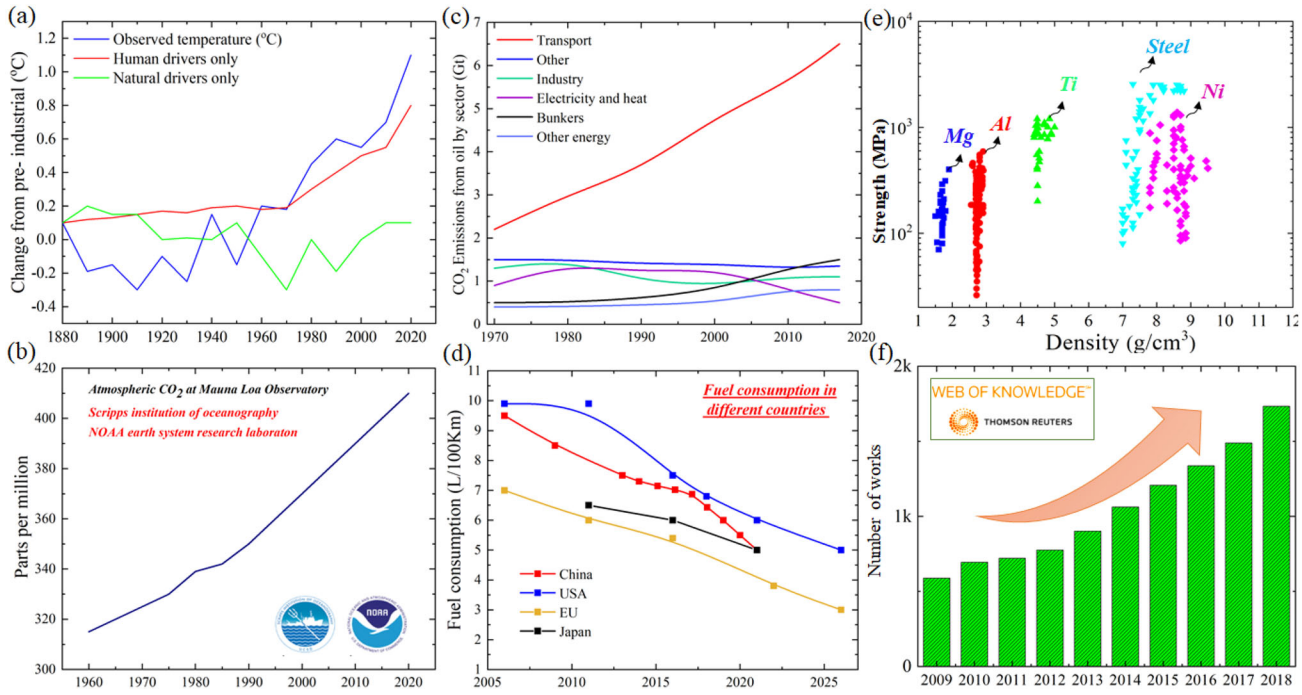

Figure 1. (a) Change in temperature occurring naturally or by human activities from pre-industrial age,[1] (b) Increase in atmospheric concentration of CO_2 over the years,[2] (c) Classification of CO_2 emissions from oil by various sectors,[3] (d) Comparison of fuel consumption standards in Major countries,[4] (e) Strength of several metals as a function of density, (f) Research output on Mg-based materials as reported in web of science from 2009 to 2018 (The data was obtained for topic: *Magnesium* and topic: *mechanical properties*).

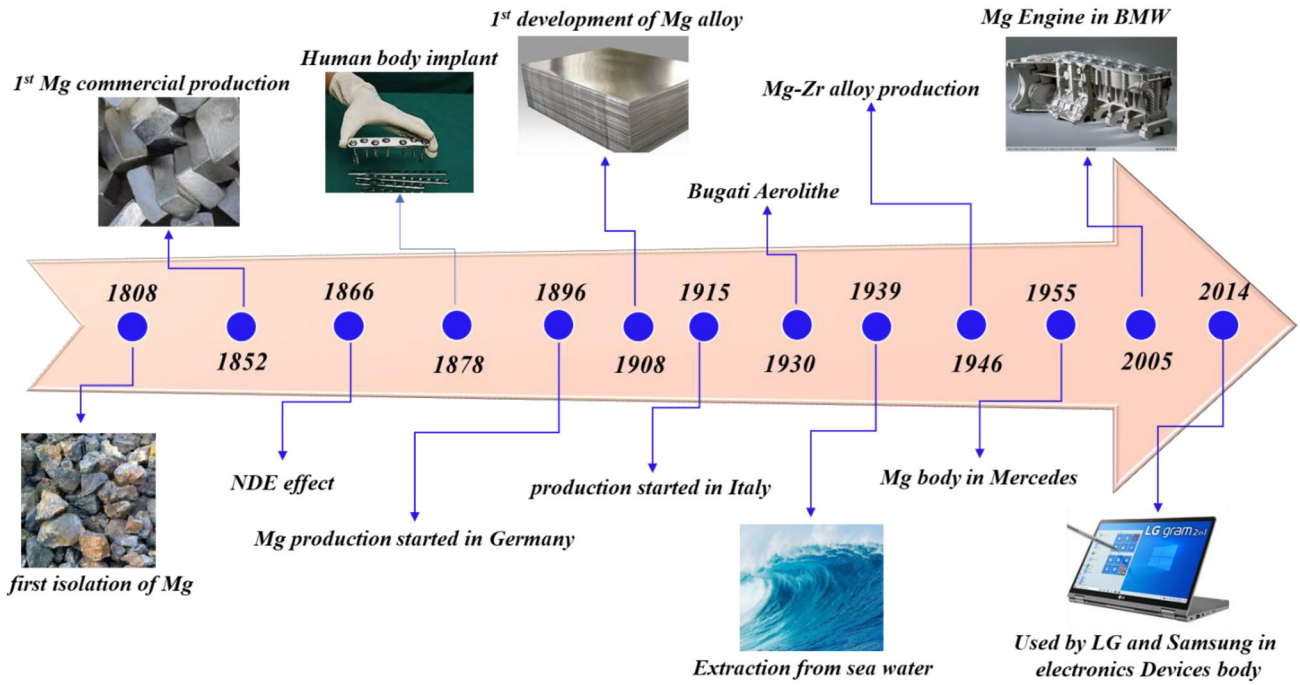

Figure 2. Scientific developments of Mg and potential applications over the years.

1.2. History of magnesium use

Figure 2 shows the historical background and scientific development of magnesium alloys. Mg was first discovered in the form of magnesium carbonate and was called "Magnesia" in ancient Greece. Sir Humphry Davy was the first chemist to successfully isolate Mg in its elemental form. Later on, in 1831, Bussey[8] reported the formation of a hydroxide layer on the surface

of Mg after exposure to moist air. The mechanism of negative difference effect (NDE) in Mg (evolution of hydrogen gas during anodic polarization) was studied by Beetz.[9] Commercial production of Mg began in 1852, when Robert Bunsen carried out electrolysis of fused magnesium chloride. Today, Mg is extracted using two different processes, high-temperature reduction of MgO by Si and electrolysis of magnesium chloride; a purity of more than 99% can be successfully achieved by both processes. The applicability of Mg in biomedical applications has been under consideration since the 1800s. Edward C. Huse was the first to use Mg wires as ligatures in 1878.[10] In 1896, Germany established the first plant for Mg production. This remained the only Mg-producing facility until 1915, when Italy started commercial production of Mg.

Since the 1900s, the global automobile industry has used Mg to make a wide range of parts, i.e., mounts, brackets, housing, and oil pumps. In the 1930s, the Bugatti Aerolithe car was built, in which the car body was fabricated using a Mg alloy (Elecktron) instead of Al alloys. Later, Mercedes Benz (1955), Porsche (1971), and BMW (2005) used Mg alloys to make car bodies and engine blocks.[11] Historically, Mg was considered a potential candidate for aerospace applications, and Wright Aeronautical first fabricated a Mg-based crankcase in the Wright duplex cyclone aviation engine. Given the remarkable characteristics of Mg, in 2010, Sony introduced a camera in which the main body is made of Mg. Samsung and LG have also introduced various devices containing Mg fabricated parts, including the world's lightest laptop, which has a Mg alloy main body.

1.3. Traditional magnesium alloys

In spite of its light weight and high natural abundance, the applicability of Mg as a structural material remains limited due to its intrinsic brittleness at room temperature (RT), which is related to its hexagonal close packed (HCP) crystal structure. The RT properties of pure Mg can be significantly enhanced by alloying Mg with various elements. During the past decade, Mg has received a tremendous amount of attention and been the subject of vigorous research, and interest in designing and developing new Mg alloys for diverse applications is currently growing (Figure 3). Mg alloys involve dispersion of intermetallic particles in the α-Mg matrix, which contributes to their superior mechanical properties. The most researched Mg alloy system contains Al and/or Zn and Mn (AZ31, AZ61, AZ91, AM60, AM61). These alloys show a broad range of mechanical properties; ductility of up to 40% and high tensile strength of 300 MPa have been reported.[12] On the other hand, the low creep resistance observed in this alloy system can be attributed to the presence of a $Mg_{17}Al_{12}$ phase with a low melting temperature, which limits the applicability of the alloys above 120 °C. Recently, next-generation Mg-Al-Zn-Ca alloys with higher

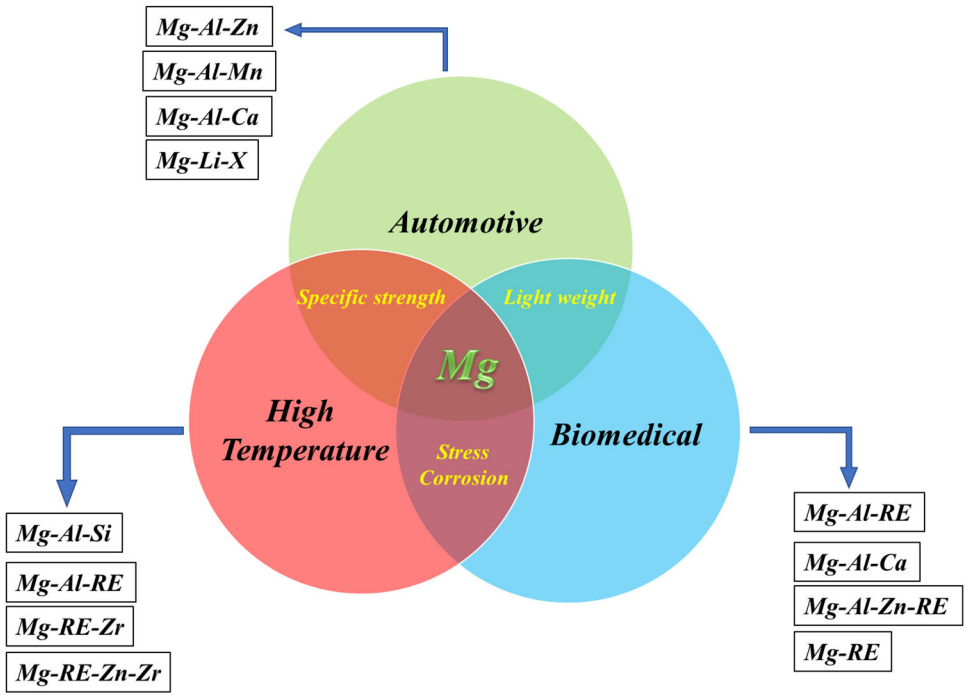

Figure 3. Conventional Mg alloys for various applications.

thermal stability have been developed; specific alloy composition along with thermo-mechanical processing have produced materials with superior properties such as high tensile ductility, high strain hardenability, and lower anisotropy. The excellent combination of properties is attributable to the intermetallic compounds (IMCs), which lead to thermally stable, weak basal textured and fine grained Mg-based materials.[13–15] In addition, Mg-Li alloys have demonstrated superplastic behavior based on their bi-phase structures, consisting of Mg-rich α (HCP) and Li-rich β (BCC) phases, when Li concentrations are between 5.7 and 11 wt%. Alloys with rare earth (RE) elements have demonstrated multiple advantages, such as strength/ductility synergy and improved creep resistance, due to the presence of IMC with higher melting points.

A $Mg_{97}Zn_1Y_2$ (at%) alloy produced by a rapid solidification powder metallurgy technique showed a yield strength of more than 600 MPa.[16] Rolled Mg-Gd-Zn alloy sheets have been reported to be highly ductile alloys with a 40% elongation to failure value.[17] A Mg-9Li-1Y (wt%) alloy has been reported to exhibit extremely high elongation of over 50%.[18] Moreover, excellent RT formability and ductility have been reported in Mg alloys with dilute (< 1%) RE alloying.[19,20] In addition, Al-free Mg alloy systems, such as Mg-Zn-Zr (ZK series), Mg-Nd-Y-Zr (WE series), Mg-Ag-Nd-Zr (QE series), Mg-Gd-Nd-Zr (Elektron 21) and Mg-Zn-RE-Zr (ZE series), have been reported to demonstrate high creep resistance and can be used at operating temperatures of up to 300 °C. The formation of various IMCs, such as $Mg_{24}Y_5$, $Mg_{14}Nd_2Y$, $NdAgMg_{11}$, Mg_7Nd, Mg_3Nd, etc., in the abovementioned Mg alloy systems can strengthen the alloy by particle hardening or particle strengthening. The presence of Zinc (Zn) along with other elements produces precipitation-hardenable magnesium alloys with superior strength and high corrosion resistance.

Over the past few years, there have been intense efforts to design Mg-based composites by adding ceramics, nano-carbon, or metal reinforcements to ensure high elastic modulus, positive creep properties, superior fatigue characteristics and to modify thermal expansion. One major obstacle is the high chemical reactivity of Mg with foreign reinforcements, which can impair the reinforcement material. Thus, there is an urgent need to identify the appropriate reinforcement and fabrication procedures that ensure the superior properties of the resultant materials for utilizing in widespread applications. Kaibo et al.[21] fabricated a TiC_p/Mg-4Zn-0.5Ca (wt%) nanocomposite using an ultrasonic-assisted semisolid stirring method and reported a yield strength (YS), ultimate tensile strength (UTS) and elongation (El) of 355 MPa, 386 MPa, and 10.2%, respectively. The improved properties were attributed to the grain refinement and high fraction of $MgZn_2$ phase due to the addition of TiC_p nanoparticles, which promoted particle-stimulated nucleation by providing a large driving force for dynamic recrystallization. Deng et al.[22] fabricated SiC_p/AZ91 with high tensile strength (441 MPa) and high elastic modulus (60 GPa) by stir casting and extrusion at 250 °C at speeds of 0.01, 0.1, and 1 mm/s. Precipitation of ultrafine $Mg_{17}Al_{12}$ during the extrusion process was suggested to be the cause of the improvements in material properties. To identify the effect of oxide nanoparticles on the wear behavior of Mg alloys, an Al_2O_3/AZ31 nanocomposite with varying amounts of Al_2O_3 (0.66, 1.11, 1.5 wt%) was fabricated by powder metallurgy with a microwave sintering technique followed by hot extrusion. The results revealed that the 1.5 wt% Al_2O_3/AZ31 nanocomposite showed the highest wear resistance of all composites tested.[23]

1.4. Potential applications of magnesium alloys

1.4.1. Automotive industry

Using Mg and its alloys as substitutes for conventional materials in the automotive industry can significantly reduce vehicle weight from 22% to 70%, which can contribute to better fuel economy and environmental protection. The excellent vibration dumping capability, castability and high strength to weight ratio make Mg an ideal candidate for such applications. In addition, vehicle weight reduction is inevitable based on the strict global policies meant to mitigate greenhouse gas emissions. As CO_2 emissions are directly related to fuel utilization, vehicle weight has emerged as the most important criterion for assessing design efficiency. The necessary weight reduction can be achieved by innovative design and use of lightweight materials (Figure 4a).[24] Since the 1900s, the automotive industry has been continuously engaged in replacing denser vehicle components with lightweight Mg alloys. The Bugatti Aerolithe, made in 1930, was the first car with a Mg main body, and, later, Porsche introduced the first car with a Mg engine. From 1990 to 2007, BMW achieved a 30% reduction in fuel utilization by introducing the world's lightest 3.0-liter inline six-cylinder gasoline engine featuring Mg alloy housing surrounding Al inserts. The innovative design lead to high power performance and enhanced fuel

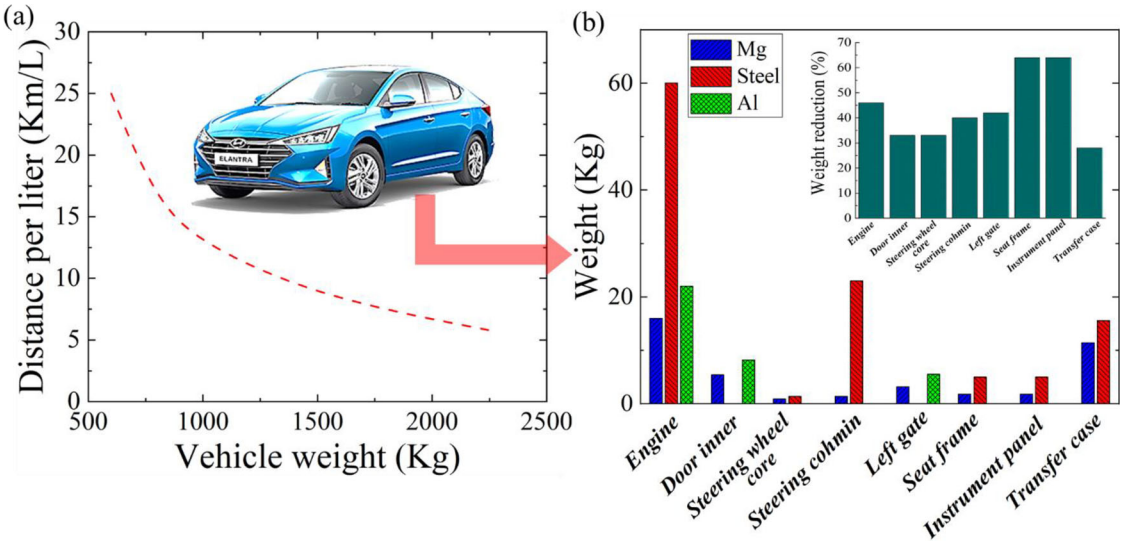

Figure 4. (a) The relation between fuel consumption and vehicle mass,[24] (b) The comparison of weight of various car components fabricated by Al, steel and Mg (The figure inset shows the % weight reduction for fabricating different parts using Mg as compared to conventional materials).

efficiency in addition to environmental benefits. Figure 4b shows the overall fraction of weight reduction that can be achieved by using Mg as an alternative to other conventional materials. Mg-Al cast alloys including Mg-(2-6)Al (wt%) (AM series) and Mg-9Al-1Zn (wt%) (AZ91) are the most common Mg alloys used to fabricate instrument panels, steering wheels, etc. because of their adequate combination of RT strength and ductility. The pre-requisites for utilizing Mg alloys in the automotive industry include metallurgical and thermal stability, superior creep properties, castability for complicated shapes and good corrosion resistance. However, the high reactivity of Mg in a molten state, low corrosion resistance, and inferior creep properties have restricted widespread applications. Accordingly, significant research is still necessary to advance alloy development, corrosion resistance, welding and joining, surface treatments and mechanical properties.

1.4.2. High temperature applications

Interest in designing a heat-resistant Mg alloy is growing based on the multiple advantages it would offer. However, due to the high grain boundary diffusion coefficient of Mg, current strengthening mechanisms are not effective at achieving superior mechanical properties at elevated temperatures. A strengthening mechanism such as the Orowan process contributes to improvements in the temperature strength of Mg-based materials since the Orowan process is not easily reduced by diffusion. Accordingly, extensive investigations have been carried out in attempts to improve the high-temperature properties of Mg alloys based on precipitation behavior and to study the underlying strengthening mechanism. Mg-RE-based alloys have emerged as new heat-resistant alloys due to the precipitation hardening and high solubility of the α-Mg matrix at high temperatures.

Liu et al.[25] fabricated a low-pressure sand-cast Mg-10Gd-3Y-0.5Zr (wt%) (GW103K) alloy with excellent properties at elevated temperature. The RT yield strength (YS), ultimate tensile strength (UTS) and ductility of the sample peak aged at 250 °C for 12 h were 247 MPa, 360 MPa and 2.7%, respectively (Figure 5a and b). The YS and UTS of the alloy were found to have a direct relationship with the temperature, and the maximum values of YS (255 MPa) and UTS (368 MPa) were achieved at 125 °C. The alloy aged at 225 °C for 14 h showed YS and UTS values of 250 MPa and 350 MPa at 200 °C, respectively. A permanent mold cast Mg-3.5Sm-2Yb-0.6Zn-0.5Zr (wt%) (SmYbZK4210) with an excellent balance of strength and ductility at elevated temperatures was fabricated by Meng et al.[26] The YS, UTS, and EL were 182 MPa, 279 MPa, and 18.2% and 127 MPa, 186 MPa, and 15% at 200 °C and 300 °C, respectively. Transmission electron microscopy (TEM) revealed that the coexistence of fine prismatic β'' and basal γ'' phases along with coarse tridentate precipitate (TP) is mainly responsible for the improved high-temperature properties of the SmYbZK4210 alloy (Figure 5c–e).

Wang et al.[27] investigated the compositional dependence of Y in a Mg-10Gd-xY-0.4Zr (x = 1,3,5 wt%) alloy and reported that the tensile properties were enhanced with an increase in Y content. As showed in Figure 5f, the Mg-10Gd-5Y-0.4Zr

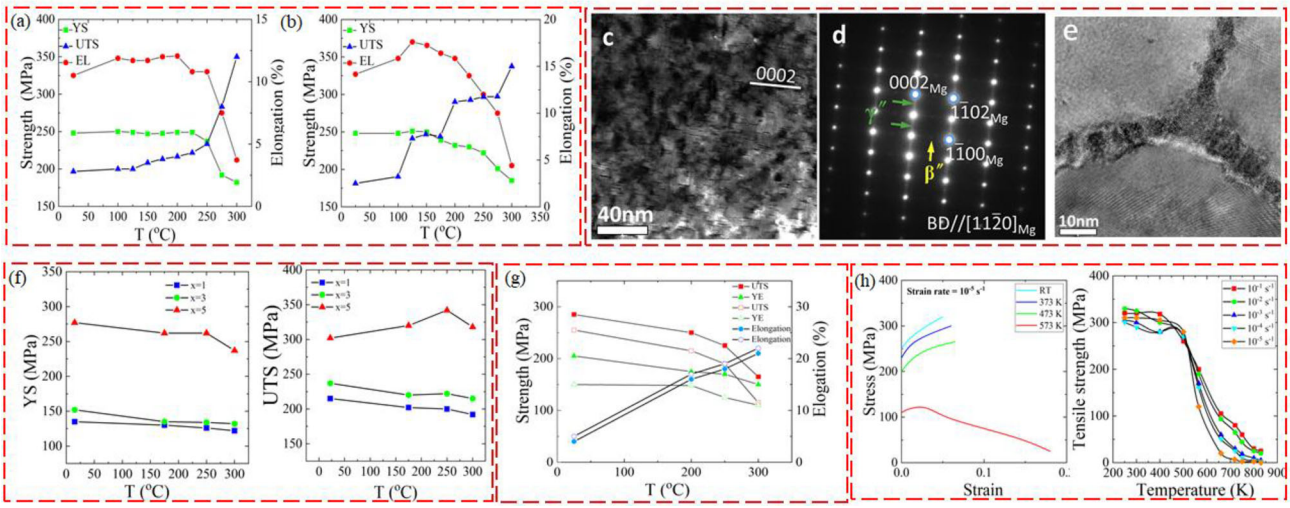

Figure 5. Tensile properties of GW103K alloys under (a) 525 °C × 12 h + 225 °C × 14 h, (b) 525 °C × 12 h + 250 °C × 12 h conditions,[25] (c,d) BF-TEM micrograph of SmYbZK4210 alloy, where yellow arrows and green arrows show β'' reflections and γ'' reflections, respectively and (e) shows the TP phase,[26] (f) Tensile properties of Mg-10Gd-xY-0.4Zr (x = 1,3,5 wt%) alloy as a function of temperature,[27] (g) High-temperature mechanical properties of Mg-2.49Nd-1.82Gd-0.19Zn-0.4Zr alloy,[28] (h) Tensile properties of peak aged Mg-4Y-3RE alloy from RT to 550 °C.[29]

alloy showed the best mechanical properties at peak aged conditions; values of 340 MPa and 267 MPa were recorded for UTS and YS, respectively, at 250 °C. The remarkable improvement was attributed to the homogeneous distribution of β and β' precipitates in the Mg matrix. The high-temperature mechanical properties of a Mg-2.49Nd-1.82Gd-0.19Zn-0.4Zr (wt%) alloy were evaluated by Liu et al.[28] The UTS and YS of peak aged alloy were 287 MPa and 206 MPa at RT, 240 MPa and 175 MPa at 200 °C, and 220 MPa and 165 MPa at 250 °C, respectively (Figure 5g). The presence of rod-shaped metastable Mg_7Nd, Mg_3Nd, coarse Zn_2Zr_3, and dispersed interdendritic $Mg_{12}Nd$ precipitates within the α-Mg matrix were responsible for the improved properties. The tensile properties of a peak-aged Mg-4Y-3RE (wt%) alloy at RT to 550 °C were studied by Mabuchi et al.,[29] and the results revealed that the alloy exhibited a strength of > 250 MPa from RT to 200 °C. The strength rapidly reduced at 300 °C, which was attributed to the initiation of the grain boundary sliding phenomenon, as shown in Figure 5h.

1.4.3. Biomedical applications

Owning to its superior biocompatibility, high specific strength, and dissolution profile in physiologic media, Mg has emerged as a potential alternative to the permanent metallic implants that have been used for the tissue healing process and fracture repairs for more than 100 years. The use of biodegradable Mg implants has been a game changer, since this avoids additional surgical procedures for implant removal. Biodegradable implants stay in the body temporarily to support a fractured bone during the healing process, and then are gradually absorbed as nutrients. One major advantage of Mg implants involves the high recommended daily intake of Mg (240–420 mg/day), which is several times higher than that of other commonly used implant materials. In addition, Mg has appropriate mechanical properties and an elastic modulus (45 GPa) close to the elastic modulus of bone (3–20 GPa), which reduces the risk of stress shielding. However, a high degradation rate, rapid non-uniform corrosion behavior and excessive hydrogen evolution have been the major drawbacks of Mg implants, all of which lead to deterioration in mechanical properties.

Since 1800, when Edward C. Huse employed Mg wires as ligatures, doctors and researchers have attempted to exploit Mg for biomedical applications. In 1948, Troitskii and Tsitrin successfully carried out pseudarthrosis surgery using a Mg-Cd alloy. Figure 6a and b display a comparison of the mechanical and corrosion properties of the most-researched elements (Fe, Zn and Mg) for biomedical applications.[30–37] During the past two decades, there has been a huge emphasis on improving the biodegradation and corrosion characteristics of Mg implants by suitable alloying, implant design optimization and further surface treatments. Heublein et al.[38] used a stent made of a Mg-2Al-1RE (wt%) alloy and confirmed the nontoxic nature of Mg alloys toward the human body. In

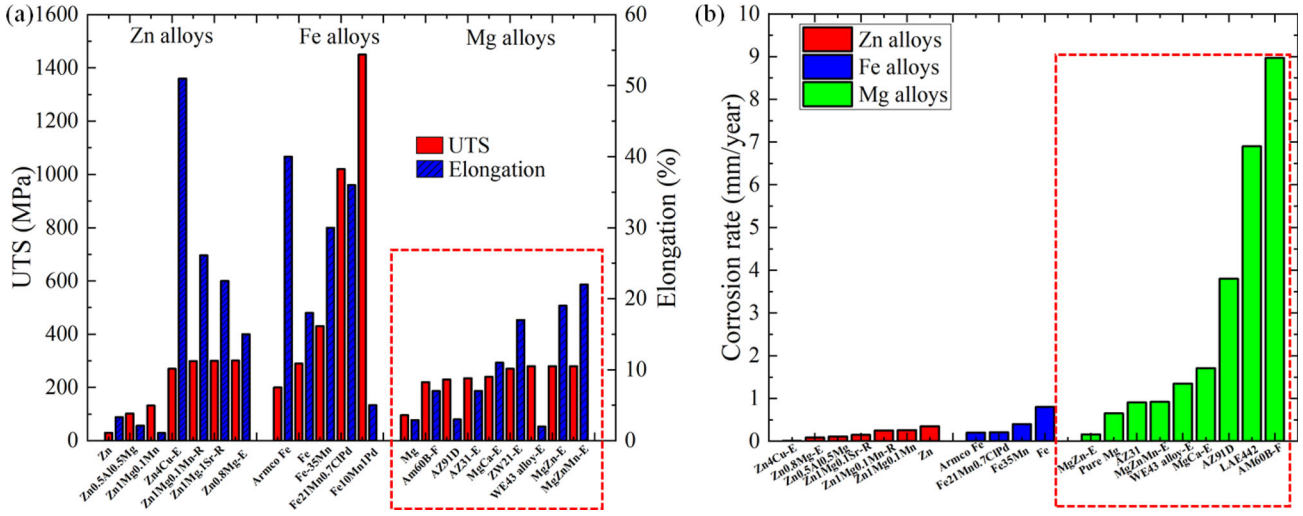

Figure 6. Comparison of (a) mechanical properties,[30–35] and (b) corrosion rate[30–37] of Zn, Fe and Mg alloys.

addition, a stent fabricated from a WE43 alloy demonstrated satisfactory mechanical properties in the physiological environment.[39] Moreover, alloying Mg with Al lead to a decrease in the corrosion rate in phosphate-buffered solution (PBS) and simulated body fluid (SBF), which was attributed to the formation of an insoluble Al_2O_3 layer instead of a soluble $Mg(OH)_2$ layer.[40] Ca-containing Mg alloys have demonstrated excellent results in terms of superior ductility and enhanced formability. In addition, it has been reported that addition of up to 0.6 wt% Ca to Mg improves the corrosion resistance of Mg-Ca alloys, whereas further increases in the Ca concentration result in the opposite trend. A higher concentration of Ca results in an increased fraction of the Mg_2Ca phase, which increases the probability of galvanic cell formation.[41]

1.5. Review summary

Magnesium (Mg) alloys have been receiving a great deal of attentions for the past 20 years owing to its widespread availability, low density, and adequate mechanical properties. The current review sheds pertinent information on the bottlenecks and obstacles impeding the vast applications of Mg alloys. Historical and most recent research in Mg and its alloys have been critically reviewed from the alloying design prospect and in terms of microstructure-processing-properties relationship and the challenges associated with designing highly ductile Mg alloys are identifies and deeply discussed. Accordingly, the novel alloy design, various pre/post processing techniques and predicting the alloying combinations using integrated computational materials engineering (ICME) and machine learning (ML) are discussed.

The current review is classified to render the comprehensive and up-to-date overview of key issues associated with intrinsic brittleness of Mg alloys. 1st section is devoted to the importance, historic background and most famous Mg alloys being used for various applications. In addition, key potential utilization areas have also been identified and discussed. Section 2 provides systemic summary of various aspects associated with the inferior properties of Mg alloys and most crucial atomistic flow mechanisms for designing highly ductile Mg alloys. Section 3 covers the important strategies including microstructure/texture modifications and altering the CRSS by appropriate alloying or pre/post processing for enhancing the properties of Mg alloys. Section 4 focuses on the recent advancements in Mg ductilization and thoroughly investigate and discuss the important Mg alloys. Moreover, the most important severe plastic deformation (SPD) techniques being employed for improving the mechanical properties of Mg alloys have been reviewed and discussed. The last part of section 4 is dedicated to the important types of Mg composites, the key processing parameters, and the strategies to achieve strength-ductility synergy in Mg composites. Section 5 reviews the most important features of Mg alloys and the pertinent obstructions in the widespread utilization is discussed. Finally, section 6 have been dedicated to the most recent opportunities for the advancements in scientific and experimental methodologies and the conclusive remarks.

It is pertinent to mention that despite the numerous research and extensive information on Mg alloys, yet there is no comprehensive literature available

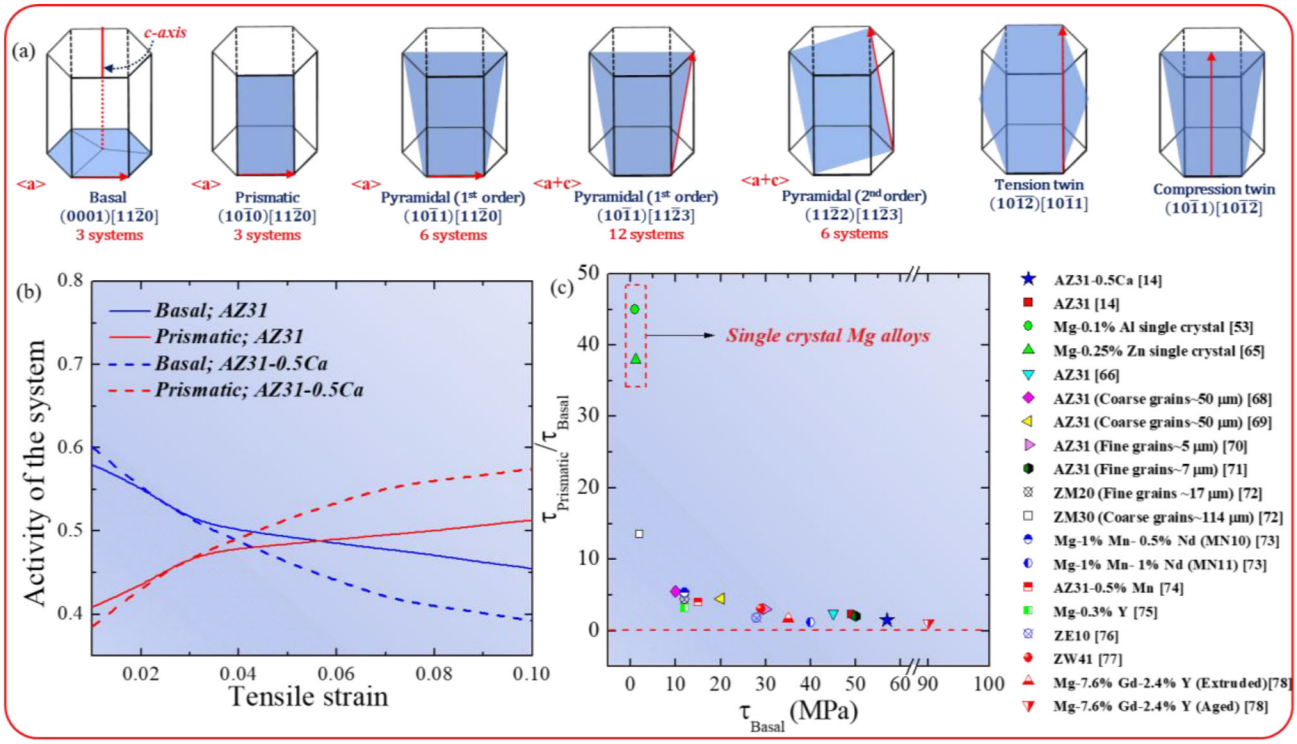

Figure 7. (a) Various slip systems in Mg, (b) Relative activities of Basal and Prismatic slip in AZ31 and AZ31-0.5Ca,[14] (c) The effective CRSSs ($CRSS_P/CRSS_B$) as a function of CRSS of basal slip for single and polycrystalline Mg alloys.[14,51–64]

discussing the fundamentals issues associated with the low ductility of Mg based materials. However, there are several important review papers on various aspects of Mg, for instance, the properties, applications and potential of Mg,[7] effect of rare-earth elements on texture evolution,[42] development of rare-earth free Mg alloys with high strength,[43] Hall-Petch relationship in Mg alloys,[44] pre-twinning in Mg alloys,[45] optimization of texture,[46] corrosion in Mg alloys,[47] properties and applications of Mg-based nanocomposites.[48] However, no review paper discusses the most fundamental impediments hindering the global growing interest in Mg alloys. The current review paper attempts to furnish a conclusive standpoint on the key fundamentals barriers and identifies gaps forestalling through understanding of diverse features.

2. Why pure magnesium is brittle?

2.1. Deformation modes in pure magnesium

2.1.1. Slip systems

Deformation of metals is facilitated by the movement of line defects along densely packed planes and in the direction of close-packed lattices. These microscopic defects are called dislocations, and their associated crystallographic features are referred to as slip systems. Slip is the most important deformation mechanism in metals as every crystal can deform along a specific direction and high deformation compatibility is required for macroscopic plasticity. According to the von Mises criterion, at least five independent slip systems need to be activated to accommodate plastic deformation in polycrystalline materials.[49] Cubic crystals demonstrate excellent plastic deformation based on a sufficiently high number of independent slip systems due to their high crystal symmetry; however, a hexagonal close-packed (HCP) structure shows a lack of independent crystallographic shears.[50] As previously mentioned, Mg and its alloys are regarded as next-generation materials and have a remarkable potential to promote energy efficiency. Despite the tantalizing properties of such materials, the widespread applications of Mg have been hampered due to its limited intrinsic ductility at RT, which can be traced to insufficient deformation slip modes owing to its HCP structure.

The slip systems in Mg can be classified into two categories, (i) basal slip system operating in the (0001) basal plane and (ii) non-basal slip system (prismatic $\{10\bar{1}1\}$, pyramidal $\{10\bar{1}1\}$ and $\{10\bar{2}2\}$) operating in non-basal planes (Figure 7a). In spite of having a large number of overall slip systems, Mg demonstrates poor ductility, which can be attributed to the fact that the relative ease with which deformation is accommodated varies among different slip systems. The

quantitative parameter, which describes the ease of slip on different slip modes, is referred to as critical resolved shear stress (CRSS), and the approximate CRSS values for different slip modes are estimated through various modeling techniques, such as elasto-plastic self-consistent (EPSC) modeling, viscoplastic self-consistent (VPSC) modeling, and others.[14,51,65,66] At RT, the plastic deformation of Mg is only governed by $\{0001\} < 10\bar{2}0 >$ basal $< a >$ dislocation slip and $\{10\bar{1}2\} < 10\bar{1}1 >$ tensile twinning owing to their low CRSS as compared to non-basal slip systems.[67–69] However, basal $< a >$ slip could not accommodate strain along the *c-axis*, rather the crystal *c-axis* is rotated parallel to the direction of stress loading, leading to strong basal textural components, and Mg eventually fails at low strains.[70] At higher temperature, more slip occurs on the pyramidal $\{10\bar{1}1\}$ plane without a change in direction.

Accordingly, the limited intrinsic ductility is associated with the inability of HCP Mg to plastically deform in the crystallographic $< c >$ direction, which can be accomplished by dislocation glide on the pyramidal II plane with $< c + a >$ Burgers vector and, hence high ductility in Mg can be achieved by generating more $< c + a >$ dislocations.[14,71,72] In polycrystalline Mg, the CRSS of slip systems is influenced by the hardening induced by grain boundaries (GBs), second phase particles, and solute atoms, which can be described by the following equation:

$$\tau = CRSS + \Delta\tau \tag{1}$$

Here, τ is the effective CRSS, and $\Delta\tau$ is the hardening contribution by the abovementioned microstructural features. The CRSS values of the basal and prismatic slip systems for single-crystal Mg are 1 and 40 MPa, respectively. Based on Eq. [1], the relative activity ratio ($CRSS_P/CRSS_B$) can be written as:

$$\frac{\tau_P}{\tau_B} = \frac{40 + \Delta\tau}{1 + \Delta\tau} \tag{2}$$

In Mg, generally, addition of dilute alloy elements leads to hardening of basal slip, while prismatic slip undergoes solute softening. Narrowing down the CRSS gap between basal and non-basal slip systems (~1–40 and 1–100 MPa for basal-prismatic and basal-pyramidal, respectively) is considered to be the key to designing highly ductile Mg alloys. This can be achieved by manipulating the relative activity of non-basal slip systems or by stabilizing the dislocations on the basal plane with the addition of various alloy elements. Several works have previously reported Mg alloys with improved properties based on the effect of added elements on dislocation mobility between the basal and non-basal systems. Addition of solid solutions has been demonstrated to impose strong hardening in the basal plane while softening the prismatic slip, resulting in activation of the non-basal slip system, and this interplay between the softer and harder slip modes determines the strength and ductility of the resulting material. In particular, dilute alloying with RE elements produces a significant improvement in RT ductility.[68,73–75] For example, elongation to failure for Mg-Zn alloys was increased by the addition of 0.2.wt% Ce, which contributed to the higher activity of the non-basal slip system.[76] Sandlobes et al. demonstrated that the addition of yttrium (Y) significantly enhances the activity of the $< c + a >$ slip system, resulting in superior properties.[67] Byong et al. introduced the AT31 (Mg-3Al-1Sn) (wt%) Mg alloy, which showed a high Erichsen value (IE) of 10.2 mm.[77] The microstructural characterization of deformed AT31 by high-resolution transmission electron microscopy (HRTEM) revealed that prismatic $< a >$ slip is the dominating deformation mechanism in addition to basal $< a >$ slip, resulting in high stretch formability. Teghtsoonian and Akhtar showed that the addition of Zn can result in higher activity of prismatic slip and hardening of basal slip.[52,53] In addition, Yuasa et al. investigated the effects of group II elements on the stretched formability of Mg-Zn alloys and concluded that adding 0.06 wt% Ca to a Mg-Zn alloy resulted in excellent stretched formability because of an increase in the activity of non-basal slip.[78] Particle-hardened basal slip was also introduced to assess the high ductility of Mg alloys containing calcium (Ca). Umer et al. introduced AZ31-0.5Ca (wt%), which demonstrated improved mechanical properties; in-grain misorientation axis (IGMA) analysis and VPSC calculations revealed the absolute activation of prismatic $< a >$ slip (Figure 7b).[14,15] Figure 7c presents the τ_P/τ_B ratio as a function of shear stress of the basal slip for various Mg-based materials.[14,51–64] Accordingly, high ductility in Mg alloys can be achieved by keeping the τ_P/τ_B ratio close to unity via hardening of basal dislocation using various kind of obstacles or by softening of non-basal slip systems.

2.1.2. Twinning systems

Twinning is an important deformation mode in Mg alloys, in addition to slip systems. At RT, the CRSS of deformation modes in Mg varies as $CRSS_{basal} < CRSS_{tension\ twins} < CRSS_{prismatic} < CRSS_{pyramidal}$ and the relative ratio ($CRSS_P/CRSS_B$) is typically in the range of 20–100 MPa. Accordingly, twinning, in

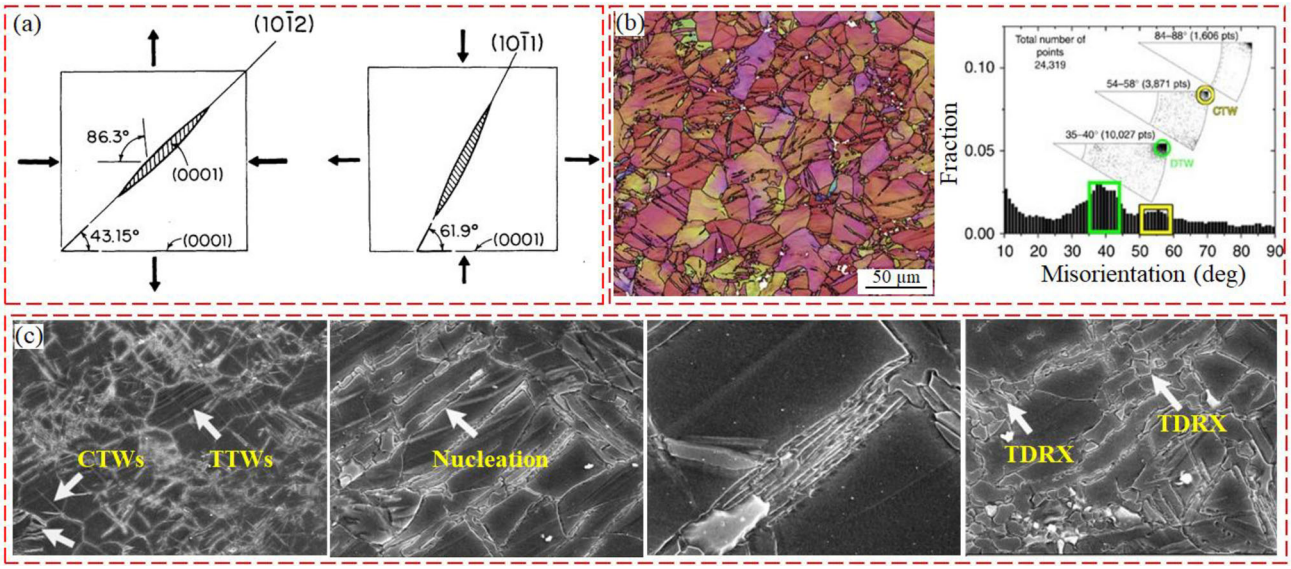

Figure 8. (a) Extension and contraction twins, (b) Formation of $\{10\bar{1}1\}-\{10\bar{1}2\}$ double twins in 24% deformed Mg-4Li (wt%) and the related misorientation distribution profile,[79] (c) TDRX in 12% cold rolled AZ31 followed by annealing at 280 °C for 10 s.[80]

addition to basal slip, acts as a secondary deformation mechanism to accommodate plastic strain by tension twinning (TTW) along $\{10\bar{1}2\}<10\bar{1}\bar{1}>$ and to some extent by compression twinning (CTW) along $\{10\bar{1}1\}<10\bar{1}2>$. Twinning on $\{10\bar{1}2\}$ leads to expansion along the *c-axis* under tensile load, with the basal plane in the twin being reoriented through ~86°. On the other hand, $\{10\bar{1}1\}$ twinning results in contraction parallel to the *c-axis*, where the basal plane is rotated through 56° under compressive loads (Figure 8a).[81] Moreover, the CRSS of TTWs is much smaller than that of CTWs, so extensive TTWs can be generated in the Mg matrix upon deformation. In addition, $\{10\bar{1}1\}-\{10\bar{1}2\}$ double twins (DTW) can also form when the crystallographic orientation of $\{10\bar{1}1\}$ is favorable for $\{10\bar{1}2\}$ twinning; in that case, $\{10\bar{1}2\}$ TTW occurs inside $\{10\bar{1}1\}$ CTW and overtakes the fine CTW lamella. The development of DTWs has been reported to cause premature failure in Mg alloys because of microcrack formation and dislocation pile-up at the twin-matrix interface, which accelerates cracking.[82–84]

Accordingly, researchers have attempted to suppress the development of CTW and DTW by using specific alloys or controlling the microstructure. Lentz et al. provided a key insight when they reported high compressive strain in a Mg-4wt% Li alloy, which was achieved by relaxing the localized stress concentration generated by DTWs by higher $<c+a>$ slip activity (Figure 8b).[79] Twinning can also strengthen the matrix, where twin boundaries act as an obstacle to dislocation slip and become a cause of high work hardening. It has been established that twinned texture formation can significantly enhance the mechanical properties of Mg alloys. Besides accommodating plastic strain, twinning deformation can also modify the microstructure as twin lamellas divide the grains, leading to grain refinement and also affecting slip activity by altering the crystal lattice orientation, resulting in improved properties.[85,86] Previously, it was reported that TTW can overtake its parent grain by growing thick under loading conditions, resulting in lower strength but higher ductility.[81,87–89] Moreover, twin-assisted dynamic recrystallization during hot deformation largely influences the microstructural and mechanical properties of a material; twins that existed before deformation and those formed during deformation can provide preferred sites for static and dynamic nucleation (Figure 8c).[80,90–92] Koike et al. noted that, in rolled Mg sheets, deformation along width strain can be accommodated by prismatic $<a>$ slip, while thickness strain can be coordinated by $<c+a>$ pyramidal slip and $\{10\bar{1}2\}$ TTWs. Due to the unavailability of $<c+a>$ slip at RT and the inability of TTWs to resolve shear stress in three directions, Mg demonstrated high plastic anisotropy (*r*-value) at RT.[93]

2.1.3. Grain boundary sliding

In addition to dislocation slip and deformation twinning, grain boundary sliding (GBS) is another plastic deformation mechanism. In GBS, grains slide against each other, resulting in superplastic behavior at elevated temperature (~0.5 T_{mp}, where T_{mp} is melting

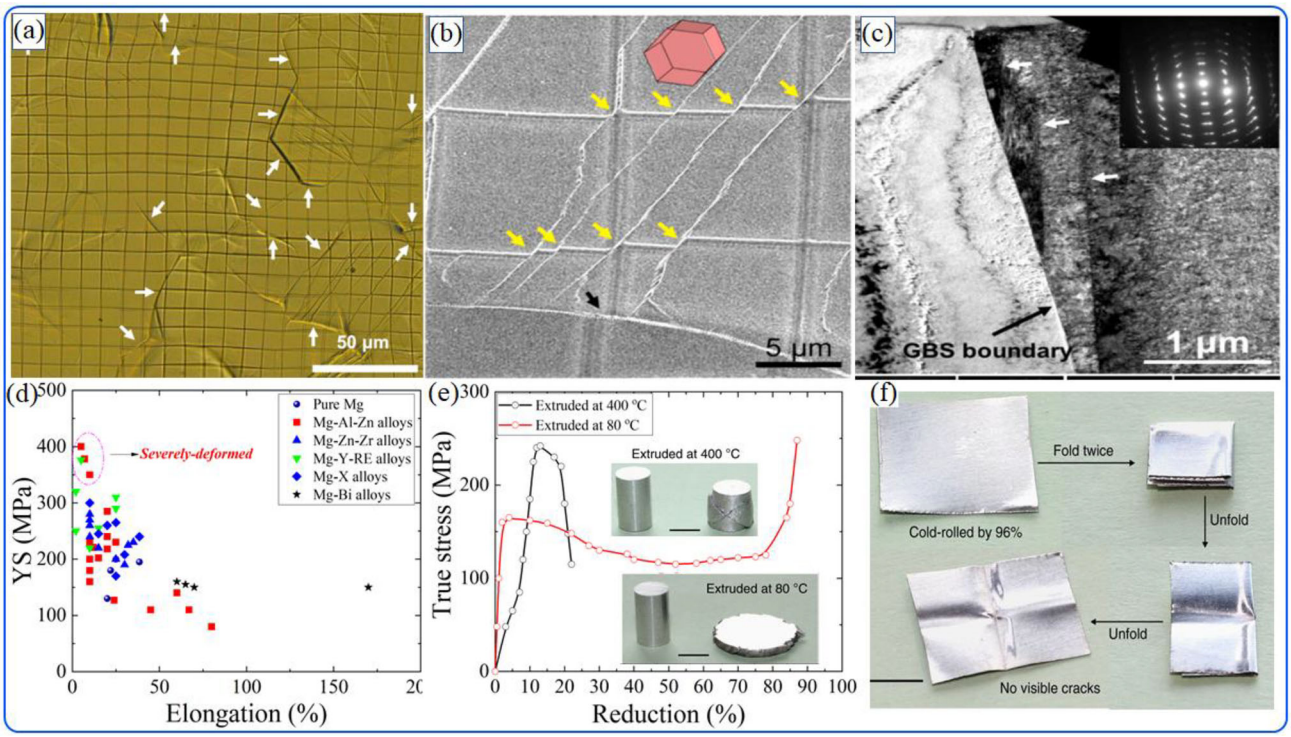

Figure 9. (a) Surface with scribed grids of 10% tensile deformed AZ31, white arrows show GBS,[97] (b) FIB image of intersection of slip line traces with GBS boundary, where yellow arrows show the slip line traces and white dotted lines represent the GBS boundary,[97] (c) TEM image of internal microstructure of GBS boundary with subgrain boundaries indicated by white arrows,[97] (d) Comparison of elongation to failure and yield strength received after RT tensile tests at a strain rate of 1×10^{-3} s^{-1},[98] (e) RT compression of pure Mg extruded at 80 °C and 300 °C,[99] (e) 96% RT rolled pure Mg showing excellent formability.[99]

point). This unique behavior is observed due to the accommodation of a high diffusion rate of GB in Mg.[94] Hence, thoroughly understanding the effect of GB structures on GB migration and GB strengthening can provide insights into the design of super ductile Mg alloys. In this regard, Somekawa et al. carried out nanoindentation creep testing and molecular dynamics (MD) simulations on pure Mg to investigate the effect of GB structures and related parameters that influence GBS behavior.[95] The results suggested that high-energy GBs showed high strain rate sensitivity, resulting in GBS. In addition, the MD calculations revealed that the addition of Al to Mg tended to suppress GBS due to a decrease in GB energy (0.32 J/m^2 as compared to 0.40 J/m^2 for pure Mg). In another quantitative work, Somekawa et al. investigated the effect of dilute solute additions (Ag, Sn, Al, Li, Pb, Y, Zn) on the tendency of GBS in Mg.[96] The GB energy values calculated by first principle calculations using density functional theory (DFT) were compared with the experimental results from the nanoindentation tests on the same alloy compositions. The results suggested that the Mg-Li and Mg-Y alloys showed the maximum and minimum values of GB energy owing to their weak and strong bonding with Mg, respectively. It was concluded that GB energy can be used to reliably predict the overall activation of GBS when developing highly ductile Mg alloys.

Moreover, the origin of GBS is considered to be slip-induced due to plastic deformation inhomogeneity near the GB, where both the basal and non-basal slip systems can be activated based on the stress/strain compatibility associated with the GB. The relationship between crystal orientation and GBS in a rolled AZ31 Mg alloy was investigated by Ando et al.[97] Electron backscattered diffraction (EBSD) analysis of the RT tensile deformed sample revealed that GBS occurred at a localized deformation region near the GB due to prismatic slip (Figure 9a and b). In addition, the internal microstructural observation of GBS showed the formation of new fine grains with high angle grain boundaries at these shear zones as shown in Figure 9c. It was proposed that GBS in AZ31 can occur at RT due to localized crystal three-dimensional rotation by dynamic recovery and dynamic recrystallization by stress concentration near the GB. Furthermore, GBS can be classified as (i) diffusion-induced GBS, which is activated when the applied resolved shear stress reaches the activation energy for GB diffusion and (ii) slip-induced GBS, which occurs

due to plastic compatibility at the GB in the presence of a plastic anisotropic strain accompanied by the absorption and dissociation of lattice dislocations at the GB. Koike et al. carried out RT tensile deformation of an AZ31 Mg alloy at different temperatures (RT to 523 K) at a strain rate of 8.3×10^{-4} s^{-1}.[100] The surface relief measurements of deformed samples taken with a scanning laser microscope and the related temperature dependence profiles revealed that diffusion-induced GBS occurred in the samples deformed above 423 K, while slip-induced GBS was observed in the samples deformed below 373 K, which resulted in severe surface undulation by operation of dislocation slip on a basal plane.

Furthermore, superplasticity due to the occurrence of GBS has frequently been observed at high temperatures, but the occurrence of GBS at ambient temperature will resolve the issues associated with the inferior mechanical properties of Mg and its alloys. The mechanism of GBS at elevated temperature has been proposed by Rachinger and Lifshitz.[101,102] According to the Rachinger model,[101] GBS occurs due to the displacement of grains without changes in grain shape, resulting in increased grain at the surface. This can lead to large plastic deformation in fine-grained material, while coarse-grained material can form cavities, resulting in premature failure. On the other hand, Lifshitz[102] proposed that GBS occurs due to diffusion of vacancies through the GB, resulting in elongation of grains in the tensile direction while the surface grains remain constant; accordingly, a large degree of plasticity can be achieved even for coarse-grained material. In this regard, Peiman et al. carried out high-temperature (230, 270, 350 °C) tensile creep tests on the AZ31 Mg alloy at stresses of 1–13 MPa to identify the mechanism of GBS during creep deformation.[103] The observed activation energy and stress exponent were 87 kJ/mol and 2, respectively, and the line patterns developed from Ga ion beam spattering confirmed the characteristics of GBS proposed by Rachinger. It is well-established that the prevalence of GBS increases with a decrease in grain size, but the static recrystallization can be initiated at elevated temperatures, leading to grain growth and, thus, suppression of GBS. Wu et al. carefully investigated the correlation between superplastic behavior with respect to energy related to grain growth and GBS for a high ratio hot extruded AZ91 Mg alloy containing various Sn additions ($0-3$ wt%).[104] The results showed that higher Sn concentration leads to an increase in the activation energy of grain growth (29.7 to 35.2 kJ/mol) and diffusion-mediated boundary sliding energy (114.1 to 126.5 kJ/mol). A compromise was made between both the energies at a certain strain rate and temperature, and superplasticity was achieved (elongation to failure > 1000%) in the AZ91-2Sn Mg alloy.

GBS is mostly witnessed at elevated temperature, however, some authors have also reported excellent mechanical properties due to the occurrence of GBS in Mg at RT.[105–110] RT-GBS in nanocrystalline Mg was reported by Hwang et al, in which strain rate sensitivity measurements showed that the stress exponent value is close to the predicted value of GBS (1.65 vs. 2), with a threshold stress value originating from the inclusions of 125 MPa.[111] Furthermore, Mg-0.3 Bi (at%) reportedly shows superior RT ductility (170%) at a strain rate of 1×10^{-3} s^{-1}, which was attributed to an enhancement of GBS during deformation by control of GB characteristics, i.e., large m-value and lower flow stress leading to equilibrium GB formation.[98] Figure 9d shows a comparison of ductility and YS for pure Mg, Mg-0.3 Bi (at%) and other famous alloys after RT tensile deformation at a strain rate of 1×10^{-3} s^{-1}. Zeng et al. reported the occurrence of GBS in pure Mg at RT.[99] Despite possessing strong texture, the sample extruded at 80 °C showed superior RT ductility, and intergranular mechanisms dominated the typical deformation mechanism (slip, twinning). The large strain rate sensitivity and small activation volume of the fine-grained microstructure (grain size ~1 μm) were the main indicators of GBS, and deformation was further accommodated by dynamic recrystallization (Figure 9e and f). Somekawa et al. performed RT Erichsen cupping tests on two samples of pure Mg with different initial grain sizes (7 and 30 μm), Mg-3Al-1Zn (wt%) and Mg-0.65 Mn (wt%), and the values of limiting dome height (LDH) at a crosshead speed of 1×10^{-5} mm/s were recorded as 4.7 and 2.9 for fine- and coarse-grained pure Mg and 2.0 and 5.2 for Mg-3Al-1Zn and Mg-0.65Mn, respectively.[112] EBSD characterization of the deformed microstructure revealed that deformation twinning was the main deformation mechanism for coarse-grained pure Mg and Mg-3Al-1Zn alloy, while the occurrence of GBS in fine-grained Mg and Mg-0.65Mn was the reason for the large LDH values of these samples. In addition, a severely deformed ultra-fine-grained Mg-8 wt% Li alloy (240 nm) has been reported to show enhanced GBS, resulting in excellent RT ductility (440%).[113] The observed superplastic behavior was attributed to the segregation of Li along the GB, which resulted in accelerated GB diffusion and the formation of Li-rich interphases.

Accordingly, it can be concluded that, for the coarse-grained microstructure which is usually present after conventional processing, dislocation slip and twinning contribute to plastic deformation. Hence, textural weakening and activation of other slip systems are pre-requisites for superior formability. However, for fine-grained Mg (in the nm range), inter-granular sliding along the GBs, which is accompanied by grain rotation and dynamic recrystallization, can be activated at RT. Accordingly, deformation slip, texture and twinning, which operate inside the grains, become less influential, and strain accumulation in fine-grained Mg will be highly unlikely to reach the level of failure.

2.2. Atomistic mechanisms in pure magnesium: Computational thermodynamics approach

2.2.1. Stacking faults energies

The origin of the inferior mechanical properties of Mg is associated with the inability of its HCP crystal structure to accommodate plastic strain in the crystallographic $< c >$ direction, which can be achieved by dislocation glide on the pyramidal II plane with the $< c + a >$ burger vector. Therefore, control of the microstructure, hardening of the basal plane, and enhancing the activity of the $< c + a >$ pyramidal slip system are essential in the design of highly ductile Mg. However, the CRSS value of the $< c + a >$ pyramidal slip system is several orders higher than that of the basal $< a >$ slip system, resulting in strong anisotropy and material fails before the pyramidal slip system can be activated.[114] In this regard, the stacking fault energy (SFE) is considered to be a crucial parameter that significantly influences the plastic deformation and mechanical properties of HCP materials. Low SFE has been reported to improve the strength and ductility of hcp materials by the formation of high density stacking faults (SFs). SFs can be described as the changes in the local crystal symmetry that occur when external layers are added or removed. The associated energy is called SFE. The SFs in Mg can be classified as intrinsic SFs (growth fault, deformation fault) and extrinsic SFs (external fault, twin fault). A growth fault (I_1) is formed by the removal of the basal plane, followed by the slip of the crystal above this fault of $1/3 < 10\bar{1}0 >$, whereas a deformation fault (I_2) is formed by the slip of $1/3 < 10\bar{1}0 >$ in a perfect hcp crystal. On the other hand, an external fault (E) is formed by the addition of an extra plane in a perfect crystal, while a twin fault (T_2) exhibits mirror symmetry about the fault plane. The layered sequencing of the various SFs is represented below:

$$
\begin{aligned}
I_1 &\quad ABABABAB \rightarrow ABABBABA \\
I_2 &\quad ABABABAB \rightarrow ABABCACA \\
E &\quad ABABABAB \rightarrow ABABCABAB \\
T_2 &\quad ABABABAB \rightarrow ABABCBABA
\end{aligned}
$$

SFs are generated by dislocation dissociation. SFE determines the width of the SFs between partial dislocations and dislocation mobility, so it can contribute to plasticity in Mg-based materials. For example, I_1SF alters the stacking in the basal plane, yet it has non-basal characteristics, where it is bounded by Frank-type partial pyramidal dislocations ($1/6 < \bar{2}203 >$). This type of dislocation is a combination of Shockley-type partial basal dislocation and partial dislocation with a burger vector normal to the basal plane (1/2[0001]). Accordingly, I_1SF forms a defected structure in the pyramidal plane, and if low energy can be obtained by the addition of some solute atoms, then I_1SF can act as a heterogeneous source of $< c + a >$ dislocations, as shown in Figure 10a. Accordingly, I_1SFE has been considered as an alloy design parameter for achieving high ductility in Mg alloys.

Over the past two decades, numerous attempts have been made to find a suitable alloying element with the greatest potential to decrease I_1SFE. Sandlobes et al. conducted an in-depth investigation of the underlying mechanisms responsible for the excellent RT mechanical properties of Mg-Y alloys.[75] TEM analysis and DFT calculations carried out on pure Mg and Mg-Y alloys revealed that the addition of yttrium (Y) significantly decreased the I_1SFE, resulting in enhanced nucleation of $< c + a >$ dislocations and activation of shear modes outside of the basal plane, as shown in Figure 10b. To extend the search for appropriate candidates, the authors carried out quantum mechanical calculations on $Mg_{15}X$ solid solutions (X = Dy, Er, Gd, Ho, Lu, Sc, Tb, Tm, Nd, Pr, Be, Ti, Zr, Zn, Tc, Re, Co, Y, Ru, Os, Tl) using DFT calculations.[115] The results revealed that addition of Sc, Y and all the lanthanide elements reduced the I_1SFE of Mg alloys. Some alloys were then fabricated, and further characterization and testing confirmed the higher activity of the non-basal slip system due to the decreased I_1SFE in terms of higher ductility (Figure 10c). Until now, Y has proven to be the best among all tested elements at decreasing the I_1SFE of Mg alloys. Recently, Zongrui et al. carried out DFT calculations on several Mg binary alloys, and concluded that the electronegativity (υ), bulk modulus (B) and atomic volume (V) of the solute atoms are the dominant factors affecting the I_1SFE of Mg alloys.[116] By comparing the impact of a solute with the impact of Y, a general numerical quantity, yttrium similarity index (YSI), was proposed to avoid the lengthy DFT-

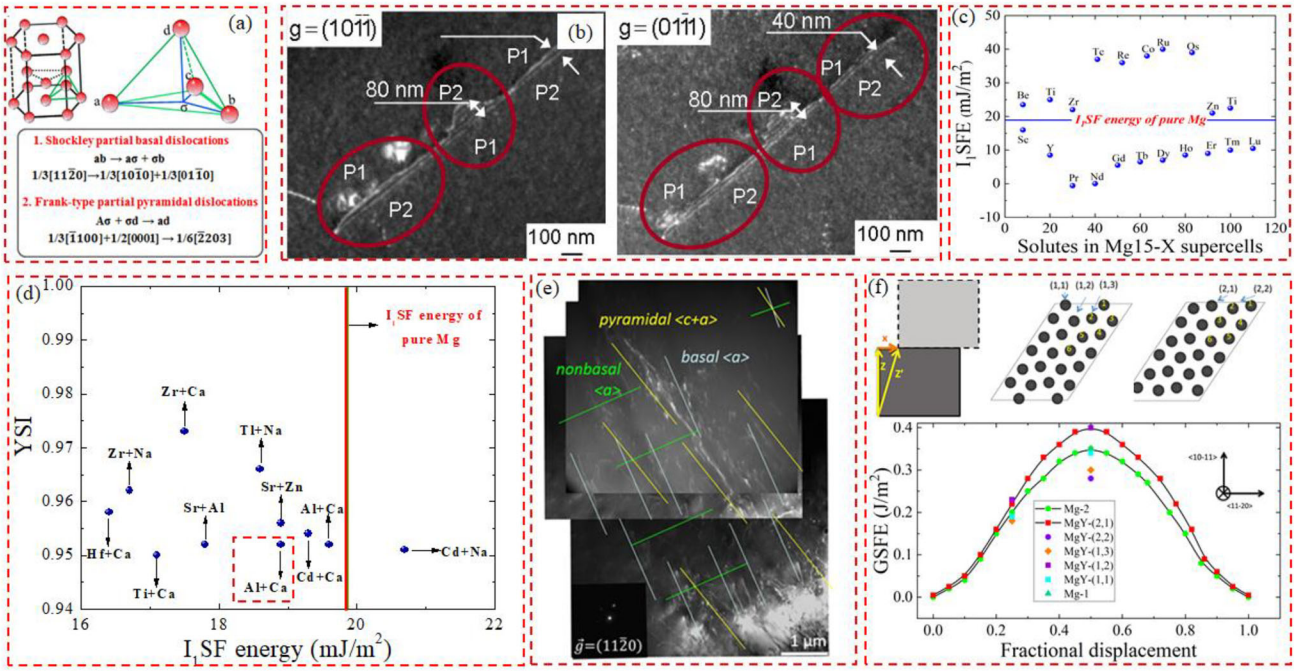

Figure 10. (a) Schematics representing the relation between I_1SFE and non-basal slip system, (b) Bright field and weak beam TEM image under different diffraction conditions showing I_1SF bounded by two partial dislocations (P1 and P2) in <1.5% cold deformed Mg-3Y (wt%),[75] (c) DFT computed I_1SFE for various $Mg_{15}X$ binary alloys in comparison to pure Mg,[115] (d) YSI calculated for different Mg ternary alloys as function to their I_1SFE,[116] (e) TEM micrograph of 2% deformed Mg-1Al-0.1Ca (wt%) alloy showing the predominant activity of pyramidal $<c+a>$ and basal $<a>$ dislocation slip,[12] (e) The schematics showing the $\{10\bar{1}1\}<11\bar{2}0>$ GSF, two $2\times2\times12$ supercells used in DFT calculations and the GSFE curve of $\{10\bar{1}1\}<11\bar{2}0>$ slip system for pure Mg and Mg-Y alloy.[117]

based calculations (Eq. [3]). An alloy system with a YSI value closer to 1 reflects a high degree of similarity with the Mg-Y alloy:

$$YSI = 1 - \sqrt{\sum w_\alpha (\alpha_c - \alpha_Y)^2} \qquad (3)$$

Here w_α is the weight fraction of the solute, α_c describes the average of the selected properties (υ, B, and V) of the solutes and α_Y is the properties of Y. From 2850 ternary solute combinations, 133 alloy combinations (excluding RE) have been identified that show YSI values greater than 0.85. DFT calculations performed on 11 solute combinations with YSI > 0.95 confirmed the reduction in I_1SFE, in alignment with the proposed correlation (Figure 10d). Based on the above YSI relationship, Sandlobes identified and fabricated an Mg-1Al-0.1Ca (wt%) alloy with excellent ductility (20%) and a tensile strength of 220 MPa.[12] Microstructural analysis confirmed that the alloy does not contain any second phase particles, and its enhanced properties were attributed to the reduced I_1SFE, which activated the $<c+a>$ pyramidal slip system, as shown by TEM observations carried on alloy samples after 2% tensile deformation as presented in Figure 10e. Besides the decrease in I_1SFE, an increase in I_2SFE enhances the probability of cross-slip of basal dislocations onto the prismatic plane while reducing the strength anisotropy through strengthening of the basal slip by specific solute addition. For instance, DFT and MD calculations were carried out to investigate the influence of solute additions on the mechanical behavior of Mg alloys in terms of basal $b = [\bar{2}110]$ dislocations and I_2 basal SFs.[118] The results revealed that the solutes that cause increased I_2SFE also cause higher activity of cross-slip of basal dislocations onto the non-basal (prismatic) plane, resulting in enhanced ductility. The solute atoms prefer to segregate at SFs, which stabilizes the SF configuration and suppresses dislocation-associated motion, resulting in higher strength.

It has been assumed that the chemical interaction between solute particles and SF is the dominant factor in altering the SFE. Liu et al. used the Vienna Ab initio Simulation Package (VASP) to perform DFT calculations on various Mg alloys in order to identify specific parameters that can explain the relationship between the electronic configuration of solute particles and the resultant properties of the alloys.[119] The results revealed that the electron work function (EWF) can be used as a guide for appropriate solute addition to improve the mechanical properties of Mg.

Addition of solutes with EWF values lower than that of Mg can result in enhanced strength/ductility synergy, while addition of solutes with high EWF values will result in improved strength but lower ductility. This finding was further explained by Wu et al., who carried out DFT calculations to evaluate the T_2 and I_2 fault energies of thirteen binary Mg alloys and suggested that the charge redistribution surrounding the solute atoms is the major factor in solute segregation and changes in SFE.[120] The charge distribution factor (F) was introduced to quantify the charge distribution induced by solute atoms and was found to have an inverse relationship with SFE. To investigate the effect of various concentrations of different solute elements on SFE, Zhang et al. calculated the I_1 basal SFE of Mg binary alloys with 1.1 and 2.5 at% solute concentration using VASP.[121] Increased solute concentration resulted in reduced SFE for the majority of solute elements, with a few notable exceptions that showed the opposite trend. Solutes with large atomic volume and low 1st ionization energy were observed to decrease the SFE, while those with high 1st ionization energy and small atomic volume displayed the opposite tendency.

It is well-established that the SFE has a strong influence on activation of the non-basal slip system, resulting in a highly ductile Mg alloy. However, it is difficult to measure the SFE accurately with current experimental methods. In contrast, the generalized stacking fault energy (GSFE) or gamma surface (γ-surface) gives a comprehensive understanding of the SFE by accurately describing the dislocation core structure and the dislocation mobility, i.e., lower values of GSFE indicate low resistance and higher dislocation mobility, and vice versa. GSFE can be calculated along the minimum energy pathway (MEP) in a faulted plane, where the local minima and maxima provide the values for stable and unstable SFE, respectively. Wen et al. computed the GSFE of pure Mg by first principle calculations and reported that the $\{11\bar{2}0\} < 10\bar{1}1 >$ slip can form a stable SF structure, but its formation is difficult due to the relatively high SFE as compared to that of the $\{0001\} < 11\bar{2}0 >$ slip system.[122] In addition, Han et al. examined the effect of addition of Li and Al on the GSFE of the basal plane of Mg and suggested that Li addition increased the SFE and facilitated dislocation mediation, while Al reduced the SFE.[123] Furthermore, to investigate the underlying deformation mechanisms in a highly ductile AT33 (Mg-3Al-3Sn) (wt%) Mg alloy, first principle calculations were carried out to compute the GSFE values for different doping concentrations of Al and Sn.[124] It was concluded that the pyramidal $\{10\bar{1}1\} < 11\bar{2}0 >$ system acted as a secondary deformation mechanism to accommodate strain along the *c-axis*, resulting in the superior mechanical properties of the AT33 Mg alloy based on its lower unstable SFE (γ_{un}) as compared to prismatic $\{10\bar{1}0\} < 11\bar{2}0 >$ slip systems (349 vs 373 mJ/m^{-2}). Moreover, Zongrui et al. studied the diverse effects of alloying Mg with Y by considering all possible solute sites and a range of solute concentrations and computed the GSFE for the $\{10\bar{1}1\} < 11\bar{2}0 >$ pyramidal slip system for all such combinations.[117] It was observed that Y reduced the GSFE for pyramidal slip, resulting in enhanced dislocation mobility in the Mg-Y alloy, as shown in Figure 10f. To quantitatively predict the basal-plane GSFE of Mg, first principle calculations were carried out on 43 Mg binary alloys.[125] The results suggested that the ionization energy and bulk modulus of solutes are directly related to the GSFE, while atomic radius, binding energy, and equilibrium volume showed the opposite trend.

Hence, it can be concluded that the SFE and GSFE are fundamental parameters associated with the plastic deformation of Mg alloys. These parameters describe plasticity-related phenomena such as dislocation nucleation, dislocation dissociation, and deformation twinning, which in turn, significantly influence the activities of various slip systems. Accordingly, the slip systems with the lowest GSFE values would be most favorable during plastic deformation. In other words, deformation by basal slip is dominant in Mg alloys since the GSFE (including I_1SFE and I_2SFE) of the basal plane are lower as compared to the GSFE values of the pyramidal and prismatic slip systems. Accordingly, modifying the GSFEs of various slip systems via suitable alloying is considered to be a benchmark for designing highly ductile Mg alloys.

2.2.2. Glissile-to-sessile transition

It has been established that the ductility of Mg is related to the behavior of $< c + a >$ pyramidal dislocations, which majorly contribute to resolution of *c-axis* strain. Hence, understanding and controlling the fundamental response of pyramidal II $< c + a >$ dislocation seems to be of primary concern, and removing any obstacles to this pursuit may catapult the field forward. Based on its primary importance, pyramidal II $< c + a >$ slip has been extensively investigated and frequently reported over the past several years. Takaaki et el. performed a *c-axis* compression test on Mg single crystal and reported that pyramidal II $< c + a >$ can be

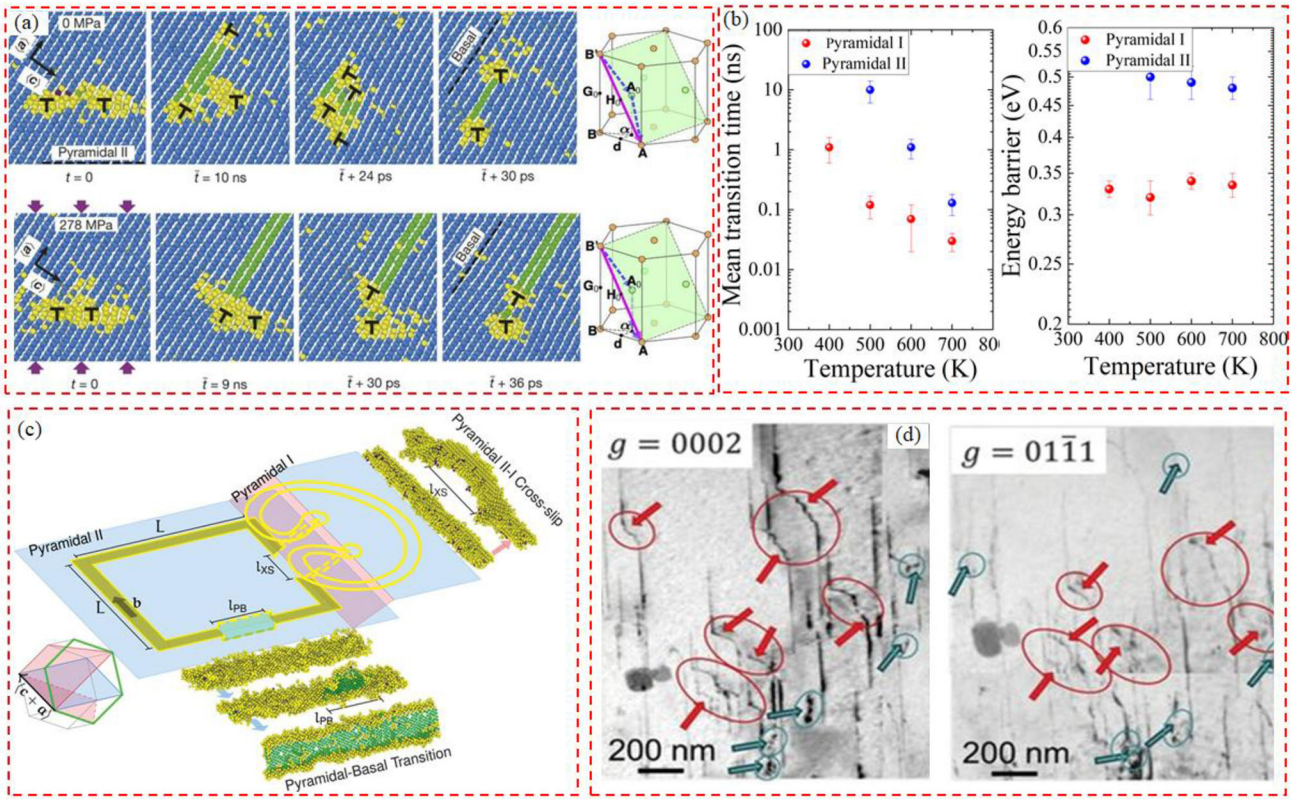

Figure 11. (a) Dislocation dissociation of pyramidal II $< c + a >$ into basal dislocations in pure Mg as observed by MD simulations for zero and moderate compressive stress,[72] (b) The mean transition time and energy barrier for pyramidal I-basal transition as a function of temperature,[128] (c and d) The schematics of $< c + a >$ cross-slip in hcp metals, and the TEM showing the dislocation switching between pyramidal II and I plane in 2.5–3% deformed Mg-3Y (wt%), respectively.[129]

activated at low temperatures ($77 - 133$ K) and low stress (20 MPa).[126] However, post-deformation microstructural TEM analysis of Mg compressed along the *c-axis* revealed that $< c + a >$ dislocation loops are dissociated on the basal planes, dominate the deformed microstructure, and are responsible for the high work hardening of Mg.[127]

In addition to this mysterious behavior, pyramidal II $< c + a >$ has also been reported to show anomalous temperature dependency, with yield shear stress increasing with increasing temperature within a certain range. This unusual behavior has been attributed to the dissociation of $< c + a >$ dislocation into glissile $< a >$ and sessile $< c >$ dislocations.[114] The results of the studies that reported on the behavior of pyramidal II $< c + a >$ over the past few decades were confusing and contradictory until Zhaoxuan et al. carried out MD simulations using DFT-validated interatomic potential to reveal the previously unexplained behavior of pyramidal II $< c + a >$.[72] MD simulations showed that pyramidal II $< c + a >$ is intrinsically unstable and readily undergoes thermally activated (transition rate of 10^5 s^{-1} at 300 K and 10^{-4} s^{-1} at 150 K) and stress-dependent transformation to basal-dissociated sessile structures with lower energies, which act as an obstacle to all slip systems and suppress plastic straining (Figure 11a). This intrinsic pyramidal-to-basal transition (PB transition) or glissile-to-sessile transformation, which occurs frequently at RT, was postulated to be the origin of high strain hardening and low ductility in Mg. Moreover, it was suggested that the thermally activated dissociation of $< c + a >$ dislocation is mainly controlled by dissociation of the $< c >$ component of the dislocation on the basal plane.[130]

One approach that could resolve this hurdle involves stabilization of the $< c + a >$ dislocations on the pyramidal I plane, as its critical *c-axis* compressive stress is seven times lower than that of the pyramidal II plane.[131] In this regard, MD simulations were carried out to investigate the stability of $< c + a >$ on the pyramidal I plane in Mg.[128] The results showed that the transition on pyramidal I had a lower energy barrier than that on pyramidal II (0.3 ev vs. 0.5 ev), and transition occurred much faster on the pyramidal I than pyramidal II plane (Figure 11b). Hence, to design a Mg alloy with excellent ductility, alloy design strategies should aim to energetically stabilize pyramidal

II $< c + a >$ dislocations and shift the PB transition to higher temperatures and longer times via appropriate alloying additions, which can suppress the easy glide of $< c + a >$ by reducing its energy. Recently, very interesting results were reported by Liu et al., who employed in situ TEM during *c-axis* compression of sub-micrometer-sized Mg single crystal to analyze the behavior of $< c + a >$ dislocations.[132] The misalignment angle was adjusted to $< 5^{\circ}$ to suppress the generation of $< a >$, $< c >$ and deformation twinning. In situ TEM, atomistic simulations and 3D image reconstruction revealed that simultaneously suppressing deformation twinning and promoting $< c + a >$ dislocation glide on both the pyramidal I and II planes contributed to the high strength and excellent ductility of Mg single crystal.

2.2.3. Cross slips

Over the past several decades, many attempts have been made to enhance the ductility of Mg-RE alloys, but concrete, reliable evidence of such alloys did not materialize and the role of RE elements remained vague. For example, in 1959, Couling et al. reported improvements in the formability of Mg alloyed with mischmetal.[133] To shed light on the underlying mechanisms responsible for the improved mechanical properties of Mg-RE alloys, Sandlobes et al. carried out an in-depth study of pure Mg and a Mg-3wt%Y alloy.[67] TEM and EBSD analysis revealed a high degree of twinning (compression and secondary) and high activity of the pyramidal $< c + a >$ slip system in the Mg-Y alloy, which were regarded as the mechanisms responsible for the improved ductility of Mg-3wt%Y as compared to pure Mg (25% vs 4%, respectively). Furthermore, increased $< c + a >$ activity was assumed to be associated with the reduction of I_1SFE upon alloying with Y, as discussed in Section 2.2.1. To solve this riddle, first principle calculations were carried out on Mg with dilute additions of Y, Al, and Zn.[134] It was found that a reduction in I_1SFE with the addition of Y can be achieved by alloying with Al and Zn in similar or slightly different concentrations. These results conflicted with the long-standing understanding of such alloys. In addition, it was speculated that alloying with Y might be responsible for stabilizing the $< c + a >$ dislocations and suppressing the detrimental PB transition in Mg. Rasool et al. was motivated to carry out MD simulations on a Mg-3wt%Y alloy to investigate the veracity of this presumption. The results showed that Y hardly influenced the transition energy barrier and time of the PB transition, and the enhanced $< c + a >$ activity in Mg-3wt%Y was not correlated with $< c + a >$ stabilization.

Hence, the mechanism behind the high ductility of Mg-RE alloys remained unclear until the solute-enhanced pyramidal cross-slip mechanism was proposed by Wu et al.[129] For pyramidal cross-slip in Mg, it is necessary that screw dislocations move from the low-energy pyramidal II planes to the higher-energy pyramidal I planes. Accordingly, additional energy is required to make up the difference in energy per unit length (ΔE_{Mg}^{I-II}) between the pyramidal II and pyramidal I screw dislocations. Hence, cross-slip of pyramidal II $< c + a >$ screw dislocations can be accelerated by a solute-driven decrease in the cross-slip energy barrier. Atomistic-scale simulations and experimental analysis revealed that Y tends to reduce the cross-slip activation energy (ΔG_{XS}) in comparison to the deleterious activation energy barrier for PB transition (ΔE_{PB}), resulting in a high rate of $< c + a >$ screw dislocation cross-slip and multiplication of $< c + a >$ dislocations, which eventually resulted in reduced CRSS of $< c + a >$ dislocation and enhanced ductility of Mg-Y alloys (Figure 11c and d). Accordingly, the proposed theory provides mechanistic insight that is vital for the development of new Mg alloys with improved ductility.

2.3. Intrinsic ductility vs extrinsic ductility

Based on the discussion and various examples given in this chapter and previous one, one can expect that suitable microstructural optimization (grain size and structure, second phase fraction and distribution, and texture) in Mg based materials can mostly lead to enhanced ductility in these materials. On the other hand, considering the changes that occur during a further processing of the optimized materials, the ductility can decline again. For example, a hot rolling of weak-basal-textured Mg alloys can result in the evolution of stronger basal textures, leading to a poor ductility. In addition, the grain growth occurring during the hot processing of Mg alloys can also alter the ductility in the processed materials. Accordingly, the method of microstructure control and the optimization of its feature just aim at enhancing the ductility through delaying the fracture (extrinsic ductility) not improving plasticity (intrinsic ductility). For enhancing the intrinsic ductility, the type of deformation modes and their critical shear stresses should be modified, and this might be achieved through alloying strategies. For example, the reducing of the 1st intrinsic stacking fault energy of pure Mg by alloying with other elements, such as Y and Ca, leads to the activation of pyramidal dislocations,[19,135] and hence, to improve the ductility. In addition, some solutes, like

Y, were found to be very significant in reducing the CRSS of the non-basal slip systems as compared to that of the basal slip system, leading to improved intrinsic ductility of the Mg alloy.[67] Up to this end, it is worth mentioning that, both the deep-rooted modification of the deformation modes in Mg based materials, and the microstructural optimization of these materials as well, are needed for ensuring the required plasticity. Next chapters will, accordingly, discuss in much more details with the various microstructural and atomistic concepts related to the extrinsic and intrinsic ductility.

2.4. Outlook

It can be summarized from the above discussion that the insufficient slip systems being activated at RT during Mg deformation are mainly responsible for the low ductility. Accordingly, non-basal slip softening, and basal slip hardening are considered to be the milestone for achieving superior ductility in Mg alloys. Moreover, twinning acts as secondary deformation mechanism to accommodate the strain but the role played by twinning is complicated. Twinning provides an additional slip system and formed the recovered regions which can increase the ductility. However, on the other hand twining acts as an obstacle to mobile dislocations and also can be the source for stress concentration, leading to inferior ductility. Hence, the consequent effect on overall mechanical properties of Mg alloys depends upon the dominated twinning behavior. In addition, GBS can be activated to contribute to overall plastic deformation when the strain rate sensitivity is higher, which can pave a new way to control RT superplasticity by GB composition and diffusion. The GBs can be engineered by the suitable alloying addition followed by severe plastic deformation (SPD) processing. Other possibilities can be the selection of appropriate alloying additions which can reduce the SFE and influences the dislocation core energy, dislocation dissociation process, and decrease the energy barrier of cross-slip are considered to be the key toward designing highly ductile-high formable Mg alloy.

3. Magnesium ductilization

3.1. Controlling the structure

3.1.1. Grain size control

Grain refinement can significantly improve the strength of polycrystalline materials based on the Hall-Petch relationship.[136]

Table 1. Variation in stress concentration factor (k) with respect to grain size for some commonly processed Mg alloys.

Sample	Processing	d (μm)	k (MPa $\mu m^{1/2}$)
AZ31[137]	Rolling	26–78	411
AZ31[137]	Rolling	26–78	228
AZ31[138]	Rolling	5–25	319
AZ31[139]	Rolling	5–17	234
AZ31[139]	Rolling	5–21	250
AZ31[140]	Rolling	2–55	209
AZ31[141]	Rolling	13–140	281
AZ31[141]	Rolling	13–140	272
AZ31[142]	Extrusion	2.5–8	304
AZ31[142]	FSP	2.6–6.1	161
AZ31[143]	Extrusion	3–23	291
AZ31[144]	Extrusion	3–11	390
AZ31[144]	Extrusion	3–11	303
AZ31[145]	FSP	1–25	119
AZ31[145]	FSP	1–25	236
AZ31[146]	Rolling	13–43	207
AZ31[146]	Rolling	13–43	472
AZ31[147]	ECAP	3–33	205
AZ31[148]	ECAP	2–8	108
AZ31[149]	ECAP	2–8	203
Pure Mg[150]	Extrusion	11–140	294
Mg-1Zn[150]	Extrusion	10–218	273
Mg-1Y[150]	Extrusion	11–190	252
Pure Mg[151]	Extrusion	4–63	157
Pure Mg[151]	Extrusion	5–28	63
Pure Mg[151]	Extrusion	10–450	188
AZ61[152]	ECAP	8–150	344
AZ91[153]	Extrusion	1–30	210

$$\sigma_y = \sigma_o + kd^{-1/2} \tag{4}$$

Here σ_y is the YS, σ_o is the friction stress when dislocations glide on the slip plane, k is the stress concentration factor, and d is the average grain size. During deformation, dislocations start to pile up in the vicinity of GBs, when the piled-up dislocations exert sufficient pressure at the GBs so that the slips can propagate from one grain to another, yielding occurs. Accordingly, the grain size substantially influences k because it controls the concentration of stress from the piling up of dislocations, and hence the overall ability of a material to deform plastically. The variation in k as a function of grain size for some commonly processed Mg alloys is illustrated in Table 1.[137–153] The strengthening effect induced by grain size is high as compared to that seen in other fcc and bcc crystal structures because Mg has a large Taylor factor.[154]

Accordingly, many studies have been devoted to enhance the strength of Mg alloys by decreasing the overall grain size in various ways, i.e., by alloying, exploiting various thermomechanical techniques, or a combination of both (Figure 12a).[155] It is evident from Figure 12a that the strength of Mg alloys increases with a decrease in grain size, which is in agreement with the Hall-Petch relationship. For example, Wang et al. extensively investigated the microstructural evolution caused by addition of Sc

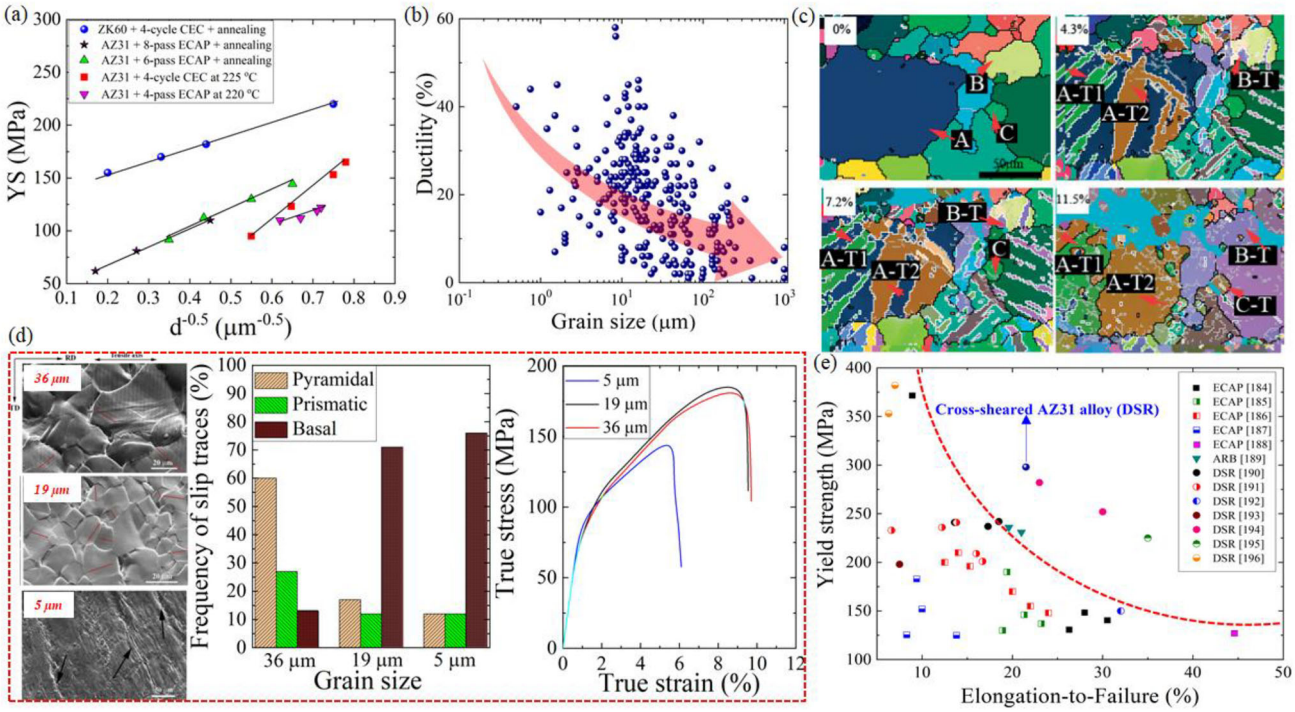

Figure 12. (a) Relationship of YS and grain size for various Mg alloys,[155] (b) The relationship of ductility and grain size for Mg alloys,[156] (c) EBSD maps of AZ31 magnesium alloy subjected to various strain levels during compression,[157] (d) SEM micrograph and frequency of slip traces with respect to various slip systems during tension test at 50 °C of pure Mg with different grain sizes and true stress-true strain curve tested at 50 °C,[158] (e) Yield strength against elongation to failure of cross-sheared AZ31 vs other severely deformed with different techniques.[159–171]

and Zr to AZ31 processed by rolling and equal channel angular extrusion (ECAE).[172] AZ31-0.15Zr-0.06Sc (wt%) processed by ECAE showed excellent mechanical properties, which were attributed to the grain refinement facilitated by alloying addition and further processing. Moreover, dispersed intermetallic particles also play a vital role by suppressing dynamic recrystallization during plastic deformation and facilitating recrystallization nucleation, exerting a strong pinning effect on grain growth. An equal channel angular pressing (ECAP)-processed AZ31-0.3RE-0.3Ca (wt%) alloy demonstrated high YS and UTS values (134.6 and 228.6 MPa, respectively), which were attributed to a refinement of grain size due to the retardation of DRX and dispersive strengthening effects of Ca- and RE-containing particles during hot deformation.[173] Identical findings have been reported for Mg-Zn-Y-Zr alloys.[174–176] Severe plastic deformation (SPD) has emerged as the most efficient method for producing an ultrafine-grained microstructure with enhanced mechanical properties.[177–180] Various SPD techniques, including equal channel angular pressing (ECAP),[181–184] high-pressure torsion (HPT),[185–187] accumulative roll bonding (ARB),[188–190] accumulative back extrusion (ABE),[191,192] etc., have been reported to significantly modify the microstructure. Interestingly, Lio et al. proposed a novel method of enhancing the hardness of Mg alloys.[193] High-speed extrusion machining (HSEM) was utilized to alter the microstructure and overall mechanical properties of an AZ31B Mg alloy. EBSD microstructural characterization of a specimen after large thickness ratio HSEM confirmed the presence of a bimodal grain structure, in which coarse grains were embedded in a fine matrix. The Vickers hardness value of an alloy with a bimodal microstructure increased by 31%, which was attributed to the incorporation of dislocations during the DRX process. In summary, high strength in Mg and its alloys can be achieved by reducing the grain size.

On the other hand, the effect of grain size on the ductility of Mg alloys seems complicated and no concrete conclusion can be drawn. In general, grain size has been reported to have an inverse relationship with ductility, where grain refinement can lead to superior ductility and vice versa. Figure 12b shows RT ductility as a function of grain size for various Mg alloys.[156] The data has been collected from the literature (~100 works) in order to demonstrate the general trend between the grain size and ductility of various Mg alloys irrespective of composition, processing technique and textural characteristics. As evident by Figure 12b, ductility increases with decreasing grain size. However, it is pertinent to

mention that there are several factors that can individually influence the ductility of Mg alloys, and grain size has been reported to have a unique effect on those factors. The factors can be summarized as follows:

1. The higher fraction of GBs that results from grain refinement acts as an obstacle and imparts greater resistance to dislocation motion, leading to inferior ductility.
2. Moreover, twins can act as a secondary deformation mechanism along with basal slip, but the activation of twins mostly leads to low ductility of a Mg alloy. This can be explained differentially based on the type of the twin. TTWs activated in the earlier stages of deformation are unable to accommodate all strains in a grain, leading to low plasticity. In addition, the evolution of DTWs (double twins) from CTWs results in brittle behavior, which is related to the formation of cracks at the tips of the DTWs.[156] Since the formation of these twins is mainly influenced by grain size, and twinning becomes extremely difficult with very small grain size,[44] one may conclude that fine-grained Mg alloys exhibit higher ductility due to less twining-ability as compared to their coarse-grained counterparts. For instance, Huajie et al. carried out EBSD analysis to investigate the deformation twinning behavior of an AZ31 magnesium alloy during quasi-in-situ compression tests at various strain levels.[157] Figure 12c shows the EBSD maps of AZ31 subjected to different strain levels (0% to 11.5%). Before the compression test, no twins were found in the grains labeled A, B and C (coarse, medium, and fine grains, respectively). At 4.3% strain, two twin lamellas (A-T1 and A-T2) appeared in grain A, while one twin was seen in grain B and no twins formed in grain C. At higher strain (7.35%), the A-T1, A-T2 and B-T twins became thicker, while no twin appeared in grain C. Finally, a small twin formed in grain C at the strain level of 11.5%. Accordingly, it was concluded that grain size played a crucial role in the differential behavior of deformation twinning.
3. It has been reported that grain refinement can enhance the activity of a non-basal slip system due to GB compatibility stress and can also reduce the intensity of concentrated stress in the grain interiors, resulting in dynamic recovery (DRV).[93,144,194,195] If two adjacent grains are to be bonded together during deformation, an additional shear stress (compatibility stress) is required to activate the non-basal system. In other words, to avoid fracture along GBs, operation of the non-basal glide system is necessary to achieve superior ductility in fine-grained Mg alloys. Koike et al. studied the deformation mechanism of an ECAE (equal channel angular extrusion)-processed fine-grained AZ31B alloy (6.5 μm) annealed at elevated temperature.[93] The RT tensile tests showed a large elongation to failure of 47% at the strain rate of 1×10^{-3} s^{-1}. TEM analysis was carried out on a 2% elongated sample to quantitatively describe the relationship of dislocation density to each slip system. The results revealed that the cross-slip of ***a*** dislocation to the non-basal plane was active because of the GB compatibility stress and DRV during deformation, which lead to superior ductility. Moreover, Shi et al. investigated the effect of grain size on the tensile ductility of Mg-1.02 Zn (wt%).[194] Their observations revealed that the grain size range of 18 – 226 μm is the transition region between slip- and twinning-dominated deformation, where the fine-grained sample demonstrated high ductility during tensile deformation. The superior ductility of the fine-grained sample was attributed to the suppression of twinning and enhancement of DRV with the high activity of the prismatic slip system through GB compatibility stress.
4. Another important aspect of grain refinement in Mg polycrystals is its influence on the cumulative activities of various slip systems, where a transition from non-basal to basal slip has been reported with decreasing grain size. This transition can be understood based on the ability of GB strengthening to differ for various slip systems; often, higher values of $CRSS_{non\text{-}basal}/CRSS_{basal}$ are observed for small grain size. To thoroughly understand the origin of the mechanism governing the transition and its consequences on work hardening capability and tensile ductility, pure Mg with various grain sizes (5, 19, and 36 μm) were tensile tested at 50 °C inside an SEM chamber.[158] EBSD-incorporated slip trace analysis confirmed the transition from non-basal to basal flow with decreasing grain size (Figure 12d). The transition was attributed to the occurrence of dissimilar non-Schmid effects for different grain sizes, where non-basal slip systems were observed to be more potently strengthened as compared to basal slip systems and the highest $CRSS_{non\text{-}basal}/CRSS_{basal}$ value was observed for the Mg sample with the smallest grain size.

5. GBS is another important deformation mechanism that occurs at elevated temperature and can result in large elongation to failure, as discussed in Section 2.1.3. GBS has a tendency to increase with decreasing grain size. Accordingly, several studies have reported the occurrence of GBS in Mg alloys at RT, which was mainly attributed to the role played by fine grains.[99,112]
6. The effect of grain size on the strain hardenability of Mg alloys and, thus, on their uniform ductility (before necking), is another factor to be considered. This is related to the activity of various slip systems (basal or multiple slip) and the dominant deformation mechanism (slip, twinning or GBS) as a function of grain size. For example, according to Cepeda-Jimenez et al., the higher non-basal slip activity seen with the coarser grains (low $CRSS_{non\text{-}basal}/CRSS_{basal}$ ratio) favors multiple slip, leading to higher strain hardening and improved ductility.[158] This effect can be further enhanced in coarse-grained samples with orientations for which multiple slip is favored (weak basal texture).

Here, the mechanisms discussed in (2), (3), and (5) improve ductility, while the mechanisms in (1), (4), and (6) reduce ductility as a result of grain refinement. All in all, grain size has dissimilar effects on the various mechanisms and the final ductility is dependent on the phenomenon which is activated by grain refinement. Hence, it is very important to devise a comprehensive strategy for grain refinement that impedes the deleterious effects on ductility and optimizes strength as well as ductility. In this regard, Hamad et al. proposed a unique technique to achieve strength and ductility synergy.[196] A cross-shear deformation method, in which the sheet was rotated by 180° around its longitudinal axis between each pass of differential speed rolling (DSR) was performed to alter the microstructure of an AZ31 alloy. The alloy processed by this innovative technique showed simultaneous improvements in UTS and ductility, which were 333 MPa and 21%, respectively. A comparison of the mechanical properties of cross-sheared AZ31 with the properties of several other samples processed by different techniques is shown in Figure 12e.[159–171] The remarkable enhancement in properties was attributed to the evolution of a fine-grained (1.2 µm) microstructure after deformation. Kim et al. fabricated an AZ91 alloy with high strength and ductility by carrying out high-ratio DSR (HRDSR) in combination with low-temperature aging.[197] The ultra-fine grained (0.3 µm) microstructure that resulted from this novel processing technique had a YS of 400 MPa and ductility of 12–14%. As compared to AZ91, grain refinement in AZ31 is very difficult owing to the lower fraction of β-Mg_{17}-Al_{12} in the matrix. However, Kim et al. suggested that ultra-high strength in AZ31 can be achieved by optimizing the processing parameters of HRDSR.[171] A sample rolled at 423 K followed by water quenching exhibited an ultrafine grain size of 0.6 µm and an exceptionally high YS of 382 MPa. Similar findings have been reported by other studies.[159,198] Interestingly, the SPD techniques have proved to be effective for refining the overall grain size of the material, but the strength is often reported to decrease instead of increasing. Careful observations have revealed that the texture softening mechanism overcomes the grain size strengthening in some specific parametric conditions.[152,161,164,170,199,200] The dependence of strength with respect to texture can be expressed by the following relationship.[201]

$$\sigma_o = M\tau_o \tag{5}$$

Here, σ_o id the friction stress, M is the Taylor orientation factor, and τ_o is the CRSS of the operative slip system. Based on the above relationship, it can be concluded that the friction stress is directly related to the CRSS of slip systems, where easy slip orientation (lower CRSS) results in lower values of σ_o and, conversely, hard orientation (high CRSS) results in enhanced strength. Some previous studies have suggested that, by the removal of deformation and frictional heat, and suppression of texture softening can substantially enhance the strength of Mg alloys at RT. Accordingly, to obtain synergy between strength and ductility, special emphasis should be placed on the overall processing conditions for SPD.

3.1.2. Texture modification

Primary processing (rolling, extrusion, etc.) of Mg typically leads to the alignment of the basal planes with the crystallographic *c-axis* parallel to the through-thickness direction of material flow and perpendicular to the loading direction.[67,202] The preferential activation of basal slip due to lower CRSS tend to rotate the *c-axis* of the crystal parallel to the loading direction, resulting in most of the grains being oriented to their basal (0001) planes close to the plane of the sheets, and, consequently, in strong basal texture.[203,204] In strong-textured Mg, most grains are found in hard orientations with lower Schmid factor (m) along with the basal slip, and the resolved shear stress (RSS) in the basal plane is essentially zero. Consequently, deformation of strong-textured Mg

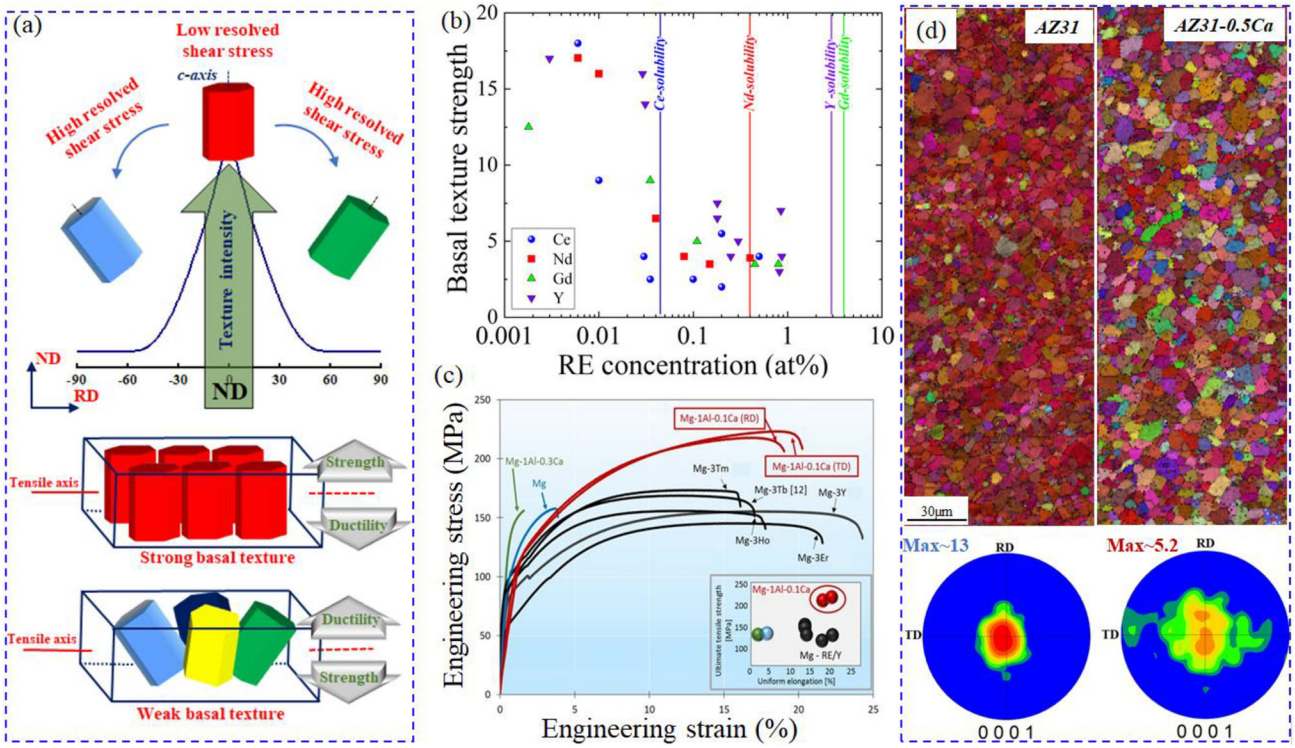

Figure 13. (a) Schematics showing the relationship of basal texture characteristics to the resolved shear stress in the basal plane, (b) Weakening of basal texture with respect to concentrations of RE elements in Mg alloy,[205] (c) Engineering stress-strain curve for Mg-Al-Ca alloy in comparison to several Mg-RE alloys,[12] (d) The inverse pole figure and pole figure of AZ31 and AZ31-0.5Ca (wt%), showing the significant texture weakening by the addition of Ca.[15]

along the rolling direction results in limited ductility and premature failure because of the limited capacity for strain accommodation due to the low RSS of the basal plane, as presented in Figure 13a.[206,207] In addition to inferior mechanical properties, the formation of a strong basal texture in Mg also results in enhanced anisotropy of plastic deformation because of significant differences in the activity of unidirectional deformation twinning. Accordingly, ductile deformation of polycrystalline Mg can be achieved by mitigating the formation of typical basal textures and encouraging non-basal texture components. Weak-textured Mg, with most grains on the *c-axis* tilted away from the normal direction of the sample, may exhibit high RT mechanical properties due to the high Schmid factor. This alternative approach to basal texture weakening improves ductility but does not tend to enhance the intrinsic ductility of Mg, instead delaying fracture. Over the past few years, various techniques have been utilized for ductilizing Mg by texture engineering. For instance, several thermomechanical techniques, such as ECAE,[163,208,209] asymmetric rolling (ASR),[210–213] and severe plastic deformation (SPD)[161,197] for grain refinement as well as alloy development,[214–216] have been exploited to weaken the basal texture. These thermomechanical processes followed by various heat treatment regimes have been reported to recrystallize textures by replacing the strong basal texture and relieving residual stresses. Very encouraging results have been reported using ECAE, in which material is subjected to pure shear stress at the intersection of two channels. Mukai et al.[163] achieved high ductility in an AZ31 Mg alloy with ECAE, with the sample exhibiting basal plane orientation inclined 45° to the extrusion direction (ED). Owing to the development of a unique weakened texture, the material showed high RT ductility (45%).

The degree to which ductility can be improved in Mg-based materials is mainly related to the amount of shear stress resolved in the basal plane due to texture modification. This, in turn, is associated with the texture characteristics that evolve in the alloy due to the effect of composition and thermomechanical processing. Mg-RE alloys, for example, show various kinds of texture, which can effectively enhance their ductility; these textures are inconsistent with those that evolve in conventional Mg alloys, such as AZ and ZK series materials (Figure 13b).[205] One example that illustrates the effect of composition on textural evolution of Mg alloys was presented by Al-Samman and Li studied the textural evolution of various ZEK100

alloys subjected to warm rolling followed by heat treatment.[73] Unexpected textures, with the basal poles broadly distributed toward the transverse direction, evolved in the Mg alloys due to the addition of RE elements, and this textural modification largely enhanced the ductility of the Mg alloys and reduced their mechanical anisotropy. Stanford et al. reported higher ductility in an extruded Mg-Gd alloy (2X that of pure Mg), even with a coarser grain size.[217] A RE textural component that formed due to oriented nucleation at shear bands and a significant reduction of 51.7% in basal texture intensity was seen in a Mg-Gd alloy, which lead to higher ductility. Similarly, several studies have shown that alloying with Y modifies basal texture and results in improved ductility.[69,75,218,219] Wu et al. reported a higher tensile ductility of 30% in a Mg-4Y alloy, which was attributed to the randomized texture which promoted more dislocation slips in the Mg-4Y alloy as compared to pure Mg.[220] Moreover, cerium (Ce) has the lowest solubility in Mg among all RE elements and has frequently been reported to produce basal texture weakening.[221–223] Misra et al. reported weakening of the basal texture in a Mg-0.2Ce (wt%) alloy, along with a combination of improved strength and ductility.[224] It was suggested that the addition of Ce to Mg decreases the volume fraction of basal-oriented grains, resulting in basal texture weakening. As a result, more non-basal slips can be activated during plastic deformation, leading to improved ductility.[225] The alloying of Mg with RE and non-RE solutes may have synergetic effects on mechanical properties by modifying textural components and reducing texture intensity. For instance, Mg-RE-Zn generates a texture with an additional basal pole split in TD and decreases the plastic anisotropy, which is highly desirable for sheet metal forming processes.[63]

Various mechanisms have been reported to be responsible for texture modification in Mg alloys, including GB mobility, particle-stimulated nucleation (PSN), and shear banding. Several studies have reported that RE solute atoms demonstrate a strong tendency to segregate at GBs because of a large atomic size misfit with Mg; the increased solute concentrations at the GB hinder the GB mobility because of the solute drag effect during recrystallization.[226–228] For example, a significant weakening in basal texture was noticed in an extruded Mg-5Y (wt%) alloy during annealing, which was attributed to the preferential growth of non-basal oriented grains due to the segregation of Y at the GBs.[229] The segregation of Y solute atoms at the GBs influenced GB mobility, and the higher fraction of off-basal-oriented grains displayed a boundary migration benefit that was not present with mostly basal-oriented grains. It has been observed that the basal texture is slightly weakened or even increased as a result of recrystallization during annealing. Usually, dynamic recrystallization (DRX) is associated with the formation of a strong basal texture.[146,230,231] The extent to which DRX can modify the texture is entirely dependent upon the processing conditions, i.e., temperature, applied strain, and strain rate, which affect the activation of various slip modes and mechanisms of DRX nucleation. In addition to the processing parameters, the type of alloy considerably influences recrystallization behavior based on solubility and the formation of precipitates, where the former leads to solute drag while the later results in a pinning effect. Accordingly, a fundamental understanding of how specific alloy elements influence nucleation and recrystallization is required. In addition, texture evolution has been suggested to be related to PSN,[232,233] shear band-induced nucleation (SBIN),[234,235] and deformation twin-induced nucleation (DTIN).[236,237] In PSN, second phase particles provide heterogeneous sites for the nucleation of recrystallized grains with randomized texture, resulting in texture weakening after recrystallization. Shear bands serve the same purpose in SBIN, in that recrystallized grains with off-basal texture grow inside the shear bands. Similarly, twins have been reported to provide the nucleation sites for recrystallized grains with randomized orientation. However, several studies have shown significant basal texture weakening even in the absence of PSN, SBIN, and DTIN phenomena, and vice versa.[80,238–240]

Despite the numerous advantages offered by RE elements, their low abundance and high cost of production have motivated engineers to find alternative elements that may serve the same purpose in Mg alloys. Of various candidates, Ca is the most promising alloying element for improving the mechanical properties. Addition of just 1% Al and 0.1% Ca to Mg generated a material with ductility like that of Mg-RE alloys with much higher strength, as shown in Figure 13c.[12] Sandlobes et al. noted that this RE-free ductile Mg alloy has two nontoxic and inexpensive alloying elements, i.e., Al and Ca, which altered the deformation mechanisms significantly with the tiny doping content of 1% Al and 0.1% Ca. These alloying additions activate non-basal deformation slip activity, such as pyramidal slip activity, in addition to basal $<a>$ slip. Recently, AZ31-0.5Ca has been reported to show improved mechanical properties,

which was attributed to weakening of the strong basal texture and enhanced activity of non-basal slip systems, as confirmed by VPSC simulations and IGMA analysis (Figure 13d).[15]

Deformation behavior and related alterations of the texture of Mg alloys are further complicated by static and/or DRX and the interactions between recrystallization and slips or twinning. Umer et al. studied the DRX behavior of warm rolled AZ31 and concluded that higher deformation leads to an increased proportion of randomly oriented DRXed grains, resulting in texture weakening.[241] Accordingly, it can be concluded that the abovementioned mechanisms do influence the texture of the material; however, weakening is not limited to the operation of these mechanisms. Hence, in-depth investigations are required to shed light on these issues and to categorize the relationship between texture engineering and related mechanisms.

3.1.3. Pre-twinning

Mg can be made intrinsically ductile by controlling the atomistic flow mechanisms, i.e., reducing the SFE or delaying the PB transition time. In addition, various strategies have been reported over the years to extrinsically enhance the ductility of Mg by utilizing thermomechanical processes. Recently, several studies have reported an enhancement in the properties of Mg alloys via introduction of twin lamellas in the microstructure by pre-deformation. As already established, twins can readily be activated due to their low CRSS value as compared to that of the non-basal slip system. Accordingly, twins can act as a secondary mechanism to accommodate strain, in addition to basal slip. Thus, pre-twinning has been suggested as a simple and effective strategy to enhance strength and stretch formability and reduce plastic anisotropy in Mg alloys. High strength in Mg alloys can be achieved by inducing fine and dense twin lamellas in the microstructure by tweaking the deformation conditions (strain rate, deformation direction, deformation temperature, amount of strain) to promote twin nucleation and suppress twinning growth during the pre-twinning period. Interestingly, pre-twinning can also result in texture hardening because $\{10\bar{1}2\}$ TTWs bring the grains into hard orientations. Strengthening via texture modifications by pre-twinning is dependent on the volume fractions of grains with hard orientations and the conditions under which the growth of pre-induced twins is more favorable as compared to twin nucleation.[242]

Moreover, twinning can alter alloy microstructure by providing preferential nucleation sites for recrystallization, resulting in grain refinement that leads to higher strength based on the Hall-Petch effect. The newly formed recrystallized grains with random orientations result in texture softening.[80,92] The mechanical properties (tensile and compressive) of an AZ31 Mg alloy were reported to be significantly enhanced by pre-rolling (thickness reduction $< 5\%$) to introduce $\{10\bar{1}2\}$ TTWs.[243] The reduction in the tension-compression asymmetry (compressive YS/tensile YS $=$ $\sim$0.65) and grain refinement by TTWs resulted in a 26% increase in tensile YS of the pre-rolled alloy as compared to the as-received alloy. Park et al. performed cold pre-forging (CPF) on an AZ31 Mg alloy before extrusion and reported a significant improvement in mechanical properties.[244] The numerous $\{10\bar{1}2\}$ TTWs (area fraction $\sim$15%) generated due to CPF provided the nucleation sites for the randomly oriented DRXed grains. The simultaneous improvement in strength and ductility in CPF-AZ31 was attributed to twinning-aided dynamic recrystallization (TDRX), which resulted in grain refinement and texture weakening (12.4 and 4.2 mrd in non-CPF and CPF-AZ31, respectively).

Pre-twinning has also been reported to enhance the overall rolling capability of Mg alloys. Xin et al. reported an extraordinary increase in maximum thickness reduction per pass during rolling at 300 °C in a pre-twinned AZ31 Mg alloy.[245] The alloy was pre-rolled (PR) to 7.5% along the TD at RT to induce TTWs in the microstructure. A 50% reduction was achieved in a single pass in PR-AZ31, without crack formation, while large cracks appeared after a 30% reduction per pass in a non-PR AZ31 Mg alloy. EBSD characterization revealed that deformation was only accommodated by the basal and pyramidal $<c+a>$ slip systems in non-PR AZ31, while the prismatic $<a>$ and the pyramidal $<c+a>$ systems contributed to plastic straining in PR-AZ31 as the PR reoriented the majority of {0002}planes toward TD. Numerous studies have reported improvements in stretch formability via introduction of twin lamellas in the microstructure of Mg alloys. A significant improvement in the stretch formability of AZ31 at RT was achieved by using a pre-compression process to introduce $\{10\bar{1}2\}$ TTWs.[246] Detwinning activation and the basal slip in the twinned region accommodated the strain in the thickness direction and resulted in a 65% improvement in the stretch formability of the pre-compressed sample, as shown in Figure 14a and b. Weijun et al. induced $\{10\bar{1}2\}$ TTWs by performing in-plane compression (IPC) in a thin AZ31 Mg alloy sheet to modify the basal texture.[248]

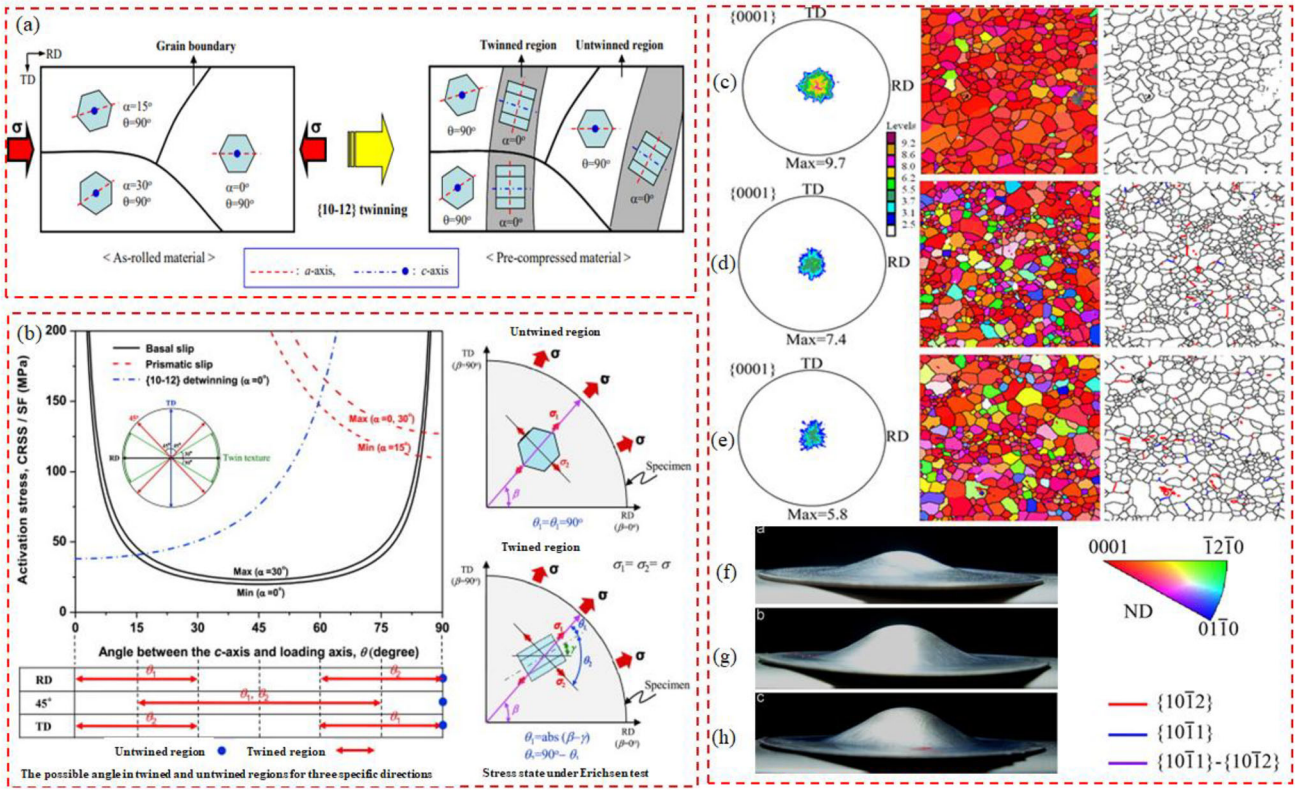

Figure 14. (a) The schematic illustration of crystallographic characteristics of as-rolled and pre-compressed material with respect to θ and α, here θ is the angle between c-axis and loading axis, α is the angle between a-axis and loading axis, when unit cell is rotated at the $\theta = 90^{o}$ position,[246] (b) stress required for activating slip systems and detwinning under twinned and untwinned region,[246] (c,f), (d,g), and (e,h) represents the EBSD maps and samples left after Erichsen test for as-received, 10% pre-rolled and annealed at 300 °C and 10% pre-rolled and annealed at 400 °C, respectively.[247]

The generated TTWs in the pre-twinned region effectively accommodated the thickness strain during the Erichsen test and resulted in a 50% increase in stretch formability in the IPC sample. It is well-established that TTWs can be generated by pre-compression or pre-rolling along TD or RD, respectively. By contract, contraction twins (CTW){10$\bar{1}$1} can be induced in the microstructure of Mg alloy sheets by performing pre-rolling along ND, and can be utilized to improve the performance of Mg alloys. Song et al. performed 10% pre-cold rolling along ND in an AZ31 Mg alloy to induce contraction twins and reported a 66% increase in stretch formability in the pre-cold rolled and annealed (400 °C) sample as compared to its non-rolled counterpart, as shown in Figure 14c–h.[247] The significant improvement in stretch formability of the pre-cold rolled and annealed AZ31 Mg alloy was attributed to nucleation and growth of randomly oriented recrystallized grains at contraction twins during annealing.

Stretch formability is mainly dependent upon elongation-to-failure, strain hardening exponent (*n*-value) and plastic anisotropy (*r*-value), where high ductility, high *n*-value, and lower *r*-value can result in enhanced stretch formability in Mg alloys. Kang et al. conducted the Erichsen test on various twin-roll cast Mg alloys at RT to identify the relationship between stretch formability and strain hardening capacity.[249] Basal texture weakening and an increase in grain size lead to high *n*-values, and a linear relationship was suggested between stretch formability and *n*-value. Typically, in rolled Mg alloy sheets with the *c*-axis parallel to ND, thickness strain can only be accommodated by < c + a > pyramidal slip, which has the highest CRSS value among all slip systems. This results in a low strain hardening capability and higher *r*-value, leading to poor stretch formability. Song et al. collected data on various Mg alloys and suggested an inverse relationship between stretch formability and *r*-value.[45] Several researchers have reported that pre-twinning can simultaneously result in higher *n*-value and reduced *r*-value, thus enhancing stretch formability. In pre-twinned Mg, the {10$\bar{1}$2} TTWs are formed with the *c*-axis parallel to TD, so the through-thickness strain can be accommodated by basal slip, prismatic < a > slip, and detwinning. Hence, basal slip and detwinning suppress dynamic recovery due to limiting non-basal slip, resulting in a reduced *r*-value

and higher strain hardening capacity. Moreover, randomization of texture and increased dislocation-twin interaction due to a higher fraction of twins can result in high strain hardening capability. When twins are formed, the twin boundaries act as an obstacle to dislocation slip and consequently become a source of work hardening.

A remarkable improvement in formability (65%) in Mg-3Al-1Zn (wt%) alloy was brought about by pre-stretching to 5% along the RD followed by annealing at 260 °C for 30 mins.[250] Microstructural and microtextural analysis revealed that the significant weakening of basal texture and grain growth in the 5% pre-stretched sample lead to higher *n*-value and lower *r*-value as compared to the as-received alloy, which eventually contributed to superior stretch formability. A very interesting result was recently reported by Weili et al..[251] Multidirectional pre-compressive deformation (TD5.38%-RD3.3%) was conducted on AZ31, followed by annealing at 450 °C for 2 h. A significant degree of texture weakening was observed in the TD5.38%-RD3.3% pre-compressed specimen, which was attributed to grain coarsening due to twin-twin interactions contributing nucleation sites for static recrystallization during annealing. Grain coarsening and basal texture weakening resulted in a 112.4% increase in the stretch formability of the TD5.38%- RD3.3% pre-compressed specimen as compared to the as-received sample. Accordingly, pre-twinning has been suggested to be a very effective and economical method of tailoring the texture and achieving high stretch formability in Mg alloys.

3.1.4. Precipitation

Precipitates (second phase particles), either those that are artificially added to a molten Mg alloy or intermetallic compounds formed by chemical reactions between alloying elements, have been reported to enhance the strength, manipulate the overall grain size by the PSN effect and modify the texture of Mg alloys, as discussed in Section 3.1.2. The constitutive roles played by precipitates largely depend on their type and size, the spacing between the precipitates, and the overall volume fraction of precipitates.[252] Therefore, desirable properties can be targeted by introducing suitable precipitates and manipulating the related characteristics. Strength can be imparted to Mg alloy by precipitation since precipitates act as an obstacle to dislocation motion during deformation, resulting in a high propensity of dislocations in the area around the precipitate particles, which effectively strengthens Mg alloys. Plate-type precipitates on the prismatic planes have been reported to effectively strengthen Mg alloys by suppressing basal slip shearing.[253,254] Accordingly, strengthening of an alloy can be explained by the shear resistance (shear ability) of precipitates to various dislocation types in Mg (<a> basal, <a> prismatic, <c + a> pyramidal), where the formation of non-shearable precipitates could result in superior strength in Mg alloys. The shear ability of the precipitates can be controlled by interface effects or by the formation of an anti-phase boundary (APB) inside the precipitates.[255] Moreover, precipitates in Mg show high anisotropy, and can thus shear more easily in some specific planes as compared to others. Ellen et al. examined the deformation behavior of the β''' and β' phases in Mg-Nd and Mg-Y alloys, respectively.[256] HAADF-STEM analysis of the deformed samples revealed that the basal plane sheared the β''' phase, while both the basal and non-basal slip planes sheared the β' phase in the Mg-Y alloy. Accordingly, the type of dislocation inside the precipitates and their relative shear resistance to various slip systems must be identified to control the coherency and morphology of the precipitates when designing high-strength Mg alloys. Kim et al. conducted hot compression and tensile tests on AZ31 and Ca-containing AZ31 (AZ31-0.7Ca, AZ31-2Ca (wt%)) and reported increased flow strength in the latter alloy.[257] TEM revealed that the high fraction of $(Mg, Al)_2Ca$ particles contributed toward suppression of grain growth in the Ca-containing alloy, resulting in superior strength. Other, similar, results have also been reported, in which precipitation hardening by dispersive precipitates resulted in improved tensile strength.[173]

Strengthening by precipitation, however, sacrifices ductility, in a manner often referred to as the strength-ductility tradeoff. Accordingly, researchers are attempting to identify the optimum conditions for alloying and microstructural design that can result in strength-ductility synergy. Yu et al. introduced an M1 (Mg-1Mn (wt%)) alloy with high strength and superior ductility.[258] Microstructural observations revealed that M1 consisted of refined grains (3.1 μm), probably because fine Mn precipitates suppressed grain growth during the extrusion process. Moreover, the M1 alloy demonstrated a high elongation to failure ratio (38.8%) and improved yield anisotropy due to the Mn precipitates and grains with[99] planes parallel to the [0001] planes of Mg, which restricted twinning initiation. Very recently, Wei et al. proposed a Mg alloy with excellent strength and ductility using a novel strategy that includes an extrusion process followed by pre-deformation and aging of the as-extruded

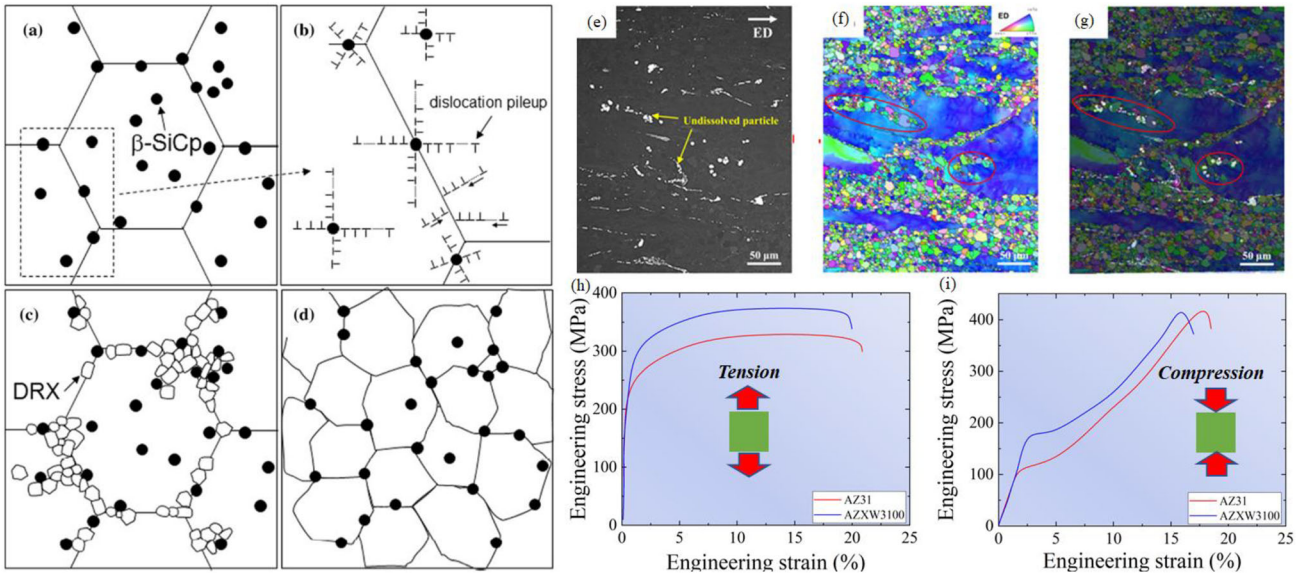

Figure 15. (a–d) Schematics showing the evolution of DRXed grains by the dislocation pile ups near precipitates, (e–f) Combined image of SEM and EBSD IPF showing the recrystallized regions of extruded AZXW3100 alloy,[260] (h–i) Tensile and compressive stress-strain curve of extruded AZ31 and AZXW3100 alloys, respectively.[260]

samples.[259] A GW83 K (Mg-8Gd-3Y-0.5Zr (wt%)) Mg alloy pre-deformed by 2% and aged for 16 h at 225 °C demonstrated excellent mechanical properties, with YS, UTS and ductility values of 371 MPa, 419 Mpa, and 15.8%, respectively. The increase in dislocation density upon pre-deformation and formation of chain-like nano-precipitates were suggested as the reason for the improved properties, as these acted as obstacles to dislocation slip, thus enabling enhanced ductility.

It is well-established that DRX behavior can significantly modify the microstructure of an alloy due to grain refinement and the increase in random texture of DRXed grains, which helps to enhance the performance of Mg alloys. In this regard, precipitates (intermetallic compounds) distributed throughout the matrix have been considered to be the most influential microstructural feature in promoting DRX. The severe deformation zones that form around the precipitates (> 1 μm diameter) during plastic deformation lead to high local lattice misorientation. The dissipation of the accumulated stored energy of lattice misorientation results in rapid sub-boundary migration in their vicinity, leading to vigorous nucleation of new DRXed grains, as shown in Figure 15a–d. Moreover, the nucleated grains usually adopt random orientations and are thus very effective at manipulating texture. Robson et al. provided direct evidence of recrystallization behavior originating from the precipitates by conducting a compression test followed by annealing at 400 °C for 2 h on Mg-Mn alloys.[261] Microstructural characterization of the deformation zones confirmed that the orientation gradient near the coarse particles (> 1 μm diameter) and particle clusters was less steep, confirming the PSN mechanism. Moreover, DRX behavior in AZ31-0.5Ca has been reported to begin at very early stages of deformation, as a rolling reduction of only 21% resulted in a significant evolution of DRXed grains.[241] Microstructural characterization confirmed the role of $(Mg, Al)_2Ca$ particles in promoting DRX. Kim et al. investigated the microstructural features and mechanical performance of extruded AZ31 following the combined addition of Ca and Y.[260] EBSD analysis revealed significant promotion of DRXed behavior in an AZXW3100 (AZ31-0.5Ca-0.2Y)(wt%) alloy as compared to AZ31, which was attributed to the PSN effect caused by the $(Mg, Al)_2Ca$ and Al_8Mn_4Y precipitates dispersed in the AZXW3100 alloy (Figure 15e–g). The mutual effects of GB hardening and grain size reduction due to the higher fraction of DRXed grains, texture softening, and strain hardening caused by increased accumulation of dislocations in un-DRXed grains suppressed the formation of twins and precipitate hardening due to undissolved precipitates and resulted in a significant increase in the tensile YS of the AZXW3100 alloy (290 MPa) as compared to AZ31 (248 MPa) (Figure 15h and i).

It is well-known that twinning can result in crack initiation, eventually leading to premature failure in Mg alloys. Precipitates have also been reported to suppress deformation twinning in cases where effective precipitation of suitable precipitates encourages deformation by slip.[262] Precipitates do not retard twin nucleation (and sometimes even promote twin

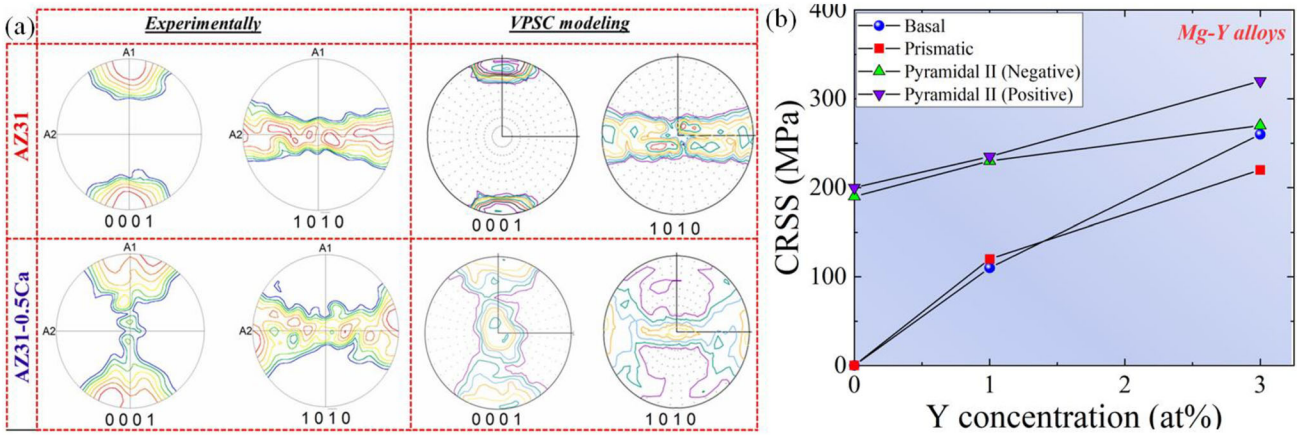

Figure 16. (a) Experimental and VPSC simulated pole figures of AZ31 and AZ31-0.5Ca,[14] (b) CRSS of Mg-Y alloys on basal, prismatic, and pyramidal II planes at 0 K.[273]

nucleation) during deformation, but restrict the total volume fraction and propagation of twin thickening by blocking the tips of twins, inhibiting twin growth.[263–265] Jian et al. reported a reduction in tension-compression yield asymmetry in an Mg-8Al-0.5Zn (wt%) alloy.[266] This was attributed to a reduction in twinning rate due to the presence of $Mg_{17}Al_{12}$ precipitates. Hence, when designing a high-strength, twinning-resistant Mg alloy, a high degree of shear resistance of the precipitate in the twinning direction is desirable in order to cope with back stresses and produce a material with sufficiently large grain size to inhibit twin growth.

3.2. Altering the relative critical resolved shear stress (non-basal/basal)

The limited ductility of Mg alloys is associated with the inability of the HCP structure to accommodate plastic strain in the crystallographic c-axis. Large differences in the CRSS values of the basal and non-basal slip systems (~1/40 MPa and 1/100 MPa for basal/prismatic and basal/pyramidal, respectively) lead to premature failure in Mg alloys before non-basal slip can be activated. Thus, widespread application of Mg alloys has been impeded due to the intrinsic brittleness of Mg. Accordingly, to fulfill the von Mises criterion, five independent slip systems need to be activated to accommodate arbitrary shape change. This can be achieved by activating non-basal slips by altering the CRSS values of the basal and non-basal slip systems ($CRSS_{non\text{-}basal}/CRSS_{basal}$), either by hardening of the basal slip system (increasing the CRSS values) or softening of the non-basal slip system (decreasing the CRSS values). Hence, remarkable improvement in the ductility of Mg alloys can be achieved when the ratio ($CRSS_{non\text{-}basal}/CRSS_{basal}$) approaches 1, when non-basal slip can be readily activated to accommodate plastic strain during deformation.

Experimentally measuring the CRSS values of various deformation mechanisms in polycrystalline Mg is a near-impossible task; hence, approximate CRSS values have been used that are obtained from crystal plasticity models, including the VPSC model, EPSC model, and others.[14,51,55,65,66,267–269] In these modeling techniques, the parameters, including plastic anisotropy, stress-strain behavior, and texture evolution, are simulated and compared with the experimentally received results. Accordingly, the absolute or relative CRSS values of slip systems have been extracted in optimized conditions. The $CRSS_{non\text{-}basal}/CRSS_{basal}$ ratio of polycrystalline Mg has been shown to be much less than that of Mg single crystal, resulting in higher activity of the non-basal slip system in strong-textured polycrystalline Mg as compared to a single crystal sample with a similar orientation.[270] Solid solutions have been reported to significantly contribute to hardening of basal slip and, sometimes, softening of non-basal slip, eventually resulting in enhanced activation of non-basal slip systems.[52,53,271] The CRSS values of polycrystalline Mg are very much related to the hardening imposed by solute segregation, GBs, and second phase particle dispersions (intermetallic compounds). For example, Ca reportedly alters the activities of the slip systems in an AZ31 alloy, thereby increasing the overall performance of the alloy.[14,272] VPSC simulation was conducted to predict the final textures of two alloys (AZ31 and AZ31-0.5Ca) deformed to 10%, and the results were compared with the texture of the alloys measured experimentally as shown in Figure 16a. The results confirmed that the formation of $(Mg,Al)_2Ca$ intermetallic compound in Ca-added AZ31 hardened the basal slip, leading to an increase in the CRSS

needed to activate this slip, and eventually reducing the $CRSS_{prismatic}/CRSS_{basal}$ ratio (1.6 vs. 2.2 in AZ31-0.5Ca and AZ31, respectively), which lead to higher ductility in AZ31-0.5Ca.[14] In another work, Sn was reported to significantly improve the stretch formability (~10.2 mm) of a Mg-3Al alloy.[77] A plasticity simulation carried out on AZ31 and AT31 (Mg-3Al-1Sn) (wt%) showed that the prismatic $<a>$ slip is the dominant deformation mode in the latter alloy, besides typical basal $<a>$ slip. Sn addition resulted in hardening of basal slip (43.86 and 62 MPa in AZ31 and AT31, respectively) and simultaneous softening of prismatic slip (109.56 and 78.09 MPa in AZ31 and AT31, respectively), which reduced the planar anisotropy and r-value in the AT31 alloy and produced improved performance.

Similarly, reducing the $CRSS_{non\text{-}basal}/CRSS_{basal}$ ratio in Mg alloys can be achieved by the strengthening imposed by solute atoms on different slip systems. For example, the CRSS of the basal slip system in Mg single crystal was reported to increase with the square root of Zn concentration (beyond 0.025 at%), which was attributed to higher forest dislocation density at the basal slip.[52] Similarly, TEM analysis of Mg-Al thin foils showed that the basal dislocation density increases parabolically with increasing solute concentration. For instance, MD simulations were conducted on Mg-Y to identify the role of Y solute on the CRSS values of an edge dislocation on the basal and non-basal slip systems, and the results were compared with those of pure Mg.[273] The solid solution strengthening effect was observed to be larger on the basal plane than the non-basal plane upon alloying with Y, based on the binding energies of solute atoms and various slip systems, as shown in Figure 16b. Basal slip hardening reduced the gap between the basal and non-basal slip systems and plastic anisotropy in the Mg-Y alloy, which was suggested to be the mechanism driving the high non-basal slip activity detected experimentally. In addition, promotion of non-basal slip systems has been reported to be significantly affected by the c/a ratio, which can reduce the CRSS gap between the basal and non-basal slip systems.[69,274,275] Accordingly, modifying the c/a ratio of an HCP crystal by specific solute addition clearly has the potential to improve the RT performance of Mg alloys. For example, substituting Mg atoms with Li has been reported to substantially reduce the c/a ratio, resulting in softening of the non-basal slip system.[276] The excellent improvement in ductility was thus attributed to the incorporation of more slip systems due to the lower activation energy of the non-basal slip system.

3.3. Controlling the atomistic flow mechanisms

The key to designing intrinsically highly ductile Mg is to attain a thorough understanding and control of various atomistic flow mechanisms, which can be summarized as follows:

1. Decreasing the SFEs
2. Suppressing and stabilizing the PB transition
3. Promoting the cross-slip of pyramidal II dislocations

Specific solute additions are required to reduce the SFE, as they increase the nucleation of non-basal dislocations. Accordingly, reduced SFE indicates a higher density of nucleations with non-basal orientations. As the non-basal orientations provide the out-of-basal plane strain, they will eventually result in enhancement of ductility in Mg alloys.[122] In addition, it has been demonstrated experimentally that the pyramidal $<c+a>$ system undergoes a thermally activated glissile-to-sessile transition upon deformation and acts as an obstacle to dislocation motion; hence, it has been tagged as the origin of lower ductility in Mg alloys.[72] These immobile dislocations pile up, and the higher rate of these transitions increases the number of immobile dislocation pile-ups. Accordingly, solute additions should be designed to enhance the PB transition time, leading to increased availability of the easy glide $<c+a>$ dislocation to accommodate c-axis plastic strain and finally resulting in enhanced ductility. The last important mechanism exploits the tendency of suitable solutes to accelerate cross-slip of pyramidal II $<c+a>$ screw dislocations by reducing the cross-slip energy barrier.[129] The resulting decrease in the energy barrier and subsequent higher cross-slip dislocations result in multiplication of $<c+a>$ dislocations, which can significantly accommodate plastic strain in the crystallographic c-axis, leading to enhanced ductility in Mg alloys.

Despite the numerous efforts that have been made to understand the precise mechanisms by which highly ductile Mg alloys can be formed, long-standing, significant obstacles remain. The above-mentioned mechanisms have been extensively investigated by exploiting various solutes, yet there is a lack of clear understanding of the individual and collaborative effect of solutes on these atomistic flow mechanisms. Accordingly, high-throughput DFT calculations should be conducted to promote our understanding of these phenomena and their mutual relationships with one another.

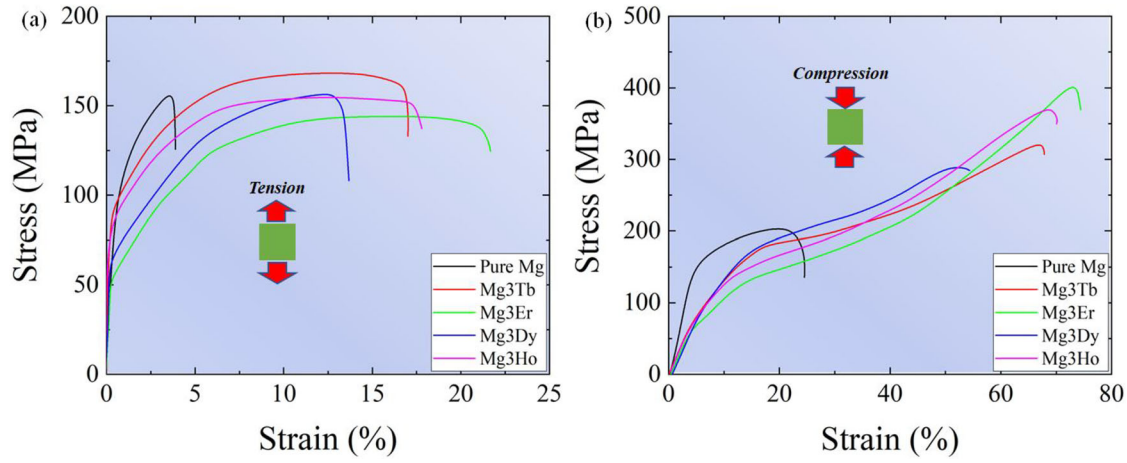

Figure 17. Stress-strain curves under (a) tension and (b) compression of various Mg-RE alloys.[115]

4. Recent advances in magnesium with improved ductility

4.1. Magnesium alloys with improved ductility

Due to its intrinsic hexagonal lattice structure, magnesium has limited RT ductility, which impedes its widespread industrial application. This inferior RT ductility is primarily due to the dominance of $\{0001\}<11\bar{2}0>$ basal $<a>$ dislocation slip and $\{10\bar{1}2\}<10\bar{1}\bar{1}>$ tensile twinning during plastic deformation.[67–69,73,277] The basal $<a>$ slip fails to accommodate strain along the crystal's c-axis and, instead, leads to the rotation of the crystal's c-axis such that it aligns parallel to the direction of loading.[277] This results in the formation of extremely strong textural components of basal/fiber textures, leading to failure at low strains.[73,278] Alternately, the strain along the crystal's c-axis is accommodated only through the activation of non-basal slip systems in HCP crystals, which consequently leads to homogenous plastic deformation of Mg even under higher strains.[70,72] Although dislocations with $<c+a>$ Burgers vectors occasionally form in pure Mg, Wu et al. used MD simulations to demonstrate that dislocations with non-basal Burgers vectors are typically unstable and, hence, relax onto the basal planes.[72] Therefore, alloying is an effective alternative strategy of manipulating the dislocation and slip systems and, thus, the stability of Mg.[279] In particular, it is often suggested that alloying with RE and other elements tremendously improves RT ductility.[279] This notion is discussed comprehensively in the following sections.

4.1.1. Magnesium-RE-based alloys

Magnesium-rare earth alloys are a class of magnesium alloys with extraordinary properties, such as excellent strength, ductility, creep resistance, etc.[279] Several commonly used RE elements include Y, Ce, Gd, La, Er, Nd, Dy, etc. Evidence of their effectiveness at improving ductility under both tensile and compressive loads is presented in Figure 17a and b.[115] The RE elements increase the ductility of Mg by more than four times. Some of the most effective RE alloying additions that lead to significant improvements in ductility are discussed below; they are classified based on their RT solid solubility in Mg.

4.1.1.1. Low solubility binary alloys

4.1.1.1.1. Mg-Ce alloys. With a negligible RT solid solubility in Mg, Ce forms a eutectic of α-Mg + $Mg_{12}Ce$ in the Mg matrix.[280] Owing to the formation of secondary phase particles, Ce aids in the dispersion strengthening of Mg.[280] Addition of trace amounts of Ce up to 0.2% contributed significantly to improving the ductility of magnesium under tensile loading from 9 to 31% (Table 2).[281] This improved ductility can be atributed to the evolution of randomized texture as a result of the dynamic recrystallization process in the course of extrusion. However, this increased ductility coincided with a reduction in the YS. Additionally, Chino et al. demonstrated that enhanced ductility was the result of increased stacking fault energy in Mg-0.2Ce, which aided in activation of non-basal slip.[68] With addition of 0.4% Ce to Mg, Tekumalla et al. demonstrated a simultaneous enhancement of strength and ductility without any textural changes.[283] Furthermore, the authors suggested that grain size refinement was the dominant factor driving the observed improvements in strength and ductility, which increased by 182% and 93% in the Mg-0.4Ce (wt%) alloy in comparison to Mg. With further addition of Ce to 0.5%, Luo et al. reported a reduction in ductility and further strengthening of the alloy, along with severe surface oxidation of the extrusions.[282] With even higher amounts of Ce of about 1% a further reduction in ductility was observed

Table 2. Tensile properties of binary Mg-Ce alloys.[279]

Alloy (wt%)	Processing condition	YS (MPa)	UTS (MPa)	Ductility (%)
Mg-0.2Ce	Cast + Extruded at 400 °C[281]	68.6	170	31
Mg-0.2Ce	Cast + Extruded at 300 °C + Rolled at 400 °C[68]	110–135	200–220	14–16
Mg-0.2Ce	Cast + Homogenized at 400 °C + Extrusion at 350 °C[282]	100	215	20.6
Mg-0.5Ce		130	230	8
Mg-0.4Ce	As cast[280]	140	160	20
Mg-0.4Ce	Cast + Annealed at 520 °C for 1 h + water quenched[280]	90	120	29
Mg-0.4Ce	Cast + Hot extruded at 350 °C[283]	206 ± 8	223 ± 6	27
Mg-0.4Ce	Cast + Hot extruded at 350 °C + Solutionized at 570 °C[283]	138 ± 5	200 ± 10	24
Mg-0.53Ce	High Pressure Die Cast[284]	80	140	5.5
Mg-0.93Ce		90	–	5
Mg-1.48Ce		100	–	4
Mg-2.87Ce		135	160	1.5
Mg-4.78Ce		150	–	0.9–1
Mg-1Ce	Cast + hot rolled at 400 °C[285]	146 ± 5.5	168.5 ± 3	7.1
Mg-1Ce	Cast + hot rolled at 400 °C + annealed for 1 h	134 ± 2.5	205.5 ± 7	2.7
Mg-1Ce	at 250 °C + Water quenched[285]	124.6 ± 1.5	212.7 ± 4.7	3.3
Mg-1Ce		106 ± 4.7	197.6 ± 4.2	11.9
Mg-1Ce		101.5 ± 1.6	203.1 ± 2.6	14.9
Mg-1Ce		99 ± 2.1	203.3 ± 4.4	16.9

Table 3. Tensile properties of binary Mg-Nd alloys.[279]

Alloy (wt%)	Processing condition	YS (MPa)	UTS (MPa)	Ductility (%)
Mg-0.47Nd	High Pressure Die-cast[284]	81	189	9.5
Mg-0.76Nd		85	–	6.75
Mg-1.25Nd		92	–	4.8
Mg-2.60Nd		115	–	4.1
Mg-3.53Nd		130	140	2.5
Mg-1.2Nd	As-cast[286]	95	123	4.61
Mg-1.85Nd		121.2	155.8	2.76
Mg-3.59Nd		141.2	153.6	1.08
Mg-2Nd	Cast + Extruded at 380 °C[287]	77	193	30
Mg-2Nd	Cast + Extruded at 380 °C + annealed for 16 h at 204 °C (T5(1))[287]	123	240	26
Mg-2Nd	Cast + Extruded at 380 °C + annealed for 48 h at 204 °C (T5(2))[287]	102	242	27.5
Mg-2Nd	Cast + Extruded at 380 °C + solution treated for 3 h at 510 °C + annealed for 16 h at 204 °C (T6(1))[287]	125	220	15
Mg-2Nd	Cast + Extruded at 380 °C + solution treated for 3 h at 510 °C + annealed for 48 h at 204 °C (T6(2))[287]	70	230	18.5

because of the formation of a higher fraction of $Mg_{12}Ce$ intermetallic compounds and associated detrimental morphologies. Table 2 lists the tensile properties of the binary Mg-Ce alloys reported thus far.[284,285]

4.1.1.1.2. Mg-Nd alloys. With an insignificant solid solubility in Mg at RT, Nd forms secondary phases (Mg_3Nd and $Mg_{12}Nd$) when added to the Mg matrix and shows good age-hardening behavior.[284,286] Nd significantly improves the YS of Mg via dispersion and precipitate strengthening mechanisms. Seitz et al. reported excellent ductility in an extruded and heat-treated Mg-2Nd alloy (Table 3) and identified this alloy as a promising bio-material for stents and other applications considering its low strength and limited degradation potential.[287]

4.1.1.2. High solubility binary alloys

4.1.1.2.1. Mg-Y alloys. With a RT solid solubility of up to 0.5 at% and 1.8 wt%, Y addition allows for strengthening by both solid solution and precipitation owing to the difference in the atomic radius of Y (atomic radius = 212 pm) and Mg (atomic radius = 145 pm).[288,289] There was a reduction in ductliity along with an improvement in strength with addition of Y up to 6.5%, as shown in Table 4. The same was also reported by Xuenan et al. for Mg-1wt%Y,[290] where rolling led to poorer ductility of the alloys when compared to their as-cast counterparts; the authors concluded that Y was detrimental for the ductility and corrosion of the Mg-1Y alloy. However, further investigations of Mg-Y alloys by Zhou et al. revealed a tremendous improvement, up to 33%, in the ductility of the as-extruded Mg-3%Y, along with an improvement in the strength (Table 4).[292] The authors attributed this tremendous improvement in ductility to the activity of multiple modes of deformation. Identical observations of simultaneous increases in strengths and ductility were reported by Tekumalla

Table 4. Tensile properties of binary Mg-Y alloys.[279]

Alloy (wt%)	Processing condition	YS (MPa)	UTS (MPa)	Ductility (%)
Mg-0.7Y	As cast + heat treated for 2-12 h at 525 °C[289]	39	150	14
Mg-1.23Y		45	155	13
Mg-3.1Y		70	160	11
Mg-4.67Y		89	175	10
Mg-6.5Y		110	230	8
Mg-1Y	As-Cast[290]	25	75	10
Mg-1Y	Cast + Hot Rolled at 400 °C[290]	148	200	9.3
Mg-0.4Y	Cast + Extruded at 350 °C[291]	120	176	7
Mg-1Y		111	166	10
Mg-1.8Y		109	167	31
Mg-3Y	Cast + Extruded at 350 °C[292]	120	200	33
Mg-2Y	Cast + Heat treated for 12 h at 480 °C + Extruded at 420 °C[220]	92	189	21
Mg-4Y		87	177	30
Mg-2Y	Cast + Hot Rolled at 450 °C + Annealed[293]	146	228	30.5
Mg-3Y	Gravity cast + Hot rolled + Annealed for 15 min at 500 °C[67]	92	165	24
Mg-5Y	Powder Metallurgy + Cold pressed (@540MPa) + Extruded at 420 °C[294]	–	350	7
Mg-10Y		–	440	9

et al.,[291] Sandlobes et al.,[67] and Edassiqi et al.[293] For Mg-4Y, Wu et al.[220] reported an increase in ductility to 30%, from 15% in pure Mg, at the expense of strength (Table 4). The authors related this drop in strength and improvement in ductility to a texture effect, as Y reduces the c/a ratio and hence the CRSS needed to activate the pyramidal slip system during deformation. Activation of the pyramidal slip system leads to extensive plasticity in Mg-Y alloys.[294] Other studies of Mg-Y alloys also highlighted enhancements in $<c+a>$ cross-slip activity and accredited the higher ductility of Mg-Y alloys relative to pure Mg to the observed activity, which allows for plastic deformation,[69,129,273] as shown in Figure 18. Sandlobes et al. credit the ductility to the reduced I_1SFE which accompanies the activation of non-basal shear with Y addition.[75]

4.1.1.2.2. Mg-Gd alloys. Gd, like Y, has a a high solublity in Mg of about 23.5 wt% at eutectic temperature.[295] Hence, it also promotes strengthening by forming a solid solution in Mg.[218,296] In fact, Mg-Gd alloys have excellent property profiles matching that of human cortical bone,[296] with superior elongation to failure (ductility) in comparison to other metal implant materials such as stainless steel, titanium alloys, etc. Gd was added to Mg in concentrations of up to 20% by weight.[297] The Mg-20Gd alloy contained α-Mg + Mg_5Gd in its microstructure along with refined grains, which led to an increase in strength (Table 5). Similar to the other RE elements, Gd addition weakens the recrystallization texture when added to Mg in concentrations up to 1%, and further addition has no further effect on the texture.[298] It forms a RE textural component that renders the alloys highly ductile, up to 30% along the extrusion direction.[217] The same authors also reported suppression of the RE textural component at higher extrusion temperatures.[285]

4.1.1.3. Ternary/complex alloys

Given the excellent ductility of Mg-RE alloys, innumerable attempts to create ternary and complex alloys with a mixture of different RE elements and/or other common alloying elements have been made in the past.[279,282,299–303] Some of the most promising ternary/complex alloys that show promising ductility under tensile loading conditions are given in Table 6. Among these, Mg-Zn-Gd alloys are noteworthy as they exhibit ductility > 40% in rolled condition; the improved ductility was attributed to Gd's texture-weakening effects.[17] Apart from Gd, other additions to the Mg-Zn alloy, such as 0.4Y, also contributed to a high ductility of 30%, as reported by Le et al.[85] Furthermore, WE43[304] and E21[306] are commercial RE-based ternary/complex alloys with extraordinary properties that are currently being used for aerospace/automobile/biomedical applications. Panigrahi et al.[304] reported improved ductility in WE 43 alloys with forging and attributed the improvement to activation of non-basal slip prior to twinning. Furthermore, Li-based alloying additions in combination with Ce also exhibited excellent ductility (as high as 33%), as reported by Wang et al.[305] The improved properties were attributed to the α (Mg) phase and β (Li) phase and refinement of the microstructure.

4.1.1.4. Modifications and properties of magnesium-RE-based alloys

4.1.1.4.1. Texture randomization and solute segregation. While "texture weakening" in Mg alloys has been mentioned several times in this article and has been attributed to improved ductility, in this section, the mechanism of texture weakening, and solute segregation is discussed using the example of a Mg-Ce alloy. As discussed earlier, Ce aids in weakening/

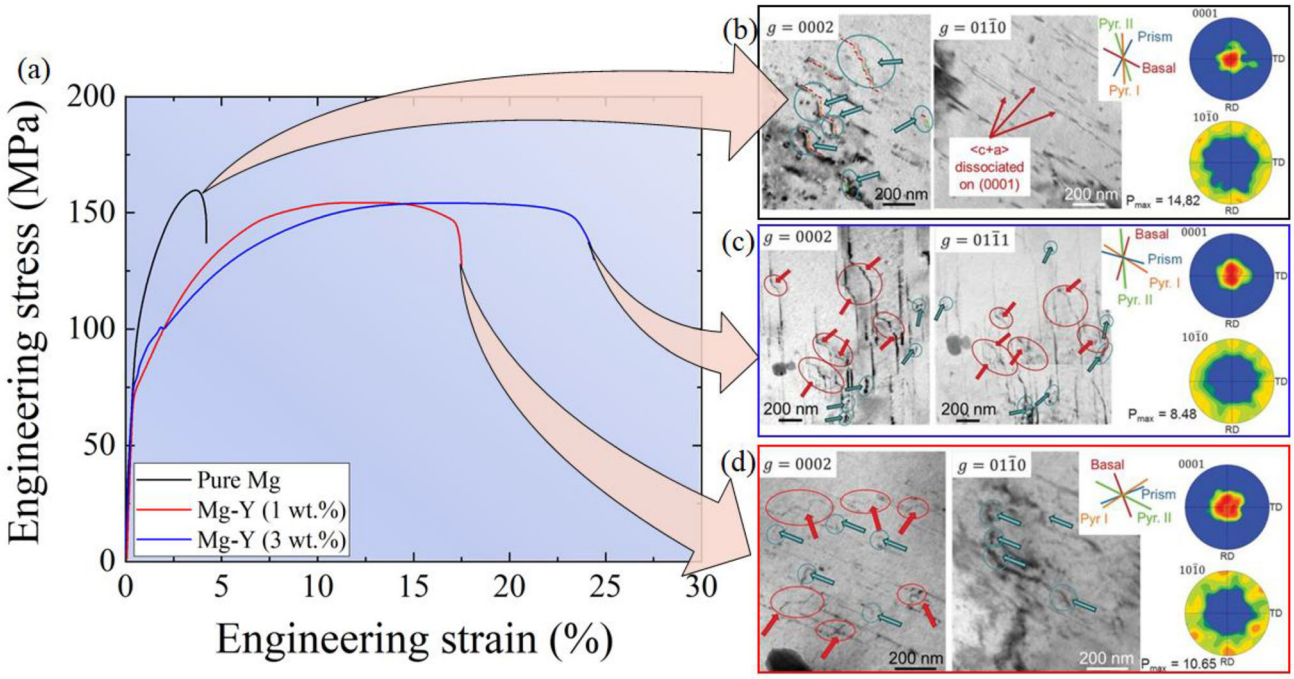

Figure 18. (a) Stress-strain curves and deformation activity of Mg-Y alloys at RT, pole figures and TEM images showing dislocation structures in strained (b) pure Mg, (c) Mg-3wt%Y, and (d) Mg-1wt%Y.[129]

Table 5. Tensile properties of binary Mg-Gd alloys.[279]

Alloy (wt%)	Processing condition	YS (MPa)	UTS (MPa)	Ductility (%)
Mg-0.22Gd	Cast + hot rolled at 400 °C + annealed at 380 °C for 1 h[298]	120	190	6
Mg-0.75Gd		145	210	12
Mg-2.75Gd		160	205	21
Mg-4.65Gd		165	210	26
Mg-1Gd	Cast + hot rolled at 400 °C[285]	138.2 ± 1.7	173.3 ± 4	4.8
Mg-1Gd	Cast + hot rolled at 400 °C + annealed at 250 °C for 1 h + Water Quenched[285]	129.3 ± 4.9	191.2 ± 5.9	3.4
Mg-1Gd	Cast + hot rolled at 400 °C + annealed at 300 °C for 1 h + Water Quenched[285]	124.5 ± 1.4	225 ± 2.6	4.2
Mg-1Gd	Cast + hot rolled at 400 °C + annealed at 350 °C for 1 h + Water Quenched[285]	111 ± 4.8	240 ± 22	29.7
Mg-1Gd	Cast + hot rolled at 400 °C + annealed at 400 °C for 1 h + Water Quenched[285]	71.3 ± 3.4	184.9 ± 2.5	29.6
Mg-1Gd	Cast + hot rolled at 400 °C + annealed at 450 °C for 1 h + Water Quenched[285]	70.4 ± 2.4	220.6 ± 2.9	29.6
Mg-1.55Gd	Cast + Solution treated for 3 h at 530 °C + 5 h at 560 °C + Extruded at 450 °C[217]	102	214	23.9
Mg-1.55Gd	Cast + Solution Treated for 3 h at 530 °C + 5 h at 560 °C + Extruded at 510 °C[217]	130	210	15.8
Mg-2Gd	As-cast[296]	37.9	103.7	6.4
Mg-2Gd	As-cast + solutionized (T4)[296]	33.4	87.0	4.9
Mg-2Gd	As-cast + solutionized + artificially aged (T6)[296]	41.2	101.3	5.6
Mg-5Gd	As-cast[296]	54.7	128.4	6.6
Mg-5Gd	As-cast + solutioned (T4)[296]	44.8	98.0	6.0
Mg-5Gd	As-cast + solutionized + artificially aged (T6)[296]	42.6	78.6	4.2
Mg-10Gd	As-cast[296]	84.1	131.1	2.5
Mg-10Gd	Cast + solutioned (T4)[296]	69.1	111.6	3.1
Mg-10Gd	Cast + solutionized + artificially aged (T6)[296]	85.4	132.2	2.1
Mg-15Gd	As-Cast[296]	127.6	175.2	0.9
Mg-15Gd	Cast + solutionized (T4)[296]	118.0	186.8	2.4
Mg-15Gd	Cast + solutionized + artificial aged (T6)[296]	201.3	250.9	0.7
Mg-3.11Gd	Cast + Solution treated at 535 °C/1.5 h[218]	60	160	13
Mg-5.73Gd	Cast + Solution treated at 535 °C/4 h[218]	80	180	11
Mg-9.28Gd	Cast + Solution treated at 535 °C/6.5 h[218]	100	190	9
Mg-14.2Gd	Cast + Solution treated at 535 °C/9 h[218]	130	225	8
Mg-19.6Gd	Cast + Solution treated at 540 °C/9.5 h[218]	150	255	7.5
Mg-20Gd	Melt Spun[297]	308	308	12
Mg-20Gd	As-cast[297]	254	254	13

randomizing the texture and reducing the CRSS for non-basal < c + a > slip, hence improving the mechanical properties of Mg.[281] Mishra et al. reported on Mg and Mg-0.5Ce alloys with distinct initial textures and grain sizes.[307] The addition of Ce reduced the average grain size of the alloy due to the presence of Mg-Ce precipitates that pin the grain boundaries and hinder grain growth during recrystallization. It is

Table 6. Tensile properties of Mg-RE ternary/complex alloys.

Alloy (wt%)	Processing condition	YS (MPa)	UTS (MPa)	Ductility (%)
Mg-3Al-0.2Ce	Cast + Homogenized at 400 °C + Extrusion at 350 °C[282]	120	235	18
Mg-3Al-0.5Ce		125	230	20
Mg-1.11Zn-1.68Gd	Cast + homogenized at 500 °C for 10 h + Rolled at 430 °C +	129.9	233.4	40.3
Mg-1.11Zn-1.68Gd	annealed at 400 °C for 1 h (Tested in RD,	113.8	221.2	44.5
Mg-1.11Zn-1.68Gd	45°, TD, RD, 45°directions, respectively[17]	110.1	218.4	44.6
Mg-1.06Zn-2.74Gd		130.6	220.0	40.3
Mg-1.06Zn-2.74Gd		121.0	220.3	47.3
Mg-1.06Zn-2.74Gd		118.0	220.9	45.1
Mg-2Zn-0.4Ce	Cast + Extruded at 310 °C[302]	190	255	18
Mg-2Zn-0.4Gd		125	220	26
Mg-2Zn-0.4Y		160	240	30
Mg-2Zn-0.4Nd		175	245	28
Mg-4Y-3RE	As Received[304]	185 ± 12	261 ± 5	31 ± 1
Mg-4Y-3RE	As Received + T5[304]	270 ± 15	348 ± 6	16 ± 3
Mg-4Y-3RE	Forged[304]	263 ± 7	311 ± 11	23 ± 3
Mg-4Y-3RE	Forged + Aged at 210 °C/32 h[304]	318 ± 9	368 ± 10	17 ± 1
Mg-4Y-3RE	Forged + Aged at 180 °C/60 h[304]	344 ± 11	388 ± 12	23 ± 1
Mg-4Y-3RE	Forged + Aged at 150 °C/104 h[304]	286 ± 10	341 ± 4	28 ± 1
Mg-3.5Li-2Al-2RE	Cast + Extruded[303]	95	190	22
Mg-5.5Li-2Al-2RE		140	235	23
Mg-8.5Li-2Al-2RE		100	150	32
Mg–8Li–1Al–1Ce	Cast[305]	141	160	16
Mg–8Li–1Al–1Ce	Cast + Extruded at 220 °C[305]	175	187	33

widely reported that GB segregation and pinning play a crucial role in texture modification by arresting migration of basal grain boundaries.[226,307] This allows for retainment of non-basal grains even after recrystallization. Texture randomization and grain boundary solute segregation are shown in the EBSD maps in Figure 19. Addition of Ce above its solubility limit, i.e., > 0.1 wt%, causes a reduction in the CRSS for < c + a > dislocations; therefore, dislocations are generated, resulting in a condition that favors nucleation of grains during the recrystallization process. Furthermore, excess Ce that is not in the solid solution forms an Mg-Ce phase which assists in grain boundary pinning and further reinforces the random orientations of the grain structure. Thus, texture randomization and solute segregation are interdependent factors, and are the mechanisms driving changes in the properties of Mg-RE alloys.

4.1.1.4.2. Long-period stacking ordered structures. Long-period stacking ordered (LPSO) structures form in several Mg alloys, especially those with higher RE content including Mg-Gd-Zn alloys with high Gd content, which have a Zn/Gd ratio of ≤ 1.0.[308] Mg-Gd-Zn alloys have been extensively studied,[309–311] and it has been reported[309] that Mg–10Gd–xZn alloys (x = 2,6) exhibits lower ductility, as shown in Table 7, despite their excellent strength due to the lamellar LPSO structures. These structures typically form as a result of heat treatment. For example, Mg–8.2Gd–3.8Y–1.0Zn–0.4Zr (wt%) exhibits eutectic compounds of Mg-(Gd,Y) in as-cast condition, but forms 14H- and 18 R-type LPSO upon heat treatment,[314,315] which aid in improving the mechanical properties. The LPSO phases are found at grain boundaries upon aging, where they lead to improved strength of Mg alloys.[312,316,317] Furthermore, in ZEK100 alloys with RE elements such as Nd, Gd, La, Ce, Al-Samman et al.[73] reported the best formability in the Gd-containing alloy at the expense of YS. This was attributed to the unique RE texture formed by Gd-containing alloys, which differs from that seen in other RE-containing alloys. LPSO structures were also reported in other alloys, such as Mg-Zn-Mn[318] and Mg-10Er-2Cu alloys[313] with an 18 R LPSO phase which resulted in excellent mechanical properties, as shown in Table 7.

4.1.1.4.3. Critical resolved shear stresses of slip systems. The critical resolved shear stress (CRSS) dictates the initiation of plastic deformation by slip in the grains. The relative CRSS values of different modes of slip in Mg are given in Table 8. It is evident that there is a significant variance in the CRSS of basal slip vs. other deformation modes. This leads to the poor ductility of Mg due to the development of strong textures and lack of activation of other slip systems for homogeneous deformation. Atomistic simulations[273,319] of Mg-Y alloys show that a reduction in the difference in CRSS between the basal < a > and non-basal < c + a > slips is crucial for the activation of the non-basal < c + a > slip, which leads to the onset of < c + a > slip in Mg-Y alloys, as shown in Figure 20, thereby rendering them highly ductile. In Mg-Al alloys, the CRSS difference between the two types of slip is large and strengthening due to the high solid solubility of Al in Mg is present; hence, <c + a>-type slip activity is not prominent. Therefore, Kim et al.

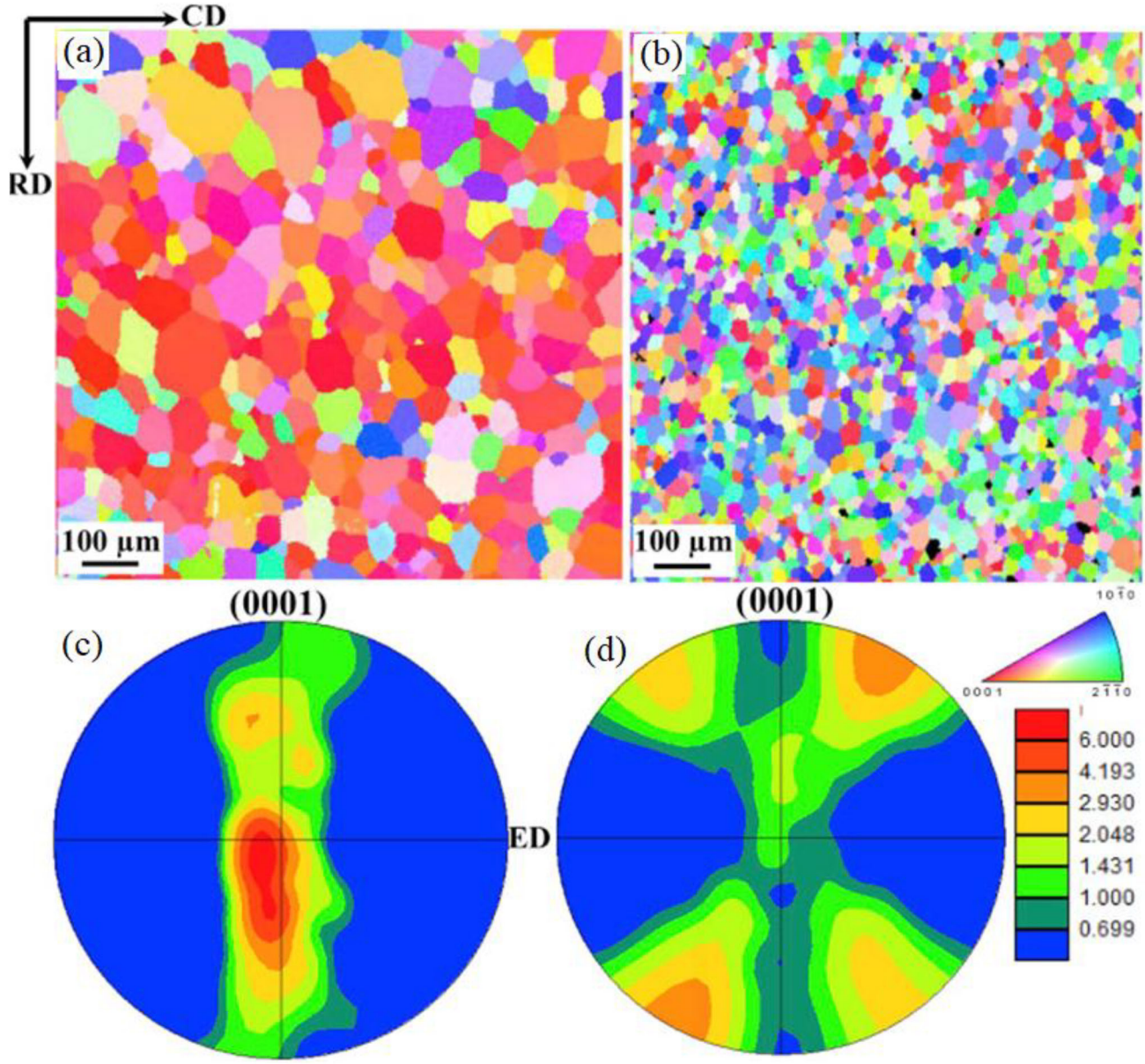

Figure 19. Extruded microstructures of (a) Pure Mg and (b) Mg-0.5Ce and their corresponding pole figures in (c) and (d), respectively.[307]

recommend simulated CRSS as a promising parameter for designing very ductile Mg-based alloys.[273]

4.1.2. Re-free magnesium alloys with improved properties

While RE elements are excellent choices for Mg alloys, particularly in terms of increasing the $< c + a >$ slip activity and, thus, improving ductility, they are complex to process, expensive, and unable to be recycled. Hence, they are not entirely suitable for large-scale production of Mg-RE-based alloys for various applications. Therefore, there is renewed interest in finding alternate, RE-free solutions to enhance the ductility of Mg. Several alloying additions are known to contribute to similar mechanisms and are viable as Mg alloy elements. These are discussed below.[12]

4.1.2.1. Mg-Sn-based alloys

Mg-Sn alloys are cost-effective and possess superior mechanical properties, such as high ductility and strength, owing to a large difference in solubility at eutectic and ambient temperatures.[320,321] Several formulations created by addition of other elements to Mg-Sn alloys, such as Mg–5Sn–2Zn (TZ52), Mg–5Sn–2Zn–2Al (TAZ522), and Mg–5Sn–5Al–1Zn–0.2Mn (TAZM5510) alloys, have been studied, and their mechanical properties are given in Figure 21. While the highest strength was seen in the TAZM5510 alloy, the highest ductility of 30% was

Table 7. Tensile properties of Mg-RE alloys with LPSO structures.

Alloy (wt%)	Processing condition	YS (MPa)	UTS (MPa)	Ductility (%)
Mg–8.2Gd–3.8Y–1.0Zn–0.4Zr	Cast + Solution treated at 510 °C for 12 h + Rolled at 400 °C + Aged at 225 °C[312]	331	436	17.8
Mg-2Zn-2Gd	Gravity permanent mold cast[309]	71	135	5.5
Mg-6Zn-2Gd		89	170	4.5
Mg-2Zn-10Gd		119	146	1.5
Mg-6Zn-10Gd		116	144	1
Mg-10Er-2Cu	Cast + homogenized at 450 °C for 24 h + Extruded at 430 °C[313]	320	380	15

Table 8. Relative CRSS of deformation modes operating in magnesium.[69]

Slip/Twinning	Plane	Direction	Relative CRSS
Basal < a>	0002	$11\bar{2}0$	1
Prismatic < a>	$1\bar{1}00$	$11\bar{2}0$	1–12
Pyramidal < c + a>	$11\bar{2}2$	$11\bar{2}3$	1–12
Extension twin	$10\bar{1}2$	$10\bar{1}1$	1–4
Contraction twin	$10\bar{1}1$	$10\bar{1}2$	–

observed in the TZ52 alloy (Mg-5Sn-2Zn). Despite the sheet texture in all of the alloys, with the basal planes of the crystals parallel to the rolling direction, the high ductility of the Mg-5Sn-2Zn alloy was attributed primarily to grain refinement. Furthermore, improvements in ductility were also observed in other Mg-Sn alloys, such as the Mg-8.32Sn-1.85Zn-0.17Mn (wt%) alloy, which shows randomized texture, <c + a> slip activity, and suppression of contraction twins.[322]

4.1.2.2. Mg-Zn-based alloys

Mg-Zn alloys such as ZK alloys, Mg-Zn-Ca alloys, etc. have recently been demonstrated to have improved strength and ductility.[323,324] Given the high solubility of Zn in Mg at RT, it is typically expected that the strengthening effects come from solid solution strengthening of Mg. Furthermore, it has been reported that the addition of trace amounts of alloying additions, such as Zr and Ca, produced ultra-fine grain sizes of <1 µm after thermomechanical treatment.[324] The formation of secondary phases such as $Ca_2Mg_6Zn_3$ precipitates and Mg_2Ca in Mg-Zn solid solution suppresses the formation of basal texture by pinning the grain boundaries and aiding in texture randomization. The Mg-2Zn-0.6Ca (wt%) alloy demonstrates an excellent elongation to failure of 30% when tensile loaded along the extrusion direction due to its weaker texture, the presence of fine precipitates of $Ca_2Mg_6Zn_3$ and refined grain size.

4.1.2.3. Mg-Ca-based alloys

Ca is one of the most effective alloying elements apart from the rare earths for improving the ductility of Mg.[12,325] Umer et al deeply investigated the effect of 0.5 wt% Ca on the mechanical properties of AZ31 magnesium alloy.[15] The results revealed that addition of Ca lead to significant improvement in RT formability at high and low punch speed as compared to the AZ31 and several other Mg and Al alloys (Figure 22). The microstructural characterization confirmed the formation of $(Mg,Al)_2Ca$ intermetallic particles in AZ31-0.5Ca, which reduced the basal texture intensity. Moreover, IGMA and VPSC calculations revealed that these alloying additions activated non-basal deformation slip activity, such as prismatic slip activity, in addition to basal < a> slip. The authors suggest that this approach can help in eliminating typical steps such as grain size reduction, texture engineering and other steps related to microstructure control. Hence, more research should be focused on this area to enable highly ductile and strong magnesium alloys doped with a tiny amount of inexpensive alloying additions.

4.1.3. Modified traditional magnesium alloys

Several commercial magnesium alloys, such as the AZ, ZK, and AM series alloys, can be modified with the addition of RE and other elements, such as Ca, Sn, Zn, etc., to realize a broad range of properties.[326,327] Fu et al. added the RE elements La and Sm and the non-RE element Ca to a commercial AZ91 alloy to study the effects these elements on the properties of the AZ91 alloy.[326] These alloying additions led to the formation of different secondary phases, such as $Al_{11}La_3$, Al_2Sm, and Al_2Ca, all of which aided in refining the microstructure, eliminating the $Mg_{17}Al_{12}$ phase, and improving the tensile strength. While all of those elements also improved ductility, the authors reported a significant increase in ductility, to 26%, with the addition of the RE elements Sm and La, as shown in Table 9.[326] Similarly, Trang et al. reported a modified RE-free alloy with the composition of Mg-3Al-1Zn-1Mn-0.5Ca (wt%) (represented as AZMX3110 in Figure 23) and demonstrated an Erichsen index (IE) value of 8 mm.[327] The IE value measures the stretch formability of the material. The IE values of traditional Mg alloys are given in Figure 23. Slight modification of traditional AZ31 alloys may make it easier to adopt a new alloy due to its similarity with the AZ31 alloy, which is commonly used in the automotive sector. Careful design of Mg alloys is

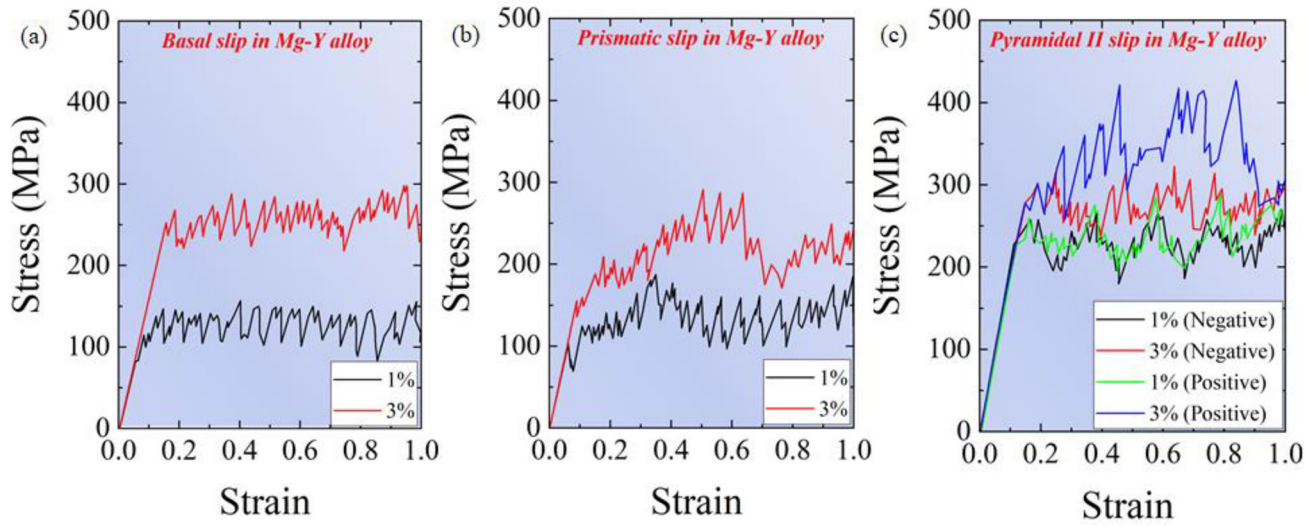

Figure 20. (a–c) Simulated stress-strain curves of Mg-(1-3)Y (at%) alloy on basal, prismatic, and pyramidal II planes at 0 K, respectively.[273]

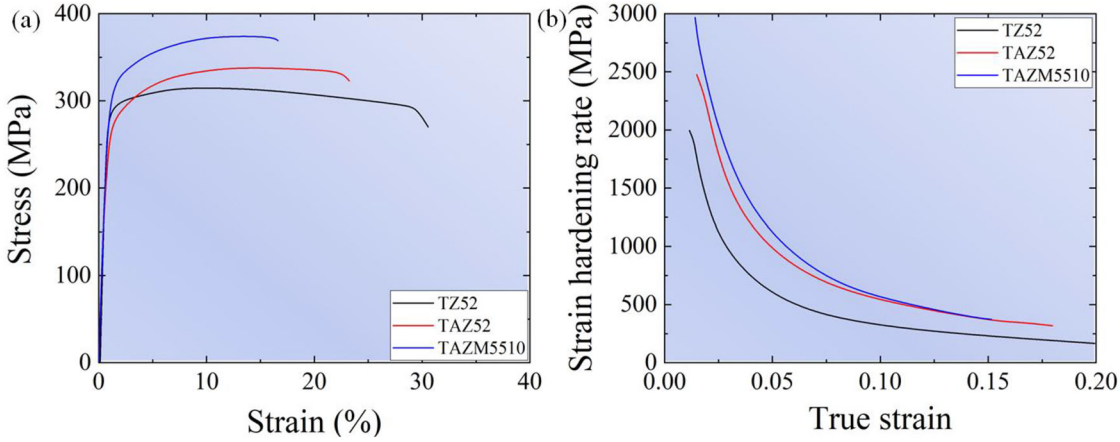

Figure 21. Engineering tensile stress-strain curves and (b) strain hardening rate of Mg-Sn alloys.[320]

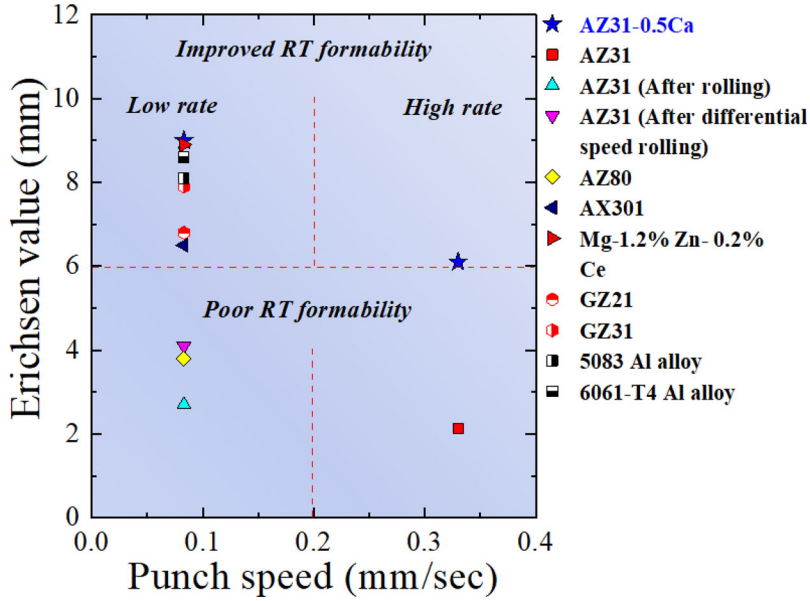

Figure 22. Erichsen values of AZ31-0.5Ca (wt%) at different punch speeds in comparison to other Mg and Al alloys.[15]

crucial such that the effects of grain refinement, solute segregation, texture engineering, etc. are realized to enhance ductility, while maintaining strength and other useful properties.

4.1.4. Outlook

In this section, the ductility response of magnesium alloys containing REs and other common alloying elements is discussed across a range of binary, ternary, and complex alloys. The mechanisms of ductilization of magnesium alloys, i.e., texture randomization, reduction in the CRSS differences between basal $<a>$ slip and non-basal $<c+a>$ slip, solute segregation, and precipitation, apart from grain refinement, are broached. These mechanisms could serve as a guide for future alloy design for improved ductility. It should be noted that thermomechanical processing is also crucial in improving the ductility of Mg alloys and will be discussed in subsequent sections. Furthermore, this section provides insight into the most promising solutes and alloying elements that can potentially accelerate the synthesis and design of extremely ductile and formable Mg alloys.

Table 9. Tensile properties of modified AZ91 alloys with RE and other alloying additions.[326]

Material	YS (MPa)	UTS (MPa)	Ductility (%)
AZ91	186	335	17
AZ91-1.5Ca	176	320	23.5
AZ91-0.5Sm	156	308	25.5
AZ91-0.3La	180	330	26
AZ91-1.5Ca-0.5Sm-0.3La	177	312	13

4.2. Severe plastic deformation for enhancing magnesium ductility

Among the various thermomechanical processes used to modify the structural features and enhance the associated mechanical properties of Mg alloys, severe plastic deformation (SPD) methods show very significant and promising results. Through SPD processes, a large degree of plastic deformation is introduced into a sample, mostly without any change in its dimensions, leading to a significant change in the structural and textural features of the SPD-processed sample. With such processing methods, ultrafine- or even nano-grained structures surrounded by non-equilibrium GBs with a high angle of misorientation (high angle grain boundaries, HAGBs) can be achieved, as shown in Figure 24. In addition to the structural modification, SPD methods can also reduce the fraction of pores that are generally observed after primary processing methods, like the powder method. In terms of Mg alloys, SPD is generally found to have a high capacity to control the texture and enhance the ductility of these alloys. The most effective SPD methods, including equal channel angular pressing (ECAP),[328–333] high pressure torsion (HPT),[185,334–338] accumulative roll bonding (ARB)[188–190,339,340] and differential speed rolling (DSR),[206,341–345] and their role in enhancing the ductility of Mg alloys will be presented in the following sections.

4.2.1. Equal channel angular pressing (ECAP)

In ECAP, a specimen is subjected to shear deformation when it is pressed through two intersecting channels with the same cross-section (die) (Figure 25a).[346] The

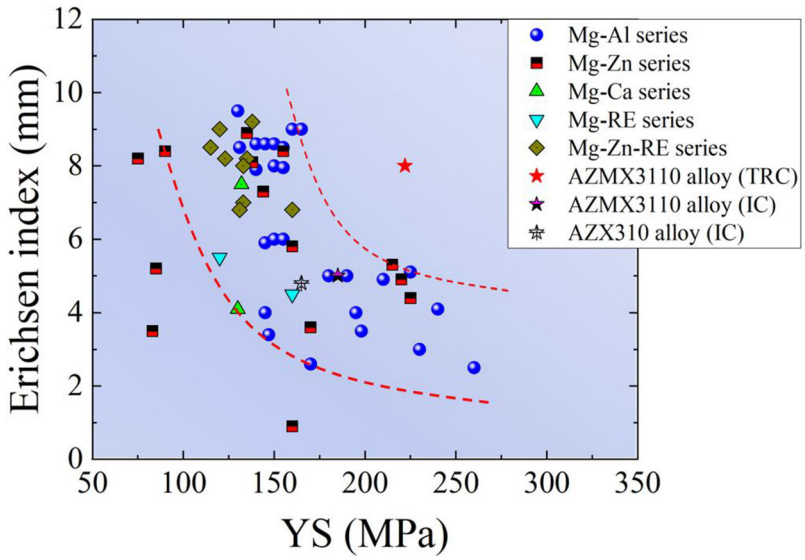

Figure 23. Yield strength and Erichsen index (indicative of the stretch formability) of different Mg alloy sheets including the recently developed TRC-AZMX3110, which exhibited excellent combination of formability and ductility. Image is reproduced with permission from Ref.[327]

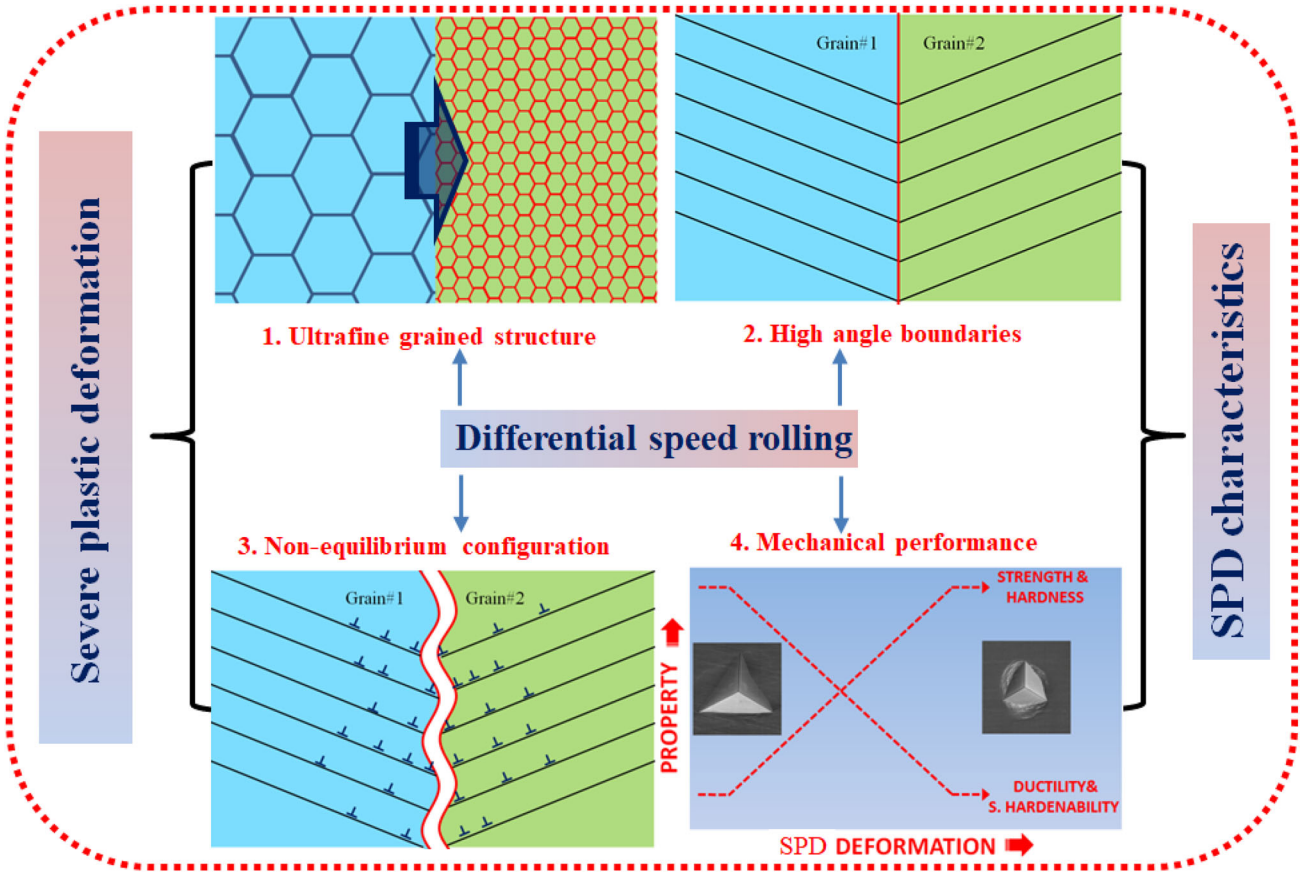

Figure 24. Microstructural features and mechanical performance of metallic materials evolved after severe plastic deformation.

nature of the shear deformation introduced by the ECAP process and the structural features that evolve from it are related to the die geometry, deformation path, processing temperature, and number of ECAP passes. For processing of Mg alloys by ECAP, elevated temperatures should be employed to avoid fracture at low temperatures. In this regard, various works have reported on the structural evolution and mechanical properties of Mg alloys subjected to elevated-temperature ECAP deformation.[173,333,348–353] Elevated-temperature deformation leads to the activation of non-basal slip systems, which in turn can enhance plasticity during the processing and result in the formation of fine DRXed grains.[199,333,351,353]

Regarding the ductility of Mg alloys subjected to ECAP deformation, several works have shown insignificant improvements in ductility as compared to non-deformed or coarse-grained specimens. For example, tensile tests carried out on WE43 Mg alloys deformed by ECAP at elevated temperatures of 285–335 °C showed that the ductility of the alloys decreased with an increasing number of ECAP passes, where a total elongation of 12% was achieved in the alloy deformed by 8 ECAP passes as compared to an elongation of ~33% in the non-deformed sample (Figure 25b).[333] This behavior is attributed to the loss of strain hardening in the sample deformed by ECAP (8 passes), which in turn is related to the formation of a dense microstructure with a large number of dislocations after ECAP deformation under the employed conditions.

In order to improve the ductility by ECAP deformations, processing parameters including processing temperature and the number of ECAP operation, in addition to the composition of the alloy, should be controlled and oriented to increase the dynamic recovery (DRV) rate of the material during deformation and, hence, to reduce dislocation density. As mentioned earlier, ECAP deformation of Mg alloys is usually carried at high temperatures to avoid fracture due to the lack of slip systems at RT. Here, one can confidently state that the optimum selection of deformation temperature is of significant importance, as the temperature should be high enough to achieve uniform plastic deformation without any fracture and to increase the rate of DRV and reduce the dislocation density without significant grain growth; all of these factors together can lead to an enhancement of the ductility of the processed alloy. He et al. investigated the microstructure and related mechanical properties

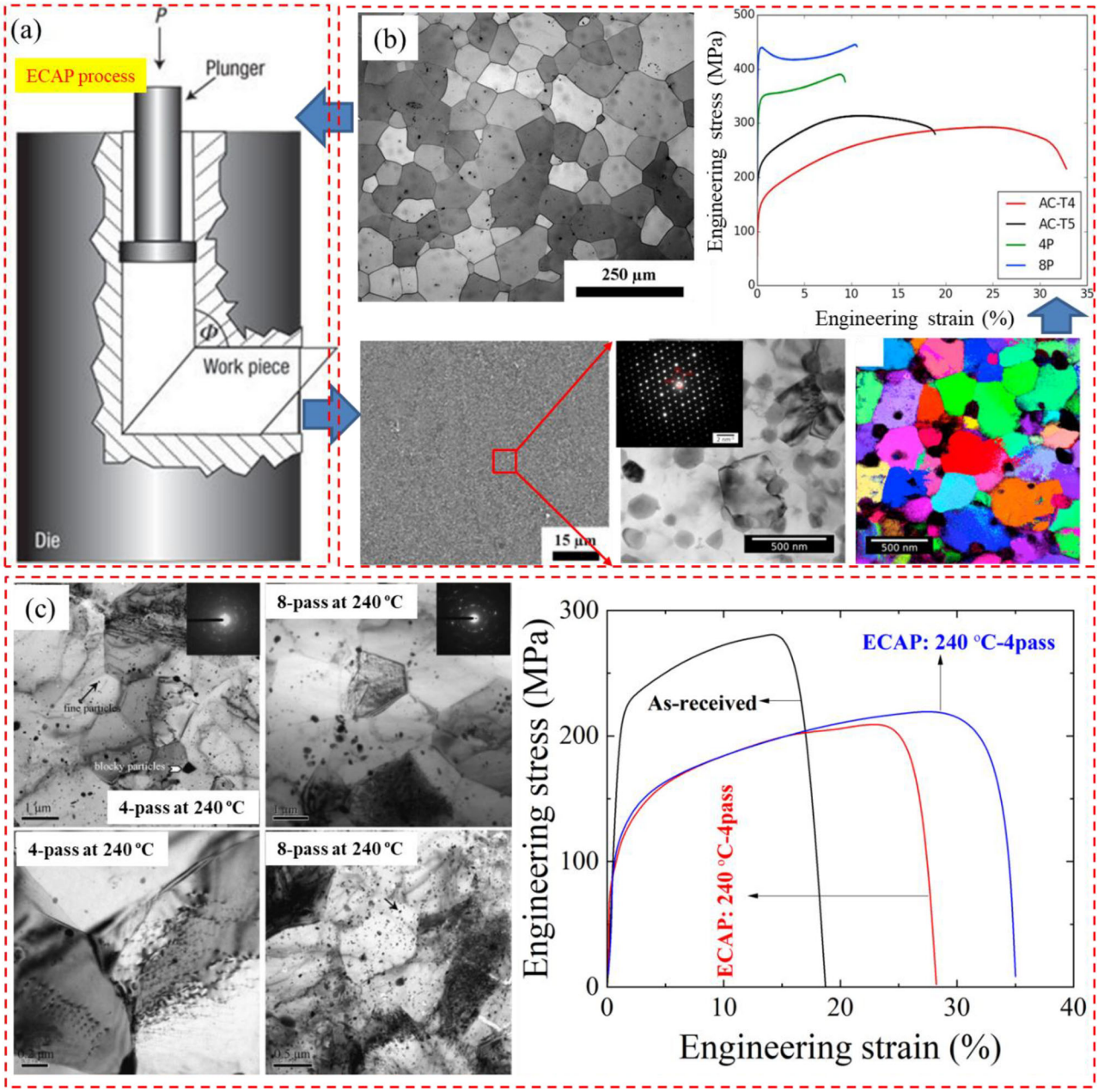

Figure 25. (a) Schematic illustration of ECAP process,[346] (b) Microstructure and tensile properties of WE43 Mg alloy samples subjected to 8-pass ECAP deformation at 285–335 °C. The OM, TEM and EBSD maps presented in this figure hows the evolution of ultrafine grained structure with a high density of dislocations,[333] (c) TEM images and tensile properties of ZK60 Mg alloy samples subjected to 4- and 8-pass ECAP deformation at 240 °C.[347]

of a ZK60 Mg alloy subjected to ECAP deformation (4 and 8 passes) at 240 °C.[347] Their results showed that ductility was improved in the sample after ECAP deformation as compared to its coarse-grained non-deformed counterpart (35% vs. 18%), and this was attributed to the occurrence of DRV at the investigated temperature (Figure 25c). The composition of the Mg alloy can also influence DRV behavior during ECAP deformation. In this regard, the manner in which the alloy constituents change the SFE of Mg is one of the key points that control the DRV rate and, accordingly, alter the ductility of the alloy. For example, alloys in which solute atoms increase the SFE of the Mg matrix are expected to show a high DRV rate during ECAP, where the high SFE leads to less dislocation dissociation and, accordingly, to easier dislocation climb and dislocation inhalation. In addition to the processing parameters, the ductility of ECAPed Mg can be improved through short-term heat treatment at a specific temperature.

4.2.2. High-pressure torsion (HPT)

High-pressure torsion (HPT)[198,354–368] has been used extensively to induce grain refinement in metallic materials through severe plastic technologies, and nano-grained metals have been fabricated using this method. In HPT, a metallic material in the form of a disk is simultaneously subjected to a hydrostatic force (compression) and torsional straining by fixing the disk between two anvils (Figure 26a). Under such conditions, a large degree of plastic deformation can be introduced into the materials, leading to significant structural changes that are usually much more pronounced as compared to those achieved by other SPD methods. In addition to the large amount of shear deformation which can be introduced by HPT, the hydrostatic force prevents the occurrence of internal cracks during deformation, and this leads to high RT deformability of Mg alloys, and thus, to a significant grain refinement.

Several studies have reported on the structural evolution and related mechanical properties of Mg alloys after HPT deformation.[369,370,372–375] One study investigated the effect of HPT deformation at two different temperatures, RT and 150 °C, on the microstructure and superplasticity of an Mg-6Al (wt%) alloy; the results showed the evolution of ultrafine-grained (UFG) structures with a grain size of ~ 150 nm and 350 nm at RT and 150 °C, respectively.[369] The UFG structure that evolved in the Mg-9 wt% Al alloy due to HPT deformation exhibited high superplasticity (~810%) at low temperature (200 °C) (Figure 26b). Despite the large number of studies that have reported on the processing of Mg alloys using HPT, very few have addressed the effect of SPD deformation by HPT on the ductility of Mg alloys; this fact is related to the small size of the sample (disk with ~1 cm diameter) that can be deformed using the HPT technique. Generally, HPT-deformed

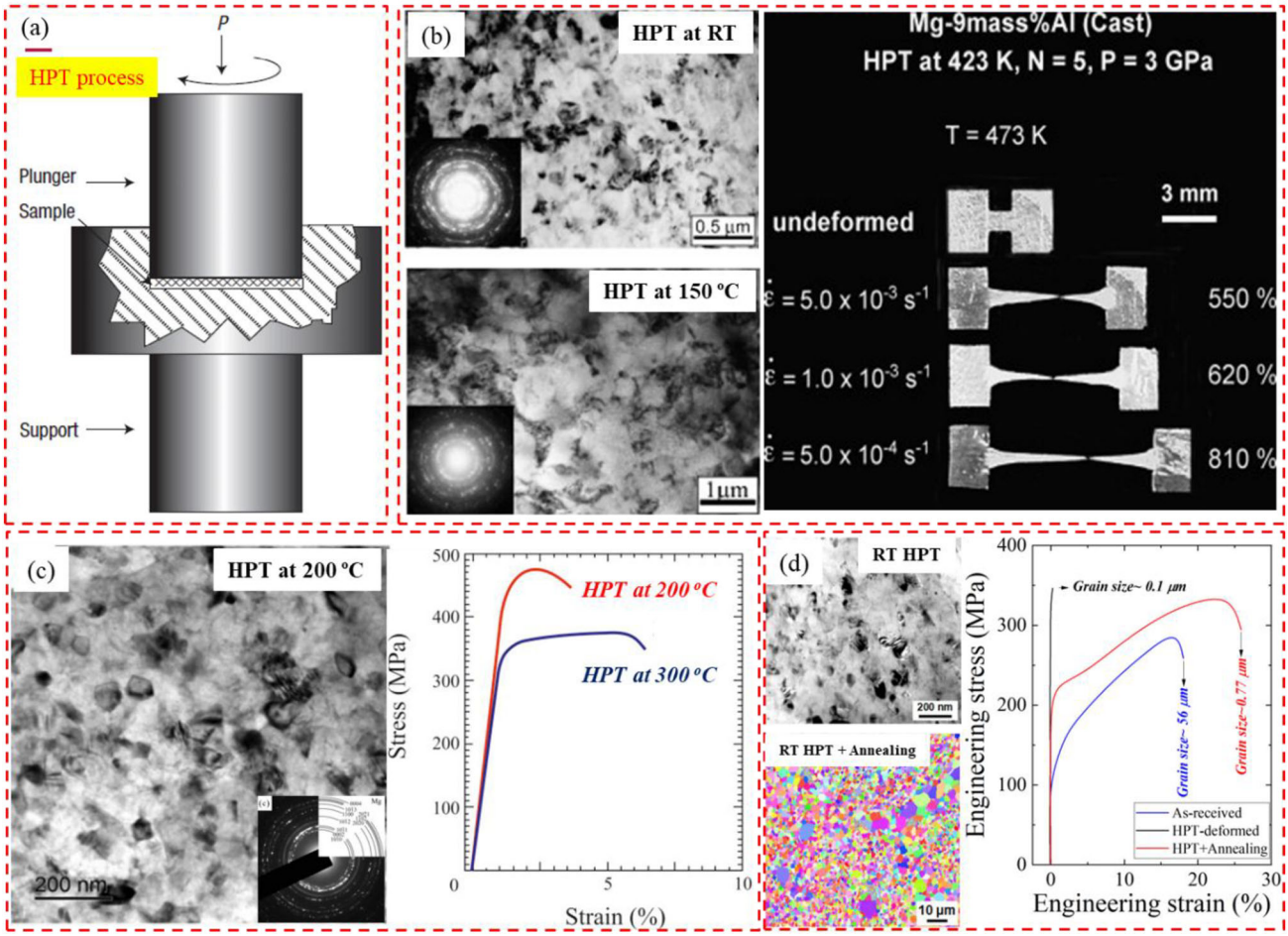

Figure 26. (a) Schematic illustration of HPT process,[355] (b) Microstructure and related superplastic behavior of Mg-9Al (wt%) alloy subjected to severe plastic deformation by HPT,[369] (c) Microstructure and tensile curves of Mg-4.7%Y-4.6%Gd-0.3%Zr (wt%) Mg alloy samples subjected to HPT deformation,[370] (d) Microstructure and tensile curves of ZKX600 Mg alloy samples subjected to HPT deformation at RT followed by annealing at 300 °C for 1 min.[371] The TEM image in (d) shows the as-HPT microstructure with ultrafine grains (~0.1 μm) and the EBSD map showing the microstructure with ultrafine grains (~0.77 μm) achieved after the HPT and annealing.

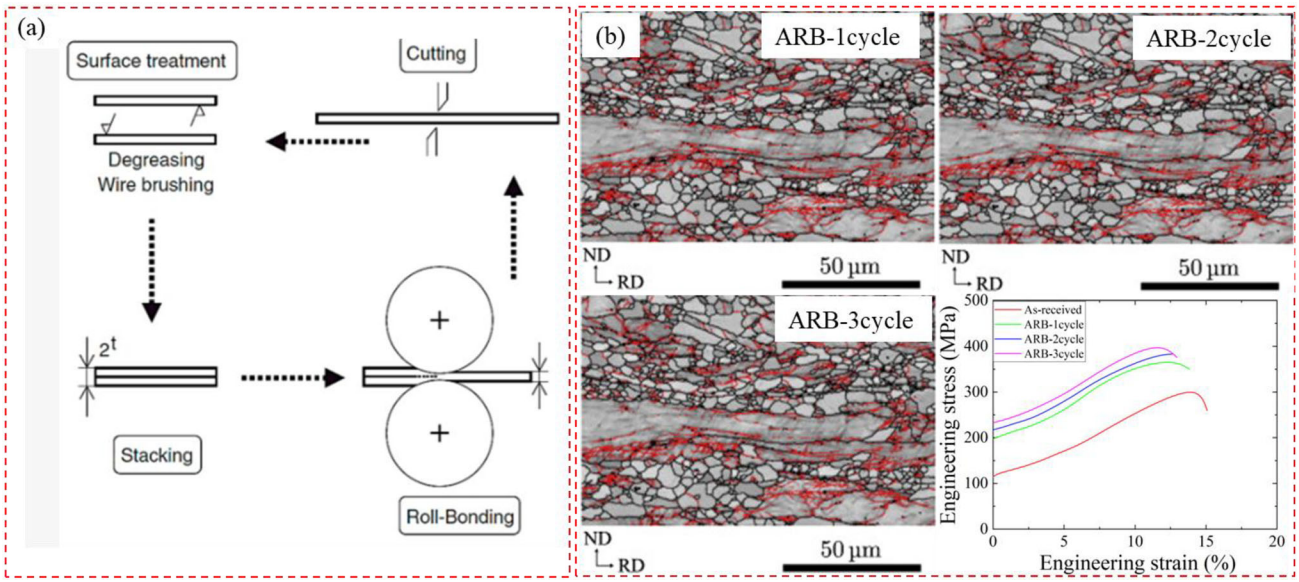

Figure 27. (a) Schematic illustration of ARB process, (b) Microstructure and tensile behavior of AM20 Mg alloy sheets fabricated by 1-pass, 2-pass, and 3-pass ARB process.[188]

Mg alloys are brittle, with a ductility of less than 5%,[370,376] which can be attributed to the low DRV rate and the large dislocation accumulation, especially when a Mg alloy is deformed at low temperatures (Figure 26c). In order to improve the ductility of HPT-processed Mg alloys without significantly reducing their strength, post-processing annealing is necessary to reduce the dislocation density through a static recovery (SRV) process. For example, high strength and improved ductility (21%) were achieved in a ZKX600 Mg alloy after HPT deformation followed by annealing at 300 °C for 1 min (Figure 26d).[371] In addition, HPT deformation followed by heat treatment at 200 °C for 20 min of a ZK60 Mg alloy resulted in improved ductility (~21.5%).[377]

4.2.3. Accumulative roll bonding (ARB)

ARB is a rolling-based SPD method that includes various processing stages, including rolling, cutting, stacking, bonding and rolling again. By repeating those stages, a large degree of plastic deformation can be introduced into a sheet sample with no changes in its thickness (Figure 27a).[188] A very early work by Perez et al. reported on the structural evolution and mechanical properties of AZ Mg alloys processed by ARB.[378] Those authors showed that grain size and grain distribution are mainly influenced by the number of ARB passes and the Al content of the alloy. To enhance bonding ability during ARB processing, elevated temperatures are usually used, but low temperatures are favorable when considering grain refinement as ARB processing at elevated temperatures can induce DRX and the growth of DRXed grains.[379] Microstructural homogeneity in the thickness direction of the processed sheet is also related to ARB processing since ARB is a rolling-based method. Schwarz et al. investigated the through-thickness microstructural homogeneity of ARB-deformed Mg alloys in an AM20 alloy (Figure 27b).[188] This work revealed that a reasonable degree of microstructural homogeneity can be achieved after three ARB cycles at 300 °C. On the other hand, under these conditions, the ductility of the alloys was dramatically reduced, and this was attributed to the formation of oxide layers in the interfaces due to the elevated processing temperature and the evolution of strong basal texture. Accordingly, a lower processing temperature should be used to avoid the formation of oxide materials within the alloy. On the other hand, the lower temperature results in a reduction of the DRV rate, leading to dislocation accumulation, and, finally, to a reduction in the ductility of the ARBed alloy. Here, it is worth noting that, to enhance ductility with the ARB process, various competing factors need to be considered, such as work hardening and grain refinement on one hand and DRV and interfacial oxidation layers on the other. Since low-temperature deformation prevents oxidation but also reduces the DRV rate and bonding-ability, a two-stage processing technique may be useful, in which warm ARB deformation, to ensure less oxidation and higher bonding-ability, is followed by heat treatment at specific temperatures for short time periods in order to reduce the dislocation density. In addition, proper

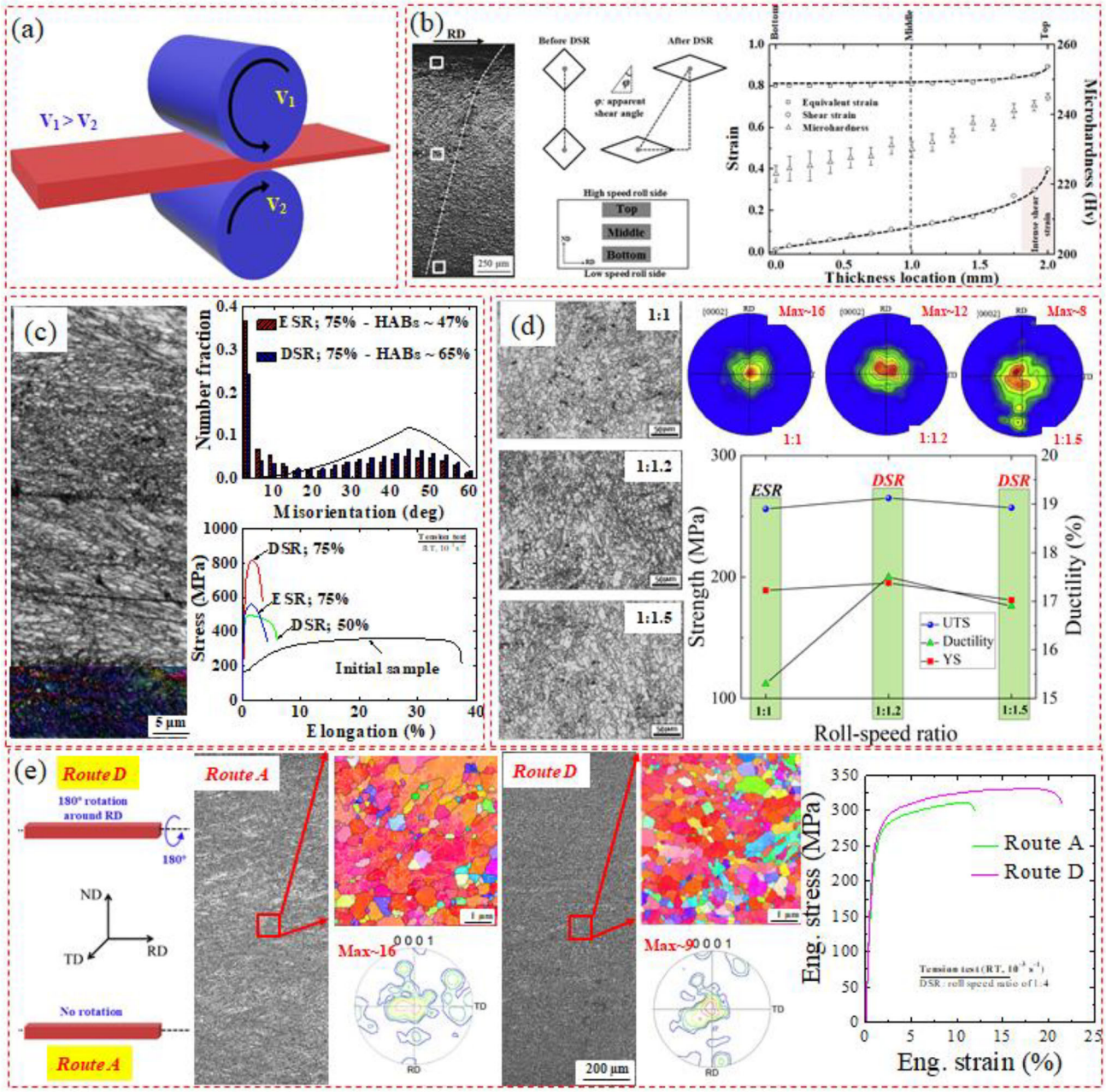

Figure 28. (a) and (b) Schematic illustration of DSR[196] and the DSR strain calculations carried out by the deviation of indentation marks,[383] respectively, (c) EBSD maps, grain misorientation distributions and mechanical properties of IF steel sample deformed by DSR and ESR processes,[384] (d) Microstructure, texture, and the related mechanical properties of AM31 Mg alloys sheets deformed by DSR process at various roll speed ratios (1:1, 1:1.2, and 1:1.5),[380] (e) Microstructure, texture, and the related mechanical properties of AZ31 Mg alloys sheets deformed by DSR process using two routes A (no rotation between successive passes) and route D (180° rotation around the rolling direction of the sheet).[206]

surface preparation and brushing before stacking and re-rolling of the sheet during ARB can also prevent the formation of oxides within the ARB-fabricated sheet.

4.2.4. Differential speed rolling (DSR)

Among the SPD methods, DSR is the only process in which the dimensions of the specimen change after deformation.[211,380–382] During DSR, metallic sheets are rolled using two identical rolls that rotate at different speeds (with the difference referred to as the roll speed ratio), leading to a reasonable amount of shear deformation introduced throughout the thickness of the sheet (Figure 28a).[196] Indentations created throughout the thickness of a sheet before DSR deformation have been used to measure shear strain and its distribution during DSR (Figure 28b).[383] The deviation of the marks proved the capability of DSR

to introduce an additional degree of deformation as compared to the equal speed rolling process (ESR) (conventional rolling).

Shear deformation and its distribution contribute more effectively to the microstructural evolution and texture modification of metallic sheets treated with DSR as compared to those deformed by ESR. Hamad et al. reported the microstructural features and mechanical properties of IF steel sheets deformed by DSR, with a roll speed ratio of 1:4, vs. sheets treated with ESR (1:1) under the same thickness reduction, rolling temperature (75%, RT), and number of passes (4) (Figure 28c).[384] This work showed that, under the employed conditions, DSR severely deformed the IF steel sheets, leading to ultrafine-grained structure (~0.4 μm) surrounded by HAGBs and to high strength (~800 MPa). Based on the structural features and the mechanical properties of DSR-deformed metals, and due to the reduction in thickness, the authors suggested that DSR can be considered an SPD-like process. In addition, owing to the open-die nature of this process (two rolls), the heat generated during DSR due to plastic deformation and the friction between the rolls and sheets is readily exchanged with the atmosphere, resulting in a lower DRV rate as compared with other SPD methods and thus a higher accumulation of dislocation.[385,386] Such behavior was used to explain the higher capability of DSR for enhancing the strength of metals as compared to ECAP under the ultrafine grain size.[386] Several works have been carried out to investigate the effect of DSR deformation on the microstructure, texture and mechanical properties of metals and their alloys, including Fe,[383,387–391] Al,[392–396] Cu,[397,398] Mg,[165,166,212,399–403] and Ti.[404–407] Most of these works reported a significant improvement in the strength of the deformed materials as compared to their non-deformed counterparts, which was always attributed to grain refinement (Hall-Petch hardening) and dislocation accumulation (work hardening). As seen with other SPD methods, this improvement in strength due to DSR deformation usually coincides with poor ductility; hence, DSR deformation should be followed by annealing to enhance ductility.

Interestingly, DSR exhibits a great deal of potential for the processing and fabrication of Mg alloys with both high strength and enhanced ductility, and this effect can largely be achieved without any further heat treatment.[206] This is because of the capacity of DSR to reduce the intensity of the strong basal texture that evolves after the conventional rolling process. The through-thickness microstructural homogeneity which can be achieved by DSR processing is another factor contributing to ductility improvement. These factors, texture weakening, and microstructural homogeneity are controlled through DSR processing parameters such as roll speed ratio. For example, Chang et al. investigated the effect of roll speed ratio (1:1, 1:1.2, and 1:1.5) on the texture evolution of an AM31 Mg alloy deformed by DSR at 300 °C, and revealed that DSR processing at a roll speed ratio of 1:1.5 resulted in a weaker basal texture as compared to the other speed ratios, leading to improved ductility under these conditions (Figure 28d).[380] In addition, the basal texture characteristics are influenced by other parameters, such as DSR temperature,[165,341] total thickness reduction,[167,408] thickness reduction per pass,[409] and number of operations.[393] Most previous studies did not consider the effect of structural homogeneity on ductility. Hamad and Ko reported on the effect of DSR route on microstructural homogeneity and texture characteristics of AZ31 Mg alloy sheets deformed at a roll speed ratio of 1:4, total thickness reduction of 50% (two passes) and rolling temperature of 150 °C.[206] The results showed that the DSR deformation using route D, in which the sheet is rotated by 180° around its rolling direction between the two passes, resulted in a homogeneous fine-grained structure (~1.2 μm) with a weak basal texture (Figure 28e). The evolution of this structure was found to enhance the ductility of the AZ31 Mg alloy sheet as compared to that of the sheet deformed by the route in which no rotation was applied between successive passes.

4.3. Magnesium composites

Magnesium matrix composites, another emerging class of magnesium-based materials, provide a unique opportunity to tailor the properties, such as strength, ductility, surface reactivity, thermal properties, etc., of the matrix through the selection of reinforcement. These materials are lightweight, generally nontoxic, and abundantly available, and hence have the potential to provide an all-in-one solution to material design problems through minor alterations of their chemistry. Over the past two decades, a significant amount of research has been done in the domain of magnesium composites, particularly relating to their mechanical behavior. The design, development and applications of magnesium matrix composites rely on some crucial factors:

i. Primary and secondary processing techniques used to synthesize the composites.

ii. Post-processing treatments such as annealing, aging, etc.
iii. Compatibility of the matrix (pure magnesium or a magnesium alloy) and reinforcement.
iv. Characteristics of reinforcement type, morphology, shape, amount, length scale and spatial distribution.
v. Interfacial integrity of matrix reinforcement.

These composites are designed based on global parameters such as particle volume fraction, particle shape, average size and orientation which serve as variables in the study of the overall strength, ductility and fracture toughness of the composites.[410] Traditionally, metal matrix composites are notorious for their very limited ductility due to the presence of reinforcements of micron and sub-micron length scales. Reinforcements, depending on their size and shape, typically act as crack initiation sites for several reasons, such as matrix-reinforcement decohesion, particle breaking, particle clustering/agglomeration, inhomogeneity in the matrix, etc. In this section, the ductility of magnesium matrix composites with both micro- and nano-scale reinforcements is broached. To promote an understanding of the deformation mechanisms and the ductility of the composites, in this article, the magnesium matrix composites are classified into different subsections based on reinforcement type, i.e., ceramic-based, carbon-based, and metal-based, with each subsection addressing both micro- and nano-composites.

4.3.1. Composite fabrication and processing parameters

Fabrication of Mg matrix composites necessitates the use of refined processing technology compared to that used to make Mg alloys to ensure uniform dispersion and homogeneity of reinforcements in the matrix. Over the years, several techniques have been specifically developed for the synthesis of magnesium micro- and nano-composites. These can be broadly classified into (i) liquid-state and (ii) solid-state processing techniques are briefly discussed below.

4.3.1.1. Liquid-state processing techniques

4.3.1.1.1. Disintegrated melt deposition (DMD). Disintegrated melt deposition (DMD) is a processing technique designed to synthesize lightweight metals such as Al and Mg, their monolithic alloys and composites. To synthesize composites, the matrix material (pure Mg or Mg alloy), in the form of chips or chunks, is added to a graphite crucible along with reinforcement particles in a sandwich pattern to ensure a homogenous presence of reinforcement particles in the matrix. These raw materials are superheated in an electric resistance furnace to a temperature of 750 °C under an inert argon (Ar) atmosphere, then the mixture of melt and reinforcing particles is mechanically stirred using a motor at a predefined speed (typically $\sim$ 450 rpm). After being stirred, the molten slurry is released through an orifice located at the base of the crucible. While the melt is being discharged, it is subjected to disintegration by two jets of Ar gas oriented normal to the melt flow direction.[411] This disintegrated melt stream is then deposited onto a steel mold, as depicted in the schematic (Figure 29). Typically, the ingot produced as a result of this technique is heat treated and hot extruded. This unique technique offers the compound merits of both spray processing and stir casting techniques as it comprises vortex mixing of reinforcements and the deposition of molten slurry onto a metallic substrate after disintegration by jets of inert gases. It also has advantages over conventional spray deposition processes, such as lower impinging velocities and moderate superheated temperatures, which aid in attaining a bulk composite material with absolutely no overspray powders. Therefore, this process offers metallurgical and other benefits, such as (i) production of finer-grained structures; (ii) lower or no segregation of reinforcements like spray processes; and (iii) simpler and more cost-effective compared to traditional stir cast processes. Hence, DMD is one of the most promising methods of fabricating Mg-based micro- and nano-composites. It should be noted, however, that this technique is viable for production of Mg nanocomposites with only $<$ 3 vol% nanoparticles as reinforcements. Addition of a higher content of nanoparticles to the matrix via this technique results in agglomeration of the particles in the matrix, leading to premature failure of the materials under mechanical loads.

4.3.1.1.2. Ultrasonic assisted casting. Ultrasonic-assisted casting is another excellent method of synthesizing Mg composites; it employs an ultrasonic probe to produce ultrasound waves, which result in acoustic streaming and cavitation in the molten slurry.[412] This method was specifically designed to improve reinforcement dispersion in the matrix of Mg nanocomposites. Figure 30a shows a schematic illustration of typical ultrasound processing of Mg composites. This technique inherits the advantages of acoustic streaming, which aids in facilitating robust convection and therefore conveying the discharged particles in

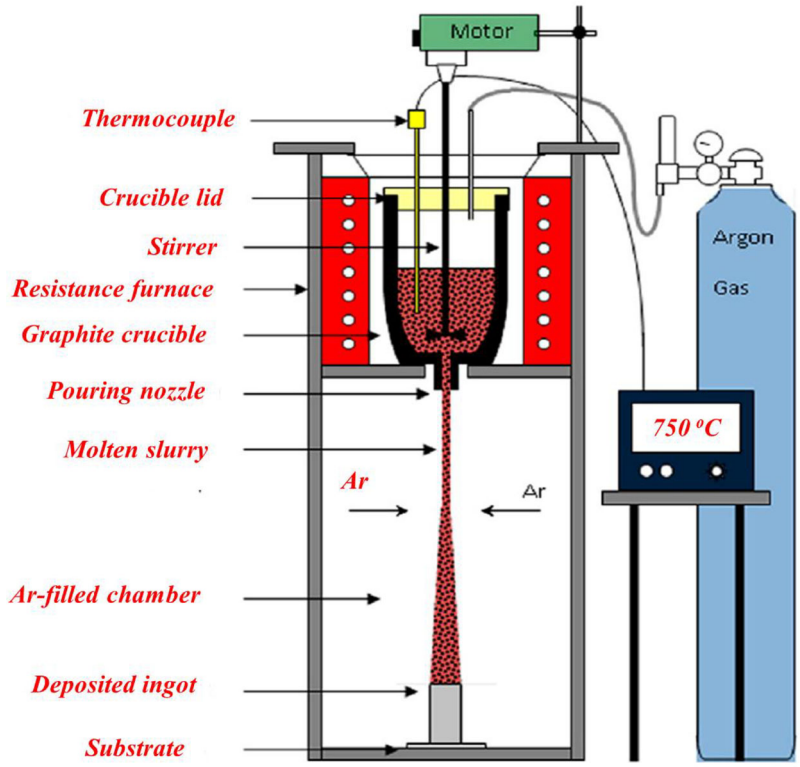

Figure 29. Disintegrated melt deposition technique.[411]

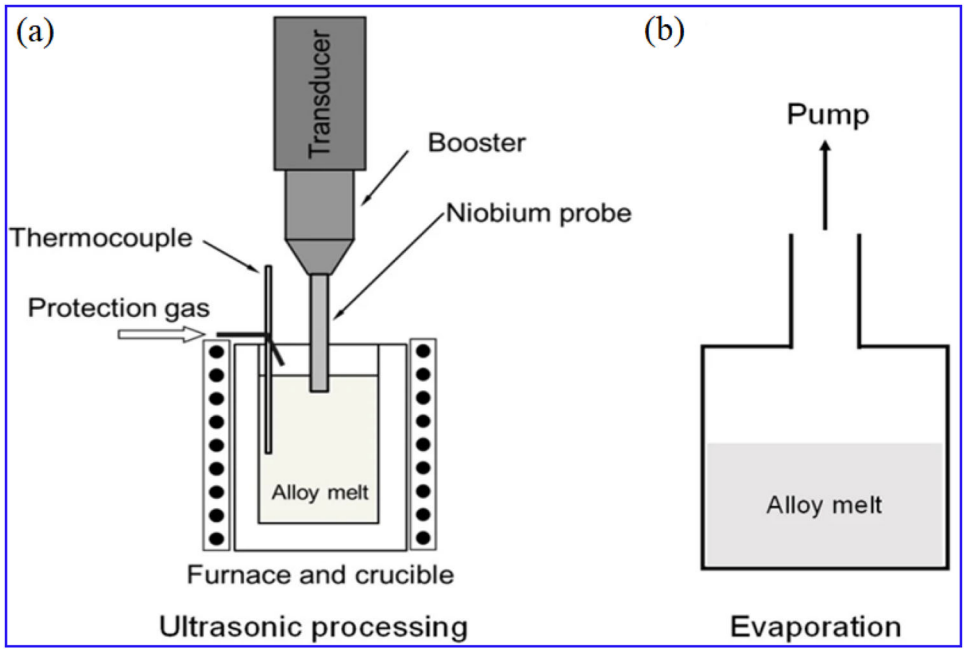

Figure 30. (a) Ultrasonic processing for nanoparticles feeding and dispersion,[412] and (b) Vacuum evaporation for concentrating nanoparticles in magnesium.[413]

the melt, and cavitation for improved reinforcement dispersion effects. It employs transient (on the order of nanoseconds) micro-hot spots that can reach extremely high temperatures (~5000 °C), heating and cooling rates (> 1010 °C/s) and pressures (> 1000 atms). Such strong conditions aid in breaking the clusters of nanoparticle agglomerates. Hence, it is particularly useful for de-agglomerating particle clusters and wetting of particles. Various matrix and reinforcement combinations of Mg alloy nanocomposites, such

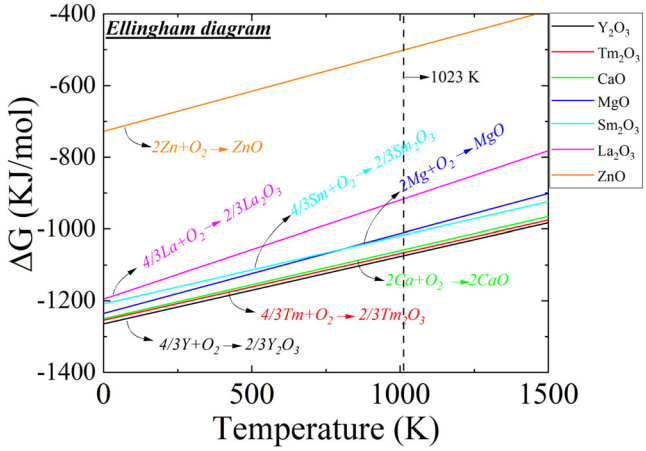

Figure 31. Ellingham diagram showing the thermodynamic stabilities of different oxides. It can be noticed that the formation of oxides of Ca, Y, and Tm is more favorable than the formation of MgO at any temperature as it lowers the free energy of the system.

as AZ31, AZ91, Z4, Z6, ZC63, ZC71, etc., have been produced using this method.

This method is also suitable for Mg nanocomposites with a lower volume fraction of reinforcements. However, recently, a simple procedural modification was demonstrated that incorporates the concept of melt vaporization to realize a Mg nanocomposite with up to 14 vol% nanoparticles uniformly dispersed in the matrix (Figure 30b).[413] Using ultrasonic processing followed by melt evaporation, a Mg-Zn melt was incorporated with 14 vol% SiC nanoparticles. As a result of this type of processing, SiC nanoparticles self-stabilized in the Mg melt. This was attributed to the synergistic effects of (i) higher thermal energy of nanoparticles; (ii) lower van der Waals forces among the particles in the Mg melt, and (iii) increased wettability of the nanoparticles in the molten Mg, resulting in an increased energy barrier that prevented nanoparticle sintering.

4.3.1.1.3. Recent advances in liquid-state processing. Recently, there have been advances in the processing of Mg nanocomposites, with the emergence of new techniques such as in-situ synthesis techniques. In-situ synthesis refers to the synthesis of nanoparticles during processing as a result of a predetermined sequence of chemical reactions. This in-situ evolution depends on the thermodynamic reactions between the matrix and reinforcements and the kinetics of the reactions. A reaction is favorable in the presence of a reactive matrix-reinforcement combination if it is thermodynamically favorable for the reaction to happen at processing temperatures, such as 750 °C. Tekumalla et al. demonstrated that the addition of ZnO to a reactive Mg-Y matrix in a Mg-1.8Y/1.53ZnO nanocomposite led to the release of new Y_2O_3 nanoparticles and formation of a Mg-Zn secondary phase in the matrix. Thus, reactive alloying elements, like Y, Ca, Th, Sm, etc., which are more reactive than Mg at processing/elevated temperatures can be employed such that they react with reinforcements in the matrix. Further ceramic reinforcements, such as CeO_2, La_2O_3, ZnO, Al_2O_3, and so on, can be chosen as they dissolve in the matrix and release ions that react with the alloying elements in the matrix to form stable in-situ nanoparticles. The thermodynamic feasibility of these reactions can be understood from the Ellingham diagram, which is shown in Figure 31. This process results in a better distribution of nanoparticles compared to conventional casting techniques, in which homogeneous dispersion of nanoparticles remains a challenge. However, this process is still in the nascent stages of development and further research is needed to understand the kinetics and thermodynamics of in-situ reactions, which eventually dictate the microstructure and properties of the resultant materials. Thus, this process has opened up a large window for the research community in the domain of magnesium-based materials.

Other advanced techniques such as additive manufacturing processes are being explored for synthesis of Mg alloys; these remain viable future directions of research into the synthesis of Mg composites.

4.3.1.2. Solid-state processing techniques

Solid-state processing techniques typically constitute traditional powder metallurgy techniques that involve blending of Mg and reinforcement powders, compaction of the powders to a billet and then sintering. This blend-press-sinter approach is depicted in Figure 32.[414] In the first stage, the metal powder is

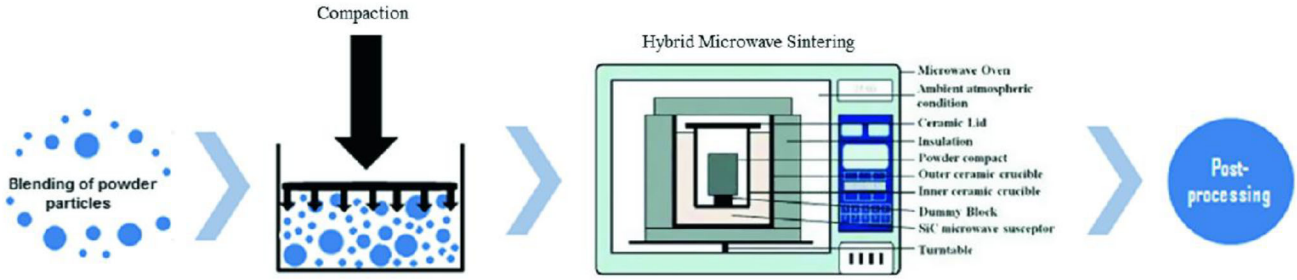

Figure 32. Blend-press-sinter-post process flow chart.[414]

Table 10. Coefficient of thermal expansion (CTE) values of different metals, ceramics and other reinforcements at 25 °C.[422]

Material	Coefficient of thermal expansion at 25 °C ($\times 10^{-6}$ K^{-1})
Mg	24.8
ZnO	2.92
CaO	12
Y_2O_3	7
Al2O3	8.1
SiC	2.77
Al3N2	5.3
Fe	10.4–12
Al	21–24
Ti	8.5–9
Y	10.6
Ca	22.3
Graphite (C)	4–8
Diamond (C)	1.1–1.3

mechanically blended with the reinforcement particles for a standard amount of time. Following the blending, the powder mixture is consolidated to a green compact. This green compact is then sintered using traditional sintering techniques or new hybrid microwave sintering techniques. Microwave sintering is an extremely promising technique for sintering of Mg-based nanocomposites that results in a ~ 90% reduction in processing time and energy consumption. One of the advantages of the solid-state approach is the ability to use multiple reinforcements, and this approach is not limited by the wettability of reinforcements in the matrix. However, one cannot synthesize complex parts using this technique. Also, there are challenges regarding the handling of reactive metal powders. In most cases, following the primary solid/liquid-state processing techniques, the obtained ingot/billet undergoes secondary (wrought) processing such as hot extrusion, rolling, forging, etc. These secondary processes aid in minimizing casting defects such as porosity, refining microstructures, improving the distribution of secondary phases and reinforcement of the Mg matrix and, lastly, breaking down the agglomerates of nanoparticles that form during casting. It is worth noting that, while several methods have been developed to synthesize Mg composites, composite technology has not yet been industrialized due to limitations in scaling up of the fabrication process to an industrial setting. Some factors limiting industrial scalability include inhomogeneity in the dispersion of nanoparticles, reactions between matrix and reinforcement, particle agglomeration, and uncontrolled distribution of the particles in the matrix. This is an interesting direction of research and development for the scientific community, and is essential to truly realize the potential of Mg composites to the fullest.

4.3.2. Magnesium/ceramic particle composites

Ceramic particles are excellent reinforcements to metallic matrices that can improve the specific strength and stiffness of a matrix. Mg has been reinforced with several micro- and nano-sized particulate reinforcements , including oxides (Al_2O_3, Y_2O_3, ZnO, TiO_2), nitrides (BN, AlN, TiN, ZrN), carbides (B_4C, SiC, TiC, ZrC), and borides (TiB_2, ZrB_2).[415,416] The addition of ceramic particles during synthesis and processing of nanocomposites results in a differential cooling rate from processing temperatures to RT due to the stark difference in the coefficient of thermal expansion and contraction of ceramic particles as compared to the Mg matrix. These varying coefficients of thermal contraction result in a mismatch in the coefficient of thermal expansion (CTE) and elastic modulus (EM) between the reinforcements and the metal matrix and is accommodated during material cooling by formation of geometrically necessary dislocations (GNDs).[417] These GNDs, formed as a result of cooling, play an influential role in the behavior of the Mg nanocomposites. The CTE values of Mg and different ceramic reinforcements are given in Table 10[419]. The CTE of most ceramics differ from that of Mg by an order of ~ 4–10. The microstructures of various ceramic reinforced micro- and nano-composites are given in Figure 33a[418] and Figure 33b.[419] An incoherent interface as a result of a mismatch in CTE is shown in Figure 33b, in a Mg/Y_2O_3 nanocomposite.

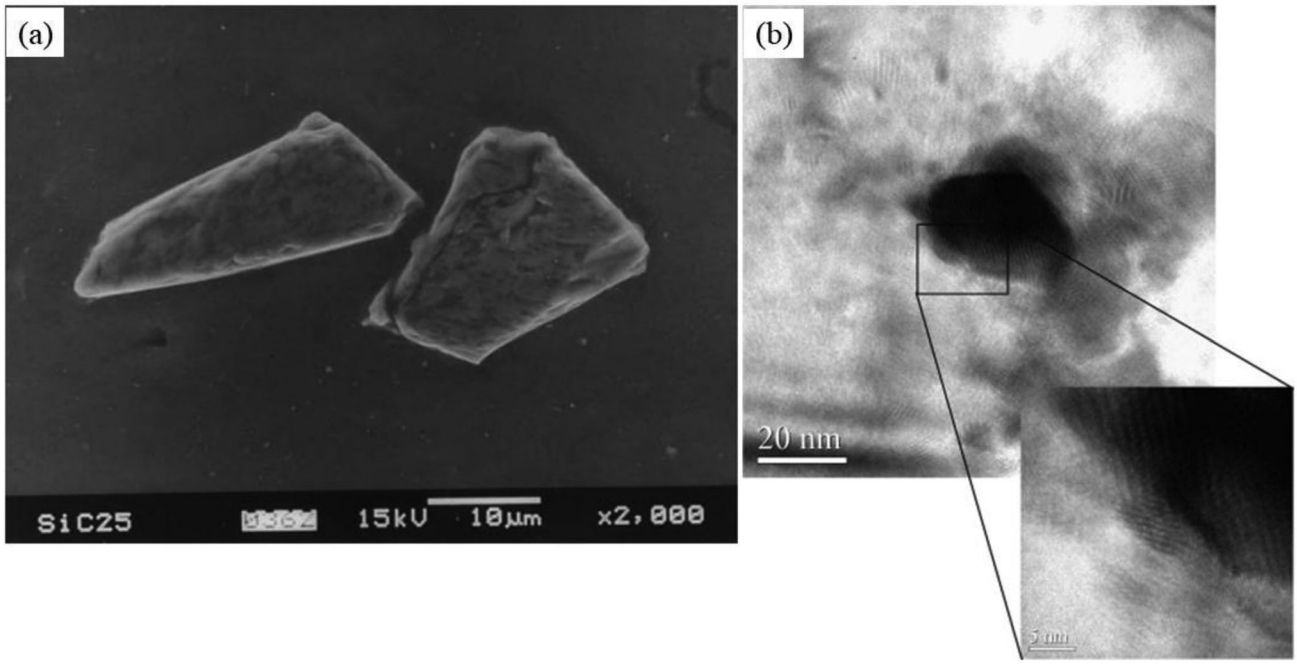

Figure 33. Microstructure of magnesium composites with (a) micro-ceramic (SiC) particles,[418] and (b) nano-ceramic (Y_2O_3) particles in pure Mg matrix.[419]

Besides pure magnesium as a matrix, these ceramic particles have also been used as reinforcements in different magnesium alloys, such as AZ31, AZ91, ZK60, El21, Mg-Y, Mg-Zn, Mg-Al, Mg-Ca, etc. The resultant materials benefit from the synergistic effects of nanoparticles and alloying elements. Their effects on ductility will be discussed in the following sections.

4.3.3. Magnesium/carbon-based particle composites

Recently, there has been a spike in interest in the use of carbon-based particles, such as graphene nanoplatelets (GNP), carbon nanotubes (CNT), carbon black, nano-diamonds, etc., as reinforcements to Mg matrix due to their tremendous potential for enhancing the strength of the matrix and reducing the weight of Mg. Figure 34 shows the microstructure of a Mg matrix with CNT and GNP reinforcements.[420,421] As seen in Table 10, the CTE of these reinforcements is lower than that of Mg by an order of about 10, which leads to generation of GNDs due to the mismatch in the CTE around the matrix-particulate interface. It should be noted that these carbon-based particles are typically added in nano-size only, and to our knowledge no attempts have been made to add micron-sized carbonaceous particles to Mg.

4.3.4. Magnesium/metallic particle composites

In addition to ceramic and carbon reinforcements, metallic particulates such as Ti, Fe, Al, Mo, Cu, Ni, etc. have been used as metallic reinforcements to Mg.[423–426] Figure 35 shows a micrograph of a Mg/15Ti micro-composite. Recently, high-entropy alloys with a combination of metallic materials and shape memory alloys such as NiTi have also been explored as reinforcements to improve the mechanical performance of Mg composites.[427] Lastly, hybrid materials with a combination of metallic and ceramic reinforcements have also been studied to realize the best combination of properties of Mg composites. Interestingly, several metallic reinforcements (such as Ti, Fe, and Y) have CTE values much lower than that of Mg.

4.3.5. Mechanical properties of magnesium composites

With the addition of micron-size reinforcements, it was generally observed that, while these reinforcements assist in improving the elastic modulus and mechanical strength of the composites, they generally lead to a substantial reduction in the ductility (by up to 80%) of the Mg matrix due to particle cracking and void formation at particle-matrix interface, leading to accelerated failure.[428] This is because micron-size reinforcements have a higher probability of containing fracture-initiating defects due to their larger size, making particle fracture more prevalent. Secondary processing such as extrusion is often used to improve the properties of composites by further consolidation of the composite and homogenization of the distribution of reinforcements, but such techniques may further increase the likelihood of particle fracture.[428] In the

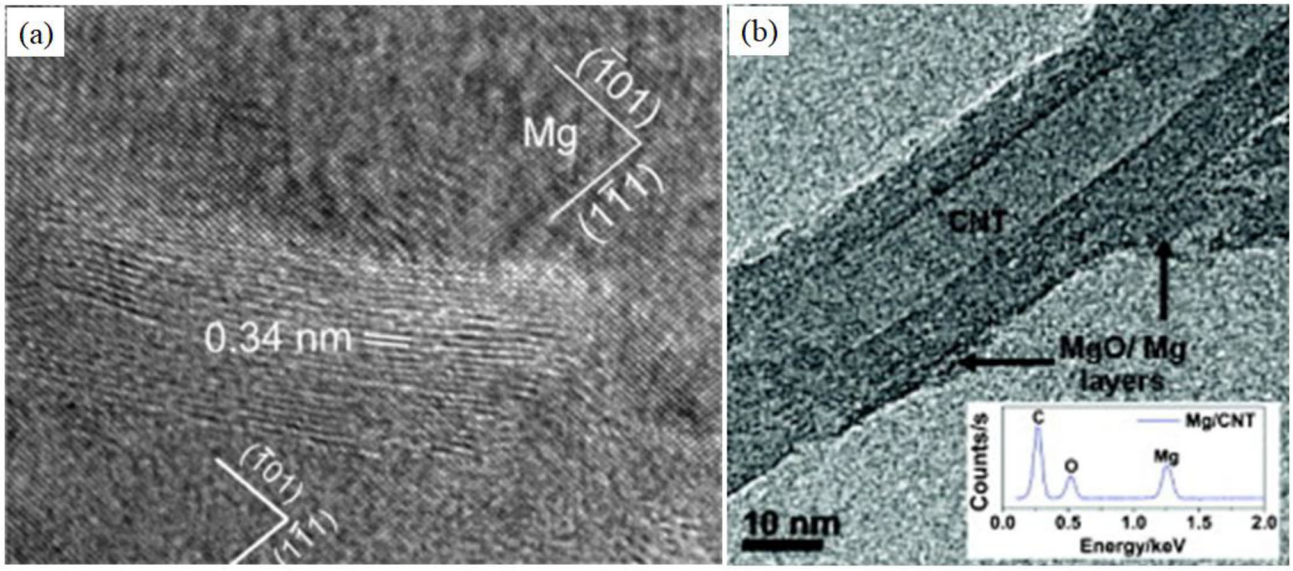

Figure 34. Magnesium matrix with (a) graphene nanoplatelets (GNP) reinforcement with an interplanar distance of 0.34 nm[420] and (b) carbon nanotubes (CNT) reinforcements.[421]

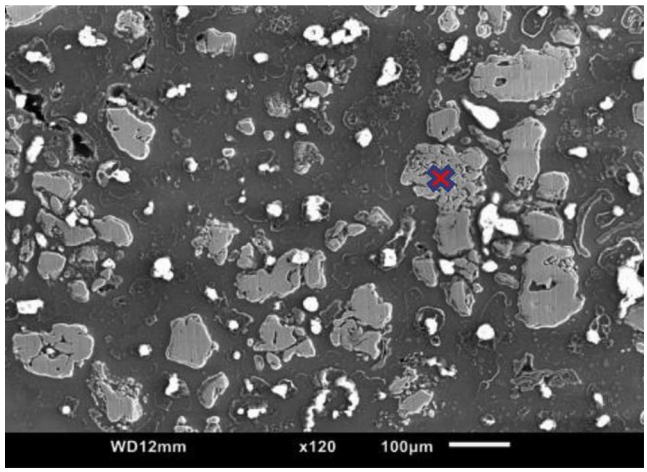

Figure 35. Micrograph of a Mg/Ti micro-composite.[427]

case of Mg nanocomposites, the addition of nano-reinforcements was revealed to aid in improving the mechanical properties of Mg; nano-reinforcements are far superior to micron-sized reinforcements, without having any adverse effects on ductility.[411,417,429] Figure 36 shows a complete picture of different reinforcements to Mg and their effects on yield strength and ductility.[411] It is clear that the addition of ceramic nano-sized reinforcements is an attractive approach to improving the mechanical properties without substantially affecting the ductility of Mg.

Furthermore, several articles have reported the possibility of improving the ductility of nanocomposites with the introduction of nanoparticles. The factors that influence the ductility of Mg composites are detailed below.

4.3.5.1. Ductility improvement through grain refinement

Grain refinement is one of the most well-substantiated methods of improving the ductility of most metals, including Mg-based materials. The ductility of a material can be improved when homogeneity during plastic deformation is established and stress concentration sites and other defects are eliminated. In the case of magnesium, owing to its HCP crystal structure, the plastic deformation ought to be homogenous when the five independent slip systems (basal and non-basal) are activated, in order to satisfy von Mises's criterion.[430] In the presence of coarse grains, deformation twinning is easily activated at high strains, leading to inhomogeneity in the deformation and, hence, premature fracture at moderate temperatures. With a refinement in the grain size, the

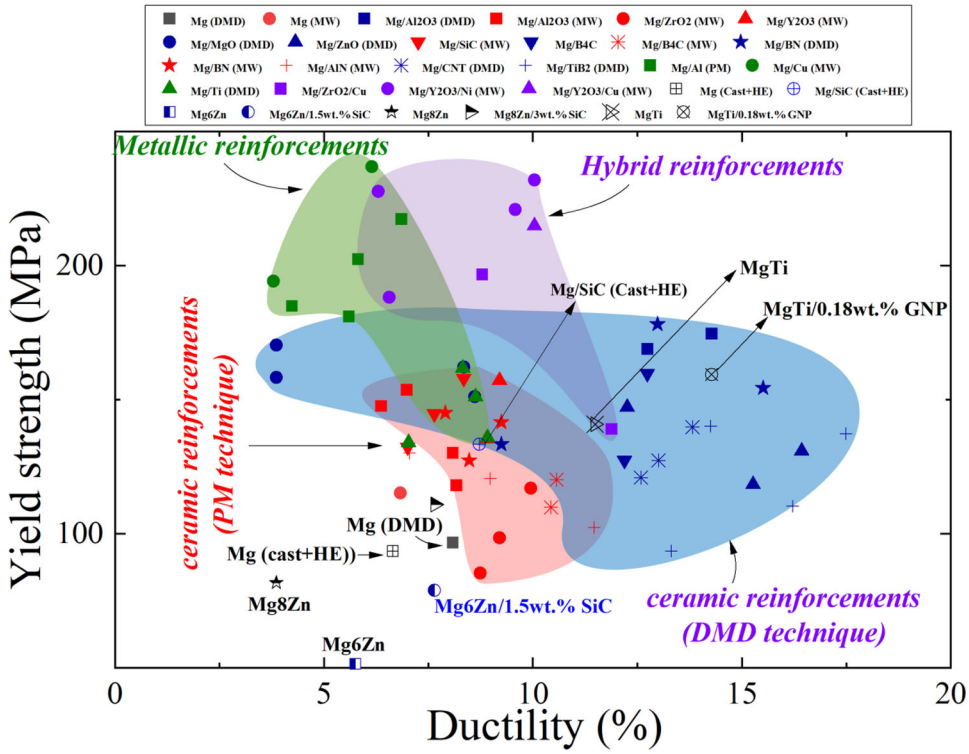

Figure 36. Bubble chart illustrating the tensile yield strength and ductility for magnesium matrix composites.[411]

resultant increased grain boundary area in the matrix allows for the homogenous distribution of stress concentration at boundaries/triple junctions, suppressing the activation of contraction twins and increasing the non-basal (<c + a>) slip activity, thereby imparting ductility at lower temperatures.[431] Hence, the grain size-dependence of ductility is attributed to the competition between contraction twinning and < c + a > slip, both of which accommodate compression along the c-axis for basal textured polycrystalline Mg.[93,432] Thus, despite the basal texture of Mg, refinement of grain size aids in improving the ductility.[433,434] However, it may be noted that this may not be valid in ultrafine-grained materials, with grain sizes on the order of submicron or lower. This is because the efficiency of storing dislocations is low in ultrafine grains, particularly alongside dynamic recovery, leaving the material susceptible to plastic instability/necking. This, in turn, limits the desirable homogenous elongation. To get around this, an alternative method of refining grain size has been identified. This route involves imparting bimodal grain characteristics, i.e., a distribution of ultrafine grains alongside a few coarse grains. While the ultrafine grains ensure the activation and homogenous distribution of non-basal slip, the coarse grains assist in increasing strain hardening, which sustains useful uniform deformation at higher strains through grain boundary sliding.[435] Thus, the presence of bimodal grains is useful to impart both high strength and uniform elongation in a material.[436] However, as shown in Figure 37, while grain refinement does have a pronounced effect on ductility, it is not the only factor that influences the ductility of Mg nanocomposites. It must be combined with other factors discussed in the following sections, as there is no general relationship between grain size and ductility among different Mg composites.

4.3.5.2. Ductility improvement by texture weakening

As discussed in the earlier sections, weakening of texture is a promising route to high ductility in Mg composites.[437,438] Creating a strong non-basal texture, e.g., by placing most of the grains in the ideal orientation with the basal plane tilting 45° from the tensile axis, has not been possible so far. There have been several reports demonstrating the ability of nanoparticles to weaken the fiber/basal texture of otherwise strongly textured magnesium by randomizing the grain orientations.[433,439] In the weakened texture, a portion of grains rotate to the direction far from the fiber texture and, hence, possess high Schmid factors. Recently, a ductility as high as 36% was reported in a Mg-1.8Y/1.5Y_2O_3 nanocomposite. This value is on par with that of commercial Al alloys and mild steels and is far superior to that of most Mg alloys and

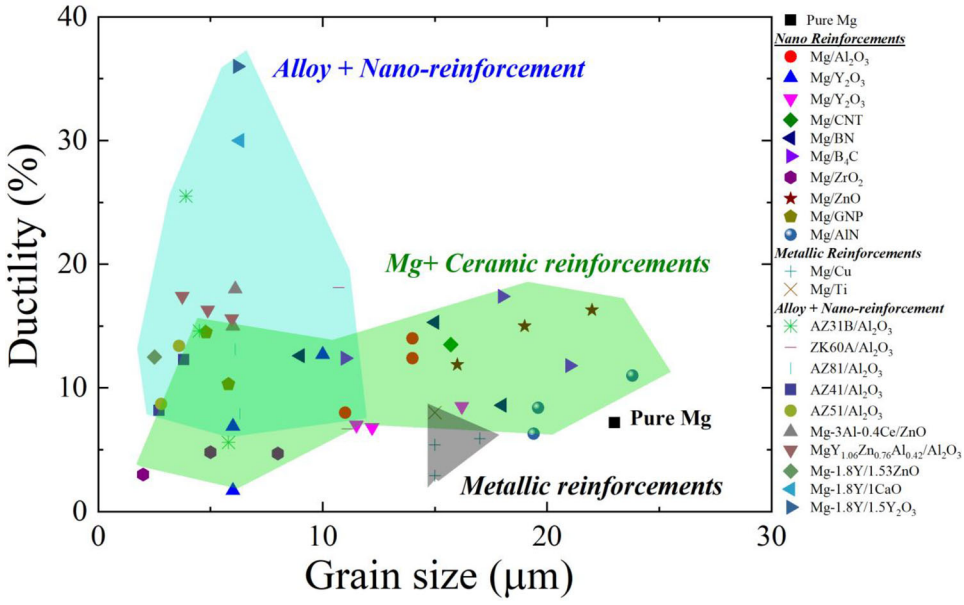

Figure 37. Influence of grain size on the ductility of magnesium nanocomposites.

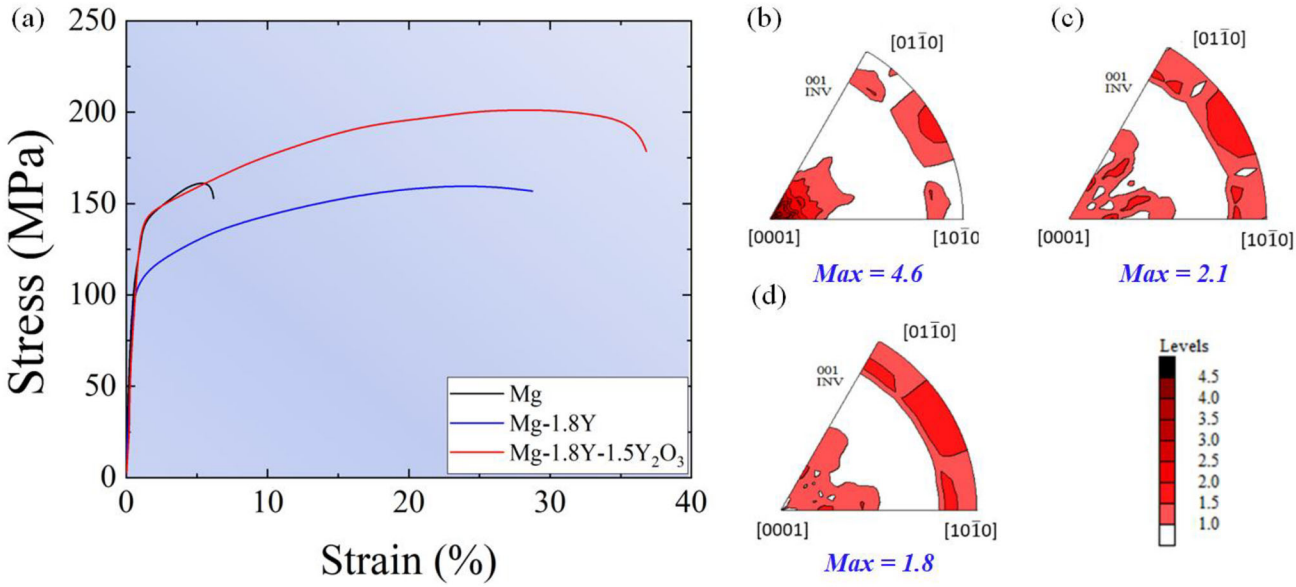

Figure 38. Influence of texture induced by Y_2O_3 nanoparticles on the ductility of a magnesium nanocomposite. (a) Tensile stress-strain curves demonstrating a ductility $>$ 35 % in Mg-1.8Y/1.5Y_2O_3 nanocomposite; Inverse pole figures from x-ray texture for (b) pure Mg; (c) Mg-1.8Y alloy; and (d) Mg-1.8Y/1.5Y_2O_3 nanocomposite, with radial direction (RD) being the projected direction.[433]

composites[411] (Figure 38). To attain such a high ductility, the weakened texture plays a dominant role over other factors such as grain refinement. While the alloying element Y did contribute to the weak texture of the nanocomposite, the presence of nanoparticles weakened the texture further, as seen in Figure 38d, which shows the lowest texture strength in the nanocomposite. This is attributed to the alteration of deformation activity owing to the interactions between nanoparticles and dislocations, which bring about an improvement in hardening behavior as well as uniform elongation, as evidenced by the tensile stress-strain curves. This contributed to an increase in slip activity, hence enhancing the ductility of the nanocomposite.[439] Similar texture weakening was induced by other nanoparticles, such as ZnO,[439] CaO,[325] GNPs,[440] CNTs,[441] B_4C,[442] etc. Thus, nanoparticle-induced texture weakening mediates a tremendously useful increase in ductility in Mg matrices.

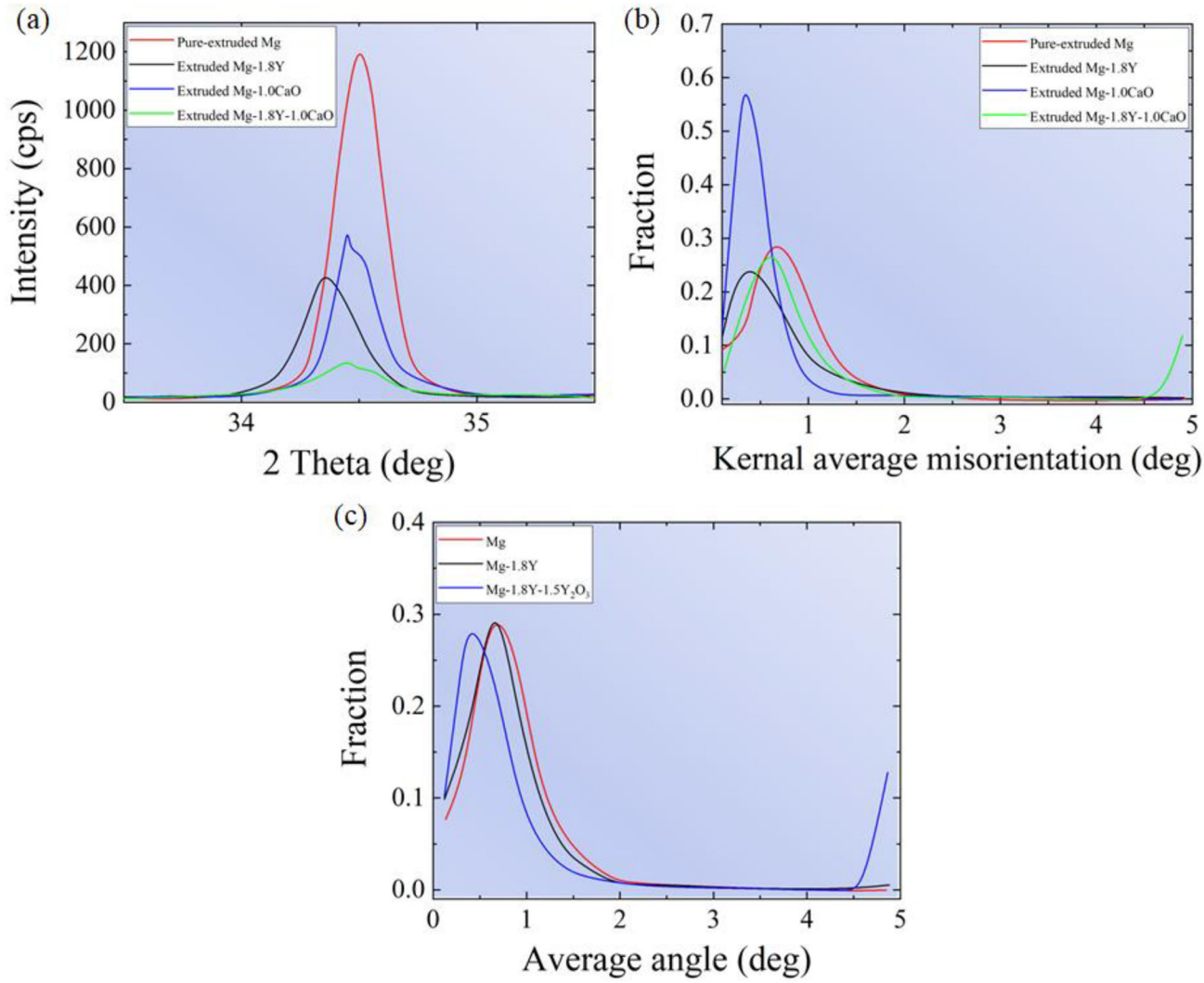

Figure 39. Schematics representing the micro-strain (elastic and plastic components) in magnesium nanocomposites. (a) Elastic micro-strain from X-ray diffraction; Plastic micro-strain as observed from the Kernel Average Misorientation (KAM) plots of (b) Mg-1.8Y/1CaO nanocomposite[443]; and (c) Mg-1.8Y/1.5Y_2O_3 nanocomposite.[433,443]

4.3.5.3. Ductility improvement through alleviation of micro-strain

Another factor that potentially contributes to the ductilization of Mg nanocomposites is alleviation of micro-strain. The micro-strain of a material is typically the sum of the elastic and plastic internal strains in the nanocomposites. Recently, Tekumalla et al.[443] estimated the elastic internal strain from XRD and the plastic strain with KAM, as depicted in Figure 39, which together provide an indirect measure of the geometrically necessary dislocations (GNDs) in the material. It is often known that the presence of lower dislocation density leads to a lower micro-strain (lower KAM value), resulting in a high ductility. Composites typically exhibit a much higher micro-strain owing to the generation of dislocations due to a mismatch in the CTE values of the matrix and reinforcements. A higher CTE differential indicates an increased dislocation density, one of the root causes of inhomogeneous deformation in a material. This is because more concentrated dislocation zones act as stress concentration sites for crack initiation and premature failure.[443] From the KAM plots, it is evident that addition of CaO and Y_2O_3 nanoparticles to a Mg-1.8Y matrix resulted in a higher micro-strain than that seen in Mg-1.8Y alone, but lower than that of pure Mg (based on the shift in the peaks). The increased micro-strain results in a substantial increase in the strain fields around the nanoparticles. To alleviate micro-strain in nanocomposites, it is necessary to carefully choose reinforcements that exhibit a lower CTE differential, i.e., CTE closer to that of the magnesium matrix, such that they result in lower GND generation.

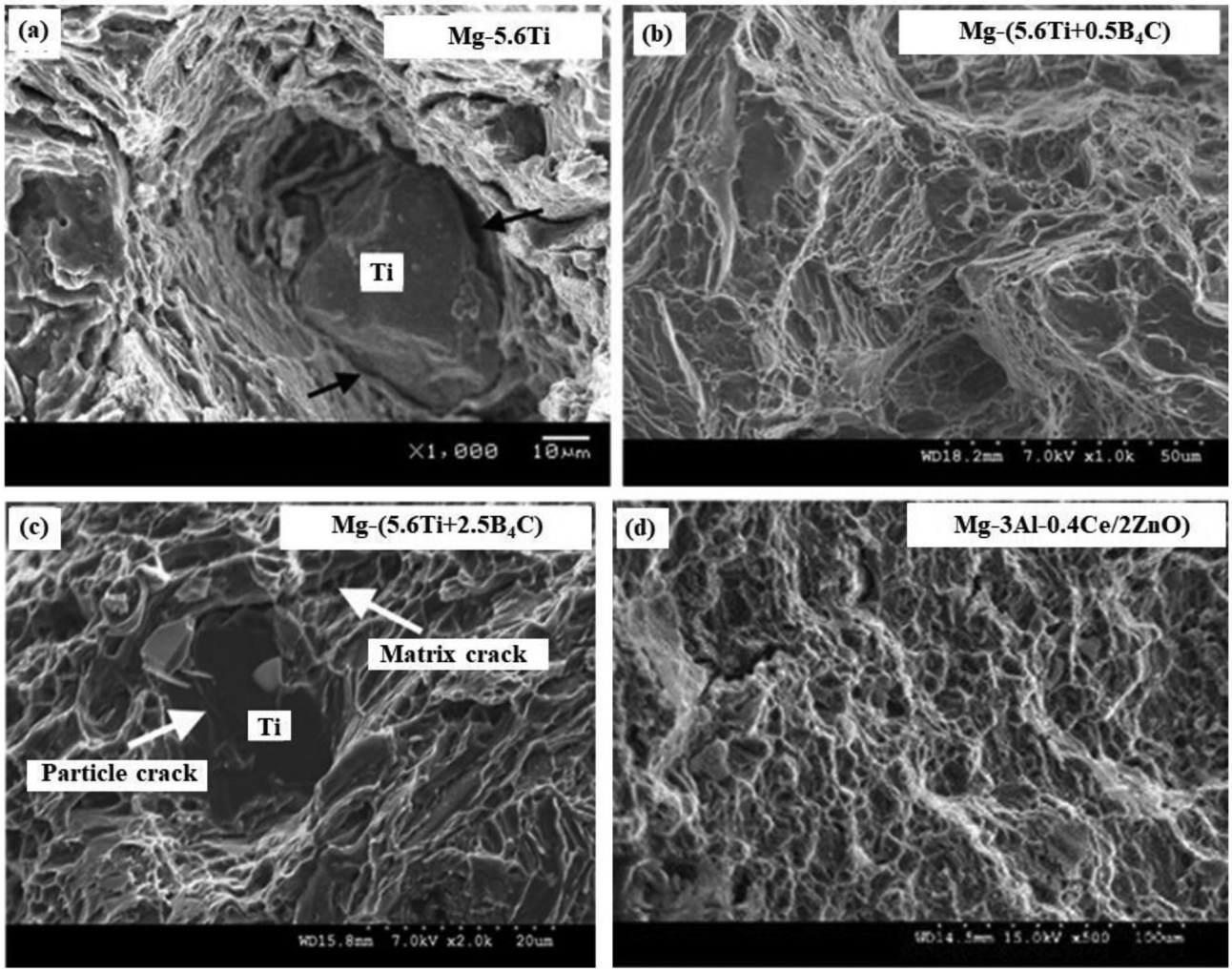

Figure 40. Representative tensile fracture surfaces of (a) Mg/5.6Ti, (b) Mg/(5.6Ti + 0.5B_4C), and (c) high magnification image showing Mg-matrix cracking extending into Ti-particle in Mg-(5.6Ti + 2.5B_4C) composite,[442] (d) Fracture surface of Mg-3Al-0.4Ce-2ZnO nanocomposite.[300]

4.3.5.4. Improving ductility through control of size, morphology and amount of reinforcement

As discussed in Section 4.3.5, the addition of micron-sized reinforcements is detrimental to the ductility of composite materials. For further elucidation, the fractured surfaces of micro-composites are shown in Figure 40. Particle cracking and void formation at the particle-matrix interface are predominant in micro-composites, leading to accelerated failure as in the case of Mg-$(5.6Ti + x\text{-}B_4C)_{BM}$ composites[442] with a ductility of about 8% and TAp/ZK51 composites with a ductility of about 5.6%.[444] The fracture surfaces in Figure 40 reveal the failure mode of the matrix; several small dimples and tearing edges, particulate fracture and Ti particle debonding attributed to a lack of chemical bonding at the Mg/Ti interface and load transfer from matrix to reinforcement are evident. In comparison, a Mg-3Al-0.4Ce/2ZnO nanocomposite[300] that exhibits a moderate ductility of 18% shows a dominant dimple mode of failure (Figure 40d), thus demonstrating the potential of nanoparticles over micro-particles for improving the ductility of the Mg matrix.

However, another concern with nanoparticles, particularly ceramic nanoparticles, is their high surface reactivity, which leads to the formation of micro-clusters and agglomerates due to the attractive van der Waals forces between nanoparticles.[445] These agglomerations of nanoparticles form clusters on the sub-micron to micron scale, as shown in Figure 41, which hamper the strength and ductility of the nanocomposites.[434] Furthermore, it is generally observed that addition of higher amounts of nanoparticles to the Mg matrix results in poor ductility of the composite. This is because of the surplus load transferred from the matrix to the reinforcement particles, resulting in particle-initiated failure. Hence, it is recommended that nanoparticles with volume fractions of

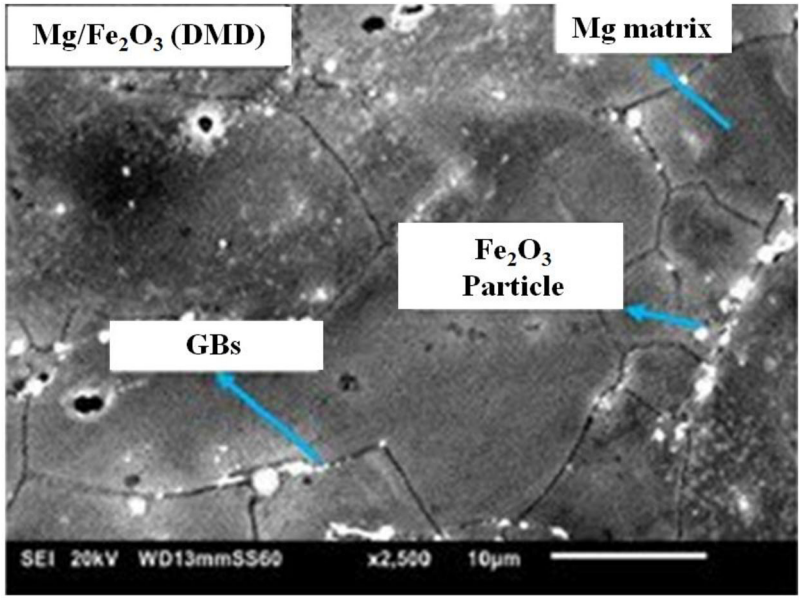

Figure 41. Agglomerates of Fe_3O_4 nanoparticles in Mg matrix that hamper the ductility of the nanocomposites.[434]

<3% are used as reinforcements to the Mg matrix to attain high ductility.

To evade the problem of agglomeration and quasi-cluster formation, Chen et al.[434] described a nanoparticle self-stabilization mechanism based on three major factors: a good wetting angle between SiC and molten Mg, a small attractive van der Waals potential between SiC nanoparticles in molten Mg, and a high thermal energy during processing, such that SiC nanoparticles overcome the van der Waals attraction in molten Mg and break free from their attraction to one another, resulting in homogenous dispersion of nanoparticles in the Mg, as evident from Figure 42.[413] This thermally activated dispersion and self-stabilization mechanism is a potential new pathway to achieving a uniform dispersion of dense nanoparticles in liquids when repulsive forces are not available through conventional methods.

Furthermore, other factors, such as interfacial bonding between the matrix and reinforcement, also affect the ductility. This is because, when a nanocomposite is stressed, load transfer from the matrix to the reinforcement occurs based on the Shear lag model,[446] which largely relies on the matrix-reinforcement interface. Hence, particles with good wettability, adhesion and interfacial bonding assist in imparting ductility to the composite.[446]

4.3.6. Strength-ductility synergy in magnesium composites

Magnesium matrix nanocomposites (MMNCs) are generally defined as materials that demonstrate extraordinarily increased strength without significantly compromising ductility due to the presence of nanoparticles that promote dislocation looping and resist immediate failure.[411,447] While texture weakening and alleviation of micro-strain aid in improving ductility, the two mechanisms are detrimental to the strength of the Mg composites. Hence, it is imperative to establish a synergy between strength and ductility in Mg composites. Recently, Tekumalla et al.[443] achieved an extraordinary combination of strength and ductility in a Mg-1.8Y/1CaO nanocomposite, as shown in Figure 43. The authors attributed the high ductility to the weakened texture and refined grain size, which are a result of the addition of the alloying element and nanoparticles. It should be noted that grain refinement is one of the only mechanisms that contributes to a simultaneous improvement in strength and ductility in Mg-based materials. The authors also attributed the tremendous improvement in strength to grain refinement as well as the presence of nanoparticles that aid in Orowan strengthening. Therefore, the appropriate strength/ductility tradeoff can be attained by carefully controlling the texture, alloying additions, type of reinforcement and its compatibility with the matrix, matrix-reinforcement interface, and reinforcement distribution.

4.3.7. Outlook

In summary, high ductility can be realized in certain classes of Mg-based composites. Micro-composites generally have poor ductility due to the micron-size reinforcements that act as fracture initiation sites. Nanocomposites generally have high strength with no compromise in ductility or improved ductility when compared to micro-composites. Nanoparticles assist in improving ductility by texture weakening and grain refinement, while also improving the strength through dislocation strengthening and Hall-Petch strengthening.

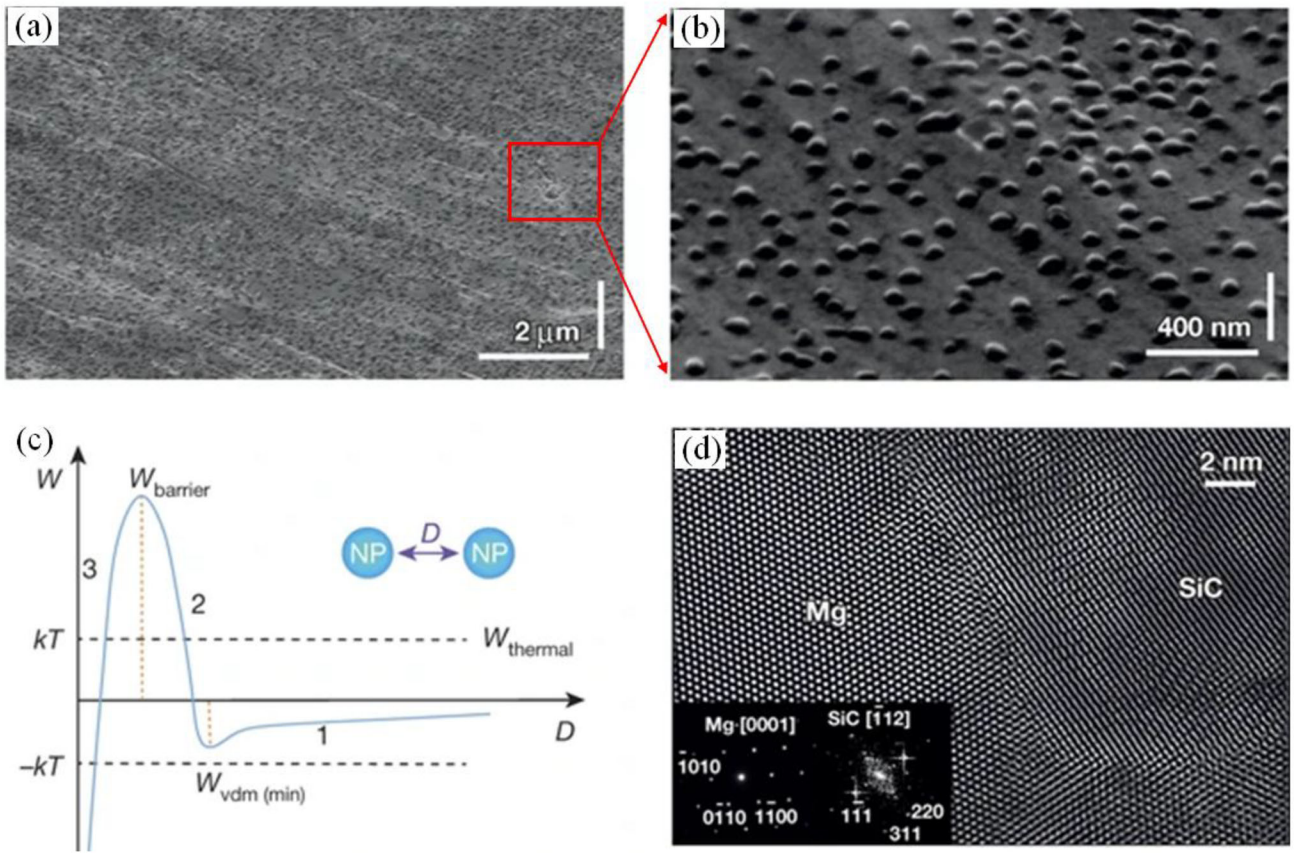

Figure 42. Uniform dispersion of SiC nanoparticles in as-solidified magnesium alloy matrix. (a), (b) Low and high magnification SEM images of Mg2Zn/14 vol%SiC showing uniform dispersion of SiC, (c) The interaction potential (W) vs inter nanoparticle distance (D) for two SiC nanoparticles shown as the blue curve, where segment 1, 2, and 3 denote the dominance of van der Waals interactions, increased interfacial energy with SiC, and decreased interfacial energy due to the contact and sintering of SiC nanoparticles, (d) TEM image of a characteristic SiC nanoparticle and Mg matrix interface.[413]

Furthermore, a careful choice of alloying elements and nano-reinforcements with a lower CTE differential could also alleviate the micro-strain, therefore granting the nanocomposite excellent strength, ductility and toughness. While there are numerous challenges to overcome before the potential of Mg nanocomposites can truly be realized, such as uniform dispersion of nanoparticles and tailoring of the matrix-reinforcement interface, Mg nanocomposites are an exciting new frontier. By manipulating and modifying existing alloys and taking advantage of nano-technology to adjust and fine-tune material properties, particularly ductility, researchers can create strong, lightweight materials with widespread applications.

5. Highly-ductile magnesium as a structural material

5.1. Creep properties

The many potential applications of Mg in the automobile industry have been restricted to only the instrument panel, steering wheel, seats, and gear boxes owing to its high reactivity and inferior properties at elevated temperatures. Automotive powertrain components, such as the engine block and transmission case, are subjected to prolonged high temperatures (150–200 °C) at increased stress (50–70 MPa).[448] This continuous exposure of material to elevated temperatures and stresses lead to slow deformation of material, or "creep," which can result in failure of the material at stresses below the YS. Creep behavior can be classified into dislocation creep, diffusional creep, GBS and GB migration depending on the exposed temperature and loading intervals, as shown in Figure 44a.[449] Creep by dislocations occurs at moderate temperatures, where dislocations are formed under the applied load. When a dislocation is forced through the stress field of another dislocation, a dislocation interaction occurs, which results in the formation of jogs or kinks. Dislocations with jogs move by thermal activation via creation of a vacancy, and this jog-vacancy pair results in dislocation climb, which leads to material failure. On the other hand, creep by

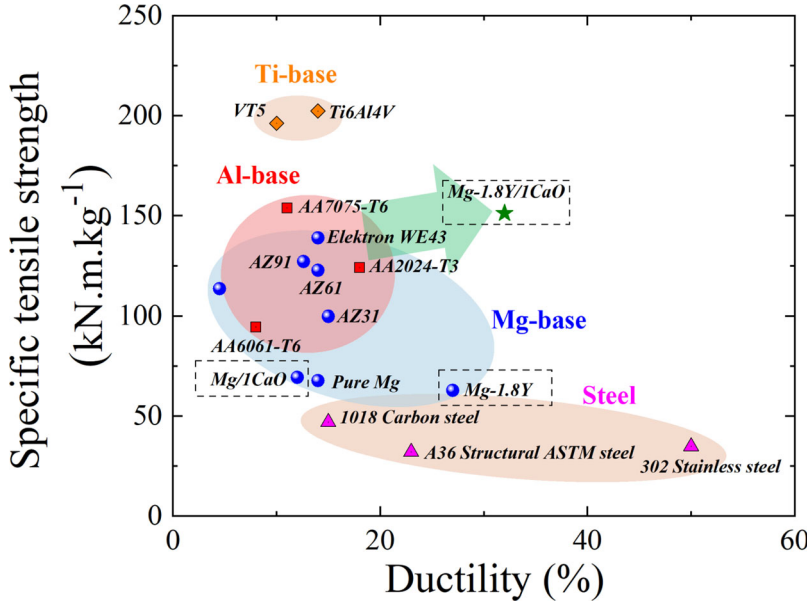

Figure 43. Magnesium nanocomposite Mg-1.8Y/1CaO exhibiting strength-ductility synergy.[443]

diffusion occurs at elevated temperatures, where self-diffusion contributes to plastic deformation. In diffusional creep, GBs serve as the sinks and sources of the vacancies.

Moreover, GBS also contributes to creep strain, because voids form due to the shear stresses acting on the GBs. The fraction of creep strain resulting from GBS is reported to be from 10% to 65% depending upon the applied stress, grain size and exposed temperature. GBS has been reported to increase with increasing stress and temperature and shares an inverse relationship with grain size.[448] Finally, GBs can migrate due to stress-induced precipitation during creep. HAGBs can migrate to relieve the increased concentration of stress caused by precipitates in supersaturated phases. The RT deformation of Mg is mainly accommodated by the (0001) basal slip system due to its low CRSS as compared to the non-basal slip system. Twinning also contributes to deformation at both RT and elevated temperatures due to low CRSS. On the other hand, GBS, GB migration and the activation of non-basal slip (pyramidal and prismatic) can occur. Raynor et al. studied the creep behavior of pure Mg and concluded that the main mechanisms of deformation at 90–300 °C and 8–70 MPa were basal slip, twinning, and formation of sub-grains.[452] However, at temperatures above 250 °C, the non-basal slip systems (pyramidal and prismatic), GB deformation and GB sliding were the primary deformation mechanisms. Vagarli et al. suggested that dislocation climb was the dominant creep mechanism at stresses between 8.2 – 21 MPa at temperatures below 477 °C, whereas cross slip occurred at stresses higher than 2.5 MPa.[453] However, for stresses lower than 2.5 MPa, lattice self-diffusion was the dominant creep mechanism. Figure 44b shows the dominant creep mechanism of various Mg alloys taken from the literature at stresses of 20–120 MPa and at temperatures of 100–300 °C.[450] Accordingly, an in-depth understanding of Mg deformation by creep and its relationship with microstructure and other material characteristics is required to design creep-resistant Mg alloys. Dargusch et al. investigated creep in an AZ91 Mg alloy at temperatures between 125 and 175 °C at 50 MPa stress and found that the activation energy was 30–45 kJ/mol.[454] The activation energy was attributed to the presence of the $Mg_{17}Al_{12}$ phase in AZ91, which contributed to GBS and GB migration. Pipe diffusion was suggested to be the dominant creep mechanism at stresses between 50 and 90 MPa. Somekawa et al. also studied the creep characteristics of AZ91 at temperatures between 200 and 350 °C and concluded that dislocation climb is the main creep mechanism.[455] At temperatures below 267 °C, the activation energy was found to be 96 kJ/mol, suggesting pipe diffusion, whereas at temperatures above 267 °C, an activation energy of 126 kJ/mol was observed, pointing toward the self-diffusion mechanism.

Very recently, Figueiredo et al. conducted a double-shear creep test on ECAPed AZ31 with an average grain size of 2.7 μm[456]; they found that GBS (stress exponent = 2, activation energy = 92 kJ/mol) occurred at the early stages of deformation, but the creep rate decreased with increasing deformation due to grain growth. On the other hand, a sample annealed (24 h at 723 K) before the creep test showed

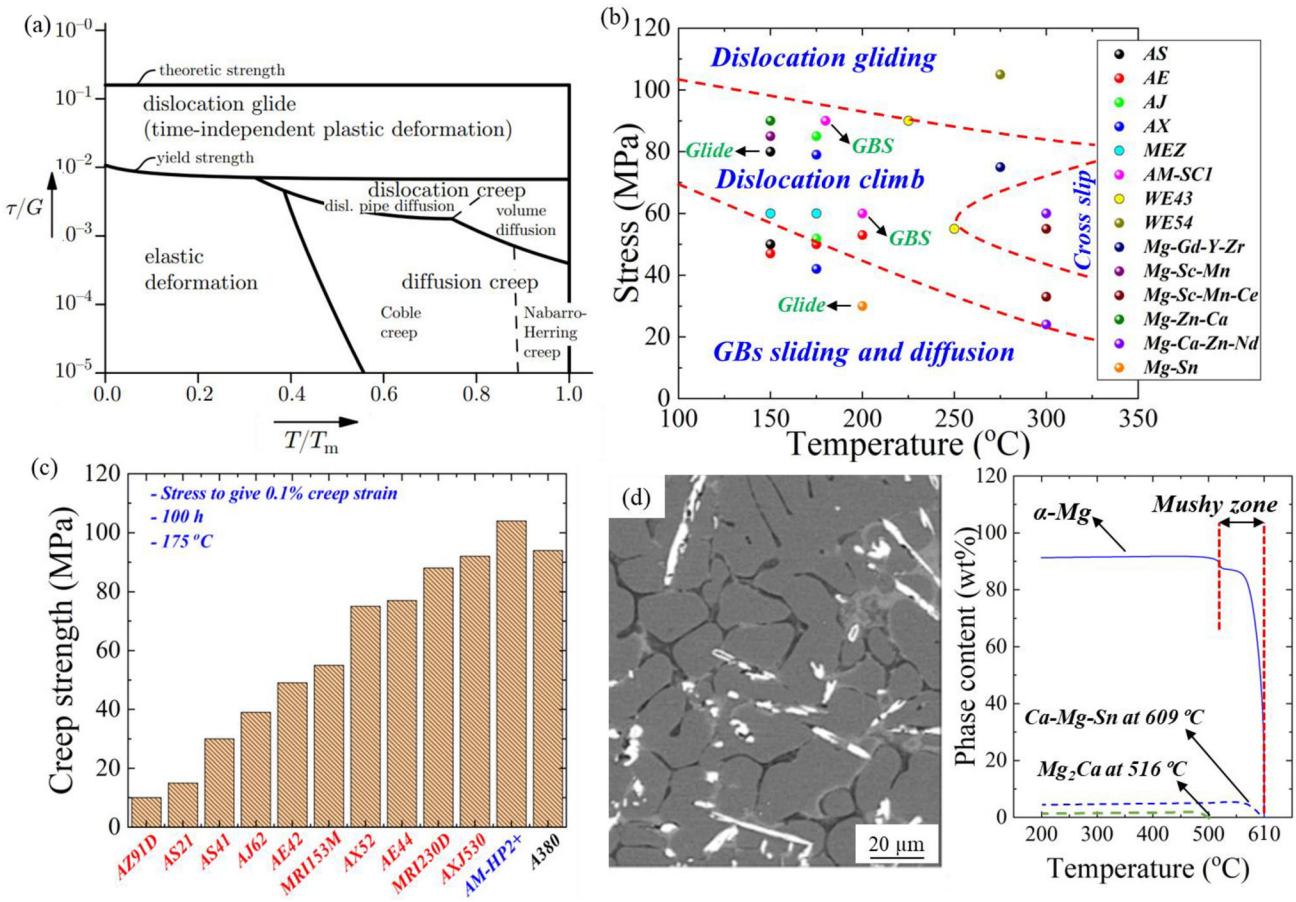

Figure 44. (a) The map illustrating various regions of deformation under specific normalized stress and temperature,[449] (b) The creep mechanism of various Mg alloys reported in the literature,[450] (c) The comparison of creep strength of several Mg die-cast alloys to produce 0.1% creep strain in 100 h at 175 °C,[450] (d) SEM image of Mg-4Sn-4Ca (wt%) alloy and the prediction for the formation of various phases after solidification by JmatPro.[451]

an increased stress exponent at higher stresses and suppression of GBS due to its coarser grain size of 50 μm. The addition of minute RE elements has been reported to modify creep resistance by solid solution strengthening and to grant an excellent age hardening response via formation of metastable semi-coherent/coherent Mg-RE precipitates (Figure 44c). Ning et al. studied the creep resistance of an Mg-2Gd-1Nd-2Ca-0.5Mn (wt%) alloy at 180 °C and 210 °C.[457] The alloy exhibited remarkable creep characteristics which were attributed to the high solid solution strengthening effect of Mg-2Gd-1Nd-2Ca-0.5Mn by the co-segregation of Nd solute atoms with other atoms. Although RE-added Mg alloys show better mechanical properties and creep characteristics, they are very costly to produce because of the expense of RE elements. Accordingly, it is important to develop a low-cost high-creep resistant alloy for commercial purposes. In this regard, Ca has been suggested as the most promising potential alternative to RE elements. Ca is not only inexpensive, but also can significantly enhance the mechanical and creep properties of alloys. Very recently, Amir et al. investigated the effect of Ca addition up to 4 wt% on the microstructure and creep characteristics of a Mg-4Sn alloy.[451] An impression creep test conducted at temperatures between 445 K and 475 K at normalized stress levels between 0.0225 and 0.035 revealed that the >2 wt% Ca-added alloy showed remarkable creep resistance. The enhanced creep properties were attributed to the formation of stable Ca-Mg-Sn and Mg_2Ca phases at the GBs instead of an unstable $MgSn_2$ phase (Figure 44d). Pipe diffusion climb was regarded as the main creep mechanism, with a stress exponent of $6.04 < n < 6.89$ and an activation energy of $101.37\ kJ/mol < Q < 113.8\ kJ/mol$. More effort and improved understanding are needed to improve the creep resistance of Mg alloys in order to exploit these materials in automotive applications.

5.2. Fatigue properties

Decreasing the weight of vehicles is considered one of the most effective approaches to enhance the fuel economy and mitigating environmentally harmful

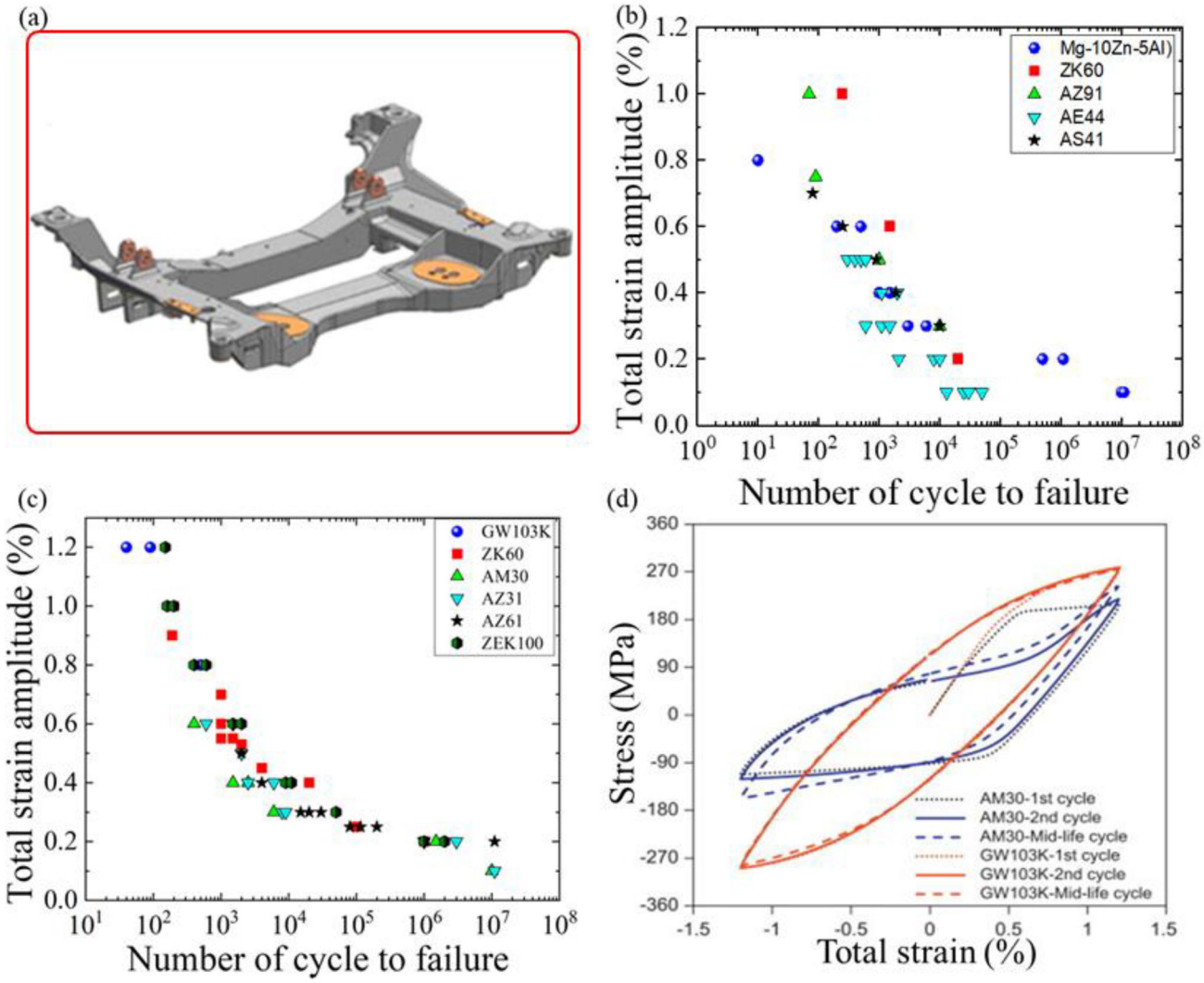

Figure 45. (a) The Mg engine cradle with 35% weight reduction as compared to the conventionally fabricated with Al alloys,[459] (b) Fatigue life of as-cast Mg alloy in comparison with other studied alloys,[460] (c) Total strain amplitude as a function of the number of cycles for ZEK100 Mg alloy in comparison to other reported in the literature,[461] (d) Stress-strain hysteresis loop of various cycles at total 1.2% strain amplitude for AM30 and GW103K.[462]

emissions. A 10% reduction in passenger vehicle weight can increase fuel economy by 6–8%.[458] Mg, the lightest metallic material, has drawn considerable attention for its potential to reduce vehicle weight based on its dimensional integrity, high strength-weight ratio, and adequate machinability and recyclability. As a structural material in the transportation industry, Mg is utilized to fabricate clutches, intake manifolds, camshaft covers and transmission housing. One potential application is shown in Figure 45a: a the weight of an engine cradle was reduced by 35% by utilizing Mg instead of conventional Al alloys.[459]

However, automobile components are inevitably subjected to repeated/fluctuating loading and unloading millions of time while in service and usually fail at stresses lower than the actual fracture stress.[154] This behavior is called fatigue failure, and it is of vital importance for the reliability and durability of structural materials. Fatigue characteristics can be analyzed by either stress-controlled fatigue (SN) behavior, where stress amplitude (S) is plotted against the number of cycles (N), or by strain-controlled low cycle fatigue (LCF), which occurs at high stress and a low number of cycles. Despite being a good potential candidate for weight reduction applications, Mg shows inferior fatigue properties owing to its high anisotropy, tension-compression yield asymmetry and the presence of a strong basal texture after primary processing. Plastic anisotropy and tension-compression yield asymmetry can hamper the irreversibility of cyclic deformation, which has an effect on the durability and in-service performance of the components.

AZ/AM series materials are the most vigorously researched of the Mg alloys with lower fatigue

Table 11. Fatigue properties of various AZ/AM alloys.

Material	Manufacturing process	Range of cycle of failure
AZ31[463]	Rolled	10^1–10^6
AZ31, AZ80[464]	Extruded	10^2–10^6
AZ31B-F[465]	Extruded	10^3–10^6
AM50[466]	Extruded	10^2–10^4
AZ31B[467]	Extruded	10^2–10^7
AM30[468]	Extruded	10^3–10^8
AZ31[469]	Extruded	10^2–10^8
AZ31[470]	Extruded	10^2–10^5
AZ31[471]	Extruded	10^3–10^7
AZ31[472]	Extruded	10^2–10^4
AZ31[473]	Rolled	10^2–10^4
AZ31[474]	Extruded	10^2–10^7
AZ31B[475]	Rolled	10^2–10^4
AZ31B[476]	Rolled	10^1–10^4
AZ31[477]	Rolled	10^2–10^8
AZ31B[478]	Extruded	10^2–10^5
AZ31, AZ61, AZ80[479]	Extruded	10^2–10^4
ZK60[480]	Extruded	10^2–10^6
AZ61A[481]	Extruded	10^2–10^6
AZ31B[482]	Extruded	10^2–10^4
AZ91[483]	Rolled	10^2–10^5
AZ31[484]	Extruded, Rolled	10^3–10^7
AZ31, ME21[485]	Extruded, TRC	10^1–10^6

properties. Table 11 shows the uniaxial tension-compression fatigue properties of wrought AZ/AM alloys.[463–485] It has been suggested that the inferior fatigue characteristics of AZ alloys are due to their strong basal texture, high plastic anisotropy and the formation of the β-Mg_{17}-Al_{12} phase. Accordingly, high fatigue strength in Mg alloys can be achieved by reducing the plastic anisotropy and weakening the strong basal texture by alloying with suitable elements. Mohammed et al. developed the a Zn-containing cast Mg-10Zn-5Al (wt%) alloy with remarkable tensile and fatigue properties as compared to other conventional alloys (Figure 45b).[460] Microstructural characterization by XRD and EBSD revealed that the addition of Zn suppressed the formation of β-Mg_{17}-Al_{12} intermetallic compound and promoted the τ-$Mg_{32}(Al,Zn)_{49}$ phase. In spite of a slight softening seen at higher strain amplitudes, the alloy demonstrated superior fatigue properties, which was attributed to the randomly oriented texture and presence of the τ-$Mg_{32}(Al,Zn)_{49}$ phase. Begum et al. studied the LCF behavior and the factors affecting the fatigue properties of an extruded AM30 Mg alloy.[468] The asymmetrical hysteresis loop was present at higher strain levels with a significant difference in tension and compression yield stress, which was due to twinning during compression and detwinning during tension. Moreover, strong cyclic hardening was observed at low strain ratios, while fatigue life was found to increase with an increase in the strain rate.

Patel et al. introduced a thixomolded AM60B Mg alloy with superior fatigue properties as compared to its die-cast counterpart.[486] Microstructural analysis revealed that it consisted primary of α-Mg and β-Mg_{17}-Al_{12} particles present in the eutectic network structure. The formation of symmetrical hysteresis loops in tension and compression and the excellent fatigue characteristics of thixomolded AM60B were attributed to the presence of β-Mg_{17}-Al_{12} particles with small grain sizes, which suppressed the formation of twinning during cyclic deformation. Similarly, excellent fatigue properties were reported for a semi-solid AZ91 Mg alloy created by the same research group.[487] The addition of RE elements results in a randomly oriented crystallographic texture, which leads to improved mechanical properties at RT and elevated temperature based on the phenomena of solid solution strengthening and precipitation strengthening. Yang et al. studied the effect of Ce addition on the stress-controlled fatigue properties of an AZ91 Mg alloy with a high-frequency fatigue testing machine.[488,489] The results revealed that the addition of 1% and 2% Ce resulted in improvements in fatigue strength of 20.3% and 9.1%, respectively. The enhanced properties were attributed to grain refinement and suppression of porosity due to Ce addition in AZ91. Similarly, Mokdad et al. studied the mechanical properties and fatigue characteristics of a 0.2 wt% Nd-containing ZEK-100 alloy compared to those of AZ31 and AM30 alloys, as illustrated in Figure 45c.[461] The ZEK100 alloy showed a combined improvement in ductility and strength, with enhanced fatigue life as compared to the other alloys studied. The skewness and asymmetry of the hysteresis loop were improved in the Nd-containing ZEK100 alloy, which was attributed to suppression of twinning based on the refined grain size and weakened texture. Mirza et al. studied the strain-controlled cyclic deformation behavior of a GW103K (Mg-10Gd-3Y-0.5Zr) alloy.[462] Fatigue testing revealed that the GW103K alloy demonstrated cyclic stabilization with a symmetrical hysteresis loop without tension-compression asymmetry (Figure 45d). The longer fatigue life of this alloy was attributed to its small grain size, texture weakening and the large number of precipitates which acted as an obstacle to twinning. Accordingly, it can be concluded that grain refinement, precipitation hardening, and texture modifications are the pre-requisites for the design of a high-fatigue strength Mg alloy.

5.3. Corrosion

Mg and its alloys have been considered extremely attractive structural materials based on the multiple

advantage it offers i.e., light weight, high strength to weight ratio, etc. However, diverse utilization of Mg has been restricted because it suffers from various handicaps, including poor formability at RT, rapid ignition in air at high temperature and, most importantly, inferior corrosion characteristics as compared to other lightweight materials such as carbon fiber-reinforced plastics and Al.[490] Discrete localized corrosion in Mg alloys is irregular, and expands laterally and spreads throughout the entire surface of the material. Owning to their high reduction potential (−2.37 V), Mg alloys are susceptible to galvanic corrosion when they come in contact with metal or intermetallic compounds with low reduction potential. The substantial corrosion rates of Mg alloys are associated with the following factors: (i) the high intrinsic reactivity of Mg, (ii) the formation of a surface film during immersion in an aqueous chloride-containing solution, which is unstable and non-protective, and (iii) micro-galvanic interactivity among the second phases or impurities, which results in significantly higher corrosion rates as compared to that of pure Mg. The corresponding anodic (1) and cathodic (2) reactions can be represented as follows:

$$Mg \rightarrow Mg^{+2} + 2e^{-} \quad (1)$$

$$2H_2O + 2e^{-} \rightarrow H_2 + 2OH^{-} \quad (2)$$

The anodic dissolution of Mg and its alloys occurs when Mg undergoes oxidization to form divalent Mg ion (Mg^{+2}). Hydrogen evolves at the cathode along with OH^{-}, which upon reacting with Mg^{+2} produces an $Mg(OH)_2$ film at the surface, which is discontinuous, does not efficiently protect the alloy and increases the pH of the solution after several hours of immersion of Mg in aqueous solution.

The overall corrosion reaction of Mg can be illustrated as[491,492]:

$$Mg + 2H_2O \rightarrow Mg^{2+} + 2(OH)^{-} + H_2 \rightarrow Mg(OH)_2 + H_2 \quad (3)$$

Due to the high electronegativity of Mg, it releases two electrons and converts to Mg^{+2}, which is stable in aqueous solution. The corrosion of one atom of Mg results in the formation of one H_2 molecule, so measurement of the amount of liberated H_2 can provide the rate of corrosion of the Mg alloy.[493] Mitigating the high corrosion rate of Mg alloys by controlling their microstructure, appropriate alloying, or applying protective coatings is of significant importance for diverse industrial applications. Different alloying additions may have dissimilar effects on the mechanical and corrosion characteristics of the alloys; some specific elements may improve both properties (corrosion and mechanical), whereas some can improve one property but cause the other to deteriorate. Accordingly, in-depth investigations are required to figure out the diverse effects of different alloying additions.

Al is known to be the most important alloying addition for Mg, along with Zn, because both control the grain size during solidification to result in improved physical properties. Mg-Al-Zn (AZ series) alloys are the most researched and versatile Mg alloys and are utilized for various structural applications owing to their adequate strength and better castability. The significant improvement in the mechanical properties of AZ alloys is attributed to the formation of the intermetallic compound $Mg_{17}Al_{12}$ (β-phase).[494] On the other hand, the $Mg_{17}Al_{12}$ phase enhances the Al content of the materials, which has a detrimental effect on the corrosion characteristics of AZ series alloys. Hence, the corrosion susceptibility of AZ alloys depends upon the distribution and morphology of $Mg_{17}Al_{12}$. Extensive investigations have been carried out on alloy design. Specific solutes react with Al or the Al-Mn phase, resulting in increased precipitation density and a highly homogeneous distribution of the $Mg_{17}Al_{12}$ phase. Figure 46a shows the corrosion potential (E_{corr}) of AZ alloys measured in quiescent 0.1 M NaCl.[47] Only small changes in the E_{corr} of various Mg alloys are measured because of the limited solubility of most of the elements in Mg.

As mentioned previously, the electrochemical characteristics of Mg alloys are highly dependent on the type of intermetallic particle involved, and they play a vital role in the localized corrosion behavior of Mg alloys. In this regard, Sudholz et al. conducted micro-capillary electrochemical tests in dilute chloride solution on the key intermetallic compounds formed in Mg alloys.[495] The results revealed that, excluding Mg_2C, all intermetallic compounds aggravated reduction reactions to rates higher than that of Mg and showed increased cathodic kinetics. Potentiodynamic polarization curves for different intermetallic compounds are shown in Figure 46b. The ability of an individual intermetallic compound to undergo a cathodic reaction depends on its composition. Accordingly, suitable alloying can enhance the corrosion resistance of Mg alloys by modifying the nature and overall distribution of intermetallic compounds. In this regard, alloying with RE elements produces excellent results in terms of mechanical properties and corrosion characteristics due to the formation of Al-RE intermetallic compounds, for example, Al_2RE,

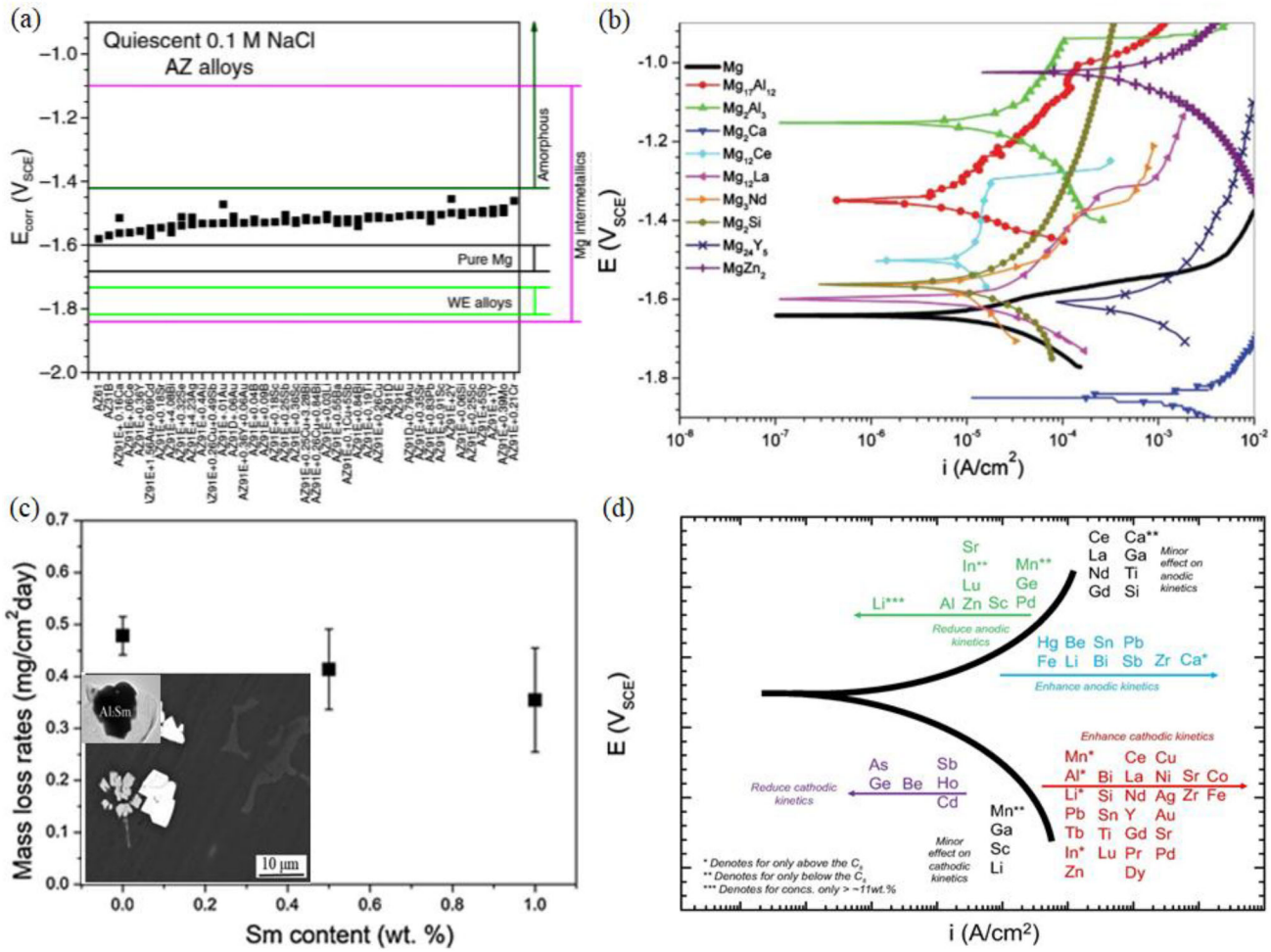

Figure 46. (a) Corrosion potential (E_{corr}) of several AZ series Mg alloys measured in 0.1 M NaCl,[47] (b) Potentiodynamic polarization curves for various intermetallic compounds present in Mg alloys,[495] (c) Mass loss in 0.1 M NaCl for AZ91 with various Sm concentration (Inset figure in figure (c) shows the SEM image in backscattered mode of AZ91-1.0Sm (wt%) alloy),[496] (d) Schematics of electrochemical effects of various alloying addition.[47]

$Al_{11}RE_3$ etc., which promote grain refinement and also enhance the homogeneous distribution of the $Mg_{17}Al_{12}$ phase.

Hu et al. studied the effect of samarium (Sm) addition on the microstructural evolution and corrosion resistance of the AZ91 Mg alloy.[496] Microstructural characterization revealed that Sm segregated with Al and formed an Al_2Sm intermetallic compound (Figure 46c), which not only altered the morphology of $Mg_{17}Al_{12}$ from coarse to fine but also reduced the overall area fraction of the $Mg_{17}Al_{12}$ phase (8.4% and 5.7% in AZ91 and AZ91-1.0Sm, respectively). The corrosion rate decreased with increasing Sm concentration. The corrosion rate, which was calculated through mass loss testing carried out for 24 h in 0.1 M NaCl solution, was 0.47 mg/cm^2 day and 0.33 mg/cm^2 day for AZ91 and AZ91-0.1Sm, respectively, as illustrated in Figure 46c. The significant improvement in the corrosion characteristics of AZ91-0.1Sm was attributed to the Al_2S phase, with more noble corrosion potential as compared to the α-Mg and $Mg_{17}Al_{12}$ phase in the same electrolyte. Similarly, microalloying of Y (0.04 wt%) to Mg-8Sn-1Zn-1Al decreases the corrosion rate by 67% (12.7 mm/y and 4.2 mm/y without and with Y microalloying, respectively).[497] The remarkable enhancement in corrosion resistance was attributed to the formation of fewer noble Al_8Fe_4Y-MgSnY duplex particles in the Y-added alloy, which formed by heterogeneous nucleation of MgSnY on the surface of Al_8Fe_4Y during solidification of the alloy. Accordingly, the duplex particles reduced the electrochemical nobility gap between the particles and α-Mg and, hence, decreased the probability of microgalvanic corrosion during NaCl immersion. Kim et al. extensively investigated the corrosion characteristics of an Mg-5Al-xCa (x = 0 to 2 wt%) alloy in NaCl alkaline solution.[498] Microstructural and electrochemical analyses of all of the alloys revealed that the addition

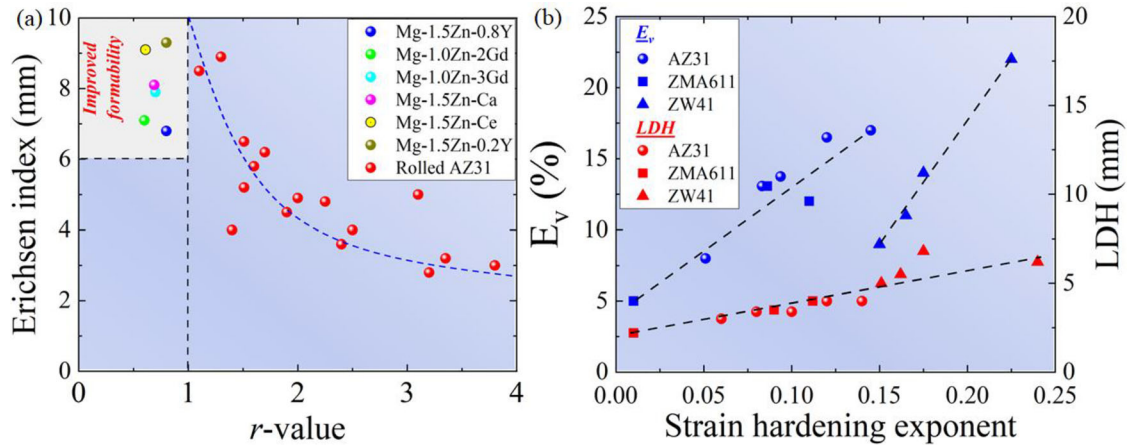

Figure 47. (a) The relationship between Erichsen value and plastic anisotropy (*r*-value) for several Mg alloys,[45] (b) Variation in ductility (E_v) and limiting dome height (LDH) with respect to the strain hardening exponent (n) for various Mg alloys.[249]

of Ca facilitated grain refinement and increased the pitting corrosion resistance of the Mg-5Al alloy. The high corrosion resistance in the Ca-added alloy was attributed to the small grain size, high precipitation density and suppression of microgalvanic cells by reduced precipitation of the $Mg_{17}Al_{12}$ phase at the grain boundaries, which were caused by increased Ca concentration. To this end, alloying can influence the overall anodic and cathodic reaction kinetics of Mg alloys and can affect the corrosion characteristics. Figure 46d gives a schematic illustration of the effect of specific alloying addition on the overall corrosion kinetics of Mg alloys.[47] The schematic explains not only the effects of a particular alloying addition on the electrochemical properties of an alloy, but also shows the extent to which the cathodic and anodic reactions are influenced by the addition. Accordingly, the schematic can be consulted to identify the appropriate alloying element that will suppress cathodic reaction kinetics in Mg alloys.

5.4. Formability

Despite various advantages, widespread application of Mg alloys has been restricted due to the poor formability of Mg at RT. The inferior formability as compared to Al arises from the inability of Mg to deform along the c-axis because of the high CRSS value of the pyramidal $< c + a >$ slip system, which causes Mg to fail in the early stages of deformation. The strong basal texture after primary processing and lack of independent slip systems are the most frequently discussed shortcomings that prevent the utilization of Mg alloys in diverse applications. Accordingly, weakening of the strong basal texture and activation of non-basal slip systems have been suggested as prerequisites for highly formable Mg alloys.

The formability of Mg alloys has been intensively investigated over the past few decades through various thermomechanical techniques and different alloying additions.[327] The addition of RE elements is better than the use of other impurities, as they lead to weak basal texture and also enhanced non-basal slip during deformation as presented in Figure 23.[67–69,75,76] Besides texture, grain size, high-strain hardening exponent (n) and plastic anisotropy have been extensively studied with respect to improving formability. Grain refinement and the implications thereof have already been discussed in previous sections. Plastic anisotropy (r-value) is considered an important parameter associated with the stretch formability of Mg alloys. A higher r-value reflects a material's inability to deform along the thickness direction, and stretch formability is mainly controlled by the capacity of materials to accommodate strain along the thickness direction. Usually, in rolled Mg sheets with the c-axis parallel to ND texture, prismatic slip is the dominant deformation mechanism during in-plane stress and thickness strain can only be accommodated by pyramidal slip. Due to the very high CRSS value of pyramidal slip, stress cannot be accommodated in the c-axis, resulting in a high r-value and lower stretch formability. Thus, to achieve high stretch formability in Mg alloys, plastic anisotropy must be reduced. Figure 47a shows the relationship between stretch formability and r-value for various Mg alloys.[45] Formability is inversely related to r-value; thus, plastic isotropy is the key factor in the design of highly formable Mg alloys. The higher plastic anisotropy of Mg alloys can be correlated with the strong basal texture created during processing. Several previous works revealed

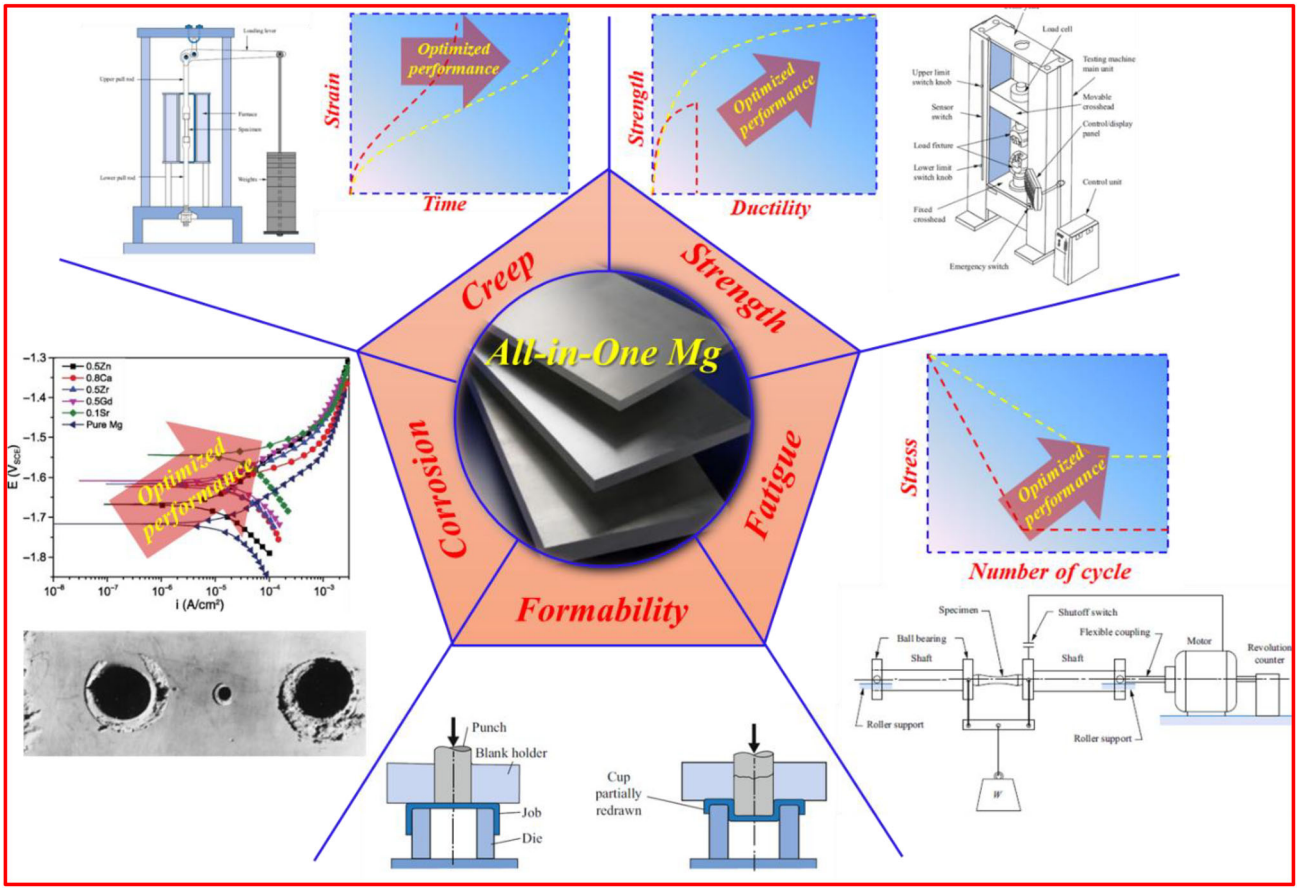

Figure 48. Schematic representing all-in-one Mg based materials.

that materials with strong basal textures showed higher anisotropy values.[17,499–502] When the basal poles are broader and split more along one direction, the r-value increases, as the angle between the tensile loading direction and texture-broadened direction increases; this is because basal slip is more favorable under tensile deformation along the texture-broadened direction. Similarly, assuming biaxial stress during stretch formation, the orthotropic texture will result in anisotropic deformation during stretching and will lead to poor formability. However, in addition to texture, the anisotropy of Mg alloys can be controlled by the relative activities of slip systems and twinning during plastic deformation. Suh et al. investigated the deformation behavior of AZ31 and AT31 (Mg-3Al-1Sn) (wt%) Mg alloys and concluded that, though there was only a small difference in the SFs of the two alloys, AT31 showed higher thickness strains along all loading directions as compared to AZ31.[77] The results suggested that through-thickness deformation (lower r-value) can be improved by the activation of the non-basal system and, thus, AT31 showed a higher stretch formability than AZ31.

In addition to lower-value, RT stretch formability of Mg alloys can be significantly enhanced by an improvement in the work hardening exponent, which can be achieved by microstructural modification. Kang et al. thoroughly investigated the relationship between work hardening exponent and stretch formability of various alloys.[249] Their findings are shown in Figure 47b. The results confirmed that stretch formability shares a linear relationship with work hardening regardless of alloy composition. Accordingly, we can conclude that a lower r-value and a higher work hardening exponent are prerequisites for high stretch formability in Mg alloys at RT. In this regard, pre-twinning has been found to be a very simple and economic approach to enhancing the strain hardening exponent and simultaneously reducing the *r*-value. TTWs alter the parent grain orientation by 86°, so a large concentration of TTWs can facilitate deformation along the thickness direction. Park et al. pre-compressed the AZ31 alloy to activate TTWs, resulting in a 65% increase in formability.[246] These results suggest that the activation of detwinning and basal slip in the twinned region accommodated

the through-thickness strain and resulted in the observed improvement in stretch formability. Similarly, Weijun et al. carried out in-plane compression to introduce TTWs to a thin AZ31 Mg alloy sheet and found that the Erichsen value of the pre-twinned alloy was improved by 50% following compression.[248] The enhancement in stretch formability was attributed to the presence of TTWs in the pre-twinned region, which effectively accommodated the through-thickness strain during deformation and resulted in improved formability. In addition, TTWs can act as a nucleation sites for dynamic recrystallization during the deformation of Mg alloys, and DRXed grains with random orientations can eventually enhance the stretch formability.

5.5. All-in-one magnesium based materials

Strength and ductility are two essential performance indicators for metallic materials which ensure the high deformability for arbitrary shape change with an adequate robustness. However, inferior mechanical properties of Mg and its alloys are the major obstacle in their global use. The strength can be enhanced by blocking the dislocation motion, which often results in the reduction of ductility, a phenomenon known as strength-ductility trade off. Therefore, the major challenge is to investigate the mechanistic origin to this dilemma and to explore new compositions of Mg alloys with strength-ductility synergy. The microstructural modification has been considered to be the most vital principle to achieve this target, where microstructure should be engineered to promote the uniform plastic flow and to suppress the dislocation pile-up during plastic deformation. As it is well established that Mg can be made strong by the grain refinement (GB-strengthening) as elaborated by Hall-Petch relationship discussed in section 3.1.1, where incoherent GBs with high boundary energy can hinder the transmission of dislocation between the adjacent grains. Interestingly, at a critical grain size the Hall-Petch relationship fails and GB softening overtake the GB hardening phenomenon. Therefore, the aim should be to modify the microstructure to a critical grain size having maximum strength with adequate ductility. In addition, the microstructure engineering can promote the intergranular deformation mechanisms (GBS, strain delocalization) resulting in super formable Mg as discussed in section 2.1.3.

Moreover, if the Mg is to be utilized in high-temperature applications (at 300 °C or above), understanding the creep behavior is of supreme importance. It is widely accepted that creep characteristics of Mg alloys are dependent on its microstructural characteristics (grain size, texture, precipitates) and the external operating conditions such as applied stress and the operating temperatures, yet the major contributor to enhance creep resistance remain unclear. The operating temperature is limited based on Mg's low melting point; hence it is required to increase the operating temperature by suitable alloying. The alloying element should be selected on the basis that it should show high solubility at high temperature and the solubility decreases at low temperatures so that the formation of precipitates could lead to age hardening. In addition to that, the precipitates should contain a high concentration of Mg which can reduce the amount of alloying elements due to an increase in the volume fraction of precipitates. Moreover, a combination of alloying elements can be exploited, which can simultaneously result in the formation of complex precipitates and increase the overall volume fraction of precipitates. Another important prerequisite of alloying elements is its lower diffusion rate in Mg which will lead to a lower tendency of dislocation climb and overageing. Hence, the utilization of calculated phase diagrams is essential to save the time/material and focus should be given to devise a relationship between the microstructural characteristics and the related deformation mechanisms (diffusion characteristics, activation of slip systems, and migration of GBs).

The existing defects, twinning lamellas, and slip bands can lead to earlier formation of fatigue cracks in Mg alloys resulting in premature material failure. Accordingly, future works should be devised to mitigate these deficiencies for achieving high fatigue strength in Mg alloys. One approach could be purification, deformation by SPD techniques followed by various annealing regimes to eliminate the metallurgical defects and exploiting the precipitation strengthening to suppress the initiation of twinning and cyclic slips. The challenge will be thoroughly understanding the slip and twinning interaction at the twin boundaries on the formation of a fatigue crack. Hence, it will be of immense advantage to utilize various in-situ techniques for mechanistically understating the interaction characteristics of slips and twins and their consequent effects on the fatigue properties of Mg alloys.

Furthermore, the widespread applications of Mg alloys have been impeded owing to its high vulnerability to corrosion, which can be attributed to the development of weakly bonded and heterogeneous oxide/hydroxide film on its surface. Accordingly, enhancing the corrosion resistance of Mg alloys is imperative for its commercial utilization. A bi-directional approach

can be opted to achieve the target. One strategy could be to carefully consider the alloying addition, deformation by SPD techniques, and followed by annealing which can result in the dispersion of second phase particles, resulting in lower susceptibility to galvanic corrosion. The second strategy could be consideration of appropriate surface engineering for developing adherent, uniform, and self-healing coatings to avoid the vigorous corrosion behavior of Mg alloys.

6. Remarks, future trends, and conclusion

The intrinsic brittleness of Mg impedes its diverse applications. Accordingly, a thorough understating of the deformation mechanisms involved can lead to a breakthrough in the design of highly ductile Mg alloys. The two globally accepted ductility-enhancing mechanisms can be summarized as dislocation nucleation and dislocation (non-basal) mobility. Dislocation nucleation can be explained based on the I_1SFE, where materials with lower SFEs can provide more sites for dislocation nucleation, resulting in an increased density of non-basal dislocations. Hence, dislocation nucleation will eventually enhance the ductility of Mg alloys by accommodating the strain in the crystallographic $<c>$ axis. Secondly, suppressing the deleterious PB transition and enhancing the mobility of non-basal dislocations result in a higher rate of $<c+a>$ cross-slip. Thus, it is imperative to fully understand the correlation between the two mechanisms as a function of solid solution alloying and provide a concrete understating of these ductility-enhancing mechanisms.

In recent years, the design of Mg alloys with superior properties has benefited greatly from the development of high-performance computing technology. The development of computationally-aided design strategies by integrated computational materials engineering (ICME) has enabled scientists and engineers to study atomistic-scale mechanisms and to successfully build reliable correlations among chemical composition, processing, and properties. This has not only boosted the design of new materials with superior properties through simulations, but also significantly reduced the cost of repeated experimentations and testing. First principle calculations and MD simulations have provided mechanistic insights and uncovered various issues related to the poor ductility of Mg and provided a roadmap for the development of high-performance Mg alloys. Although ICME offers great predictability and unprecedented tools for temporally and spatially resolved materials simulations, it is hindered by its high cost and laborious and time-intensive computations. Accordingly, the discovery of a new material can be significantly expedited by exploiting machine learning (ML). Ultrafast, efficient, and accurate predictions of yet-to-be-synthesized materials can be made by employing simplified machine learning methods trained on data from either computations or experimental results. The main concept of ML is to establish a relationship between a given data set (chemical composition, microstructural characteristics, etc.) and the targeted property (strength, ductility, etc.). ML is then performed by training an algorithm to predict the targeted property based on the given input data. The trained algorithm is then further tested against a new set of input features to predict changes in the property at negligible computational cost, once a sufficient level of accuracy has been achieved. ML can be used to extract insights, establish a relationship between various attributes, and make predictions based on learned trends. Hence, harnessing these paradigms can systematically explore the vast chemical space and can accelerate the prediction of new materials with targeted properties.

Recently, with the development of the materials genome philosophy and data mining strategies, data-based statistical ML approaches have contributed to materials engineering; some recent studies successfully predicted the transformation temperature of NiTi-based shape memory alloys,[503] the composition of ultrahigh-strength stainless steel[504] and the stress-strain curve and final texture of an FCC polycrystalline material.[505] Moreover, ML tools are now being utilized to successfully unearth specific behavior in Mg alloys and to provide insight into the correlations between various parameters. For instance, Andrew et al. utilized a ML framework and data obtained from EBSD to predict factors that affect twinning behavior in the AZ31 Mg alloy.[506] A decision tree algorithm was selected to establish the relationship between microstructural features and twin formation. The results revealed that grain size, basal Schmid factor and dislocation density control twin nucleation, while twin propagation is affected by GB length, GB misorientation, angle from GB plane to RD plane and basal Schmid factor. Recently, Pie et al. utilized ML to successfully identify promising alloying elements to create ductile Mg alloys.[507] Twenty-one elements (out of 76) with 22 properties were used as a training data set and the Gaussian process clarification (GPC) algorithm was employed. The GPC algorithm efficiently and reliably predicted promising solutes for ductile Mg alloys. The results were further used to evaluate the correlation between the ductility mechanisms

(dislocation nucleation and dislocation mobility), and it was shown that the two mechanisms are strongly linked. This postulate was further verified in another work by the same authors, in which high-throughput calculations were performed to investigate the effects of the same solute elements on the two ductility-enhancing mechanisms.[508] The results revealed that the two pro-ductility mechanisms are strongly linked, such that a specific solute had the same effect on both of the mechanisms. Accordingly, ML can pave the way toward discovery of new compositions of Mg alloys. It can remove the fundamental bottleneck and eliminate conventional trial-and-error fabrications and testing methodologies. A simple ML algorithm, based either on configurational or compositional information, can predict the targeted property at ultrafast speed and enormously reduced cost.

Mg has been under intensive investigations for utilizing it in structural applications, owing to its low density and high natural abundance. Despite the various tantalizing properties, the vast applications has been impeded due to the low ductility of Mg at RT. Accordingly, in the present review, the major factors associated with the intrinsic brittleness of Mg and the strategies that should be exploited to enhance the mechanical properties are deeply discussed. It can be concluded from the above discussion that the atomic flow mechanisms including PB transition, SFEs (1st, 2nd, and GSFE) and the cross-slip of pyramidal II dislocations are most significant mechanisms for designing highly ductile Mg alloys. Specific alloying additions can not only modify the PB transition time or lower the energy barrier for pyramidal II cross-slip but can also alter the relative CRSS activating the non-basal slip system at the initial stages of deformation leading to superior ductility. Moreover, structural, and textural modification by various thermo-mechanical treatments or different SPD techniques can result in strength/ductility synergy of Mg alloys. Finally, the ceramic nanoparticles based Mg composites showed promising performance, which can be further optimized by the appropriate particle selection and by increasing the homogeneous distribution throughout the matrix.

Acknowledgments

This research was supported by National Research Foundation (NRF) of South Korea (2020R1A2C1004720).

References

1. Wuebbles, D. J.; Fahey, D. W.; Hibbard, K. A. *Climate Science Special Report: Fourth National Climate Assessment*. Vol. I. 2017. Washington, DC, USA: U.S. Global Change Research Program.
2. Carbon and Climate. 2017. https://galenmckinley.github.io/CarbonCycle
3. IEA, World Energy Outlook. 2019, Paris: IEA. https://www.iea.org/reports/world-energy-outlook-2019
4. Liping, L.; John, G.; Sijia, S.; Chengyuan, W. 2017 Global Primary Magnesium Supply and Demand Balance 2016. IMA Annual Conference. Singapore.
5. Halada, K.; Ijima, K. Resource Productivity of Magnesium. *Mater. Japan* 2004, *43*, 264–269. doi:10.2320/materia.43.264
6. Pollock, T. M. Materials Science. Weight Loss with Magnesium Alloys. *Science* 2010, *328*, 986–987. doi:10.1126/science.1182848
7. Mordike, B.; Ebert, T. Magnesium: Properties—Applications—Potential. *Mater. Sci. Eng. A* 2001, *302*, 37–45. doi:10.1016/S0921-5093(00)01351-4
8. Bussy, A. Mémoire sur le Radical Métallique de la Magnésie. *Ann. Chim.* 1831, *46*, 434–437.
9. Beetz, W. XXXIV. On the Development of Hydrogen from the Anode. *Lond. Edinb. Dublin Philos. Mag. J. Sci.* 1866, *32*, 269–278. doi:10.1080/14786446608644179
10. Witte, F. Reprint of: The History of Biodegradable Magnesium Implants: A Review. *Acta Biomater.* 2015, *23*, S28–S40. doi:10.1016/j.actbio.2015.07.017
11. Visnic, B. BMW N52. 2006. https://www.wardsauto.com/news-analysis/10-best-engines-2006
12. Sandlöbes, S.; Friák, M.; Korte-Kerzel, S.; Pei, Z.; Neugebauer, J.; Raabe, D. A Rare-Earth Free Magnesium Alloy with Improved Intrinsic Ductility. *Sci. Rep.* 2017, *7*, 1–8. doi:10.1038/s41598-017-10384-0
13. Pei, R.; Korte-Kerzel, S.; Al-Samman, T. Superior Microstructure and Mechanical Properties of a Next-Generation AZX310 Magnesium Sheet Alloy. *Mater. Sci. Eng. A* 2019, *763*, 138112. doi:10.1016/j.msea.2019.138112
14. Chaudry, U. M.; Kim, T. H.; Park, S. D.; Kim, Y. S.; Hamad, K.; Kim, J.-G. Effects of Calcium on the Activity of Slip Systems in AZ31 Magnesium Alloy. *Mater. Sci. Eng. A* 2019, *739*, 289–294. doi:10.1016/j.msea.2018.10.060
15. Masood Chaudry, U.; Hoo Kim, T.; Duck Park, S.; Sik Kim, Y.; Hamad, K.; Kim, J.-G. On the High Formability of AZ31-0.5 Ca Magnesium Alloy. *Materials* 2018, *11*, 2201. doi:10.3390/ma11112201
16. Kawamura, Y.; Hayashi, K.; Inoue, A.; Masumoto, T. Rapidly Solidified Powder Metallurgy Mg97Zn1Y2Alloys with Excellent Tensile Yield Strength above 600 MPa. *Mater. Trans.* 2001, *42*, 1172–1176. doi:10.2320/matertrans.42.1172
17. Wu, D.; Chen, R.; Han, E. Excellent Room-Temperature Ductility and Formability of Rolled Mg–Gd–Zn Alloy Sheets. *J. Alloys Compd.* 2011, *509*, 2856–2863. doi:10.1016/j.jallcom.2010.11.141
18. Takuda, H.; Kikuchi, S.; Yoshida, N.; Okahara, H. Tensile Properties and Press Formability of a Mg-9Li-1Y Alloy Sheet. *Mater. Trans.* 2003, *44*, 2266–2270. doi:10.2320/matertrans.44.2266

19. Chino, Y.; Sassa, K.; Mabuchi, M. Texture and Stretch Formability of a Rolled Mg–Zn Alloy Containing Dilute Content of Y. *Mater. Sci. Eng. A* 2009, *513-514*, 394–400. doi:10.1016/j.msea.2009.01.074
20. Yan, H.; Chen, R.; Han, E. Room-Temperature Ductility and Anisotropy of Two Rolled Mg–Zn–Gd Alloys. *Mater. Sci. Eng. A* 2010, *527*, 3317–3322. doi:10.1016/j.msea.2010.02.038
21. Nie, K.; Guo, Y.; Deng, K.; Kang, X. High Strength TiCp/Mg-Zn-Ca Magnesium Matrix Nanocomposites with Improved Formability at Low Temperature. *J. Alloys Compd.* 2019, *792*, 267–278. doi:10.1016/j.jallcom.2019.04.028
22. Sun, X-f.; Wang, C-j.; Deng, K-k.; Nie, K-b.; Zhang, X-c.; Xiao, X-y. High Strength SiCp/AZ91 Composite Assisted by Dynamic Precipitated Mg17Al12 Phase. *J. Alloys Compd.* 2018, *732*, 328–335. doi:10.1016/j.jallcom.2017.10.164
23. Kaviti, R. V. P.; Jeyasimman, D.; Parande, G.; Gupta, M.; Narayanasamy, R.; Koppad, P. G. Improving the Friction and Wear Characteristics of AZ31 Alloy with the Addition of Al_2O_3 Nanoparticles. *Mater. Res. Express* 2019, *6*, 126505. doi:10.1088/2053-1591/ab531d
24. Eliezer, D.; Aghion, E.; Froes, F. S. Magnesium Science, Technology and Applications. *Adv. Perform. Mater.* 1998, *5*, 201–212. doi:10.1023/A:1008682415141
25. Liu, W.; Zhou, B.; Wu, G.; Zhang, L.; Peng, X.; Cao, L. High Temperature Mechanical Behavior of Low-Pressure Sand-Cast Mg–Gd–Y–Zr Magnesium Alloy. *J. Magnesium Alloys* 2019, *7*, 597–604. doi:10.1016/j.jma.2019.07.006
26. Zhang, D.; Yang, Q.; Li, B.; Guan, K.; Wang, N.; Jiang, B.; Sun, C.; Zhang, D.; Li, X.; Cao, Z.; et al. Improvement on Both Strength and Ductility of Mg − Sm − Zn − Zr Casting Alloy via Yb Addition. *J. Alloys Compd.* 2019, *805*, 811–821. doi:10.1016/j.jallcom.2019.07.094
27. Wang, J.; Meng, J.; Zhang, D.; Tang, D. Effect of Y for Enhanced Age Hardening Response and Mechanical Properties of Mg–Gd–Y–Zr Alloys. *Mater. Sci. Eng. A* 2007, *456*, 78–84. doi:10.1016/j.msea.2006.11.096
28. Liu, S.; Yang, G.; Luo, S.; Jie, W. Microstructure Evolution during Heat Treatment and Mechanical Properties of Mg–2.49 Nd–1.82 Gd–0.19 Zn–0.4 Zr Cast Alloy. *Mater. Charact.* 2015, *107*, 334–342. doi:10.1016/j.matchar.2015.07.034
29. Mabuchi, M.; Chino, Y.; Iwasaki, H. Tensile Properties at Room Temperature to 823 K of Mg-4Y-3RE Alloy. *Mater. Trans.* 2002, *43*, 2063–2068. doi:10.2320/matertrans.43.2063
30. Kubasek, J.; Vojtěch, D. Zn-Based Alloys as an Alternative Biodegradable Materials. *Proc. Metal.* 2012, *5*, 23–25.
31. Liu, X.; Sun, J.; Zhou, F.; Yang, Y.; Chang, R.; Qiu, K.; Pu, Z.; Li, L.; Zheng, Y. Micro-Alloying with Mn in Zn–Mg Alloy for Future Biodegradable Metals Application. *Mater. Des.* 2016, *94*, 95–104. doi:10.1016/j.matdes.2015.12.128
32. Bowen, P. K.; Shearier, E. R.; Zhao, S.; Guillory, R. J.; Zhao, F.; Goldman, J.; Drelich, J. W. Biodegradable Metals for Cardiovascular Stents: From Clinical Concerns to Recent Zn-Alloys. *Adv. Healthc. Mater.* 2016, *5*, 1121–1140. doi:10.1002/adhm.201501019
33. Kubásek, J.; Vojtěch, D.; Jablonská, E.; Pospíšilová, I.; Lipov, J.; Ruml, T. Structure, Mechanical Characteristics and in Vitro Degradation, Cytotoxicity, Genotoxicity and Mutagenicity of Novel Biodegradable Zn-Mg Alloys. *Mater. Sci. Eng. C Mater. Biol. Appl.* 2016, *58*, 24–35. doi:10.1016/j.msec.2015.08.015
34. Liu, X.; Sun, J.; Yang, Y.; Zhou, F.; Pu, Z.; Li, L.; Zheng, Y. Microstructure, Mechanical Properties, in Vitro Degradation Behavior and Hemocompatibility of Novel Zn–Mg–Sr Alloys as Biodegradable Metals. *Mater. Lett.* 2016, *162*, 242–245. doi:10.1016/j.matlet.2015.07.151
35. Witte, F.; Fischer, J.; Nellesen, J.; Crostack, H.-A.; Kaese, V.; Pisch, A.; Beckmann, F.; Windhagen, H. In Vitro and in Vivo Corrosion Measurements of Magnesium Alloys. *Biomaterials* 2006, *27*, 1013–1018. doi:10.1016/j.biomaterials.2005.07.037
36. Sanchez, A. H. M.; Luthringer, B. J.; Feyerabend, F.; Willumeit, R. Mg and Mg Alloys: How Comparable Are in Vitro and in Vivo Corrosion Rates? A Review. *Acta Biomater.* 2015, *13*, 16–31. doi:10.1016/j.actbio.2014.11.048
37. Cheng, J.; Liu, B.; Wu, Y.; Zheng, Y. Comparative in Vitro Study on Pure Metals (Fe, Mn, Mg, Zn and W) as Biodegradable Metals. *J. Mater. Sci. Technol.* 2013, *29*, 619–627. doi:10.1016/j.jmst.2013.03.019
38. Heublein, B.; Rohde, R.; Kaese, V.; Niemeyer, M.; Hartung, W.; Haverich, A. Biocorrosion of Magnesium Alloys: A New Principle in Cardiovascular Implant Technology? *Heart* 2003, *89*, 651–656. doi:10.1136/heart.89.6.651
39. Di Mario, C.; Griffiths, H.; Goktekin, O.; Peeters, N.; Verbist, J.; Bosiers, M.; Deloose, K.; Heublein, B.; Rohde, R.; Kasese, V.; et al. Drug-Eluting Bioabsorbable Magnesium Stent. *J. Interv. Cardiol.* 2004, *17*, 391–395. doi:10.1111/j.1540-8183.2004.04081.x
40. Esmaily, M.; Blücher, D.; Svensson, J.-E.; Halvarsson, M.; Johansson, L.-G. New Insights into the Corrosion of Magnesium Alloys—The Role of Aluminum. *Scr. Mater.* 2016, *115*, 91–95. doi:10.1016/j.scriptamat.2016.01.008
41. Wan, Y.; Xiong, G.; Luo, H.; He, F.; Huang, Y.; Zhou, X. Preparation and Characterization of a New Biomedical Magnesium–Calcium Alloy. *Mater. Des.* 2008, *29*, 2034–2037. doi:10.1016/j.matdes.2008.04.017
42. Imandoust, A.; Barrett, C.; Al-Samman, T.; Inal, K.; El Kadiri, H. A Review on the Effect of Rare-Earth Elements on Texture Evolution during Processing of Magnesium Alloys. *J. Mater. Sci.* 2017, *52*, 1–29. doi:10.1007/s10853-016-0371-0
43. Pan, H.; Ren, Y.; Fu, H.; Zhao, H.; Wang, L.; Meng, X.; Qin, G. Recent Developments in Rare-Earth Free Wrought Magnesium Alloys Having High Strength:

A Review. *J. Alloys Compd.* 2016, *663*, 321–331. doi:10.1016/j.jallcom.2015.12.057
44. Yu, H.; Xin, Y.; Wang, M.; Liu, Q. Hall-Petch Relationship in Mg Alloys: A Review. *J. Mater. Sci. Technol.* 2018, *34*, 248–256. doi:10.1016/j.jmst.2017.07.022
45. Song, B.; Guo, N.; Liu, T.; Yang, Q. Improvement of Formability and Mechanical Properties of Magnesium Alloys via Pre-Twinning: A Review. *Mater. Des.* 2014, *62*, 352–360. doi:10.1016/j.matdes.2014.05.034
46. Wu, J.; Jin, L.; Dong, J.; Wang, F.; Dong, S. The Texture and Its Optimization in Magnesium Alloy. *J. Mater. Sci. Technol.* 2020, *42*, 175–189. doi:10.1016/j.jmst.2019.10.010
47. Esmaily, M.; Svensson, J. E.; Fajardo, S.; Birbilis, N.; Frankel, G. S.; Virtanen, S.; Arrabal, R.; Thomas, S.; Johansson, L. G. Fundamentals and Advances in Magnesium Alloy Corrosion. *Prog. Mater. Sci.* 2017, *89*, 92–193. doi:10.1016/j.pmatsci.2017.04.011
48. Tekumalla, S.; Processing, G. M. Properties and Potential Applications of Magnesium Alloy-Based Nanocomposites: A Review. In *Nanocomposites VI: Nanoscience and Nanotechnology in Advanced Composites*. Springer, 2019; pp. 3–18. https://doi.org/10.1007/978-3-030-35790-0_1
49. Bishop, J.; Hill, R. XLVI. A Theory of the Plastic Distortion of a Polycrystalline Aggregate under Combined Stresses. *Lond. Edinb. Dublin Philos. Mag. J. Sci.* 1951, *42*, 414–427. doi:10.1080/14786445108561065
50. Partridge, P. The Crystallography and Deformation Modes of Hexagonal Close Packed Metals. *Metallur. Rev.* 1967, *12*, 169–194.
51. Agnew, S.; Brown, D.; Tomé, C. Validating a Polycrystal Model for the Elastoplastic Response of Magnesium Alloy AZ31 Using in Situ Neutron Diffraction. *Acta Mater.* 2006, *54*, 4841–4852. doi:10.1016/j.actamat.2006.06.020
52. Akhtar, A.; Teghtsoonian, E. Solid Solution Strengthening of Magnesium Single Crystals—I Alloying Behaviour in Basal Slip. *Acta Metall.* 1969, *17*, 1339–1349. doi:10.1016/0001-6160(69)90151-5
53. Akhtar, A.; Teghtsoonian, E. Solid Solution Strengthening of Magnesium Single Crystals—II The Effect of Solute on the Ease of Prismatic Slip. *Acta Metall.* 1969, *17*, 1351–1356. doi:10.1016/0001-6160(69)90152-7
54. Agnew, S.; Liu, K.; Kenik, E.; Viswanathan, S. Magnesium Technology 2002. TMS, USA. 2002, 169.
55. Agnew, S.; Tomé, C.; Brown, D.; Holden, T.; Vogel, S. Study of Slip Mechanisms in a Magnesium Alloy by Neutron Diffraction and Modeling. *Scr. Mater.* 2003, *48*, 1003–1008. doi:10.1016/S1359-6462(02)00591-2
56. Muránsky, O.; Carr, D.; Barnett, M.; Oliver, E.; Šittner, P. Investigation of Deformation Mechanisms Involved in the Plasticity of AZ31 Mg Alloy: In Situ Neutron Diffraction and EPSC Modelling. *Mater. Sci. Eng. A* 2008, *496*, 14–24. doi:10.1016/j.msea.2008.07.031
57. Barnett, M.; Keshavarz, Z.; Ma, X. A Semianalytical Sachs Model for the Flow Stress of a Magnesium Alloy. *Metall. Mat. Trans. A.* 2006, *37*, 2283–2293. doi:10.1007/BF02586147
58. Muránsky, O.; Barnett, M.; Carr, D.; Vogel, S.; Oliver, E. Investigation of Deformation Twinning in a Fine-Grained and Coarse-Grained ZM20 Mg Alloy: Combined in Situ Neutron Diffraction and Acoustic Emission. *Acta Mater.* 2010, *58*, 1503–1517. doi:10.1016/j.actamat.2009.10.057
59. Herrera-Solaz, V.; Hidalgo-Manrique, P.; Pérez-Prado, M.; Letzig, D.; Llorca, J.; Segurado, J. Effect of Rare Earth Additions on the Critical Resolved Shear Stresses of Magnesium Alloys. *Mater. Lett.* 2014, *128*, 199–203. doi:10.1016/j.matlet.2014.04.144
60. Pan, H.; Wang, F.; Feng, M.; Jin, L.; Dong, J.; Wu, P. Mechanical Behavior and Microstructural Evolution in Rolled Mg-3Al-1Zn-0.5 Mn Alloy under Large Strain Simple Shear. *Mater. Sci. Eng. A* 2018, *712*, 585–591. doi:10.1016/j.msea.2017.11.123
61. Wang, L.; Huang, Z.; Wang, H.; Maldar, A.; Yi, S.; Park, J.-S.; Kenesei, P.; Lilleodden, E.; Zeng, X. Study of Slip Activity in a Mg-Y Alloy by in Situ High Energy X-Ray Diffraction Microscopy and Elastic Viscoplastic Self-Consistent Modeling. *Acta Mater.* 2018, *155*, 138–152. doi:10.1016/j.actamat.2018.05.065
62. Steglich, D.; Jeong, Y. Texture-Based Forming Limit Prediction for Mg Sheet Alloys ZE10 and AZ31. *Int. J. Mech. Sci.* 2016, *117*, 102–114. doi:10.1016/j.ijmecsci.2016.08.013
63. Bohlen, J.; Nürnberg, M. R.; Senn, J. W.; Letzig, D.; Agnew, S. R. The Texture and Anisotropy of Magnesium–Zinc–Rare Earth Alloy Sheets. *Acta Mater.* 2007, *55*, 2101–2112. doi:10.1016/j.actamat.2006.11.013
64. Sun, J.; Jin, L.; Dong, S.; Dong, J.; Zhang, Z.; Wang, F.; Ding, W.; Luo, A. A. A Combined Electron Backscattered Diffraction and Visco-Plastic Self-Consistent Analysis on the Anisotropic Deformation Behavior in a Mg-Gd-Y Alloy. *Mater. Des.* 2017, *122*, 164–171. doi:10.1016/j.matdes.2017.02.093
65. Staroselsky, A.; Anand, L. A Constitutive Model for Hcp Materials Deforming by Slip and Twinning: Application to Magnesium Alloy AZ31B. *Int. J. Plast.* 2003, *19*, 1843–1864. doi:10.1016/S0749-6419(03)00039-1
66. Raeisinia, B.; Agnew, S. R.; Akhtar, A. Incorporation of Solid Solution Alloying Effects into Polycrystal Modeling of Mg Alloys. *Metall. Mat. Trans. A.* 2011, *42*, 1418–1430. doi:10.1007/s11661-010-0527-5
67. Sandlöbes, S.; Zaefferer, S.; Schestakow, I.; Yi, S.; Gonzalez-Martinez, R. On the Role of Non-Basal Deformation Mechanisms for the Ductility of Mg and Mg–Y Alloys. *Acta Mater.* 2011, *59*, 429–439. doi:10.1016/j.actamat.2010.08.031
68. Chino, Y.; Kado, M.; Mabuchi, M. Enhancement of Tensile Ductility and Stretch Formability of Magnesium by Addition of 0.2 wt%(0.035 at%) Ce. *Mater. Sci. Eng. A* 2008, *494*, 343–349. doi:10.1016/j.msea.2008.04.059
69. Agnew, S.; Yoo, M.; Tome, C. Application of Texture Simulation to Understanding Mechanical Behavior of Mg and Solid Solution Alloys

Containing Li or Y. *Acta Mater.* 2001, *49*, 4277–4289. doi:10.1016/S1359-6454(01)00297-X
70. Agnew, S.; Horton, J.; Yoo, M. Transmission Electron Microscopy Investigation of < c+a > Dislocations in Mg and α-Solid Solution Mg-Li Alloys. *Metallur. Mater. Trans. A* 2002, *33*, 851–858.
71. Nogaret, T.; Curtin, W.; Yasi, J.; Hector, L.; Jr.; Trinkle, D. Atomistic Study of Edge and Screw < c+a > Dislocations in Magnesium. *Acta Mater.* 2010, *58*, 4332–4343.
72. Wu, Z.; Curtin, W. The Origins of High Hardening and Low Ductility in Magnesium. *Nature* 2015, *526*, 62–67. doi:10.1038/nature15364
73. Al-Samman, T.; Li, X. Sheet Texture Modification in Magnesium-Based Alloys by Selective Rare Earth Alloying. *Mater. Sci. Eng. A* 2011, *528*, 3809–3822. doi:10.1016/j.msea.2011.01.080
74. Hantzsche, K.; Bohlen, J.; Wendt, J.; Kainer, K.; Yi, S.; Letzig, D. Effect of Rare Earth Additions on Microstructure and Texture Development of Magnesium Alloy Sheets. *Scr. Mater.* 2010, *63*, 725–730. doi:10.1016/j.scriptamat.2009.12.033
75. Sandlöbes, S.; Friák, M.; Zaefferer, S.; Dick, A.; Yi, S.; Letzig, D.; Pei, Z.; Zhu, L.-F.; Neugebauer, J.; Raabe, D. The Relation between Ductility and Stacking Fault Energies in Mg and Mg–Y Alloys. *Acta Mater.* 2012, *60*, 3011–3021. doi:10.1016/j.actamat.2012.02.006
76. Chino, Y.; Kado, M.; Mabuchi, M. Compressive Deformation Behavior at Room Temperature–773 K in Mg–0.2 Mass%(0.035 at.%) Ce Alloy. *Acta Mater.* 2008, *56*, 387–394. doi:10.1016/j.actamat.2007.09.036
77. Suh, B.-C.; Kim, J. H.; Bae, J. H.; Hwang, J. H.; Shim, M.-S.; Kim, N. J. Effect of Sn Addition on the Microstructure and Deformation Behavior of Mg-3Al Alloy. *Acta Mater.* 2017, *124*, 268–279. doi:10.1016/j.actamat.2016.11.020
78. Yuasa, M.; Miyazawa, N.; Hayashi, M.; Mabuchi, M.; Chino, Y. Effects of Group II Elements on the Cold Stretch Formability of Mg–Zn Alloys. *Acta Mater.* 2015, *83*, 294–303. doi:10.1016/j.actamat.2014.10.005
79. Lentz, M.; Risse, M.; Schaefer, N.; Reimers, W.; Beyerlein, I. Strength and Ductility with {10 - 11}—{10 - 12} Double Twinning in a Magnesium Alloy. *Nat. Commun.* 2016, *7*, 1–7. doi:10.1038/ncomms11068
80. Li, X.; Yang, P.; Wang, L.-N.; Meng, L.; Cui, F.-e. Orientational Analysis of Static Recrystallization at Compression Twins in a Magnesium Alloy AZ31. *Mater. Sci. Eng.* 2009, *517*, 160–169. doi:10.1016/j.msea.2009.03.045
81. Lentz, M.; Coelho, R. S.; Camin, B.; Fahrenson, C.; Schaefer, N.; Selve, S.; Link, T.; Beyerlein, I. J.; Reimers, W. In-Situ, Ex-Situ EBSD and (HR-) TEM Analyses of Primary, Secondary and Tertiary Twin Development in an Mg–4 wt% Li Alloy. *Mater. Sci. Eng. A* 2014, *610*, 54–64. doi:10.1016/j.msea.2014.05.025
82. Cizek, P.; Barnett, M. Characteristics of the Contraction Twins Formed Close to the Fracture Surface in Mg–3Al–1Zn Alloy Deformed in Tension. *Scr. Mater.* 2008, *59*, 959–962. doi:10.1016/j.scriptamat.2008.06.041
83. Mu, S.; Jonas, J. J.; Gottstein, G. Variant Selection of Primary, Secondary and Tertiary Twins in a Deformed Mg Alloy. *Acta Mater.* 2012, *60*, 2043–2053. doi:10.1016/j.actamat.2012.01.014
84. Ando, D.; Koike, J.; Sutou, Y. The Role of Deformation Twinning in the Fracture Behavior and Mechanism of Basal Textured Magnesium Alloys. *Mater. Sci. Eng. A* 2014, *600*, 145–152. doi:10.1016/j.msea.2014.02.010
85. Hong, S.-G.; Park, S. H.; Lee, C. S. Role of {10–12} Twinning Characteristics in the Deformation Behavior of a Polycrystalline Magnesium Alloy. *Acta Mater.* 2010, *58*, 5873–5885. doi:10.1016/j.actamat.2010.07.002
86. Lou, X.; Li, M.; Boger, R.; Agnew, S.; Wagoner, R. Hardening Evolution of AZ31B Mg Sheet. *Int. J. Plast.* 2007, *23*, 44–86. doi:10.1016/j.ijplas.2006.03.005
87. Lentz, M.; Behringer, A.; Fahrenson, C.; Beyerlein, I. J.; Reimers, W. Grain Size Effects on Primary, Secondary, and Tertiary Twin Development in Mg-4 wt Pct Li (-1 wt Pct Al) Alloys. *Metall. Mat. Trans. A.* 2014, *45*, 4737–4741. doi:10.1007/s11661-014-2491-y
88. Brown, D.; Agnew, S.; Bourke, M.; Holden, T.; Vogel, S.; Tomé, C. Internal Strain and Texture Evolution during Deformation Twinning in Magnesium. *Mater. Sci. Eng. A* 2005, *399*, 1–12. doi:10.1016/j.msea.2005.02.016
89. El Kadiri, H.; Barrett, C. D.; Wang, J.; Tomé, C. N. Why Are {101\bar 2} Twins Profuse in Magnesium? *Acta Mater.* 2015, *85*, 354–361. doi:10.1016/j.actamat.2014.11.033
90. Kim, H.; Lee, J.-H.; Lee, C.; Bang, W.; Ahn, S.; Chang, Y. Shear Band Formation during Hot Compression of AZ31 Mg Alloy Sheets. *Mater Sci. Eng. A* 2012, *558*, 431–438. doi:10.1016/j.msea.2012.08.023
91. Ma, Q.; Li, B.; Marin, E.; Horstemeyer, S. Twinning-Induced Dynamic Recrystallization in a Magnesium Alloy Extruded at 450 C. *Scr. Mater.* 2011, *65*, 823–826. doi:10.1016/j.scriptamat.2011.07.046
92. Park, C. H.; Oh, C.-S.; Kim, S. Dynamic Recrystallization of the H-and O-Tempered Mg AZ31 Sheets at Elevated Temperatures. *Mater. Sci. Eng. A* 2012, *542*, 127–139. doi:10.1016/j.msea.2012.02.042
93. Koike, J.; Kobayashi, T.; Mukai, T.; Watanabe, H.; Suzuki, M.; Maruyama, K.; Higashi, K. The Activity of Non-Basal Slip Systems and Dynamic Recovery at Room Temperature in Fine-Grained AZ31B Magnesium Alloys. *Acta Mater.* 2003, *51*, 2055–2065. doi:10.1016/S1359-6454(03)00005-3
94. Sherby, O. D.; Wadsworth, J. Superplasticity—Recent Advances and Future Directions. *Prog. Mater. Sci.* 1989, *33*, 169–221. doi:10.1016/0079-6425(89)90004-2
95. Somekawa, H.; Mukai, T. Effect of Grain Boundary Structures on Grain Boundary Sliding in Magnesium. *Mater. Lett.* 2012, *76*, 32–35. doi:10.1016/j.matlet.2012.02.010

96. Somekawa, H.; Tsuru, T. Effect of Alloying Elements on Grain Boundary Sliding in Magnesium Binary Alloys: Experimental and Numerical Studies. *Mater. Sci. Eng. A* 2017, *708*, 267–273. doi:10.1016/j.msea.2017.09.095
97. Ando, D.; Sutou, Y.; Koike, J. Internal Microstructure Observation of Enhanced Grain-Boundary Sliding at Room Temperature in AZ31 Magnesium Alloy. *Mater. Sci. Eng. A* 2016, *666*, 94–99. doi:10.1016/j.msea.2016.04.030
98. Somekawa, H.; Singh, A. Superior Room Temperature Ductility of Magnesium Dilute Binary Alloy via Grain Boundary Sliding. *Scr. Mater.* 2018, *150*, 26–30. doi:10.1016/j.scriptamat.2018.02.034
99. Zeng, Z.; Nie, J.-F.; Xu, S.-W.; Davies, C. H.; Birbilis, N. Super-Formable Pure Magnesium at Room Temperature. *Nat. Commun.* 2017, *8*, 1–6. doi:10.1038/s41467-017-01330-9
100. Koike, J.; Ohyama, R.; Kobayashi, T.; Suzuki, M.; Maruyama, K. Grain-Boundary Sliding in AZ31 Magnesium Alloys at Room Temperature to 523 K. *Mater. Trans.* 2003, *44*, 445–451. doi:10.2320/matertrans.44.445
101. Rachinger, W. Relative Grain Translations in the Plastic Flow of Aluminium. *J. Inst. Metals* 1952, *81*, 33–41.
102. Lifshitz, I. On the Theory of Diffusion-Viscous Flow of Polycrystalline Bodies. *Soviet Phys. JETP* 1963, *17*, 909.
103. Roodposhti, P. S.; Sarkar, A.; Murty, K. L.; Brody, H.; Scattergood, R. Grain Boundary Sliding Mechanism during High Temperature Deformation of AZ31 Magnesium Alloy. *Mater. Sci. Eng. A* 2016, *669*, 171–177. doi:10.1016/j.msea.2016.05.076
104. Wu, K.-C.; Chang, S.-Y.; Yeh, J.-W. Optimizing Superplasticity of AZ91− xSn Magnesium Alloys with Competitive Grain Growth and Boundary Sliding. *Mater. Sci. Eng. A* 2015, *646*, 201–206. doi:10.1016/j.msea.2015.08.066
105. Figueiredo, R. B.; Sabbaghianrad, S.; Giwa, A.; Greer, J. R.; Langdon, T. G. Evidence for Exceptional Low Temperature Ductility in Polycrystalline Magnesium Processed by Severe Plastic Deformation. *Acta Mater.* 2017, *122*, 322–331. doi:10.1016/j.actamat.2016.09.054
106. Choi, H.; Kim, Y.; Shin, J.; Bae, D. Deformation Behavior of Magnesium in the Grain Size Spectrum from Nano-to Micrometer. *Mater. Sci. Eng. A* 2010, *527*, 1565–1570. doi:10.1016/j.msea.2009.10.035
107. Wang, C.; Mukai, T.; Nieh, T. Room Temperature Creep of Fine-Grained Pure Mg: A Direct Comparison between Nanoindentation and Uniaxial Tension. *J. Mater. Res.* 2009, *24*, 1615–1618. doi:10.1557/jmr.2009.0187
108. Somekawa, H.; Mukai, T. Nanoindentation Creep Behavior of Grain Boundary in Pure Magnesium. *Philos. Mag. Lett.* 2010, *90*, 883–890. doi:10.1080/09500839.2010.514577
109. Somekawa, H.; Mukai, T. Hall–Petch Breakdown in Fine-Grained Pure Magnesium at Low Strain Rates. *Metall. Mat. Trans. A.* 2015, *46*, 894–902. doi:10.1007/s11661-014-2641-2
110. Figueiredo, R. B.; Poggiali, F. S.; Silva, C. L.; Cetlin, P. R.; Langdon, T. G. The Influence of Grain Size and Strain Rate on the Mechanical Behavior of Pure Magnesium. *J. Mater. Sci.* 2016, *51*, 3013–3024. doi:10.1007/s10853-015-9612-x
111. Hwang, S.; Nishimura, C.; McCormick, P. Deformation Mechanism of Nanocrystalline Magnesium in Compression. *Scr. Mater.* 2001, *44*, 1507–1511. doi:10.1016/S1359-6462(01)00716-3
112. Somekawa, H.; Kinoshita, A.; Washio, K.; Kato, A. Enhancement of Room Temperature Stretch Formability via Grain Boundary Sliding in Magnesium Alloy. *Mater. Sci. Eng. A* 2016, *676*, 427–433. doi:10.1016/j.msea.2016.09.014
113. Edalati, K.; Masuda, T.; Arita, M.; Furui, M.; Sauvage, X.; Horita, Z.; Valiev, R. Z. Room-Temperature Superplasticity in an Ultrafine-Grained Magnesium Alloy. *Sci. Rep.* 2017, *7*, 1–9. doi:10.1038/s41598-017-02846-2
114. Tonda, H.; Ando, S. Effect of Temperature and Shear Direction on Yield Stress by {11\Bar2\Bar 22}< \Overline11\Overline {11} 23> Slip in HCP metals23> Slip in HCP Metals. *Metall. Mater. Trans. A* 2002, *33*, 831–836.
115. Sandlöbes, S.; Pei, Z.; Friák, M.; Zhu, L.-F.; Wang, F.; Zaefferer, S.; Raabe, D.; Neugebauer, J. Ductility Improvement of Mg Alloys by Solid Solution: Ab Initio Modeling, Synthesis and Mechanical Properties. *Acta Mater.* 2014, *70*, 92–104. doi:10.1016/j.actamat.2014.02.011
116. Pei, Z.; Friák, M.; Sandlöbes, S.; Nazarov, R.; Svendsen, B.; Raabe, D.; Neugebauer, J. Rapid Theory-Guided Prototyping of Ductile Mg Alloys: From Binary to Multi-Component Materials. *New J. Phys.* 2015, *17*, 093009. doi:10.1088/1367-2630/17/9/093009
117. Pei, Z.; Li, R. The Effect of Yttrium on the Generalized Stacking Fault Energies in Mg. *Comput. Mater. Sci.* 2017, *133*, 1–5. doi:10.1016/j.commatsci.2017.02.030
118. Yasi, J. A.; Hector, L. G.; Jr.; Trinkle, D. R. First-Principles Data for Solid-Solution Strengthening of Magnesium: From Geometry and Chemistry to Properties. *Acta Mater.* 2010, *58*, 5704–5713. doi:10.1016/j.actamat.2010.06.045
119. Liu, Z.; Li, D. The Electronic Origin of Strengthening and Ductilizing Magnesium by Solid Solutes. *Acta Mater.* 2015, *89*, 225–233. doi:10.1016/j.actamat.2015.01.051
120. Wu, Y.; Li, S.; Ding, Z.; Liu, W.; Zhao, Y.; Zhu, Y. Effect of Charge Redistribution Factor on Stacking-Fault Energies of Mg-Based Binary Alloys. *Scr. Mater.* 2016, *112*, 101–105. doi:10.1016/j.scriptamat.2015.09.023
121. Zhang, J.; Dou, Y.; Liu, G.; Guo, Z. First-Principles Study of Stacking Fault Energies in Mg-Based Binary Alloys. *Comput. Mater. Sci.* 2013, *79*, 564–569. doi:10.1016/j.commatsci.2013.07.012
122. Wen, L.; Chen, P.; Tong, Z.-F.; Tang, B.-Y.; Peng, L.-M.; Ding, W.-J. A Systematic Investigation of Stacking Faults in Magnesium via First-Principles

Calculation. *Eur. Phys. J. B.* 2009, *72*, 397–403. doi:10.1140/epjb/e2009-00365-2

123. Han, J.; Su, X.; Jin, Z.-H.; Zhu, Y. Basal-Plane Stacking-Fault Energies of Mg: A First-Principles Study of Li-and Al-Alloying Effects. *Scr. Mater.* 2011, *64*, 693–696. doi:10.1016/j.scriptamat.2010.11.034
124. Wang, H.-Y.; Zhang, N.; Wang, C.; Jiang, Q.-C. First-Principles Study of the Generalized Stacking Fault Energy in Mg–3Al–3Sn Alloy. *Scr. Mater.* 2011, *65*, 723–726. doi:10.1016/j.scriptamat.2011.07.016
125. Dong, Q.; Luo, Z.; Zhu, H.; Wang, L.; Ying, T.; Jin, Z.; Li, D.; Ding, W.; Zeng, X. Basal-Plane Stacking-Fault Energies of Mg Alloys: A First-Principles Study of Metallic Alloying Effects. *J. Mater. Sci. Technol.* 2018, *34*, 1773–1780. doi:10.1016/j.jmst.2018.02.009
126. Kitahara, T.; Ando, S.; Tsushida, M.; Kitahara, H.; Tonda, H. Deformation Behavior of Magnesium Single Crystals in c-Axis Compression. *KEM* 2007, *345-346*, 129–132. doi:10.4028/www.scientific.net/KEM.345-346.129
127. Geng, J.; Chisholm, M. F.; Mishra, R.; Kumar, K. The Structure of⟨ c + a⟩ Type Dislocation Loops in Magnesium. *Philos. Mag. Lett.* 2014, *94*, 377–386. doi:10.1080/09500839.2014.916423
128. Wu, Z.; Curtin, W. Intrinsic Structural Transitions of the Pyramidal I < c+ a > Dislocation in Magnesium. *Scr. Mater.* 2016, *116*, 104–107.
129. Wu, Z.; Ahmad, R.; Yin, B.; Sandlöbes, S.; Curtin, W. Mechanistic Origin and Prediction of Enhanced Ductility in Magnesium Alloys. *Science* 2018, *359*, 447–452. doi:10.1126/science.aap8716
130. Fan, H.; Tang, J.; Tian, X.; Wang, Q.; Tian, X.; El-Awady, J. A. Core Structures and Mobility of⟨ c⟩ Dislocations in Magnesium. *Scr. Mater.* 2017, *135*, 37–40. doi:10.1016/j.scriptamat.2017.03.012
131. Fan, H.; El-Awady, J. A. Towards Resolving the Anonymity of Pyramidal Slip in Magnesium. *Mater. Sci. Eng. A* 2015, *644*, 318–324. doi:10.1016/j.msea.2015.07.080
132. Liu, B.-Y.; Liu, F.; Yang, N.; Zhai, X.-B.; Zhang, L.; Yang, Y.; Li, B.; Li, J.; Ma, E.; Nie, J.-F.; et al. Large Plasticity in Magnesium Mediated by Pyramidal Dislocations. *Science* 2019, *365*, 73–75. doi:10.1126/science.aaw2843
133. Couling, S.; Pashak, J.; Sturkey, L. Unique Deformation and Aging Characteristics of Certain Magnesium-Base Alloys. *Trans. ASM* 1959, *51*, 94–107.
134. Yin, B.; Wu, Z.; Curtin, W. First-Principles Calculations of Stacking Fault Energies in Mg-Y, Mg-Al and Mg-Zn Alloys and Implications for < c+ a > Activity. *Acta Mater.* 2017, *136*, 249–261.
135. Zhu, G.; Wang, L.; Zhou, H.; Wang, J.; Shen, Y.; Tu, P.; et al. Improving Ductility of a Mg Alloy via Non-Basal < a> Slip Induced by Ca Addition. *Int. J. Plast.* 2019, *120*, 164–179.
136. Hall, E. The Deformation and Ageing of Mild Steel: III Discussion of Results. *Proc. Phys. Soc. B.* 1951, *64*, 747–753. doi:10.1088/0370-1301/64/9/303
137. Yuan, W.; Panigrahi, S.; Su, J.-Q.; Mishra, R. Influence of Grain Size and Texture on Hall–Petch Relationship for a Magnesium Alloy. *Scr. Mater.* 2011, *65*, 994–997. doi:10.1016/j.scriptamat.2011.08.028
138. Yu, H.; Li, C.; Xin, Y.; Chapuis, A.; Huang, X.; Liu, Q. The Mechanism for the High Dependence of the Hall-Petch Slope for Twinning/Slip on Texture in Mg Alloys. *Acta Mater.* 2017, *128*, 313–326. doi:10.1016/j.actamat.2017.02.044
139. Tong, L. B.; Zheng, M. Y.; Kamado, S.; Zhang, D. P.; Meng, J.; Cheng, L. R.; Zhang, H. J. Reducing the Tension–Compression Yield Asymmetry of Extruded Mg–Zn–Ca Alloy via Equal Channel Angular Pressing. *J. Magnesium Alloys* 2015, *3*, 302–308. doi:10.1016/j.jma.2015.08.007
140. Doiphode, R.; Murty, S. N.; Prabhu, N.; Kashyap, B. Grain Growth in Calibre Rolled Mg–3Al–1Zn Alloy and Its Effect on Hardness. *J. Magnesium Alloys* 2015, *3*, 322–329. doi:10.1016/j.jma.2015.11.003
141. Wang, Y.; Choo, H. Influence of Texture on Hall–Petch Relationships in an Mg Alloy. *Acta Mater.* 2014, *81*, 83–97. doi:10.1016/j.actamat.2014.08.023
142. Guo, L.; Chen, Z.; Gao, L. Effects of Grain Size, Texture and Twinning on Mechanical Properties and Work-Hardening Behavior of AZ31 Magnesium Alloys. *Mater. Sci. Eng. A* 2011, *528*, 8537–8545. doi:10.1016/j.msea.2011.07.076
143. Chino, Y.; Mabuchi, M.; Kishihara, R.; Hosokawa, H.; Yamada, Y.; Wen, C&r;e.; Shimojima, K.; Iwasaki, H. Mechanical Properties and Press Formability at Room Temperature of AZ31 Mg Alloy Processed by Single Roller Drive Rolling. *Mater. Trans.* 2002, *43*, 2554–2560. doi:10.2320/matertrans.43.2554
144. Del Valle, J.; Carreño, F.; Ruano, O. A. Influence of Texture and Grain Size on Work Hardening and Ductility in Magnesium-Based Alloys Processed by ECAP and Rolling. *Acta Mater.* 2006, *54*, 4247–4259. doi:10.1016/j.actamat.2006.05.018
145. Shaw, L. L.; Ortiz, A. L.; Villegas, J. C. Hall–Petch Relationship in a Nanotwinned Nickel Alloy. *Scr. Mater.* 2008, *58*, 951–954. doi:10.1016/j.scriptamat.2008.01.025
146. Jain, A.; Duygulu, O.; Brown, D.; Tomé, C.; Agnew, S. Grain Size Effects on the Tensile Properties and Deformation Mechanisms of a Magnesium Alloy, AZ31B, Sheet. *Mater. Sci. Eng. A* 2008, *486*, 545–555. doi:10.1016/j.msea.2007.09.069
147. Barnett, M.; Keshavarz, Z.; Beer, A.; Atwell, D. Influence of Grain Size on the Compressive Deformation of Wrought Mg–3Al–1Zn. *Acta Mater.* 2004, *52*, 5093–5103. doi:10.1016/j.actamat.2004.07.015
148. Chang, L.; Wang, Y.; Zhao, X.; Qi, M. Grain Size and Texture Effect on Compression Behavior of Hot-Extruded Mg–3Al–1Zn Alloys at Room Temperature. *Mater. Charact.* 2009, *60*, 991–994. doi:10.1016/j.matchar.2009.04.001
149. Somekawa, H.; Mukai, T. Hall–Petch Relation for Deformation Twinning in Solid Solution Magnesium Alloys. *Mater. Sci. Eng. A* 2013, *561*, 378–385. doi:10.1016/j.msea.2012.10.040
150. Wang, Y.; Chang, C.; Lee, C.; Lin, H.; Huang, J. Texture and Weak Grain Size Dependence in Friction

Stir Processed Mg–Al–Zn Alloy. *Scr. Mater.* 2006, *55*, 637–640. doi:10.1016/j.scriptamat.2006.06.005

151. Razavi, S. M.; Foley, D. C.; Karaman, I.; Hartwig, K. T.; Duygulu, O.; Kecskes, L. J.; Mathaudhu, S. N.; Hammond, V. H. Effect of Grain Size on Prismatic Slip in Mg–3Al–1Zn Alloy. *Scr. Mater.* 2012, *67*, 439–442. doi:10.1016/j.scriptamat.2012.05.017
152. Kim, W. J.; Jeong, H. T. Grain-Size Strengthening in Equal-Channel-Angular-Pressing Processed AZ31 Mg Alloys with a Constant Texture. *Mater. Trans.* 2005, *46*, 251–258. doi:10.2320/matertrans.46.251
153. Kim, H.-K. The Grain Size Dependence of Flow Stress in an ECAPed AZ31 Mg Alloy with a Constant Texture. *Mater. Sci. Eng. A* 2009, *515*, 66–70. doi:10.1016/j.msea.2009.02.039
154. Dieter, G. E.; Bacon, D. J. *Mechanical Metallurgy*. McGraw-Hill: New York; 1986.
155. Lin, J.; Ren, W.; Wang, Q.; Ma, L.; Chen, Y. Influence of Grain Size and Texture on the Yield Strength of Mg Alloys Processed by Severe Plastic Deformation. *Adv. Mater. Sci. Eng.* 2014, *2014*, 1–9. doi:10.1155/2014/356572
156. Chaudry, U. M.; Hamad, K.; Kim, J.-G. On the Ductility of Magnesium Based Materials: A Mini Review. *J. Alloys Compd.* 2019, *792*, 652–664. doi:10.1016/j.jallcom.2019.04.031
157. Yang, H. J.; Yin, S. M.; Huang, C. X.; Zhang, Z. F.; Wu, S. D.; Li, S. X.; Liu, Y. D. EBSD Study on Deformation Twinning in AZ31 Magnesium Alloy during Quasi-in-Situ Compression. *Adv. Eng. Mater.* 2008, *10*, 955–960. doi:10.1002/adem.200800111
158. Cepeda-Jiménez, C.; Molina-Aldareguia, J.; Pérez-Prado, M. Effect of Grain Size on Slip Activity in Pure Magnesium Polycrystals. *Acta Mater.* 2015, *84*, 443–456. doi:10.1016/j.actamat.2014.10.001
159. Ding, S.; Lee, W.; Chang, C.; Chang, L.; Kao, P. Improvement of Strength of Magnesium Alloy Processed by Equal Channel Angular Extrusion. *Scr. Mater.* 2008, *59*, 1006–1009. doi:10.1016/j.scriptamat.2008.07.007
160. Suh, J.; Victoria-Hernandez, J.; Letzig, D.; Golle, R.; Yi, S.; Bohlen, J.; Volk, W. Improvement in Cold Formability of AZ31 Magnesium Alloy Sheets Processed by Equal Channel Angular Pressing. *J. Mater. Process. Technol.* 2015, *217*, 286–293. doi:10.1016/j.jmatprotec.2014.11.029
161. Agnew, S.; Horton, J.; Lillo, T.; Brown, D. Enhanced Ductility in Strongly Textured Magnesium Produced by Equal Channel Angular Processing. *Scr. Mater.* 2004, *50*, 377–381. doi:10.1016/j.scriptamat.2003.10.006
162. Kim, H.; Kim, W. Microstructural Instability and Strength of an AZ31 Mg Alloy after Severe Plastic Deformation. *Mater. Sci. Eng. A* 2004, *385*, 300–308. doi:10.1016/S0921-5093(04)00882-2
163. Mukai, T.; Yamanoi, M.; Watanabe, H.; Higashi, K. Ductility Enhancement in AZ31 Magnesium Alloy by Controlling Its Grain Structure. *Scr. Mater.* 2001, *45*, 89–94. doi:10.1016/S1359-6462(01)00996-4
164. Zhan, M.; Li, Y.; Chen, W.; Chen, W. Microstructure and Mechanical Properties of Mg–Al–Zn Alloy Sheets Severely Deformed by Accumulative Roll-Bonding. *J. Mater. Sci.* 2007, *42*, 9256–9261. doi:10.1007/s10853-007-1885-2
165. Watanabe, H.; Mukai, T.; Ishikawa, K. Effect of Temperature of Differential Speed Rolling on Room Temperature Mechanical Properties and Texture in an AZ31 Magnesium Alloy. *J. Mater. Process. Technol.* 2007, *182*, 644–647. doi:10.1016/j.jmatprotec.2006.08.010
166. Kim, W.; Hwang, B.; Lee, M.; Park, Y. Effect of Speed-Ratio on Microstructure, and Mechanical Properties of Mg–3Al–1Zn Alloy, in Differential Speed Rolling. *J. Alloys Compd.* 2011, *509*, 8510–8517. doi:10.1016/j.jallcom.2011.05.063
167. Xia, W.; Chen, Z.; Chen, D.; Zhu, S. Microstructure and Mechanical Properties of AZ31 Magnesium Alloy Sheets Produced by Differential Speed Rolling. *J. Mater. Process. Technol.* 2009, *209*, 26–31. doi:10.1016/j.jmatprotec.2008.01.045
168. Hamad, K.; Chung, B. K.; Ko, Y. G. Microstructure and Mechanical Properties of Severely Deformed Mg–3% Al–1% Zn Alloy via Isothermal Differential Speed Rolling at 453 K. *J. Alloys Compd.* 2014, *615*, S590–S4. doi:10.1016/j.jallcom.2013.12.195
169. Kim, W.; Lee, H.; Yoo, S.; Park, Y. Texture and Mechanical Properties of Ultrafine-Grained Mg–3Al–1Zn Alloy Sheets Prepared by High-Ratio Differential Speed Rolling. *Mater. Sci. Eng. A* 2011, *528*, 874–879. doi:10.1016/j.msea.2010.09.007
170. Kim, W.; Yoo, S.; Chen, Z.; Jeong, H. Grain Size and Texture Control of Mg–3Al–1Zn Alloy Sheet Using a Combination of Equal-Channel Angular Rolling and High-Speed-Ratio Differential Speed-Rolling Processes. *Scr. Mater.* 2009, *60*, 897–900. doi:10.1016/j.scriptamat.2009.02.005
171. Kim, W.; Lee, Y.; Lee, M.; Wang, J.; Park, Y. Exceptionally High Strength in Mg–3Al–1Zn Alloy Processed by High-Ratio Differential Speed Rolling. *Scr. Mater.* 2011, *65*, 1105–1108. doi:10.1016/j.scriptamat.2011.09.029
172. Wang, S.; Chou, C. Effect of Adding Sc and Zr on Grain Refinement and Ductility of AZ31 Magnesium Alloy. *J. Mater. Process. Technol.* 2008, *197*, 116–121. doi:10.1016/j.jmatprotec.2007.06.021
173. Masoudpanah, S.; Mahmudi, R. Effects of Rare-Earth Elements and Ca Additions on the Microstructure and Mechanical Properties of AZ31 Magnesium Alloy Processed by ECAP. *Mater. Sci. Eng. A* 2009, *526*, 22–30. doi:10.1016/j.msea.2009.08.027
174. Xu, S.; Zheng, M.; Kamado, S.; Wu, K. The Microstructural Evolution and Superplastic Behavior at Low Temperatures of Mg–5.00 Zn–0.92 Y–0.16 Zr (wt.%) Alloys after Hot Extrusion and ECAP Process. *Mater. Sci. Eng. A* 2012, *549*, 60–68. doi:10.1016/j.msea.2012.03.116
175. Zheng, M.; Xu, S.; Wu, K.; Kamado, S.; Kojima, Y. Superplasticity of Mg–Zn–Y Alloy Containing Quasicrystal Phase Processed by Equal Channel Angular Pressing. *Mater. Lett.* 2007, *61*, 4406–4408. doi:10.1016/j.matlet.2007.02.013
176. Bae, D.; Kim, Y.; Kim, I. Thermally Stable Quasicrystalline Phase in a Superplastic

Mg–Zn–Y–Zr Alloy. *Mater. Lett.* 2006, *60*, 2190–2193. doi:10.1016/j.matlet.2005.12.096
177. Valiev, R. Z.; Islamgaliev, R. K.; Alexandrov, I. V. Bulk Nanostructured Materials from Severe Plastic Deformation. *Prog. Mater. Sci.* 2000, *45*, 103–189. doi:10.1016/S0079-6425(99)00007-9
178. Furukawa, M.; Horita, Z.; Langdon, T. G. Factors Influencing the Shearing Patterns in Equal-Channel Angular Pressing. *Mater. Sci. Eng. A* 2002, *332*, 97–109. doi:10.1016/S0921-5093(01)01716-6
179. Sklenicka, V.; Dvorak, J.; Kral, P.; Svoboda, M.; Kvapilova, M.; Langdon, T. Factors Influencing Creep Flow and Ductility in Ultrafine-Grained Metals. *Mater. Sci. Eng. A* 2012, *558*, 403–411. doi:10.1016/j.msea.2012.08.019
180. Valiev, R. Z. Paradoxes of Severe Plastic Deformation. *Adv. Eng. Mater.* 2003, *5*, 296–300. doi:10.1002/adem.200310089
181. Kang, S.-H.; Lee, Y.; Lee, J. Effect of Grain Refinement of Magnesium Alloy AZ31 by Severe Plastic Deformation on Material Characteristics. *J. Mater. Process. Technol.* 2008, *201*, 436–440. doi:10.1016/j.jmatprotec.2007.11.305
182. Figueiredo, R. B.; Langdon, T. G. The Development of Superplastic Ductilities and Microstructural Homogeneity in a Magnesium ZK60 Alloy Processed by ECAP. *Mater. Sci. Eng. A* 2006, *430*, 151–156. doi:10.1016/j.msea.2006.05.056
183. Xia, K.; Wang, J.; Wu, X.; Chen, G.; Gurvan, M. Equal Channel Angular Pressing of Magnesium Alloy AZ31. *Mater. Sci. Eng. A* 2005, *410-411*, 324–327. doi:10.1016/j.msea.2005.08.123
184. Figueiredo, R. B.; Langdon, T. G. Grain Refinement and Mechanical Behavior of a Magnesium Alloy Processed by ECAP. *J. Mater. Sci.* 2010, *45*, 4827–4836. doi:10.1007/s10853-010-4589-y
185. Alsubaie, S. A.; Huang, Y.; Langdon, T. G. Hardness Evolution of AZ80 Magnesium Alloy Processed by HPT at Different Temperatures. *J. Mater. Res. Technol.* 2017, *6*, 378–384. doi:10.1016/j.jmrt.2017.05.004
186. Torbati-Sarraf, S. A.; Sabbaghianrad, S.; Figueiredo, R. B.; Langdon, T. G. Orientation Imaging Microscopy and Microhardness in a ZK60 Magnesium Alloy Processed by High-Pressure Torsion. *J. Alloys Compd.* 2017, *712*, 185–193. doi:10.1016/j.jallcom.2017.04.054
187. Bryła, K.; Morgiel, J.; Faryna, M.; Edalati, K.; Horita, Z. Effect of High-Pressure Torsion on Grain Refinement, Strength Enhancement and Uniform Ductility of EZ Magnesium Alloy. *Mater. Lett.* 2018, *212*, 323–326. doi:10.1016/j.matlet.2017.10.113
188. Schwarz, F.; Eilers, C.; Krüger, L. Mechanical Properties of an AM20 Magnesium Alloy Processed by Accumulative Roll-Bonding. *Mater. Charact.* 2015, *105*, 144–153. doi:10.1016/j.matchar.2015.03.032
189. Wang, Q.; Xiao, X.; Hu, J.; Xu, W.; Zhao, X.; Zhao, S. An Ultrafine-Grained AZ31 Magnesium Alloy Sheet with Enhanced Superplasticity Prepared by Accumulative Roll Bonding. *J. Iron Steel Res. Int.* 2007, *14*, 167–172. doi:10.1016/S1006-706X(08)60073-4
190. Zhan, M.-Y.; Zhang, W.-W.; Zhang, D.-T. Production of Mg-Al-Zn Magnesium Alloy Sheets with Ultrafine-Grain Microstructure by Accumulative Roll-Bonding. *Trans. Nonferrous Met. Soc. China* 2011, *21*, 991–997. doi:10.1016/S1003-6326(11)60811-X
191. Fatemi-Varzaneh, S.; Zarei-Hanzaki, A.; Cabrera, J.; Calvillo, P. EBSD Characterization of Repetitive Grain Refinement in AZ31 Magnesium Alloy. *Mater. Chem. Phys.* 2015, *149-150*, 339–343. doi:10.1016/j.matchemphys.2014.10.026
192. Fatemi-Varzaneh, S.; Zarei-Hanzaki, A. Processing of AZ31 Magnesium Alloy by a New Noble Severe Plastic Deformation Method. *Mater. Sci. Eng. A* 2011, *528*, 1334–1339. doi:10.1016/j.msea.2010.10.033
193. Liu, Y.; Cai, S.; Dai, L. A New Method for Grain Refinement in Magnesium Alloy: High Speed Extrusion Machining. *Mater. Sci. Eng. A* 2016, *651*, 878–885. doi:10.1016/j.msea.2015.11.046
194. Shi, B.; Chen, R.; Ke, W. Influence of Grain Size on the Tensile Ductility and Deformation Modes of Rolled Mg–1.02 wt.% Zn Alloy. *J. Magnesium Alloys* 2013, *1*, 210–216. doi:10.1016/j.jma.2013.09.001
195. Margolin, H.; Stanescu, M. S. Polycrystalline Strengthening. *Acta Metall.* 1975, *23*, 1411–1418. doi:10.1016/0001-6160(75)90150-9
196. Hamad, K.; Ko, Y. G. A Cross-Shear Deformation for Optimizing the Strength and Ductility of AZ31 Magnesium Alloys. *Sci. Rep.* 2016, *6*, 1–8. doi:10.1038/srep29954
197. Kim, W.; Jeong, H.; Jeong, H. Achieving High Strength and High Ductility in Magnesium Alloys Using Severe Plastic Deformation Combined with Low-Temperature Aging. *Scr. Mater.* 2009, *61*, 1040–1043. doi:10.1016/j.scriptamat.2009.08.020
198. Chang, C.; Du, X.; Huang, J. Achieving Ultrafine Grain Size in Mg–Al–Zn Alloy by Friction Stir Processing. *Scr. Mater.* 2007, *57*, 209–212. doi:10.1016/j.scriptamat.2007.04.007
199. Kim, W.; Hong, S.; Kim, Y.; Min, S.; Jeong, H.; Lee, J. Texture Development and Its Effect on Mechanical Properties of an AZ61 Mg Alloy Fabricated by Equal Channel Angular Pressing. *Acta Mater.* 2003, *51*, 3293–3307. doi:10.1016/S1359-6454(03)00161-7
200. Pérez-Prado, M. T.; Del Valle, J.; Ruano, O. A. Achieving High Strength in Commercial Mg Cast Alloys through Large Strain Rolling. *Mater. Lett.* 2005, *59*, 3299–3303. doi:10.1016/j.matlet.2005.04.061
201. Armstrong, R.; Codd, I.; Douthwaite, R.; Petch, N. The Plastic Deformation of Polycrystalline Aggregates. *Philos. Mag.* 1962, *7*, 45–58. doi:10.1080/14786436208201857
202. Styczynski, A.; Hartig, C.; Bohlen, J.; Letzig, D. Cold Rolling Textures in AZ31 Wrought Magnesium Alloy. *Scr. Mater.* 2004, *50*, 943–947. doi:10.1016/j.scriptamat.2004.01.010
203. Steiner, M.; Bhattacharyya, J.; Agnew, S. The Origin and Enhancement of $\{0001\}<112\bar{0}>$ Texture during Heat Treatment of Rolled AZ31B Magnesium Alloys. *Acta Mater.* 2015, *95*, 443–455.
204. Li, Z.; Liu, F.; Yuan, A.; Duan, B.; Li, Y.; Li, X. Effect of Rolling Deformation on Microstructure and Texture of Spray-Deposited Magnesium Alloy Containing Mg-Nd-Zn Typed LPSO. *J. Mater. Sci.*

Technol. 2017, *33*, 630–636. doi:10.1016/j.jmst.2017.02.003
205. Griffiths, D. Explaining Texture Weakening and Improved Formability in Magnesium Rare Earth Alloys. *Mater. Sci. Technol.* 2015, *31*, 10–24. doi:10.1179/1743284714Y.0000000632
206. Ko, Y. G.; Hamad, K. Structural Features and Mechanical Properties of AZ31 Mg Alloy Warm-Deformed by Differential Speed Rolling. *J. Alloys Compd.* 2018, *744*, 96–103. doi:10.1016/j.jallcom.2018.02.095
207. Agnew, S. R.; Duygulu, Ö. Plastic Anisotropy and the Role of Non-Basal Slip in Magnesium Alloy AZ31B. *Int. J. Plast.* 2005, *21*, 1161–1193. doi:10.1016/j.ijplas.2004.05.018
208. Jain, A.; Agnew, S. Effect of Twinning on the Mechanical Behavior of a Magnesium Alloy Sheet during Strain Path Changes. *Magnesium Technol.* 2006, *2006*, 219–224.
209. Yoshida, Y.; Cisar, L.; Kamado, S.; Kojima, Y. Effect of Microstructural Factors on Tensile Properties of an ECAE-Processed AZ31 Magnesium Alloy. *Mater. Trans.* 2003, *44*, 468–475. doi:10.2320/matertrans.44.468
210. Kim, S.-H.; You, B.-S.; Yim, C. D.; Seo, Y.-M. Texture and Microstructure Changes in Asymmetrically Hot Rolled AZ31 Magnesium Alloy Sheets. *Mater. Lett.* 2005, *59*, 3876–3880. doi:10.1016/j.matlet.2005.07.024
211. Huang, X.; Suzuki, K.; Saito, N. Microstructure and Mechanical Properties of AZ80 Magnesium Alloy Sheet Processed by Differential Speed Rolling. *Mater. Sci. Eng. A* 2009, *508*, 226–233. doi:10.1016/j.msea.2008.12.052
212. Kim, W.; Park, J.; Kim, W. Effect of Differential Speed Rolling on Microstructure and Mechanical Properties of an AZ91 Magnesium Alloy. *J. Alloys Compd.* 2008, *460*, 289–293. doi:10.1016/j.jallcom.2007.06.050
213. Biswas, S.; Kim, D.-I.; Suwas, S. Asymmetric and Symmetric Rolling of Magnesium: Evolution of Microstructure, Texture and Mechanical Properties. *Mater. Sci. Eng. A* 2012, *550*, 19–30. doi:10.1016/j.msea.2012.03.099
214. Chino, Y.; Sassa, K.; Kamiya, A.; Mabuchi, M. Stretch Formability at Elevated Temperature of a Cross-Rolled AZ31 Mg Alloy Sheet with Different Rolling Routes. *Mater. Sci. Eng. A* 2008, *473*, 195–200. doi:10.1016/j.msea.2007.05.109
215. Wu, W. X.; Jin, L.; Wang, F. H.; Sun, J.; Zhang, Z. Y.; Ding, W. J.; Dong, J. Microstructure and Texture Evolution during Hot Rolling and Subsequent Annealing of Mg–1Gd Alloy. *Mater. Sci. Eng. A* 2013, *582*, 194–202. doi:10.1016/j.msea.2013.05.080
216. Jin, L.; Dong, J.; Wang, R.; Peng, L. Effects of Hot Rolling Processing on Microstructures and Mechanical Properties of Mg–3% Al–1% Zn Alloy Sheet. *Mater. Sci. Eng. A* 2010, *527*, 1970–1974. doi:10.1016/j.msea.2009.11.047
217. Stanford, N.; Barnett, M. R. The Origin of "Rare Earth" Texture Development in Extruded Mg-Based Alloys and Its Effect on Tensile Ductility. *Mater. Sci. Eng. A* 2008, *496*, 399–408. doi:10.1016/j.msea.2008.05.045
218. Gao, L.; Chen, R.; Han, E. Effects of Rare-Earth Elements Gd and Y on the Solid Solution Strengthening of Mg Alloys. *J. Alloys Compd.* 2009, *481*, 379–384. doi:10.1016/j.jallcom.2009.02.131
219. Stanford, N. Micro-Alloying Mg with Y, Ce, Gd and La for Texture Modification—A Comparative Study. *Mater. Sci. Eng. A* 2010, *527*, 2669–2677. doi:10.1016/j.msea.2009.12.036
220. Wu, B.; Zhao, Y.; Du, X.; Zhang, Y.; Wagner, F.; Esling, C. Ductility Enhancement of Extruded Magnesium via Yttrium Addition. *Mater. Sci. Eng. A* 2010, *527*, 4334–4340. doi:10.1016/j.msea.2010.03.054
221. Sabat, R.; Brahme, A.; Mishra, R.; Inal, K.; Suwas, S. Ductility Enhancement in Mg-0.2% Ce Alloys. *Acta Mater.* 2018, *161*, 246–257. doi:10.1016/j.actamat.2018.09.023
222. Hadorn, J. P.; Mulay, R. P.; Hantzsche, K.; Yi, S.; Bohlen, J.; Letzig, D.; Agnew, S. R. Texture Weakening Effects in Ce-Containing Mg Alloys. *Metall. Mat. Trans. A.* 2013, *44*, 1566–1576. doi:10.1007/s11661-012-1486-9
223. Imandoust, A.; Barrett, C. D.; Oppedal, A. L.; Whittington, W. R.; Paudel, Y.; El Kadiri, H. Nucleation and Preferential Growth Mechanism of Recrystallization Texture in High Purity Binary Magnesium-Rare Earth Alloys. *Acta Mater.* 2017, *138*, 27–41. doi:10.1016/j.actamat.2017.07.038
224. Mishra, R. K.; Gupta, A. K.; Rao, P. R.; Sachdev, A. K.; Kumar, A. M.; Luo, A. A. Influence of Cerium on Texture and Ductility of Magnesium Extrusions. In *Essential Readings in Magnesium Technology*. Springer, 2016; p. 363–368. https://doi.org/10.1007/978-3-319-48099-2_58
225. Masoumi, M.; Hoseini, M.; Pekguleryuz, M. The Influence of Ce on the Microstructure and Rolling Texture of Mg–1% Mn Alloy. *Mater. Sci. Eng. A* 2011, *528*, 3122–3129. doi:10.1016/j.msea.2010.12.096
226. Robson, J. D.; Haigh, S. J.; Davis, B.; Griffiths, D. Grain Boundary Segregation of Rare-Earth Elements in Magnesium Alloys. *Metall. Mat. Trans. A.* 2016, *47*, 522–530. doi:10.1007/s11661-015-3199-3
227. Robson, J. D. Effect of Rare-Earth Additions on the Texture of Wrought Magnesium Alloys: The Role of Grain Boundary Segregation. *Metall. Mat. Trans. A.* 2014, *45*, 3205–3212. doi:10.1007/s11661-013-1950-1
228. Basu, I.; Pradeep, K.; Mießen, C.; Barrales-Mora, L.; Al-Samman, T. The Role of Atomic Scale Segregation in Designing Highly Ductile Magnesium Alloys. *Acta Mater.* 2016, *116*, 77–94. doi:10.1016/j.actamat.2016.06.024
229. Huang, G. H.; Yin, D. D.; Lu, J. W.; Zhou, H.; Zeng, Y.; Quan, G. F.; Wang, Q. D. Microstructure, Texture and Mechanical Properties Evolution of Extruded Fine-Grained Mg-Y Sheets during Annealing. *Mater. Sci. Eng. A* 2018, *720*, 24–35. doi:10.1016/j.msea.2018.02.045
230. Bohlen, J.; Yi, S.; Swiostek, J.; Letzig, D.; Brokmeier, H.; Kainer, K. Microstructure and Texture Development during Hydrostatic Extrusion of

Magnesium Alloy AZ31. *Scr. Mater.* 2005, *53*, 259–264. doi:10.1016/j.scriptamat.2005.03.036
231. Bhattacharyya, J. J.; Agnew, S.; Muralidharan, G. Texture Enhancement during Grain Growth of Magnesium Alloy AZ31B. *Acta Mater.* 2015, *86*, 80–94. doi:10.1016/j.actamat.2014.12.009
232. Ball, E.; Prangnell, P. Tensile-Compressive Yield Assymetries in High Strength Wrought Magnesium Alloys. *Scr. Metall. Mater.* 1994, *31*, 111–116. doi:10.1016/0956-716X(94)90159-7
233. Robson, J.; Zhou, X.; Thompson, G. Magnesium Research: Scientific Challenges. *Mater. Technol.* 2009, *24*, 133–136. doi:10.1179/106678509X12489506475430
234. Basu, I.; Al-Samman, T.; Gottstein, G. Shear Band-Related Recrystallization and Grain Growth in Two Rolled Magnesium-Rare Earth Alloys. *Mater. Sci. Eng. A* 2013, *579*, 50–56. doi:10.1016/j.msea.2013.04.076
235. Kim, K.-H.; Suh, B.-C.; Bae, J. H.; Shim, M.-S.; Kim, S.; Kim, N. J. Microstructure and Texture Evolution of Mg Alloys during Twin-Roll Casting and Subsequent Hot Rolling. *Scr. Mater.* 2010, *63*, 716–720. doi:10.1016/j.scriptamat.2009.12.010
236. Beer, A.; Barnett, M. Microstructural Development during Hot Working of Mg-3Al-1Zn. *Metall. Mat. Trans. A.* 2007, *38*, 1856–1867. doi:10.1007/s11661-007-9207-5
237. Molodov, K. D.; Al-Samman, T.; Molodov, D. A.; Gottstein, G. Mechanisms of Exceptional Ductility of Magnesium Single Crystal during Deformation at Room Temperature: Multiple Twinning and Dynamic Recrystallization. *Acta Mater.* 2014, *76*, 314–330. doi:10.1016/j.actamat.2014.04.066
238. Mackenzie, L.; Pekguleryuz, M. The Recrystallization and Texture of Magnesium–Zinc–Cerium Alloys. *Scr. Mater.* 2008, *59*, 665–668. doi:10.1016/j.scriptamat.2008.05.021
239. Stanford, N.; Barnett, M. Effect of Composition on the Texture and Deformation Behaviour of Wrought Mg Alloys. *Scr. Mater.* 2008, *58*, 179–182. doi:10.1016/j.scriptamat.2007.09.054
240. Barnett, M. R.; Nave, M. D.; Bettles, C. J. Deformation Microstructures and Textures of Some Cold Rolled Mg Alloys. *Mater. Sci. Eng. A* 2004, *386*, 205–211. doi:10.1016/S0921-5093(04)00942-6
241. Chaudry, U. M.; Kim, T. H.; Kim, Y. S.; Hamad, K.; Ko, Y. G.; Kim, J.-G. Dynamic Recrystallization Behavior of AZ31-0.5 Ca Magnesium Alloy during Warm Rolling. *Mater. Sci. Eng. A* 2019, *762*, 138085. doi:10.1016/j.msea.2019.138085
242. Song, B.; Xin, R.; Chen, G.; Zhang, X.; Liu, Q. Mechanical Properties and Anisotropy of Mg Alloys with Twin Lamellae. 33rd Risoe International Symposium on Materials Science 2012; p. 337–347.
243. Song, B.; Xin, R.; Chen, G.; Zhang, X.; Liu, Q. Improving Tensile and Compressive Properties of Magnesium Alloy Plates by Pre-Cold Rolling. *Scr. Mater.* 2012, *66*, 1061–1064. doi:10.1016/j.scriptamat.2012.02.047
244. Park, S. H.; Kim, H. S.; Bae, J. H.; Yim, C. D.; You, B. S. Improving the Mechanical Properties of Extruded Mg–3Al–1Zn Alloy by Cold Pre-Forging. *Scr. Mater.* 2013, *69*, 250–253. doi:10.1016/j.scriptamat.2013.04.011
245. Xin, Y.; Wang, M.; Zeng, Z.; Huang, G.; Liu, Q. Tailoring the Texture of Magnesium Alloy by Twinning Deformation to Improve the Rolling Capability. *Scr. Mater.* 2011, *64*, 986–989. doi:10.1016/j.scriptamat.2011.02.010
246. Park, S. H.; Hong, S.-G.; Lee, C. S. Enhanced Stretch Formability of Rolled Mg–3Al–1Zn Alloy at Room Temperature by Initial {10–12} Twins. *Mater. Sci. Eng. A* 2013, *578*, 271–276. doi:10.1016/j.msea.2013.04.084
247. Song, B.; Xin, R.; Liao, A.; Yu, W.; Liu, Q. Enhancing Stretch Formability of Rolled Mg Sheets by Pre-Inducing Contraction Twins and Recrystallization Annealing. *Mater. Sci. Eng. A* 2015, *627*, 369–373. doi:10.1016/j.msea.2015.01.027
248. He, W.; Zeng, Q.; Yu, H.; Xin, Y.; Luan, B.; Liu, Q. Improving the Room Temperature Stretch Formability of a Mg Alloy Thin Sheet by Pre-Twinning. *Mater. Sci. Eng. A* 2016, *655*, 1–8. doi:10.1016/j.msea.2015.12.070
249. Kang, D.; Kim, D.-W.; Kim, S.; Bae, G.; Kim, K.; Kim, N. J. Relationship between Stretch Formability and Work-Hardening Capacity of Twin-Roll Cast Mg Alloys at Room Temperature. *Scr. Mater.* 2009, *61*, 768–771. doi:10.1016/j.scriptamat.2009.06.026
250. Zhang, H.; Huang, G.; Wang, L.; Li, J. Improved Formability of Mg–3Al–1Zn Alloy by Pre-Stretching and Annealing. *Scr. Mater.* 2012, *67*, 495–498. doi:10.1016/j.scriptamat.2012.06.017
251. Cheng, W.; Wang, L.; Zhang, H.; Cao, X. Enhanced Stretch Formability of AZ31 Magnesium Alloy Thin Sheet by Pre-Crossed Twinning Lamellas Induced Static Recrystallizations. *J. Mater. Process. Technol.* 2018, *254*, 302–309. doi:10.1016/j.jmatprotec.2017.11.052
252. Humphreys, F. J.; Hatherly, M. *Recrystallization and Related Annealing Phenomena.* Elsevier; 2012. https://doi.org/10.1016/B978-008044164-1/50005-0
253. Robson, J. D.; Stanford, N.; Barnett, M. R. Effect of Precipitate Shape on Slip and Twinning in Magnesium Alloys. *Acta Mater.* 2011, *59*, 1945–1956. doi:10.1016/j.actamat.2010.11.060
254. Nie, J.-F. Precipitation and Hardening in Magnesium Alloys. *Metall. Mat. Trans. A.* 2012, *43*, 3891–3939. doi:10.1007/s11661-012-1217-2
255. Bhattacharyya, J.; Wang, F.; Stanford, N.; Agnew, S. Slip Mode Dependency of Dislocation Shearing and Looping of Precipitates in Mg Alloy WE43. *Acta Mater.* 2018, *146*, 55–62. doi:10.1016/j.actamat.2017.12.043
256. Solomon, E. L.; Marquis, E. A. Deformation Behavior of β' and β''' Precipitates in Mg-RE Alloys. *Mater. Lett.* 2018, *216*, 67–69. doi:10.1016/j.matlet.2017.12.149
257. Kim, J. H.; Kang, N. E.; Yim, C. D.; Kim, B. K. Effect of Calcium Content on the Microstructural Evolution and Mechanical Properties of Wrought Mg–3Al–1Zn Alloy. *Mater. Sci. Eng. A* 2009, *525*, 18–29. doi:10.1016/j.msea.2009.07.048

258. Yu, Z.; Tang, A.; Wang, Q.; Gao, Z.; He, J.; She, J.; Song, K.; Pan, F. High Strength and Superior Ductility of an Ultra-Fine Grained Magnesium–Manganese Alloy. *Mater. Sci. Eng. A* 2015, *648*, 202–207. doi:10.1016/j.msea.2015.09.065
259. Wei, X.; Jin, L.; Wang, F.; Li, J.; Ye, N.; Zhang, Z.; Dong, J. High Strength and Ductility Mg-8Gd-3Y-0.5 Zr Alloy with Bimodal Structure and Nano-Precipitates. *J. Mater. Sci. Technol.* 2020, *44*, 19–23. doi:10.1016/j.jmst.2019.10.024
260. Kim, S.-H.; Bae, S. W.; Lee, S. W.; Moon, B. G.; Kim, H. S.; Kim, Y. M.; Yoon, J.; Park, S. H. Microstructural Evolution and Improvement in Mechanical Properties of Extruded AZ31 Alloy by Combined Addition of Ca and Y. *Mater. Sci. Eng. A* 2018, *725*, 309–318. doi:10.1016/j.msea.2018.04.031
261. Robson, J.; Henry, D.; Davis, B. Particle Effects on Recrystallization in Magnesium–Manganese Alloys: Particle-Stimulated Nucleation. *Acta Mater.* 2009, *57*, 2739–2747. doi:10.1016/j.actamat.2009.02.032
262. Chun, J.; Byrne, J.; Bornemann, A. The Inhibition of Deformation Twinning by Precipitates in a Magnesium-Zinc Alloy. *Philos. Mag.* 1969, *20*, 291–300. doi:10.1080/14786436908228701
263. Stanford, N.; Taylor, A. S.; Cizek, P.; Siska, F.; Ramajayam, M.; Barnett, M. R. {101\bar 2} Twinning in Magnesium-Based Lamellar Microstructures. *Scr. Mater.* 2012, *67*, 704–707. doi:10.1016/j.scriptamat.2012.06.035
264. Stanford, N.; Barnett, M. Effect of Particles on the Formation of Deformation Twins in a Magnesium-Based Alloy. *Mater. Sci. Eng. A* 2009, *516*, 226–234. doi:10.1016/j.msea.2009.04.001
265. Robson, J. D.; Stanford, N.; Barnett, M. R. Effect of Particles in Promoting Twin Nucleation in a Mg–5 wt.% Zn Alloy. *Scr. Mater.* 2010, *63*, 823–826. doi:10.1016/j.scriptamat.2010.06.026
266. Jain, J.; Poole, W.; Sinclair, C.; Gharghouri, M. Reducing the Tension–Compression Yield Asymmetry in a Mg–8Al–0.5 Zn Alloy via Precipitation. *Scr. Mater.* 2010, *62*, 301–304. doi:10.1016/j.scriptamat.2009.11.024
267. Raeisinia, B.; Agnew, S. R. Using Polycrystal Plasticity Modeling to Determine the Effects of Grain Size and Solid Solution Additions on Individual Deformation Mechanisms in Cast Mg Alloys. *Scr. Mater.* 2010, *63*, 731–736. doi:10.1016/j.scriptamat.2010.03.054
268. Herrera-Solaz, V.; LLorca, J.; Dogan, E.; Karaman, I.; Segurado, J. An Inverse Optimization Strategy to Determine Single Crystal Mechanical Behavior from Polycrystal Tests: Application to AZ31 Mg Alloy. *Int. J. Plast.* 2014, *57*, 1–15. doi:10.1016/j.ijplas.2014.02.001
269. Fernández, A.; Prado, M. T. P.; Wei, Y.; Jérusalem, A. Continuum Modeling of the Response of a Mg Alloy AZ31 Rolled Sheet during Uniaxial Deformation. *Int. J. Plast.* 2011, *27*, 1739–1757. doi:10.1016/j.ijplas.2011.05.002
270. Hutchinson, W.; Barnett, M. Effective Values of Critical Resolved Shear Stress for Slip in Polycrystalline Magnesium and Other Hcp Metals. *Scr. Mater.* 2010, *63*, 737–740. doi:10.1016/j.scriptamat.2010.05.047
271. Akhtar, A.; Teghtsoonian, E. Substitutional Solution Hardening of Magnesium Single Crystals. *Philos. Mag.* 1972, *25*, 897–916. doi:10.1080/14786437208229311
272. Kim, S.-J.; Lee, Y.-S.; Kim, D. Analysis of Formability of Ca-Added Magnesium Alloy Sheets at Low Temperatures. *Mater. Charact.* 2016, *113*, 152–159. doi:10.1016/j.matchar.2016.01.013
273. Kim, K.-H.; Jeon, J. B.; Kim, N. J.; Lee, B.-J. Role of Yttrium in Activation of $< c+a >$ Slip in Magnesium: An Atomistic Approach. *Scr. Mater.* 2015, *108*, 104–108.
274. Hehmann, F.; Sommer, F.; Predel, B. Extension of Solid Solubility in Magnesium by Rapid Solidification. *Mater. Sci. Eng. A* 1990, *125*, 249–265. doi:10.1016/0921-5093(90)90175-3
275. Miura, S.; Yamamoto, S.; Ohkubo, K.; Mohri, T. Deformation Behavior of Mg Alloy Single Crystals at Various Temperatures. *MSF* 2000, *350-351*, 183–190. doi:10.4028/www.scientific.net/MSF.350-351.183
276. Al-Samman, T. Comparative Study of the Deformation Behavior of Hexagonal Magnesium–Lithium Alloys and a Conventional Magnesium AZ31 Alloy. *Acta Mater.* 2009, *57*, 2229–2242. doi:10.1016/j.actamat.2009.01.031
277. Yoo, M. H. Slip, Twinning, and Fracture in Hexagonal Close-Packed Metals. *MTA* 1981, *12*, 409–418. doi:10.1007/BF02648537
278. Tekumalla, S.; Bibhanshu, N.; Shabadi, R.; Suwas, S.; Ha, T. M. H.; Gupta, M. Evolution of Texture and Asymmetry and Its Impact on the Fatigue Behaviour of an in-Situ Magnesium Nanocomposite. *Mater. Sci. Eng. A* 2018, *727*, 61–69. doi:10.1016/j.msea.2018.04.101
279. Tekumalla, S.; Seetharaman, S.; Almajid, A.; Gupta, M. Mechanical Properties of Magnesium-Rare Earth Alloy Systems: A Review. *Metals* 2014, *5*, 1–39. doi:10.3390/met5010001
280. Zhang, B.; Nagasekhar, A. V.; Tao, X.; Ouyang, Y.; Cáceres, C. H.; Easton, M. Strengthening by the Percolating Intergranular Eutectic in an HPDC Mg–Ce Alloy. *Mater. Sci. Eng. A* 2014, *599*, 204–211. doi:10.1016/j.msea.2014.01.074
281. Mishra, R. K.; Gupta, A. K.; Rao, P. R.; Sachdev, A. K.; Kumar, A. M.; Luo, A. A. Influence of Cerium on the Texture and Ductility of Magnesium Extrusions. *Scr. Mater.* 2008, *59*, 562–565. doi:10.1016/j.scriptamat.2008.05.019
282. Luo, A. A.; Wu, W.; Mishra, R. K.; Jin, L.; Sachdev, A. K.; Ding, W. Microstructure and Mechanical Properties of Extruded Magnesium-Aluminum-Cerium Alloy Tubes. *Metall. Mat. Trans. A.* 2010, *41*, 2662–2674. doi:10.1007/s11661-010-0278-3
283. Tekumalla, S.; Seetharaman, S.; Quy Bau, N.; Leong Eugene Wong, W.; Sim Goh, C.; Shabadi, R.; Gupta, M. Influence of Cerium on the Deformation and Corrosion of Magnesium. *J. Eng. Mater. Technol.* 2016, *138*, 031011. doi:10.1115/1.4033033
284. Chia, T. L.; Easton, M. A.; Zhu, S. M.; Gibson, M. A.; Birbilis, N.; Nie, J. F. The Effect of Alloy Composition on the Microstructure and Tensile

Properties of Binary Mg-Rare Earth Alloys. *Intermetallics* 2009, *17*, 481–490. doi:10.1016/j.intermet.2008.12.009

285. Basu, I.; Al-Samman, T. Triggering Rare Earth Texture Modification in Magnesium Alloys by Addition of Zinc and Zirconium. *Acta Mater.* 2014, *67*, 116–133. doi:10.1016/j.actamat.2013.12.015
286. Yan, J.; Sun, Y.; Xue, F.; Xue, S.; Tao, W. Microstructure and Mechanical Properties in Cast Magnesium–Neodymium Binary Alloys. *Mater. Sci. Eng. A* 2008, *476*, 366–371. doi:10.1016/j.msea.2007.05.058
287. Seitz, J. M.; Eifler, R.; Stahl, J.; Kietzmann, M.; Bach, F. W. Characterization of MgNd2 Alloy for Potential Applications in Bioresorbable Implantable Devices. *Acta Biomater.* 2012, *8*, 3852–3864. doi:10.1016/j.actbio.2012.05.024
288. Zhao, H. D.; Qin, G. W.; Ren, Y. P.; Pei, W. L.; Chen, D.; Guo, Y. The Maximum Solubility of Y in α-Mg and Composition Ranges of Mg24Y5 and Mg2Y1 Intermetallic Phases in Mg–Y Binary System. *J. Alloys Compd.* 2011, *509*, 627–631. doi:10.1016/j.jallcom.2010.09.120
289. Gao, L.; Chen, R. S.; Han, E. H. Solid Solution Strengthening Behaviors in Binary Mg–Y Single Phase Alloys. *J. Alloys Compd.* 2009, *472*, 234–240. doi:10.1016/j.jallcom.2008.04.049
290. Gu, X.; Zheng, Y.; Cheng, Y.; Zhong, S.; Xi, T. In Vitro Corrosion and Biocompatibility of Binary Magnesium Alloys. *Biomaterials* 2009, *30*, 484–498. doi:10.1016/j.biomaterials.2008.10.021
291. Tekumalla, S.; Yang, C.; Seetharaman, S.; Wong, W. L. E.; Goh, C. S.; Shabadi, R.; et al. Enhancing Overall Static/Dynamic/Damping/Ignition Response of Magnesium through the Addition of Lower Amounts (<2%) of Yttrium. *J. Alloys Compd.* 2016, *689*, 350–358.
292. Zhou, N.; Zhang, Z.; Jin, L.; Dong, J.; Chen, B.; Ding, W. Ductility Improvement by Twinning and Twin–Slip Interaction in a Mg-Y Alloy. *Mater. Des.* 2014, *56*, 966–974. doi:10.1016/j.matdes.2013.12.014
293. Essadiqi Mts, E.; Javaid, A.; Shen, G.; Aljarrah, M.; Verma, R.; Mishra, R. Alloying and Process Design of Mg Sheet. CANMET – Materials. Canada 2011.
294. Sugamata, M.; Hanawa, S.; Kaneko, J. Structures and Mechanical Properties of Rapidly Solidified Mg-Y Based Alloys. *Mater. Sci. Eng. A* 1997, *226-228*, 861–866. doi:10.1016/S0921-5093(97)80089-5
295. Nayeb-Hashemi, A. A. *Phase Diagrams of Binary Magnesium Alloys*. ASM International: Metals Park, OH, 1998.
296. Hort, N.; Huang, Y.; Fechner, D.; Störmer, M.; Blawert, C.; Witte, F.; Vogt, C.; Drücker, H.; Willumeit, R.; Kainer, K. U.; et al. Magnesium Alloys as Implant Materials-Principles of Property Design for Mg-RE Alloys. *Acta Biomater.* 2010, *6*, 1714–1725. doi:10.1016/j.actbio.2009.09.010
297. Peng, Q.; Wu, Y.; Fang, D.; Meng, J.; Wang, L. Microstructures and Properties of Melt-Spun and as-Cast Mg-20Gd Binary Alloy. *J. Rare Earths* 2006, *24*, 466–470. doi:10.1016/S1002-0721(06)60145-2
298. Stanford, N.; Atwell, D.; Barnett, M. R. The Effect of Gd on the Recrystallisation, Texture and Deformation Behaviour of Magnesium-Based Alloys. *Acta Mater.* 2010, *58*, 6773–6783. doi:10.1016/j.actamat.2010.09.003
299. Yang, W.; Tekumalla, S.; Gupta, M. Cumulative Effect of Strength Enhancer—Lanthanum and Ductility Enhancer—Cerium on Mechanical Response of Magnesium. *Metals* 2017, *7*, 241. doi:10.3390/met7070241
300. Tekumalla, S.; Farhan, N.; Srivatsan, T. S.; Gupta, M. Nano-ZnO Particles' Effect in Improving the Mechanical Response of Mg-3Al-0.4Ce Alloy. *Metals* 2016, *6*, 276. doi:10.3390/met6110276
301. Chen, Y.; Tekumalla, S.; Guo, Y. B.; Shabadi, R.; Shim, V. P. W.; Gupta, M. The Dynamic Compressive Response of a High-Strength Magnesium Alloy and Its Nanocomposite. *Mater. Sci. Eng. A* 2017, *702*, 65–72. doi:10.1016/j.msea.2017.07.005
302. Le, Q.-C.; Zhang, Z-q.; Shao, Z-w.; Cui, J-z.; Yi, X. Microstructures and Mechanical Properties of Mg-2% Zn-0.4% RE Alloys. *Trans. Nonferrous Met. Soc. China* 2010, *20*, s352–s356. doi:10.1016/S1003-6326(10)60496-7
303. Zhou, W.; Zheng, Y.; Leeflang, M.; Zhou, J. Mechanical Property, Biocorrosion and in Vitro Biocompatibility Evaluations of Mg-Li-(Al)-(RE) Alloys for Future Cardiovascular Stent Application. *Acta Biomater.* 2013, *9*, 8488–8498. doi:10.1016/j.actbio.2013.01.032
304. Panigrahi, S. K.; Yuan, W.; Mishra, R. S.; DeLorme, R.; Davis, B.; Howell, R. A.; Cho, K. A Study on the Combined Effect of Forging and Aging in Mg–Y–RE Alloy. *Mater. Sci. Eng. A* 2011, *530*, 28–35. doi:10.1016/j.msea.2011.08.065
305. Wang, T.; Zhang, M.; Wu, R. Microstructure and Properties of Mg–8Li–1Al–1Ce Alloy. *Mater. Lett.* 2008, *62*, 1846–1848. doi:10.1016/j.matlet.2007.10.017
306. Tekumalla, S.; Joo Yuan, N.; Haghshenas, M.; Gupta, M. Enhancing Properties of Aerospace Alloy Elektron 21 Using Boron Carbide Nanoparticles as Reinforcement. *Appl. Sci.* 2019, *9*, 5470. doi:10.3390/app9245470
307. Mishra, R. K.; Brahme, A.; Sabat, R. K.; Jin, L.; Inal, K. Twinning and Texture Randomization in Mg and Mg-Ce Alloys. *Int. J. Plast.* 2019, *117*, 157–172. doi:10.1016/j.ijplas.2019.03.001
308. Zhang, S.; Yuan, G. Y.; Lu, C.; Ding, W. J. Effect of Zn/Gd Ratio on Phase Constitutions in Mg-Zn-Gd Alloys. In *Magnesium Technology 2011*, Sillekens, W. H., Agnew, S. R., Neelameggham, N. R, Mathaudhu, S. N., Eds.; Springer International Publishing: Cham, 2016; p. 157–159.
309. Srinivasan, A.; Huang, Y.; Mendis, C. L.; Blawert, C.; Kainer, K. U.; Hort, N. Investigations on Microstructures, Mechanical and Corrosion Properties of Mg–Gd–Zn Alloys. *Mater. Sci. Eng. A* 2014, *595*, 224–234. doi:10.1016/j.msea.2013.12.016
310. Singh, A.; Somekawa, H.; Mukai, T. High Temperature Processing of Mg–Zn–Y Alloys Containing Quasicrystal Phase for High Strength.

Mater. Sci. Eng. A 2011, *528*, 6647–6651. doi:10.1016/j.msea.2011.05.001

311. Seetharaman, S.; Tekumalla, S.; Lalwani, B.; Patel, H.; Bau, N. Q.; Gupta, M. Microstructure and Mechanical Properties New Magnesium-Zinc-Gadolinium Alloys. In *Magnesium Technology 2016*, Singh, A., Solanki, K., Manuel, M. V., Neelameggham, N. R., Eds.; Springer International Publishing: Cham, 2016; p. 159–163.
312. Xu, C.; Zheng, M. Y.; Xu, S. W.; Wu, K.; Wang, E. D.; Fan, G. H.; Kamado, S.; Liu, X. D.; Wang, G. J.; Lv, X. Y.; et al. Microstructure and Mechanical Properties of Mg–Gd–Y–Zn–Zr Alloy Sheets Processed by Combined Processes of Extrusion, Hot Rolling and Ageing. *Mater. Sci. Eng. A* 2013, *559*, 844–851. doi:10.1016/j.msea.2012.09.032
313. Du, X. H.; Duan, G. S.; Hong, M.; Wang, D. P.; Wu, B. L.; Zhang, Y. D.; Esling, C. Effect of V on the Microstructure and Mechanical Properties of Mg–10Er–2Cu Alloy with a Long Period Stacking Ordered Structure. *Mater. Lett.* 2014, *122*, 312–314. doi:10.1016/j.matlet.2014.02.056
314. Xu, C.; Zheng, M. Y.; Xu, S. W.; Wu, K.; Wang, E. D.; Kamado, S.; Wang, G. J.; Lv, X. Y. Microstructure and Mechanical Properties of Rolled Sheets of Mg–Gd–Y–Zn–Zr Alloy: As-Cast versus as-Homogenized. *J. Alloys Compd.* 2012, *528*, 40–44. doi:10.1016/j.jallcom.2012.03.023
315. Xu, C.; Xu, S. W.; Zheng, M. Y.; Wu, K.; Wang, E. D.; Kamado, S.; Wang, G. J.; Lv, X. Y. Microstructures and Mechanical Properties of High-Strength Mg–Gd–Y–Zn–Zr Alloy Sheets Processed by Severe Hot Rolling. *J. Alloys Compd.* 2012, *524*, 46–52. doi:10.1016/j.jallcom.2012.02.050
316. Freeney, T. A.; Mishra, R. S. Effect of Friction Stir Processing on Microstructure and Mechanical Properties of a Cast-Magnesium–Rare Earth Alloy. *Metall. Mat. Trans. A.* 2010, *41*, 73–84. doi:10.1007/s11661-009-0080-2
317. Yang, Z.; Li, J. P.; Guo, Y. C.; Liu, T.; Xia, F.; Zeng, Z. W.; Liang, M. X. Precipitation Process and Effect on Mechanical Properties of Mg–9Gd–3Y–0.6Zn–0.5Zr Alloy. *Mater. Sci. Eng. A* 2007, *454-455*, 274–280. doi:10.1016/j.msea.2006.11.047
318. Stulikova, I.; Smola, B. Mechanical Properties and Phase Composition of Potential Biodegradable Mg–Zn–Mn–Base Alloys with Addition of Rare Earth Elements. *Mater. Charact.* 2010, *61*, 952–958. doi:10.1016/j.matchar.2010.06.004
319. Wu, J.; Si, S.; Takagi, K.; Li, T.; Mine, Y.; Takashima, K.; et al. Study of Basal $<a>$ and Pyramidal $<c+a>$ Slips in Mg-Y Alloys Using Micro-Pillar Compression. *Philos. Mag.* 2020, *100*, 1454–1475.
320. Li, Y.; Wang, F.; Hu, T.; Zheng, R.; Xiao, W.; Lyu, S.; Ma, C. Microstructure and Mechanical Property of High Strength Mg–Sn–Zn–Al Alloys. *Mater. Sci. Technol.* 2019, *35*, 1046–1052. doi:10.1080/02670836.2019.1603901
321. Sasaki, T. T.; Elsayed, F. R.; Nakata, T.; Ohkubo, T.; Kamado, S.; Hono, K. Strong and Ductile Heat-Treatable Mg–Sn–Zn–Al Wrought Alloys. *Acta Mater.* 2015, *99*, 176–186. doi:10.1016/j.actamat.2015.06.060
322. Zhong, L.; Wang, Y.; Dou, Y. On the Improved Tensile Strength and Ductility of Mg–Sn–Zn–Mn Alloy Processed by Aging Prior to Extrusion. *J. Magnesium Alloys* 2019, *7*, 637–647. doi:10.1016/j.jma.2019.07.007
323. Zheng, R.; Bhattacharjee, T.; Gao, S.; Gong, W.; Shibata, A.; Sasaki, T.; Hono, K.; Tsuji, N. Change of Deformation Mechanisms Leading to High Strength and Large Ductility in Mg-Zn-Zr-Ca Alloy with Fully Recrystallized Ultrafine Grained Microstructures. *Sci. Rep.* 2019, *9*, 11702. doi:10.1038/s41598-019-48271-5
324. Tu, T.; Chen, X.-H.; Chen, J.; Zhao, C.-Y.; Pan, F.-S. A High-Ductility Mg–Zn–Ca Magnesium Alloy. *Acta Metall. Sin.* 2019, *32*, 23–30. doi:10.1007/s40195-018-0804-7
325. Tekumalla, S.; Gupta, M.; Min, K. H. Using CaO Nanoparticles to Improve Mechanical and Ignition Response of Magnesium. *CNM* 2018, *3*, 44–51. doi:10.2174/2405461503666180502101957
326. Fu, L.; Wang, X. B.; Gou, P. L.; Le, Q. C.; Jia, W. T.; Tang, Y. Microstructures and Tensile Properties of AZ91 Magnesium Alloys with Ca, Sm, and La Elements Additions. *Adv. Eng. Mater.* 2017, *19*, 1700230. doi:10.1002/adem.201700230
327. Trang, T. T. T.; Zhang, J. H.; Kim, J. H.; Zargaran, A.; Hwang, J. H.; Suh, B.-C.; Kim, N. J. Designing a Magnesium Alloy with High Strength and High Formability. *Nat. Commun.* 2018, *9*, 1–6. doi:10.1038/s41467-018-04981-4
328. Xu, B.; Sun, J.; Yang, Z.; Xiao, L.; Zhou, H.; Han, J.; Liu, H.; Wu, Y.; Yuan, Y.; Zhuo, X.; et al. Microstructure and Anisotropic Mechanical Behavior of the High-Strength and Ductility AZ91 Mg Alloy Processed by Hot Extrusion and Multi-Pass RD-ECAP. *Mater. Sci. Eng. A* 2020, *780*, 139191. doi:10.1016/j.msea.2020.139191
329. Sun, J.; Xu, B.; Yang, Z.; Zhuo, X.; Han, J.; Wu, Y.; Song, D.; Liu, H.; Jiang, J.; Ma, A.; et al. Developing an Industrial-Scale ECAP Mg-Al-Zn Alloy with Multi-Heterostructure for Synchronously High Strength and Good Ductility. *Mater. Charact.* 2020, *164*, 110341. doi:10.1016/j.matchar.2020.110341
330. Huang, H.; Liu, H.; Wang, C.; Sun, J.; Bai, J.; Xue, F.; Jiang, J.; Ma, A. Potential of Multi-Pass ECAP on Improving the Mechanical Properties of a High-Calcium-Content Mg-Al-Ca-Mn Alloy. *J. Magnesium Alloys* 2019, *7*, 617–627. doi:10.1016/j.jma.2019.04.008
331. Liu, H.; Huang, H.; Zhang, Y.; Xu, Y.; Wang, C.; Sun, J.; Jiang, J.; Ma, A.; Xue, F.; Bai, J.; et al. Evolution of Mg–Zn Second Phases during ECAP at Different Processing Temperatures and Its Impact on Mechanical Properties of Zn-1.6 Mg (wt.%) Alloys. *J. Alloys Compd.* 2019, *811*, 151987. doi:10.1016/j.jallcom.2019.151987
332. Yan, K.; Sun, J.; Bai, J.; Liu, H.; Huang, X.; Jin, Z.; Wu, Y. Preparation of a High Strength and High Ductility Mg-6Zn Alloy Wire by Combination of

ECAP and Hot Drawing. *Mater. Sci. Eng. A* 2019, *739*, 513–518. doi:10.1016/j.msea.2018.09.007
333. Minárik, P.; Veselý, J.; Král, R.; Bohlen, J.; Kubásek, J.; Janeček, M.; Stráská, J. Exceptional Mechanical Properties of Ultra-Fine Grain Mg-4Y-3RE Alloy Processed by ECAP. *Mater. Sci. Eng. A* 2017, *708*, 193–198. doi:10.1016/j.msea.2017.09.106
334. Li, Y.; Wang, J.; Xu, R. The Microstructure and Mechanical Properties of Nanocrystalline Mg-Zn-Y Alloy Achieved by a Combination of Aging and High Pressure Torsion. *Vacuum* 2020, *178*, 109396. doi:10.1016/j.vacuum.2020.109396
335. Li, Y.; Qu, C.; Wang, J.; Xu, R. Exceptional Aging Hardening Behaviour of Nanocrystalline Mg–Y-Nd-Gd-Zr Alloy Prepared by High Pressure Torsion. *J. Alloys Compd.* 2020, *813*, 152123. doi:10.1016/j.jallcom.2019.152123
336. Chen, X.; Xiao, L.; Liu, Y.; Xu, M.; Xu, T.; Gao, B.; Hu, Z.; Zhou, H. High Strength-Ductility of Heterogeneous Sandwich Mg–Y Alloys Produced by High Pressure Torsion. *Vacuum* 2020, *179*, 109568. doi:10.1016/j.vacuum.2020.109568
337. Sun, W. T.; Qiao, X. G.; Zheng, M. Y.; He, Y.; Hu, N.; Xu, C.; Gao, N.; Starink, M. J. Exceptional Grain Refinement in a Mg Alloy during High Pressure Torsion Due to Rare Earth Containing Nanosized Precipitates. *Mater. Sci. Eng. A* 2018, *728*, 115–123. doi:10.1016/j.msea.2018.05.021
338. Sun, W.; Qiao, X.; Zheng, M.; Xu, C.; Gao, N.; Starink, M. Microstructure and Mechanical Properties of a Nanostructured Mg-8.2 Gd-3.8 Y-1.0 Zn-0.4 Zr Supersaturated Solid Solution Prepared by High Pressure Torsion. *Mater. Des.* 2017, *135*, 366–376. doi:10.1016/j.matdes.2017.09.048
339. Rao, X.; Wu, Y.; Pei, X.; Jing, Y.; Luo, L.; Liu, Y.; Lu, J. Influence of Rolling Temperature on Microstructural Evolution and Mechanical Behavior of AZ31 Alloy with Accumulative Roll Bonding. *Mater. Sci. Eng. A* 2019, *754*, 112–120. doi:10.1016/j.msea.2019.03.047
340. Chang, H.; Zheng, M.; Wu, K.; Gan, W.; Tong, L.; Brokmeier, H.-G. Microstructure and Mechanical Properties of the Accumulative Roll Bonded (ARBed) Pure Magnesium Sheet. *Mater. Sci. Eng. A* 2010, *527*, 7176–7183. doi:10.1016/j.msea.2010.07.065
341. Kaseem, M.; Chung, B. K.; Yang, H. W.; Hamad, K.; Ko, Y. G. Effect of Deformation Temperature on Microstructure and Mechanical Properties of AZ31 Mg Alloy Processed by Differential-Speed Rolling. *J. Mater. Sci. Technol.* 2015, *31*, 498–503. doi:10.1016/j.jmst.2014.08.016
342. Luo, D.; Wang, H.-Y.; Zhao, L.-G.; Wang, C.; Liu, G.-J.; Liu, Y.; Jiang, Q.-C. Effect of Differential Speed Rolling on the Room and Elevated Temperature Tensile Properties of Rolled AZ31 Mg Alloy Sheets. *Mater. Charact.* 2017, *124*, 223–228. doi:10.1016/j.matchar.2016.12.007
343. Kim, W.; Kim, W. Fabrication of Ultrafine-Grained Mg–3Al–1Zn Magnesium Alloy Sheets Using a Continuous High-Ratio Differential Speed Rolling Technique. *Mater. Sci. Eng. A* 2014, *594*, 189–192. doi:10.1016/j.msea.2013.11.066
344. Ru, M.; Yue, L.; Ling, W.; Wang, Y-n. Influence of Rolling Route on Microstructure and Mechanical Properties of AZ31 Magnesium Alloy during Asymmetric Reduction Rolling. *Trans. Nonferrous Met. Soc. China* 2018, *28*, 902–911. doi:10.1016/S1003-6326(18)64724-7
345. Gong, X.; Kang, S. B.; Cho, J. H.; Li, S. Effect of Annealing on Microstructure and Mechanical Properties of ZK60 Magnesium Alloy Sheets Processed by Twin-Roll Cast and Differential Speed Rolling. *Mater. Charact.* 2014, *97*, 183–188. doi:10.1016/j.matchar.2014.09.014
346. Valiev, R. Z.; Langdon, T. G. Principles of Equal-Channel Angular Pressing as a Processing Tool for Grain Refinement. *Prog. Mater. Sci.* 2006, *51*, 881–981. doi:10.1016/j.pmatsci.2006.02.003
347. He, Y.; Pan, Q.; Qin, Y.; Liu, X.; Li, W.; Chiu, Y.; Chen, J. J. J. Microstructure and Mechanical Properties of ZK60 Alloy Processed by Two-Step Equal Channel Angular Pressing. *J. Alloys Compd.* 2010, *492*, 605–610. doi:10.1016/j.jallcom.2009.11.192
348. Cabibbo, M.; Paoletti, C.; Minárik, P.; Král, R.; Zemková, M. Secondary Phase Precipitation and Thermally Stable Microstructure Refinement Induced by ECAP on Mg-Y-Nd (WN43) Alloy. *Mater. Lett.* 2019, *237*, 5–8. doi:10.1016/j.matlet.2018.09.107
349. Wang, C.; Ma, A.; Sun, J.; Liu, H.; Huang, H.; Yang, Z.; Jiang, J. Effect of ECAP Process on as-Cast and as-Homogenized Mg-Al-Ca-Mn Alloys with Different Mg2Ca Morphologies. *J. Alloys Compd.* 2019, *793*, 259–270. doi:10.1016/j.jallcom.2019.04.202
350. Afifi, M. A.; Wang, Y. C.; Pereira, P. H. R.; Huang, Y.; Wang, Y.; Cheng, X.; Li, S.; Langdon, T. G. Effect of Heat Treatments on the Microstructures and Tensile Properties of an Ultrafine-Grained Al-Zn-Mg Alloy Processed by ECAP. *J. Alloys Compd.* 2018, *749*, 567–574. doi:10.1016/j.jallcom.2018.03.206
351. Liu, T.; Wang, Y. D.; Wu, S. D.; Lin Peng, R.; Huang, C. X.; Jiang, C. B.; Li, S. X. Textures and Mechanical Behavior of Mg–3.3% Li Alloy after ECAP. *Scr. Mater.* 2004, *51*, 1057–1061. doi:10.1016/j.scriptamat.2004.08.007
352. Fan, G.; Zheng, M.; Hu, X.; Xu, C.; Wu, K.; Golovin, I. Improved Mechanical Property and Internal Friction of Pure Mg Processed by ECAP. *Mater. Sci. Eng. A* 2012, *556*, 588–594. doi:10.1016/j.msea.2012.07.031
353. Krajňák, T.; Minárik, P.; Gubicza, J.; Máthis, K.; Kužel, R.; Janeček, M. Influence of Equal Channel Angular Pressing Routes on Texture, Microstructure and Mechanical Properties of Extruded AX41 Magnesium Alloy. *Mater. Charact.* 2017, *123*, 282–293. doi:10.1016/j.matchar.2016.11.044
354. Malheiros, L. R. C.; Figueiredo, R. B.; Langdon, T. G. Grain Size and Microhardness Evolution during Annealing of a Magnesium Alloy Processed by High-Pressure Torsion. *J. Mater. Res. Technol.* 2015, *4*, 14–17. doi:10.1016/j.jmrt.2014.10.008
355. Zhilyaev, A. P.; Langdon, T. G. Using High-Pressure Torsion for Metal Processing: Fundamentals and Applications. *Prog. Mater. Sci.* 2008, *53*, 893–979. doi:10.1016/j.pmatsci.2008.03.002

356. Torbati-Sarraf, S. A.; Langdon, T. G. Properties of a ZK60 Magnesium Alloy Processed by High-Pressure Torsion. *J. Alloys Compd.* 2014, *613*, 357–363. doi:10.1016/j.jallcom.2014.06.056
357. Tang, L.; Zhao, Y.; Liang, N.; Islamgaliev, R.; Valiev, R.; Zhu, Y. Localized Deformation via Multiple Twinning in a Mg–Gd–Y–Zr Alloy Processed by High-Pressure Torsion. *Mater. Sci. Eng. A* 2016, *677*, 68–75. doi:10.1016/j.msea.2016.09.005
358. Kulyasova, O. B.; Islamgaliev, R. K.; Zhao, Y.; Valiev, R. Z. Enhancement of the Mechanical Properties of an Mg–Zn–Ca Alloy Using High-Pressure Torsion. *Adv. Eng. Mater.* 2015, *17*, 1738–1741. doi:10.1002/adem.201500176
359. Meng, F.; Rosalie, J. M.; Singh, A.; Somekawa, H.; Tsuchiya, K. Ultrafine Grain Formation in Mg–Zn Alloy by in Situ Precipitation during High-Pressure Torsion. *Scr. Mater.* 2014, *78-79*, 57–60. doi:10.1016/j.scriptamat.2014.01.036
360. Starink, M. J.; Cheng, X.; Yang, S. Hardening of Pure Metals by High-Pressure Torsion: A Physically Based Model Employing Volume-Averaged Defect Evolutions. *Acta Mater.* 2013, *61*, 183–192. doi:10.1016/j.actamat.2012.09.048
361. Čížek, J.; Procházka, I.; Smola, B.; Stulíková, I.; Kužel, R.; Matěj, Z.; Cherkaska, V.; Islamgaliev, R. K.; Kulyasova, O. Microstructure and Thermal Stability of Ultra Fine Grained Mg-Based Alloys Prepared by High-Pressure Torsion. *Mater. Sci. Eng. A* 2007, *462*, 121–126. doi:10.1016/j.msea.2006.01.177
362. Alizadeh, R.; Mahmudi, R.; Ngan, A.; Huang, Y.; Langdon, T. Superplasticity of a Nano-Grained Mg–Gd–Y–Zr Alloy Processed by High-Pressure Torsion. *Mater. Sci. Eng. A* 2016, *651*, 786–794. doi:10.1016/j.msea.2015.10.094
363. Al-Zubaydi, A. S.; Zhilyaev, A. P.; Wang, S. C.; Kucita, P.; Reed, P. A. Evolution of Microstructure in AZ91 Alloy Processed by High-Pressure Torsion. *J. Mater. Sci.* 2016, *51*, 3380–3389. doi:10.1007/s10853-015-9652-2
364. Sun, W.; Qiao, X.; Zheng, M.; Hu, N.; Gao, N.; Starink, M. Evolution of Long-Period Stacking Ordered Structure and Hardness of Mg-8.2 Gd-3.8 Y-1.0 Zn-0.4 Zr Alloy during Processing by High Pressure Torsion. *Mater. Sci. Eng. A* 2018, *738*, 238–252. doi:10.1016/j.msea.2018.09.063
365. Huang, Y.; Figueiredo, R. B.; Baudin, T.; Brisset, F.; Langdon, T. G. Evolution of Strength and Homogeneity in a Magnesium AZ31 Alloy Processed by High-Pressure Torsion at Different Temperatures. *Adv. Eng. Mater.* 2012, *14*, 1018–1026. doi:10.1002/adem.201200016
366. Serre, P.; Figueiredo, R. B.; Gao, N.; Langdon, T. G. Influence of Strain Rate on the Characteristics of a Magnesium Alloy Processed by High-Pressure Torsion. *Mater. Sci. Eng. A* 2011, *528*, 3601–3608. doi:10.1016/j.msea.2011.01.066
367. Sun, W. T.; Qiao, X. G.; Zheng, M. Y.; Xu, C.; Kamado, S.; Zhao, X. J.; Chen, H. W.; Gao, N.; Starink, M. J. Altered Ageing Behaviour of a Nanostructured Mg-8.2 Gd-3.8 Y-1.0 Zn-0.4 Zr Alloy Processed by High Pressure Torsion. *Acta Mater.* 2018, *151*, 260–270. doi:10.1016/j.actamat.2018.04.003
368. Figueiredo, R. B.; Langdon, T. G. Processing Magnesium and Its Alloys by High-Pressure Torsion: An Overview. *Adv. Eng. Mater.* 2019, *21*, 1801039. doi:10.1002/adem.201801039
369. Kai, M.; Horita, Z.; Langdon, T. G. Developing Grain Refinement and Superplasticity in a Magnesium Alloy Processed by High-Pressure Torsion. *Mater. Sci. Eng. A* 2008, *488*, 117–124. doi:10.1016/j.msea.2007.12.046
370. Dobatkin, S.; Rokhlin, L.; Lukyanova, E.; Murashkin, M. Y.; Dobatkina, T.; Tabachkova, N. Y. Structure and Mechanical Properties of the Mg-Y-Gd-Zr Alloy after High Pressure Torsion. *Mater. Sci. Eng. A* 2016, *667*, 217–223. doi:10.1016/j.msea.2016.05.003
371. Zheng, R.; Bhattacharjee, T.; Shibata, A.; Sasaki, T.; Hono, K.; Joshi, M.; Tsuji, N. Simultaneously Enhanced Strength and Ductility of Mg-Zn-Zr-Ca Alloy with Fully Recrystallized Ultrafine Grained Structures. *Scr. Mater.* 2017, *131*, 1–5. doi:10.1016/j.scriptamat.2016.12.024
372. Qiao, X. G.; Zhao, Y. W.; Gan, W. M.; Chen, Y.; Zheng, M. Y.; Wu, K.; Gao, N.; Starink, M. J. Hardening Mechanism of Commercially Pure Mg Processed by High Pressure Torsion at Room Temperature. *Mater. Sci. Eng. A* 2014, *619*, 95–106. doi:10.1016/j.msea.2014.09.068
373. Kocich, R.; Kunčická, L.; Král, P.; Lowe, T. C. Texture, Deformation Twinning and Hardening in a Newly Developed Mg–Dy–Al–Zn–Zr Alloy Processed with High Pressure Torsion. *Mater. Des.* 2016, *90*, 1092–1099. doi:10.1016/j.matdes.2015.11.062
374. Sun, W. T.; Xu, C.; Qiao, X. G.; Zheng, M. Y.; Kamado, S.; Gao, N.; Starink, M. J. Evolution of Microstructure and Mechanical Properties of an as-Cast Mg-8.2 Gd-3.8 Y-1.0 Zn-0.4 Zr Alloy Processed by High Pressure Torsion. *Mater. Sci. Eng. A* 2017, *700*, 312–320. doi:10.1016/j.msea.2017.05.115
375. Harai, Y.; Kai, M.; Kaneko, K.; Horita, Z.; Langdon, T. G. Microstructural and Mechanical Characteristics of AZ61 Magnesium Alloy Processed by High-Pressure Torsion. *Mater. Trans.* 2008, *49*, 76–83. doi:10.2320/matertrans.ME200718
376. Lukyanova, E. A.; Martynenko, N. S.; Serebryany, V. N.; Belyakov, A. N.; Rokhlin, L. L.; Dobatkin, S. V.; Estrin, Y. Z. Structure and Mechanical and Corrosion Properties of a Magnesium Mg–Y–Nd–Zr Alloy after High Pressure Torsion. *Russ. Metall.* 2017, *2017*, 912–921. doi:10.1134/S0036029517110088
377. Torbati-Sarraf, S. A.; Sabbaghianrad, S.; Langdon, T. G. Using Post-Deformation Annealing to Optimize the Properties of a ZK60 Magnesium Alloy Processed by High-Pressure Torsion. *Adv. Eng. Mater.* 2018, *20*, 1700703. doi:10.1002/adem.201700703
378. Pérez-Prado, M. T.; Valle, d.; Ruano, O. A. Grain Refinement of Mg–Al–Zn Alloys via Accumulative Roll Bonding. Scr. Mater. 2004, *51*, 1093–1097. doi:10.1016/j.scriptamat.2004.07.028

379. Del Valle, J.; Pérez-Prado, M. T.; Ruano, O. A. Accumulative Roll Bonding of a Mg-Based AZ61 Alloy. *Mater. Sci. Eng. A* 2005, *410-411*, 353–357. doi:10.1016/j.msea.2005.08.097
380. Chang, L.; Cho, J.; Kang, S. Microstructure and Mechanical Properties of AM31 Magnesium Alloys Processed by Differential Speed Rolling. J. Mater. Process. Technol. 2011, *211*, 1527–1533. doi:10.1016/j.jmatprotec.2011.04.003
381. Cho, J.-H.; Kim, H.-W.; Kang, S.-B.; Han, T.-S. Bending Behavior, and Evolution of Texture and Microstructure during Differential Speed Warm Rolling of AZ31B Magnesium Alloys. *Acta Mater.* 2011, *59*, 5638–5651. doi:10.1016/j.actamat.2011.05.039
382. Gong, X.; Kang, S. B.; Li, S.; Cho, J. H. Enhanced Plasticity of Twin-Roll Cast ZK60 Magnesium Alloy through Differential Speed Rolling. *Mater. Des.* 2009, *30*, 3345–3350. doi:10.1016/j.matdes.2009.03.040
383. Park, J.; Hamad, K.; Widiantara, I.; Ko, Y. Strain and Crystallographic Texture Evaluation of Interstitial Free Steel Cold Deformed by Differential Speed Rolling. *Mater. Lett.* 2015, *147*, 38–41. doi:10.1016/j.matlet.2015.02.030
384. Ko, Y. G.; Widiantara, I.; Hamad, K. On the Considerability of DSR (Differential Speed Rolling) as a Severe Plastic Deformation Method. *Adv. Eng. Mater.* 2017, *19*, 1600722. doi:10.1002/adem.201600722
385. Hamad, K.; Ko, Y. G. Continuous Differential Speed Rolling for Grain Refinement of Metals: Processing, Microstructure, and Properties. *Crit. Rev. Solid State Mater. Sci.* 2019, *44*, 470–525. doi:10.1080/10408436.2018.1525528
386. Ko, Y. G.; Chaudry, U. M.; Hamad, K. Microstructure and Mechanical Properties of AA6061 Alloy Deformed by Differential Speed Rolling. Mater. Lett. 2020, *259*, 126870. doi:10.1016/j.matlet.2019.126870
387. Ko, Y. G.; Kim, Y. G.; Hamad, K. Microstructure Optimization of Low-Carbon Steel Using Differential Speed Rolling Deformation Followed by Annealing. Mater. Lett. 2020, *261*, 127154. doi:10.1016/j.matlet.2019.127154
388. Hamad, K.; Megantoro, R. B.; Ko, Y. G. Microstructure and Texture Evolution in Low Carbon Steel Deformed by Differential Speed Rolling (DSR) Method. J. Mater. Sci. 2014, *49*, 6608–6619. doi:10.1007/s10853-014-8280-6
389. Hamad, K.; Chung, B. K.; Ko, Y. G. Effect of Deformation Path on Microstructure, Microhardness and Texture Evolution of Interstitial Free Steel Fabricated by Differential Speed Rolling. Mater. Charact. 2014, *94*, 203–214. doi:10.1016/j.matchar.2014.05.019
390. Ko, Y.; Suharto, J.; Lee, J.; Park, B.; Shin, D. Effect of Roll Speed Ratio on Deformation Characteristics of IF Steel Subjected to Differential Speed Rolling. *Met. Mater. Int.* 2013, *19*, 603–609. doi:10.1007/s12540-013-3033-7
391. Ko, Y. G.; Kim, M. J.; Hamad, K. Structural Evolutions and Mechanical Properties of IF Steel Deformed by Differential Speed Rolling at Various per-Pass-Thickness Reductions. Mater. Lett. 2019, *250*, 178–181. doi:10.1016/j.matlet.2019.04.109
392. Ko, Y. G. Microstructure Evolution and Mechanical Properties of Severely Deformed Al Alloy Processed by Differential Speed Rolling. *J. Alloys Compd.* 2012, *536*, S122–S5. doi:10.1016/j.jallcom.2011.12.009
393. Ko, Y. G. Effect of Differential Speed Rolling Strain on Microstructure and Mechanical Properties of Nanostructured 5052 Al Alloy. *J. Alloys Compd.* 2014, *586*, S205–S9. doi:10.1016/j.jallcom.2012.10.128
394. Ko, Y. G.; Hamad, K. Annealing Behavior of 6061 Al Alloy Subjected to Differential Speed Rolling Deformation. *Metals* 2017, *7*, 494. doi:10.3390/met7110494
395. Hamad, K.; Park, J.; Ko, Y. Finite Element Analysis of Deformation Behavior in Al-2.2 wt.% Mg Alloy Subjected to Differential Speed Rolling. *J. Mater. Eng. Perform.* 2015, *24*, 2990–3001. doi:10.1007/s11665-015-1598-7
396. Ko, Y. G.; Hamad, K. Microstructure Stability and Mechanical Properties of Ultrafine Grained 5052 Al Alloy Fabricated by Differential Speed Rolling. *Mater. Sci. Eng. A* 2018, *733*, 24–27. doi:10.1016/j.msea.2018.07.033
397. Polkowski, W.; Jóźwik, P.; Polański, M.; Bojar, Z. Microstructure and Texture Evolution of Copper Processed by Differential Speed Rolling with Various Speed Asymmetry Coefficient. *Mater. Sci. Eng. A* 2013, *564*, 289–297. doi:10.1016/j.msea.2012.12.006
398. Kim, W.; Lee, K.; Choi, S.-H. Mechanical Properties and Microstructure of Ultra Fine-Grained Copper Prepared by a High-Speed-Ratio Differential Speed Rolling. *Mater. Sci. Eng. A* 2009, *506*, 71–79. doi:10.1016/j.msea.2008.11.029
399. Kim, W.; Kim, M.; Wang, J. Ultrafine-Grained Mg–9Li–1Zn Alloy Sheets Exhibiting Low Temperature Superplasticity. *Mater. Sci. Eng. A* 2009, *516*, 17–22. doi:10.1016/j.msea.2009.03.089
400. !!! INVALID CITATION !!!
401. Huang, X.; Suzuki, K.; Watazu, A.; Shigematsu, I.; Saito, N. Microstructure and Texture of Mg–Al–Zn Alloy Processed by Differential Speed Rolling. J. Alloys *Compd.* 2008, *457*, 408–412. doi:10.1016/j.jallcom.2007.02.144
402. Watanabe, H.; Mukai, T.; Ishikawa, K. Differential Speed Rolling of an AZ31 Magnesium Alloy and the Resulting Mechanical Properties. J. Mater. Sci. 2004, *39*, 1477–1480. doi:10.1023/B:JMSC.0000013922.16079.d3
403. Kaseem, M.; Yang, H.; Hamad, K.; Kim, Y.; Park, B.; Ko, Y. Microstructure and Plastic Anisotropy of Fine Grained AZ31 Magnesium Alloy Fabricated by Differential Speed Rolling at 473 and 573 K. Mater. Res. Innovations 2015, *19*, S5-477– 80. doi:10.1179/1432891714Z.0000000001135
404. Kim, W.; Yoo, S.; Jeong, H.; Kim, D.; Choe, B.; Lee, J. Effect of the Speed Ratio on Grain Refinement and Texture Development in Pure Ti during Differential Speed Rolling. Scr. Mater. 2011, *64*, 49–52. doi:10.1016/j.scriptamat.2010.09.002

405. Kim, W.; Yoo, S.; Lee, J. Microstructure and Mechanical Properties of Pure Ti Processed by High-Ratio Differential Speed Rolling at Room Temperature. Scr. Mater. 2010, *62*, 451–454. doi:10.1016/j.scriptamat.2009.12.008
406. Huang, X.; Suzuki, K.; Chino, Y. Improvement of Stretch Formability of Pure Titanium Sheet by Differential Speed Rolling. Scr. Mater. 2010, *63*, 473–476. doi:10.1016/j.scriptamat.2010.05.005
407. Kim, H. S.; Yoo, S. J.; Ahn, J. W.; Kim, D. H.; Kim, W. J. Ultrafine Grained Titanium Sheets with High Strength and High Corrosion Resistance. *Mater. Sci. Eng. A* 2011, *528*, 8479–8485. doi:10.1016/j.msea.2011.07.074
408. Kim, W.; Lee, J.; Kim, W.; Jeong, H.; Jeong, H. Microstructure and Mechanical Properties of Mg–Al–Zn Alloy Sheets Severely Deformed by Asymmetrical Rolling. Scr. Mater. 2007, *56*, 309–312. doi:10.1016/j.scriptamat.2006.09.034
409. Huang, X.; Suzuki, K.; Watazu, A.; Shigematsu, I.; Saito, N. Effects of Thickness Reduction per Pass on Microstructure and Texture of Mg–3Al–1Zn Alloy Sheet Processed by Differential Speed Rolling. Scr. Mater. 2009, *60*, 964–967. doi:10.1016/j.scriptamat.2009.02.022
410. Kolednik, O.; Unterweger, K. The Ductility of Metal Matrix Composites – Relation to Local Deformation Behavior and Damage Evolution. Eng. Fract. Mech. 2008, *75*, 3663–3676. doi:10.1016/j.engfracmech.2007.08.011
411. Gupta, M.; Wong, W. L. E. Magnesium-Based Nanocomposites: Lightweight Materials of the Future. Mater. Charact. 2015, *105*, 30–46. doi:10.1016/j.matchar.2015.04.015
412. Dieringa, H. Processing of Magnesium-Based Metal Matrix Nanocomposites by Ultrasound-Assisted Particle Dispersion: A Review. *Metals* 2018, *8*, 431. doi:10.3390/met8060431
413. Chen, L.-Y.; Xu, J.-Q.; Choi, H.; Pozuelo, M.; Ma, X.; Bhowmick, S.; Yang, J.-M.; Mathaudhu, S.; Li, X.-C. Processing and Properties of Magnesium Containing a Dense Uniform Dispersion of Nanoparticles. *Nature* 2015, *528*, 539–543. doi:10.1038/nature16445
414. Tekumalla, S.; Gupta, M. Processing, Properties and Potential Applications of Magnesium Alloy-Based Nanocomposites: A Review. In *Nanocomposites VI: Nanoscience and Nanotechnology in Advanced Composites*, Srivatsan, T. S., Gupta, M., Eds.; Springer International Publishing: Cham, 2019; p. 3–18.
415. Moll, F.; Kainer, K. U. Particle-Reinforced Magnesium Alloys. In *Magnesium – Alloys and Technology 2004*, Kainer, K. U., Ed. Weinheim, Germany: DGM, Wiley-VCH, 2003, 197 https://doi.org/10.1002/3527602046.ch12
416. Ye, H. Z.; Liu, X. Y. Review of Recent Studies in Magnesium Matrix Composites. J. Mater. Sci. 2004, *39*, 6153–6171. doi:10.1023/B:JMSC.0000043583.47148.31
417. Casati, R.; Vedani, M. Metal Matrix Composites Reinforced by Nano-Particles—A Review. *Metals* 2014, *4*, 65–83. doi:10.3390/met4010065
418. Lim, S. C. V.; Gupta, M.; Lu, L. Processing, Microstructure, and Properties of Mg–SiC Composites Synthesised Using Fluxless Casting Process. Mater. Sci. Technol. 2001, *17*, 823–832. doi:10.1179/026708301101510591
419. Goh, C. S.; Wei, J.; Lee, L. C.; Gupta, M. Properties and Deformation Behaviour of Mg–Y_2O_3 Nanocomposites. *Acta Mater.* 2007, *55*, 5115–5121. doi:10.1016/j.actamat.2007.05.032
420. Chen, L.-Y.; Konishi, H.; Fehrenbacher, A.; Ma, C.; Xu, J.-Q.; Choi, H.; Xu, H.-F.; Pfefferkorn, F. E.; Li, X.-C. Novel Nanoprocessing Route for Bulk Graphene Nanoplatelets Reinforced Metal Matrix Nanocomposites. Scr. Mater. 2012, *67*, 29–32. doi:10.1016/j.scriptamat.2012.03.013
421. Nai, M. H.; Wei, J.; Gupta, M. Interface Tailoring to Enhance Mechanical Properties of Carbon Nanotube Reinforced Magnesium Composites. *Mater. Des.* 2014, *60*, 490–495. doi:10.1016/j.matdes.2014.04.011
422. ToolBox E. Coefficients of Linear Thermal Expansion. https://www.engineeringtoolbox.com/linear-expansion-coefficients-d_95.html; 2003.
423. Hassan, S. F.; Gupta, M. Development of a Novel Magnesium/Nickel Composite with Improved Mechanical Properties. J. Alloys *Compd.* 2002, *335*, L10–L5. doi:10.1016/S0925-8388(01)01841-2
424. Hassan, S. F.; Gupta, M. Development of Ductile Magnesium Composite Materials Using Titanium as Reinforcement. J. Alloys *Compd.* 2002, *345*, 246–251. doi:10.1016/S0925-8388(02)00413-9
425. Hassan, S. F.; Ho, K. F.; Gupta, M. Increasing Elastic Modulus, Strength and CTE of AZ91 by Reinforcing Pure Magnesium with Elemental Copper. Mater. Lett. 2004, *58*, 2143–2146. doi:10.1016/j.matlet.2004.01.011
426. Wong, W. L. E.; Gupta, M. Enhancing Thermal Stability, Modulus and Ductility of Magnesium Using Molybdenum as Reinforcement. *Adv. Eng. Mater.* 2005, *7*, 250–256. doi:10.1002/adem.200400137
427. Pandey, R.; Tekumalla, S.; Gupta, M. Enhanced (X-Band) Microwave Shielding Properties of Pure Magnesium by Addition of Diamagnetic Titanium Micro-Particulates. J. Alloys *Compd.* 2019, *770*, 473–482. doi:10.1016/j.jallcom.2018.08.147
428. Lloyd, D. J. Particle Reinforced Aluminium and Magnesium Matrix Composites. Int. Mater. Rev. 1994, *39*, 1–23. doi:10.1179/imr.1994.39.1.1
429. Gupta, M.; Wong, W. L. An Insight into Processing and Characteristics of Magnesium Based Composites. In *Magnesium Technology 2014*, Alderman, M., Manuel, M., Hort, N., Neelameggham, N. R., Eds.; 2014. Springer, Cham. https://doi.org/10.1007/978-3-319-48231-6_78
430. Yang, W. H. A Generalized Von Mises Criterion for Yield and Fracture. *J. Appl. Mech.* 1980, *47*, 297–300. doi:10.1115/1.3153658
431. Biswas, S.; Singh Dhinwal, S.; Suwas, S. Room-Temperature Equal Channel Angular Extrusion of Pure Magnesium. *Acta Mater.* 2010, *58*, 3247–3261. doi:10.1016/j.actamat.2010.01.051
432. Peng, J.; Zhang, Z.; Liu, Z.; Li, Y.; Guo, P.; Zhou, W.; Wu, Y. The Effect of Texture and Grain Size on

Improving the Mechanical Properties of Mg-Al-Zn Alloys by Friction Stir Processing. Sci. Rep. 2018, *8*, 4196. doi:10.1038/s41598-018-22344-3

433. Tekumalla, S.; Bibhanshu, N.; Suwas, S.; Gupta, M. Superior Ductility in Magnesium Alloy-Based Nanocomposites: The Crucial Role of Texture Induced by Nanoparticles. J. Mater. Sci. 2019, *54*, 8711–8718. doi:10.1007/s10853-019-03460-5
434. Johanes, M.; Tekumalla, S.; Gupta, M. Fe3O4 Nanoparticle-Reinforced Magnesium Nanocomposites Processed via Disintegrated Melt Deposition and Turning-Induced Deformation Techniques. *Metals* 2019, *9*, 1225. doi:10.3390/met9111225
435. Wang, Y.; Chen, M.; Zhou, F.; Ma, E. High Tensile Ductility in a Nanostructured Metal. *Nature* 2002, *419*, 912–915. doi:10.1038/nature01133
436. Wang, H.-Y.; Yu, Z.-P.; Zhang, L.; Liu, C.-G.; Zha, M.; Wang, C.; Jiang, Q.-C. Achieving High Strength and High Ductility in Magnesium Alloy Using Hard-Plate Rolling (HPR) Process. Sci. Rep. 2015, *5*, 17100. doi:10.1038/srep17100
437. Wu, D.; Chen, R. S.; Tang, W. N.; Han, E. H. Influence of Texture and Grain Size on the Room-Temperature Ductility and Tensile Behavior in a Mg–Gd–Zn Alloy Processed by Rolling and Forging. *Mater. Des.* 2012, *41*, 306–313. doi:10.1016/j.matdes.2012.04.033
438. Sabat, R. K.; Mishra, R. K.; Sachdev, A. K.; Suwas, S. The Deciding Role of Texture on Ductility in a Ce Containing Mg Alloy. Mater. Lett. 2015, *153*, 158–161. doi:10.1016/j.matlet.2015.03.036
439. Sankaranarayanan, S.; Pranav Nayak, U.; Sabat, R. K.; Suwas, S.; Almajid, A.; Gupta, M. Nano-ZnO Particle Addition to Monolithic Magnesium for Enhanced Tensile and Compressive Response. *J. Alloys Compd.* 2014, *615*, 211–219. doi:10.1016/j.jallcom.2014.06.163
440. Xiang, S. L.; Gupta, M.; Wang, X. J.; Wang, L. D.; Hu, X. S.; Wu, K. Enhanced Overall Strength and Ductility of Magnesium Matrix Composites by Low Content of Graphene Nanoplatelets. *Compos. Part A: Appl. Sci. Manuf.* 2017, *100*, 183–193. doi:10.1016/j.compositesa.2017.05.011
441. Paramsothy, M.; Hassan, S. F.; Srikanth, N.; Gupta, M. Simultaneous Enhancement of Tensile/Compressive Strength and Ductility of Magnesium Alloy AZ31 Using Carbon Nanotubes. J. Nanosci. Nanotechnol. 2010, *10*, 956–964. doi:10.1166/jnn.2010.1809
442. Sankaranarayanan, S.; Sabat, R. K.; Jayalakshmi, S.; Suwas, S.; Gupta, M. Microstructural Evolution and Mechanical Properties of Mg Composites Containing nano-B4C Hybridized micro-Ti Particulates. Mater. Chem. Phys. 2014, *143*, 1178–1190. doi:10.1016/j.matchemphys.2013.11.019
443. Tekumalla, S.; Nandigam, Y.; Bibhanshu, N.; Rajashekara, S.; Yang, C.; Suwas, S.; Gupta, M. A Strong and Deformable in-Situ Magnesium Nanocomposite Igniting above 1000 °C. Sci. Rep. 2018, *8*, 7038. doi:10.1038/s41598-018-25527-0
444. Xi, Y. L.; Chai, D. L.; Zhang, W. X.; Zhou, J. E. Titanium Alloy Reinforced Magnesium Matrix Composite with Improved Mechanical Properties. Scr. Mater. 2006, *54*, 19–23. doi:10.1016/j.scriptamat.2005.09.020
445. Min, Y.; Akbulut, M.; Kristiansen, K.; Golan, Y.; Israelachvili, J. The Role of Interparticle and External Forces in Nanoparticle Assembly. Nat. Mater. 2008, *7*, 527–538. doi:10.1038/nmat2206
446. Rashad, M.; Pan, F.; Tang, A.; Lu, Y.; Asif, M.; Hussain, S.; She, J.; Gou, J.; Mao, J. Effect of Graphene Nanoplatelets (GNPs) Addition on Strength and Ductility of Magnesium-Titanium Alloys. J. Magnesium *Alloys* 2013, *1*, 242–248. doi:10.1016/j.jma.2013.09.004
447. Ferguson, J. B.; Sheykh-Jaberi, F.; Kim, C.-S.; Rohatgi, P. K.; Cho, K. On the Strength and Strain to Failure in Particle-Reinforced Magnesium Metal-Matrix Nanocomposites (Mg MMNCs). *Mater. Sci. Eng. A* 2012, *558*, 193–204. doi:10.1016/j.msea.2012.07.111
448. Pekguleryuz, M.; Celikin, M. Creep Resistance in Magnesium Alloys. Int. Mater. Rev. 2010, *55*, 197–217. doi:10.1179/095066010X12646898728327
449. Pekguleryuz, M. O.; Kaya, A. A. Creep Resistant Magnesium Alloys for Powertrain Applications. *Adv. Eng. Mater.* 2003, *5*, 866–878. doi:10.1002/adem.200300403
450. Mo, N.; Tan, Q.; Bermingham, M.; Huang, Y.; Dieringa, H.; Hort, N.; Zhang, M.-X. Current Development of Creep-Resistant Magnesium Cast Alloys: A Review. *Mater. Des.* 2018, *155*, 422–442. doi:10.1016/j.matdes.2018.06.032
451. Baghani, A.; Khalilpour, H.; Miresmaeili, S. M. Microstructural Evolution and Creep Properties of Mg-4Sn Alloys by Addition of Calcium up to 4 wt.%. *Trans. Nonferrous Met. Soc. China* 2020, *30*, 896–904. doi:10.1016/S1003-6326(20)65263-3
452. Raynor, G. V. *The Physical Metallurgy of Magnesium and Its Alloys*. New York: Pergamon, 1959.
453. Vagarali, S. S.; Langdon, T. G. Deformation Mechanisms in Hcp Metals at Elevated Temperatures—II. Creep Behavior of a Mg-0.8% Al Solid Solution Alloy. *Acta Metall.* 1982, *30*, 1157–1170. doi:10.1016/0001-6160(82)90009-8
454. Dargusch, M.; Dunlop, G.; Pettersen, K. Elevated Temperature Creep and Microstructure of Die Cast Mg-Al Alloys. In *Magnesium Alloys and Their Applications*, Mordike, B. L., Kainer, K. U., Eds.; Werkstoff-Informationsgesellschaft mbH: Wolfsburg, Germany, 1998; p. 277–282.
455. Somekawa, H.; Hirai, K.; Watanabe, H.; Takigawa, Y.; Higashi, K. Dislocation Creep Behavior in Mg–Al–Zn Alloys. *Mater. Sci. Eng. A* 2005, *407*, 53–61. doi:10.1016/j.msea.2005.06.059
456. Figueiredo, R. B.; Langdon, T. G. Analysis of the Creep Behavior of Fine-Grained AZ31 Magnesium Alloy. *Mater. Sci. Eng. A* 2020, *787*, 139489. doi:10.1016/j.msea.2020.139489
457. Mo, N.; McCarroll, I.; Tan, Q.; Ceguerra, A.; Cairney, J.; Dieringa, H.; Huang, Y.; Jiang, B.; Pan, F.; Bermingham, M.; et al. Roles of Nd and Mn in a

New Creep-Resistant Magnesium Alloy. *Mater. Sci. Eng. A* 2020, *779*, 139152. doi:10.1016/j.msea.2020.139152

458. Mirza, F.; Chen, D.; Li, D.; Zeng, X. Effect of Strain Ratio on Cyclic Deformation Behavior of a Rare-Earth Containing Extruded Magnesium Alloy. *Mater. Sci. Eng. A* 2013, *588*, 250–259. doi:10.1016/j.msea.2013.09.023
459. Joost, W. J. Reducing Vehicle Weight and Improving US Energy Efficiency Using Integrated Computational Materials Engineering. *Jom* 2012, *64*, 1032–1038. doi:10.1007/s11837-012-0424-z
460. Mohammed, S.; Li, D.; Zeng, X.; Chen, D. Cyclic Deformation Behavior of a High Zinc-Containing Cast Magnesium Alloy. Int. J. Fatigue 2019, *125*, 1–10. doi:10.1016/j.ijfatigue.2019.03.015
461. Mokdad, F.; Chen, D. Strain-Controlled Low Cycle Fatigue Properties of a Rare-Earth Containing ZEK100 Magnesium Alloy. *Mater. Des.* 2015, *67*, 436–447. doi:10.1016/j.matdes.2014.11.058
462. Mirza, F.; Chen, D.; Li, D.; Zeng, X. Low Cycle Fatigue of a Rare-Earth Containing Extruded Magnesium Alloy. *Mater. Sci. Eng. A* 2013, *575*, 65–73. doi:10.1016/j.msea.2013.03.041
463. Noster, U.; Scholtes, B. Isothermal Strain-Controlled Quasi-Static and Cyclic Deformation Behavior of Magnesium Wrought Alloy AZ31: Dedicated to Professor Dr. Otmar Vöhringer on the Occasion of His 65th Birthday. *MEKU* 2003, *94*, 559–563. doi:10.3139/146.030559
464. Renner, F. *Einflussgrössen auf die Schwingfestigkeit von Magnesium-Guss-und-Knet-Legierungen und Lebensdauerrechnungen*. Papierflieger, 2004.
465. Hasegawa, S.; Tsuchida, Y.; Yano, H.; Matsui, M. Evaluation of Low Cycle Fatigue Life in AZ31 Magnesium Alloy. Int. J. Fatigue 2007, *29*, 1839–1845. doi:10.1016/j.ijfatigue.2006.12.003
466. Chen, L.; Wang, C.; Wu, W.; Liu, Z.; Stoica, G. M.; Wu, L.; Liaw, P. K. Low-Cycle Fatigue Behavior of an as-Extruded AM50 Magnesium Alloy. Metall. *Mat.* Trans. A. 2007, *38*, 2235–2241. doi:10.1007/s11661-007-9181-y
467. Lin, X.; Chen, D. Strain Controlled Cyclic Deformation Behavior of an Extruded Magnesium Alloy. *Mater. Sci. Eng. A* 2008, *496*, 106–113. doi:10.1016/j.msea.2008.05.016
468. Begum, S.; Chen, D.; Xu, S.; Luo, A. A. Strain-Controlled Low-Cycle Fatigue Properties of a Newly Developed Extruded Magnesium Alloy. Metall. *Mat.* Trans. A. 2008, *39*, 3014–3026. doi:10.1007/s11661-008-9677-0
469. Begum, S.; Chen, D.; Xu, S.; Luo, A. A. Low Cycle Fatigue Properties of an Extruded AZ31 Magnesium Alloy. Int. J. Fatigue 2009, *31*, 726–735. doi:10.1016/j.ijfatigue.2008.03.009
470. Matsuzuki, M.; Horibe, S. Analysis of Fatigue Damage Process in Magnesium Alloy AZ31. *Mater. Sci. Eng. A* 2009, *504*, 169–174. doi:10.1016/j.msea.2008.10.034
471. Ishihara, S.; McEvily, A.; Sato, M.; Taniguchi, K.; Goshima, T. The Effect of Load Ratio on Fatigue Life and Crack Propagation Behavior of an Extruded Magnesium Alloy. Int. J. Fatigue 2009, *31*, 1788–1794. doi:10.1016/j.ijfatigue.2009.02.034
472. Kwon, S.; Song, K.; Shin, K.; Kwun, S. Low Cycle Fatigue Properties and Cyclic Deformation Behavior of as-Extruded AZ31 Magnesium Alloy. *Trans. Nonferrous Met. Soc. China* 2010, *20*, s533–s539. doi:10.1016/S1003-6326(10)60533-X
473. Hong, S.-G.; Park, S. H.; Huh, Y.-H.; Lee, C. S. Anisotropic Fatigue Behavior of Rolled Mg–3Al–1Zn Alloy. *J. Mater. Res.* 2010, *25*, 966–971. doi:10.1557/JMR.2010.0123
474. Huppmann, M.; Lentz, M.; Brömmelhoff, K.; Reimers, W. Fatigue Properties of the Hot Extruded Magnesium Alloy AZ31. *Mater. Sci. Eng. A* 2010, *527*, 5514–5521. doi:10.1016/j.msea.2010.05.036
475. Park, S. H.; Hong, S.-G.; Lee, B. H.; Bang, W.; Lee, C. S. Low-Cycle Fatigue Characteristics of Rolled Mg–3Al–1Zn Alloy. Int. J. Fatigue 2010, *32*, 1835–1842. doi:10.1016/j.ijfatigue.2010.05.002
476. Wu, L.; Agnew, S. R.; Ren, Y.; Brown, D. W.; Clausen, B.; Stoica, G. M.; Wenk, H. R.; Liaw, P. K. The Effects of Texture and Extension Twinning on the Low-Cycle Fatigue Behavior of a Rolled Magnesium Alloy, AZ31B. *Mater. Sci. Eng. A* 2010, *527*, 7057–7067. doi:10.1016/j.msea.2010.07.047
477. Lv, F.; Yang, F.; Duan, Q. Q.; Yang, Y. S.; Wu, S. D.; Li, S. X.; Zhang, Z. F. Fatigue Properties of Rolled Magnesium Alloy (AZ31) Sheet: Influence of Specimen Orientation. Int. J. Fatigue 2011, *33*, 672–682. doi:10.1016/j.ijfatigue.2010.10.013
478. Albinmousa, J.; Jahed, H.; Lambert, S. Cyclic Axial and Cyclic Torsional Behaviour of Extruded AZ31B Magnesium Alloy. Int. J. Fatigue 2011, *33*, 1403–1416. doi:10.1016/j.ijfatigue.2011.04.012
479. Shiozawa, K.; Kitajima, J.; Kaminashi, T.; Murai, T.; Takahashi, T. Low-Cycle Fatigue Deformation Behavior and Evaluation of Fatigue Life on Extruded Magnesium Alloys. *Procedia Eng.* 2011, *10*, 1244–1249. doi:10.1016/j.proeng.2011.04.207
480. Yu, Q.; Zhang, J.; Jiang, Y.; Li, Q. An Experimental Study on Cyclic Deformation and Fatigue of Extruded ZK60 Magnesium Alloy. Int. J. Fatigue 2012, *36*, 47–58. doi:10.1016/j.ijfatigue.2011.08.016
481. Yu, Q.; Zhang, J.; Jiang, Y.; Li, Q. Effect of Strain Ratio on Cyclic Deformation and Fatigue of Extruded AZ61A Magnesium Alloy. Int. J. Fatigue 2012, *44*, 225–233. doi:10.1016/j.ijfatigue.2012.04.013
482. Geng, C. J.; Wu, B. L.; Du, X. H.; Wang, Y. D.; Zhang, Y. D.; Wagner, F.; Esling, C. Low Cycle Fatigue Behavior of the Textured AZ31B Magnesium Alloy under the Asymmetrical Loading. *Mater. Sci. Eng. A* 2013, *560*, 618–626. doi:10.1016/j.msea.2012.10.004
483. Lin, Y.; Chen, X.-M.; Liu, Z.-H.; Chen, J. Investigation of Uniaxial Low-Cycle Fatigue Failure Behavior of Hot-Rolled AZ91 Magnesium Alloy. Int. J. Fatigue 2013, *48*, 122–132. doi:10.1016/j.ijfatigue.2012.10.010
484. Lugo, M.; Jordon, J. B.; Solanki, K. N.; Hector, L. G.; Bernard, J. D.; Luo, A. A.; Horstemeyer, M. F. Role of Different Material Processing Methods on the Fatigue Behavior of an AZ31 Magnesium Alloy. Int.

J. Fatigue 2013, *52*, 131–143. doi:10.1016/j.ijfatigue.2013.02.017

485. Dallmeier, J.; Huber, O.; Saage, H.; Eigenfeld, K.; Hilbig, A. Quasi-Static and Fatigue Behavior of Extruded ME21 and Twin Roll Cast AZ31 Magnesium Sheet Metals. *Mater. Sci. Eng. A* 2014, *590*, 44–53. doi:10.1016/j.msea.2013.09.088
486. Patel, H.; Chen, D.; Bhole, S.; Sadayappan, K. Low Cycle Fatigue Behavior of a Semi-Solid Processed AM60B Magnesium Alloy. *Mater. Des.* 2013, *49*, 456–464. doi:10.1016/j.matdes.2013.01.015
487. Patel, H.; Chen, D.; Bhole, S.; Sadayappan, K. Cyclic Deformation and Twinning in a Semi-Solid Processed AZ91D Magnesium Alloy. *Mater. Sci. Eng. A* 2010, *528*, 208–219. doi:10.1016/j.msea.2010.09.016
488. Yang, Y.; Liu, Y.; Qin, S.; Fang, Y. High Cycle Fatigue Properties of Die-Cast Magnesium Alloy AZ91D with Addition of Different Concentrations of Cerium. J. Rare *Earths* 2006, *24*, 591–595. doi:10.1016/S1002-0721(06)60170-1
489. Yang, Y.; Liu, Y. The Effect of Cerium on High-Cycle Fatigue Properties of Die-Cast Magnesium Alloy. Fat. Frac. Eng. Mat. Struct. 2007, *30*, 1149–1157. doi:10.1111/j.1460-2695.2007.01184.x
490. You, B.-S.; Park, W.-W.; Chung, I.-S. The Effect of Calcium Additions on the Oxidation Behavior in Magnesium Alloys. Scr. Mater. 2000, *42*, 1089–1094. doi:10.1016/S1359-6462(00)00344-4
491. Song, G.; Atrens, A. Understanding Magnesium Corrosion—A Framework for Improved Alloy Performance. *Adv. Eng. Mater.* 2003, *5*, 837–858. doi:10.1002/adem.200310405
492. Song, G. L.; Atrens, A. Corrosion Mechanisms of Magnesium Alloys. *Adv. Eng. Mater.* 1999, *1*, 11–33. doi:10.1002/(SICI)1527-2648(199909)1:1<11::AID-ADEM11>3.0.CO;2-N
493. Song, G.; Atrens, A.; StJohn, D. *Magnesium Technology 2001*. TMS: New Orleans. 2001, p. 255.
494. Jing, B.; Yangshan, S.; Shan, X.; Feng, X.; Tianbai, Z. Microstructure and Tensile Creep Behavior of Mg–4Al Based Magnesium Alloys with Alkaline-Earth Elements Sr and Ca Additions. *Mater. Sci. Eng. A* 2006, *419*, 181–188. doi:10.1016/j.msea.2005.12.017
495. SüDholz, A. D.; Kirkland, N. T.; Buchheit, R. G.;; Birbilis, N. Electrochemical Properties of Intermetallic Phases and Common Impurity Elements in Magnesium Alloys. *Electrochem. Solid-State Lett.* 2011, *14*, C5–C7. doi:10.1149/1.3523229
496. Hu, Z.; Liu, R.; Kairy, S.; Li, X.; Yan, H.; Birbilis, N. Effect of Sm Additions on the Microstructure and Corrosion Behavior of Magnesium Alloy AZ91. Corros. Sci. 2019, *149*, 144–152. doi:10.1016/j.corsci.2019.01.024
497. Lee, D.; Kim, B.; Lee, S.; Baek, S.-M.; Kim, J. C.; Son, H.-T.; Lee, J. G.; Lee, K.-S.; Park, S. S. Enhanced Corrosion Resistance of Mg–Sn–Zn–Al Alloy by Y Microalloying. Scr. Mater. 2019, *163*, 125–129. doi:10.1016/j.scriptamat.2019.01.015
498. Kim, K. H.; Nam, N. D.; Kim, J. G.; Shin, K. S.; Jung, H. C. Effect of Calcium Addition on the Corrosion Behavior of Mg–5Al Alloy. *Intermetallics* 2011, *19*, 1831–1838. doi:10.1016/j.intermet.2011.07.024
499. Chino, Y.; Huang, X.; Suzuki, K.; Sassa, K.; Mabuchi, M. Influence of Zn Concentration on Stretch Formability at Room Temperature of Mg–Zn–Ce Alloy. *Mater. Sci. Eng. A* 2010, *528*, 566–572. doi:10.1016/j.msea.2010.09.081
500. Huang, X.; Suzuki, K.; Chino, Y. Influences of Initial Texture on Microstructure and Stretch Formability of Mg–3Al–1Zn Alloy Sheet Obtained by a Combination of High Temperature and Subsequent Warm Rolling. Scr. Mater. 2010, *63*, 395–398. doi:10.1016/j.scriptamat.2010.04.032
501. Huang, X.; Suzuki, K.; Chino, Y.; Mabuchi, M. Improvement of Stretch Formability of Mg–3Al–1Zn Alloy Sheet by High Temperature Rolling at Finishing Pass. J. Alloys *Compd.* 2011, *509*, 7579–7584. doi:10.1016/j.jallcom.2011.04.132
502. Huang, X.; Suzuki, K.; Watazu, A.; Shigematsu, I.; Saito, N. Improvement of Formability of Mg–Al–Zn Alloy Sheet at Low Temperatures Using Differential Speed Rolling. J. Alloys *Compd.* 2009, *470*, 263–268. doi:10.1016/j.jallcom.2008.02.029
503. Xue, D.; Xue, D.; Yuan, R.; Zhou, Y.; Balachandran, P. V.; Ding, X.; Sun, J.; Lookman, T. An Informatics Approach to Transformation Temperatures of NiTi-Based Shape Memory Alloys. *Acta Mater.* 2017, *125*, 532–541. doi:10.1016/j.actamat.2016.12.009
504. Shen, C.; Wang, C.; Wei, X.; Li, Y.; van der Zwaag, S.; Xu, W. Physical Metallurgy-Guided Machine Learning and Artificial Intelligent Design of Ultrahigh-Strength Stainless Steel. *Acta Mater.* 2019, *179*, 201–214. doi:10.1016/j.actamat.2019.08.033
505. Yuan, M.; Paradiso, S.; Meredig, B.; Niezgoda, S. R. Machine Learning–Based Reduce Order Crystal Plasticity Modeling for ICME Applications. Integr. Mater. Manuf. Innov. 2018, *7*, 214–230. doi:10.1007/s40192-018-0123-x
506. Orme, A. D.; Chelladurai, I.; Rampton, T. M.; Fullwood, D. T.; Khosravani, A.; Miles, M. P.; Mishra, R. K. Insights into Twinning in Mg AZ31: A Combined EBSD and Machine Learning Study. Comput. Mater. Sci. 2016, *124*, 353–363. doi:10.1016/j.commatsci.2016.08.011
507. Pei, Z.; Yin, J. Machine Learning as a Contributor to Physics: Understanding Mg Alloys. *Mater. Des.* 2019, *172*, 107759. doi:10.1016/j.matdes.2019.107759
508. Pei, Z.; Yin, J. The Relation between Two Ductility Mechanisms for Mg Alloys Revealed by High-Throughput Simulations. *Mater. Des.* 2020, *186*, 108286. doi:10.1016/j.matdes.2019.108286